GRAVITY WAVE MOTIONS IN THE TROPOSPHERE AND LOWER STRATOSPHERE

By

Simon J. Allen

Thesis

submitted for the degree of

DOCTOR OF PHILOSOPHY

at the

UNIVERSITY OF ADELAIDE

(Department of Physics and Mathematical Physics)

August 1996

This work contains no material which has been accepted for the award of any other degree or diploma in any university or other tertiary institution and, to the best of my knowledge and belief, contains no material previously published or written by another person, except where due reference has been made in the text.

I give consent to this copy of my thesis, when deposited in the University Library, being available for loan and photocopying.

Signed: .... dated: ....1/8/96.....

Simon J. Allen

Abstract

The large-scale circulation structures of the atmosphere are thought to be influenced by gravity wave motions. Therefore, the climatological characteristics of such waves must be determined if the basic state atmosphere is to be fully understood and modelled. Radiosonde measurements provide one means of approaching the problem and this thesis is concerned with the determination of gravity wave characteristics using operational radiosondes. The data considered include soundings from 22 stations whose locations range from the tropics to the Antarctic. All measurements were supplied by the Australian Bureau of Meteorology, with the exception of the South Pole data used in appendix C.

The first chapter introduces some background theory regarding gravity waves and discusses their importance in relation to the large scale dynamics of the atmosphere. In addition, a brief review of the cognate research field of gravity waves in oceans is provided. A review of the relevant atmospheric literature is presented in chapter 2 which includes both theoretical and experimental aspects of recent gravity wave research. It is noted that a gravity wave study which uses high-vertical-resolution radiosonde measurements from a network of stations in the southern hemisphere is unique. In chapter 3, the radiosonde data that were utilized and the analysis techniques that were employed, are described. Also presented are discussions regarding important issues such as measurement accuracy, measurement sensor response times and the observational geometry of radiosonde soundings.

The large majority of scientific research is presented in chapters 4, 5, 6 and 7. In chapter 4, the seasonal and geographic variations of gravity wave temperature variance are investigated. This is made possible by the extensive geographic and temporal coverage of the available radiosonde data. Chapters 5 and 6 investigate additional aspects of the gravity wave field over Macquarie Island (55°S, 159°E) and the Cocos Islands (12°S, 97°E), respectively. The availability of good quality horizontal wind velocity measurements from these sites, which were obtained simultaneously with the temperature measurements, allows qualitative information

about wave field directionality to be inferred. Furthermore, knowledge of both wave energy and directionality suggests that the net vertical flux of zonal momentum can be estimated. This possibility is explored in chapter 7.

Acknowledgements

The research presented in this thesis was conducted under the supervision of Dr. Bob Vincent whose support and advice are gratefully acknowledged. Furthermore, some parts of chapters 3 and 4 also appear in a journal publication [*Allen and Vincent*, 1995; see appendix D] which was written in collaboration with Bob. I would also like to thank the more general support and encouragement of the various staff and students of the Atmospheric Physics Group of the Department of Physics and Mathematical Physics.

Early versions of some chapters have been reviewed by Dr. Steve Eckermann, Dr. Tom VanZandt and Dr. Bob Vincent. Their comments and advice have greatly improved the final manuscript. I would also like to thank Steve for valuable discussions and correspondence. Chapter 7, and in particular section 7.2, is based on an unpublished manuscript written by Dr. Steve Eckermann in collaboration with Dr. Bob Vincent. I must also thank Dr. Wayne Hocking, my Honours year project supervisor, for first bringing to my attention the response time problem discussed in section 3.4.

The majority of the data that were utilized were provided by the National Climate Centre of the Australian Bureau of Meteorology. Their prompt provision of these data is gratefully acknowledged. I would especially like to thank Bruce Gunn, Jeff Stickland, Dr. Peter May and Alan Sharp for providing me with a basic understanding of the radiosonde systems used by the Australian Bureau of Meteorology. I would also like to thank Vaisala Pty. Ltd. for the provision of the response time technical reports.

The radiosonde data from the Antarctic and sub-Antarctic bases were provided on a weekly basis by the staff at each station. Their efforts on my behalf are greatly appreciated. I would especially like to thank Dr. Damian Murphy, Mike Ball and Shaun Johnson for helping to organize the system of data transfer. In addition, I must also thank the Antarctic Division for the use of their computing facilities. The radiosonde data from the South Pole were kindly supplied by Matt Pfenninger of the University of Illinois.

The support and encouragement of the Department Physics and Mathematical Physics has been very helpful. I would especially like to thank Mark Ferraretto, Dr. Trevor Harris (who provided me with the DCDFT program code) and Dr. Brenton Vandepeer for their help in improving my computing skills. Discussions with visiting scientists have also been valuable. These have included Dr. S. K. Avery, Dr. D. G. Andrews, Dr. D. J. Karoly, Dr. P. T. May and Dr. T. Tsuda. My research has been supported financially for 3.5 years by an Australian Postgraduate Award.

Contents

List of Tables

List of Figures

Chapter 1

Introduction

1.1 Gravity Waves and the Earth's Atmosphere

The Earth's atmosphere is often divided into four regions based on the observed vertical temperature structure. This is illustrated in Figure 1.1 where an example from the COSPAR International Reference Atmosphere [*CIRA*, 1986] between 0 and 120 km is presented. This profile is representative of mean conditions at 30°S and the COSPAR reference atmosphere is an internationally recognized standard. The four regions are called the troposphere, the stratosphere, the mesosphere and the thermosphere, and are characterized by the sign of the vertical gradient of air temperature. The boundaries between regions are called the tropopause, stratopause and mesopause and are shown in the diagram.

Another classification scheme relies on characteristics of the atmosphere's composition. The so-called homosphere, between approximately 0 and 100 km, is that region of the atmosphere where significant turbulent mixing maintains the relative abundance of major atmospheric constituents at constant values. Above this region, the process of molecular diffusion is more important and gaseous constituents are found to be separated according to mass with heavier gases relatively more abundant at lower altitudes. This region of the atmosphere is called the heterosphere and its lower boundary is called the turbopause. The exact position of the turbopause[1] is not clearly defined since the altitude at which molecular diffusion becomes important is different for different gases.

A further scheme of classification separates the atmosphere into two spheres, the barosphere and the exosphere, on the basis of the mean free path of neutral gas molecules. The

[1]The turbopause is defined as the altitude at which the eddy diffusion and molecular diffusion coefficients are equal [e.g., *Bauer*, 1973]. Both terms are dependent upon the gaseous constituent being considered.

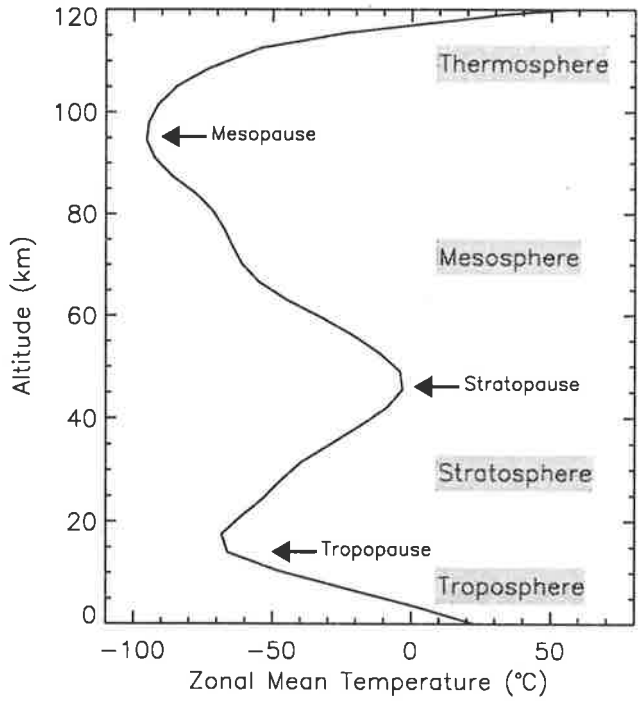

Figure 1.1: A typical zonal-mean temperature profile during January at 30°S. The diagram uses temperature data from *CIRA* [1986].

exosphere, above approximately 400 km, is that region of the atmosphere where gaseous escape is significant owing to the large mean free path of gas molecules. In this region the velocity distribution of molecules is non-Maxwellian since high velocity particles, in particular those with velocities exceeding their gravitational escape velocity, suffer few collisions and are typically lost from the atmosphere. The exosphere is separated from the barosphere, so called because in this region barometric laws hold, by the baropause. The baropause is defined [e.g., *Bauer*, 1973] as the altitude at which the mean free path is equal to the local scale height[2].

The ionosphere is the region of the atmosphere, between approximately 60 and 400 km, where the number density of plasma becomes large and has significant influence on radio wave propagation. It can be subdivided into various layers or regions [e.g., *Bauer*, 1973; *Rees*, 1989] based on the observed characteristics and structure of the plasma number density profile. The main sources of ionization are believed to be solar ultra-violet (UV) and X-ray radiation and energetic particles of either solar system or cosmic origin. The study of the Earth's ionosphere has particular historical significance owing to its affects on radio wave communication.

[2]The scale height is the vertical distance over which atmospheric pressure decreases by 37%.

The atmosphere is often divided into lower, middle and upper atmosphere regions. There are no strict definitions of these terms although it is most commonly understood [e.g., *Andrews et al.,* 1987] that the term lower atmosphere refers to the troposphere, the term middle atmosphere refers to the region between the tropopause and the turbopause and the term upper atmosphere is used to describe the atmosphere above the turbopause. The work of this thesis is concerned primarily with the region of the atmosphere, between ground level and approximately 30 km, that can be probed using conventional meteorological radiosondes. Although this includes only the lowest portions of the middle atmosphere, the work is nonetheless of relevance to all regions of the middle atmosphere as will be discussed later.

Some of the above classification schemes are illustrated schematically in Figure 1.2. These are based on extensive observational studies of the atmosphere which provide climatological mean profiles of primary geophysical variables such as pressure, temperature and wind velocity, and also of atmospheric constituents [e.g., *U.S. Standard Atmosphere Supplements*, 1966; *CIRA*, 1986]. The purpose of such reference atmospheres is to provide hypothetical profiles "which, by international agreement, are roughly representative of the various geographical and seasonal conditions over the Earth" [*CIRA*, 1972, p. XVI]. They provide a basic observational framework within which most atmospheric research is undertaken.

The altitude dependence of air temperature in the lower and middle atmospheres varies with season and geographic location but the general structure presented in Figure 1.1 is reproduced in all circumstances. This basic structure is broadly explained in terms of radiative and photochemical processes and that explanation, put simply, is as follows. In the troposphere the Earth's surface behaves as a heat source (due to its absorption of visible light) and this results in a temperature maximum at ground level. The temperature minimum at the tropopause is due to radiative emission whereas absorption of long-wavelength solar UV radiation by ozone[3] results in the temperature maximum at the stratopause [e.g., *Andrews et al.,* 1987]. Once again radiative emission and decreasing ozone concentrations explain the temperature minimum at the mesopause while increasing thermospheric temperatures result from absorption of short-wavelength UV and X-ray radiation by various constituents but predominantly by atomic and molecular oxygen. Details of the various radiative and photochemical processes that are involved are described elsewhere [e.g., *Banks and Kockarts*, 1973; *Brasseur and Solomon*, 1984] and are believed to be well understood.

While radiative and photochemical processes are successful in explaining many broad

[3] A minor atmospheric constituent that is typically most abundant near 20 km.

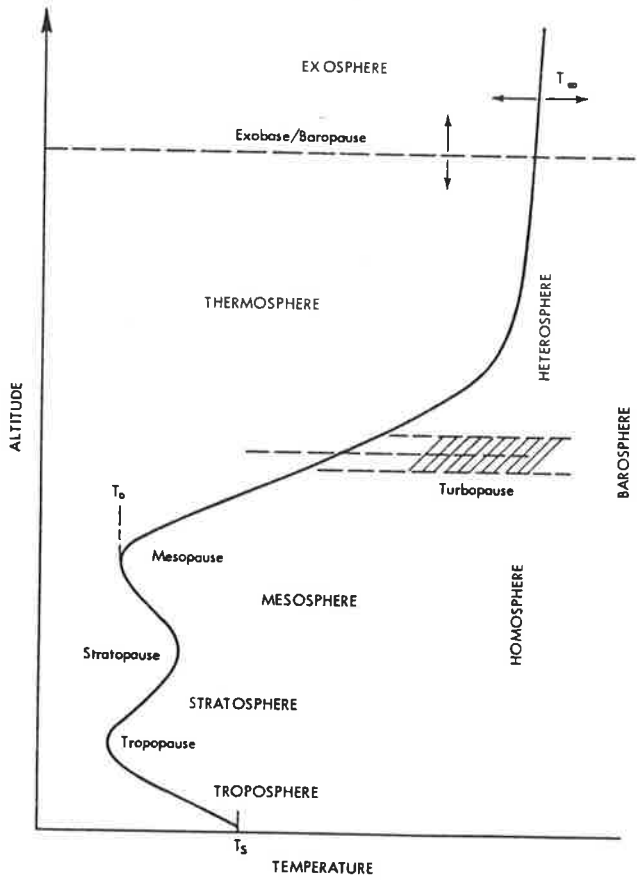

Figure 1.2: A schematic illustration of different atmospheric regions [from *Bauer*, 1973].

features of the observed temperature structure, certain features cannot be explained in such a manner. Figure 1.3 displays a schematic illustration of the latitude-height distribution of zonal-mean atmospheric temperature for the solstice case following *Geller* [1983]. Two features of this diagram that are difficult to explain, at least from the viewpoint of radiative and photochemical arguements, are: one, the local temperature minimum at the tropical tropopause and two, the reversal of the meridional temperature gradient at heights near the mesopause [*Geller*, 1983]. Models of zonal-mean temperature which attain local thermodynamic equilibrium, thereby allowing no vertical or meridional motion, and which include known photochemical processes cannot account for either of these features [e.g., *Geller*, 1983]. Such hypothetical temperatures are termed radiative equilibrium temperatures. They serve to highlight the importance of dynamical processes since the models which generate them specifically exclude dynamical effects. It is now widely understood that dynamical, photochemical and radiative process are all important and must be considered together if a

comprehensive understanding of the climatological-mean structures of the atmosphere is to be achieved.

The latitude-height structure of zonal-mean zonal winds is illustrated schematically in Figure 1.3. Climatological mean horizontal winds are typically in geostrophic balance[4] and the zonal winds are related to the latitudinal distribution of temperature according to the thermal wind equation [e.g., *Andrews et al.*, 1987]. It is therefore possible to obtain model zonal winds based on the calculated radiative equilibrium temperatures and to compare these with the representative solstice wind structure of Figure 1.3. Given the differences between observed and radiative equilibrium temperatures it is not surprising that there should be differences between model and reference atmosphere winds as has been found by, for example, *Geller* [1983]. Since the latitudinal gradient of radiative equilibrium temperature does not change sign with height, the corresponding geostrophic winds at midlatitude must increase monotonically with height. This is in contrast to midlatitude reference atmosphere winds which increase more slowly with height and which peak near 60 km and decline thereafter (Figure 1.3).

It is now understood that the difference between radiative equilibrium and observed temperatures is the result of important dynamical processes which occur within the atmosphere [e.g., *Andrews et al.*, 1987]. Strong convection and adiabatic cooling are responsible for the temperature minimum at the tropical tropopause while wave motions are believed to have significant effects at mesospheric heights. Indeed the reversal of the meridional temperature gradient at these heights is thought to be due to dynamical thermal transport associated with eddy or wave motions[5] [*Andrews et al.*, 1987]. *Leovy* [1964] was the first to parameterize this effect by assuming that it acted to decelerate mean winds where the deceleration or drag (called Rayleigh drag) was proportional to the mean winds themselves. Using this approach, *Leovy* [1964], and later *Schoeberl and Strobel* [1978] and *Holton and Wehrbein* [1980], were able to model successfully the observed departures from radiative equilibrium wind or temperature structures. *Houghton* [1978] argued that gravity waves, which are medium-scale atmospheric wave motions, were likely to be responsible for the deceleration effect while *Lindzen* [1981] provided a physical picture as to how this might occur.

According to the picture of *Lindzen* [1981], gravity waves are generated predominantly within the troposphere and propagate vertically with increasing amplitude. This increasing

[4]This is not true at equatorial latitudes where Coriolis effects become negligible and the geostrophic approximation is no longer valid.

[5]These are first order perturbations about some mean background structure.

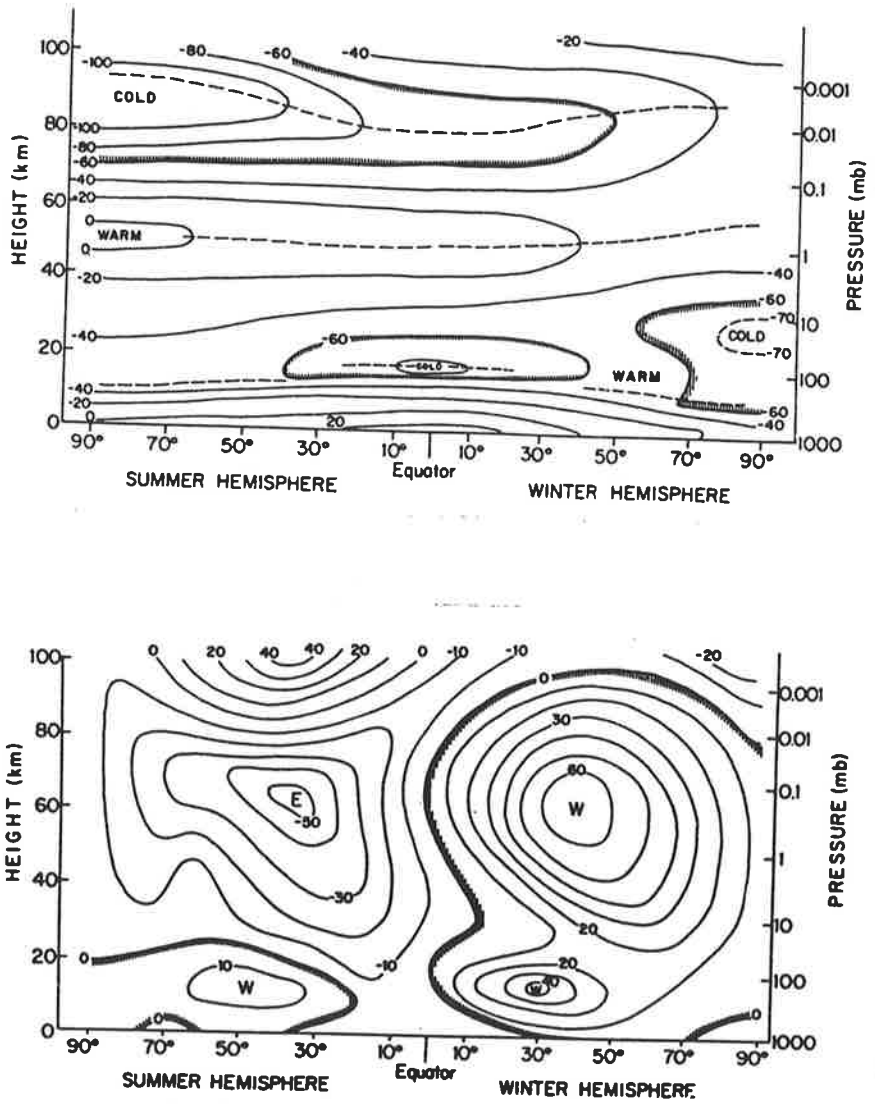

Figure 1.3: Schematic latitude-height sections of zonal-mean temperatures (°C, upper panel) and zonal-mean zonal winds (m s^{-1}, lower panel) during solstice conditions [from *Andrews et al.*, 1987]. Dashed lines indicate the tropopause, stratopause and mesopause while W and E designate westerly and easterly winds, respectively [*Andrews et al.*, 1987]. R. J. Reed is acknowledged by *Andrews et al.* [1987] for the preparation of these diagrams.

amplitude results from the exponential decrease of density with height and from energy conservation considerations. Relatively small amplitude waves in the troposphere thus have large amplitudes upon reaching the mesosphere and may become unstable and break by approximate analogy with breaking surf. Breaking gravity waves act to accelerate mean winds in the direction of the horizontal phase speed of the wave [*Lindzen*, 1981]. This effect is similar to the Rayleigh drag parameterization used by e.g., *Leovy* [1964] if the waves' phase speeds are zero. Such an assumption is entirely plausible in many situations if topographic forcing can be considered as a dominant source mechanism. While gravity waves do not possess momentum they do act to redistribute it [e.g., *McIntyre*, 1981; *Fritts*, 1984] and this point will be discussed in more detail later.

The above description of gravity waves and their effects upon the mean structures of the mesosphere is vastly oversimplified and ignores important processes such as the filtering of certain waves before reaching the mesosphere. These will be discussed later. However, it does highlight the importance of gravity waves in determining even the most basic observed structures of the atmosphere such as the climatological mean temperature and zonal wind structures of the mesosphere. More recently gravity waves have been found to play a similar role, albeit a much less dramatic one, in determining the circulation structures of the troposphere and the lower stratosphere [e.g., *Palmer et al.*, 1986; McFarlane, 1987] and it is now believed that they influence all regions of the atmosphere through which they propagate [e.g., *Fritts and VanZandt*, 1993; *Fritts and Lu*, 1993; *Lu and Fritts*, 1993]. Quite clearly the study of atmospheric gravity waves is both a valid and necessary branch of atmospheric research and is already broadly successful in explaining many observed features of the atmosphere. This thesis is concerned with the study of atmospheric gravity waves in the troposphere and lower stratosphere using an extensive experimental data base of meteorological radiosonde measurements. Before describing the relevance of this work, however, it is first necessary to discuss the basic theoretical framework within which the work is undertaken.

1.2 Theoretical Framework

The atmosphere is capable of supporting several different classes of wave motions which cover a broad range of spatial and temporal scales. The various classification schemes are described by, for example, *Gossard and Hooke* [1975] and *Andrews et al.* [1987], and only certain points will be reported here. Most commonly waves are classified according to their important

restoring forces [*Gossard and Hooke*, 1975; *Andrews et al.*, 1987]. For example, gravity waves are so named since gravity is an important restoring force for this wave class whereas Rossby or planetary waves require Coriolis effects to provide a restoring mechanism. Other important wave classes include trapped or evanescent waves which are constrained to certain regions of the atmosphere, stationary waves which have phase fronts that remain fixed with respect to a ground-based observer, and forced waves which must be continuously maintained by a given excitation mechanism [*Andrews et al.*, 1987]. Equatorial waves such as the Kelvin and mixed Rossby-gravity wave modes are examples of trapped waves, thermal tides are examples of forced waves, and topographically generated gravity waves, often called mountain or lee waves, can be examples of stationary waves. The various schemes of classification are not exclusive and often overlap.

In this thesis atmospheric gravity waves are the focus of study due to their importance in influencing the large scale dynamics of the lower and middle atmospheres. However, other wave motions are also important in this regard. For example, dissipating Kelvin and mixed Rossby-gravity waves are thought to provide a mechanism for maintenance of the quasi-biennial oscillation (QBO) which is observed in the equatorial lower and middle stratosphere [e.g., *Lindzen and Holton*, 1968; *Wallace*, 1973]. Planetary waves, on the other hand, are largely responsible for stratospheric sudden warmings and for weakening the northern-hemisphere polar vortex [e.g., *Matsuno*, 1971; *Andrews et al.*, 1987]. It appears that several classes of wave motion are important in influencing the dynamics of the Earth's atmosphere.

Atmospheric wave motions of all scales, and indeed the large-scale circulation structures themselves, are defined by the three fundamental equations of fluid dynamics which express Newton's second law, the first law of thermodynamics and the law of mass conservation [e.g., *Holton*, 1992]. Newton's second law is expressed mathematically by the equation of motion which, for conditions appropriate to the lower and middle atmospheres, is given by [e.g., *Brasseur and Solomon*, 1985; *Holton*, 1992]

$$\frac{D\vec{\mathrm{U}}}{Dt} + \frac{1}{\rho}\vec{\nabla}\mathrm{p} + 2\vec{\Omega} \times \vec{\mathrm{U}} = \vec{g} + \vec{F} \tag{1.1}$$

where $\vec{\mathrm{U}} = (u, v, w)$ is the velocity vector of an air parcel in Cartesian coordinates, ρ is air density, p is air pressure, $\vec{\Omega}$ is the Earth's angular rotation rate, $\vec{g}$ is the acceleration due to gravity[6], $\vec{F}$ represents the frictional force and $\frac{D}{Dt} = \frac{\partial}{\partial t} + \vec{\mathrm{U}} \cdot \vec{\nabla}$ is the total time derivative and corresponds physically to the rate of change of a given atmospheric variable in the frame of

[6]It is assumed that the gravitational force term in (1.1) includes centrifugal force effects [e.g., *Holton*, 1992].

reference moving with an air parcel[7]. Electromagnetic force terms are legitimately ignored here since the number density of ions is small throughout the lower and middle atmospheres and these force terms are negligible at all scales of motion. The first law of thermodynamics and the law of mass conservation may be written, respectively, as follows [e.g., *Brasseur and Solomon*, 1985; *Holton*, 1992]

$$c_p \frac{DT}{Dt} - \frac{1}{\rho}\frac{D\mathrm{p}}{Dt} = Q \tag{1.2}$$

$$\frac{D\rho}{Dt} + \rho\vec{\nabla}\cdot\vec{\mathrm{U}} = 0 \tag{1.3}$$

where c_p is the specific heat of air at constant pressure, T is air temperature and Q is the net heating rate per unit mass.

Equations (1.1), (1.2) and (1.3) are often simplified by scale analysis. This involves removing certain terms which can be demonstrated to have negligible or unimportant effects at certain scales of motion [e.g., *Holton*, 1992]. The pressure gradient and gravitational forces are the most important at scales of motion common to gravity waves, essentially by definition. In the Earth's atmosphere this occurs at horizontal scales between a few tens and several hundreds of kilometres, at vertical scales between a few hundred metres and several kilometres, and at time scales ranging from a few minutes to several hours. Atmospheric gravity waves are commonly referred to as mesoscale wave motions as a consequence and are intermediate to global-scale planetary waves and small-scale turbulence. Coriolis and frictional forces have only minor influences at such scales and the relevant force terms of (1.1) can be legitimately removed in order to simplify this equation.

The gravity wave solution of (1.1), (1.2) and (1.3) has been well documented [e.g., *Hines*, 1960; *Gossard and Hooke*, 1975; *Andrews et al.*, 1987; *Holton*, 1992] and will not be reproduced here. The perturbation method is used to attain this solution and is a reputable mathematical technique. It assumes that all field variables can be decomposed into basic state and perturbation components. If ψ is any one of ρ, p, T, u, v, or w then $\psi = \overline{\psi} + \psi'$ where $\overline{\psi}$ is some long-term climatological mean (for example a zonal mean) and ψ' is the local deviation from the basic state $\overline{\psi}$. The perturbation components ψ' are assumed to be sufficiently small that the product of any two such quantities can be legitimately ignored while both ψ and $\overline{\psi}$ are assumed to satisfy the fundamental equations of motion [e.g., *Holton*, 1992]. Substitution of mean and perturbation components into simplified versions of (1.1), (1.2) and (1.3) yields, after some mathematical manipulation, a set of linear equations which

[7]The Lagrangian frame of reference

govern the system in question. This procedure is called linearization and the now linearized equations can be solved by looking for wave solutions of the form $\psi' \propto \exp(i[kx+ly+mz-\omega t])$ where $\vec{K} = (k, l, m)$ is the wavenumber vector, ω is the observed frequency in the Lagrangian frame of reference or the intrinsic frequency, $i = \sqrt{-1}$ and the complex notation has its usual meaning [e.g., *Gill*, 1982].

Valid wave solutions are found to satisfy both dispersion and polarization equations. The dispersion equation relates the wave frequency to its component wavenumbers while the polarization equations relate the amplitude and phases of different perturbation quantities such as u' and v'. The exact form of these equations depends on the degree to which (1.1), (1.2) and (1.3) have been simplified and on the approximations employed to achieve the wave solutions. One commonly used approximation is called the Boussinesq approximation and treats atmospheric density as a constant, except where it appears coupled with buoyancy force terms in the vertical component of the equation of motion [*Holton*, 1992]. Other approximation strategies can also be used but the Boussinesq approximation is generally considered to be valid for the gravity wave scales that are investigated in this thesis [e.g., *Sidi et al.*, 1988]. Coriolis effects are negligible for many gravity wave motions, but they can play a significant role at large gravity wave scales. It is therefore prudent to retain the Coriolis force term in (1.1) although its omission will not preclude the gravity wave solution. Gravity wave motions which are significantly influenced by the Coriolis force are called inertio-gravity waves.

The gravity wave dispersion relation, under the Boussinesq approximation and allowing for Coriolis and nonhydrostatic effects, is given by [e.g., *Gossard and Hooke*, 1975; *Gill*, 1982]

$$m^2 = K_h^2 \frac{(N^2 - \omega^2)}{(\omega^2 - f^2)} \tag{1.4}$$

where

$$N^2 = \frac{g}{\overline{T}} \left(\frac{d\overline{T}}{dz} + \frac{g}{c_p} \right) \tag{1.5}$$

$$f = 2\Omega \sin\theta \tag{1.6}$$

$$K_h^2 = k^2 + l^2 \tag{1.7}$$

and where $\overline{T}$ is the basic state temperature, $\Omega = |\vec{\Omega}|$ is the angular frequency of the Earth's rotation, θ is the latitude, (k, l, m) are the component wavenumbers in Cartesian coordinates, ω is the intrinsic frequency, N is the Väisälä-Brunt frequency and f is the inertial frequency. Some important polarization equations under the same approximations and assuming $Q = 0$

are [e.g., *Gossard and Hooke*, 1975; *Gill*, 1982]

$$v' = \frac{l\omega - ikf}{k\omega + ilf} u' \tag{1.8}$$

$$w' = \frac{-\omega m(\omega^2 - f^2)}{(N^2 - \omega^2)(\omega k + ifl)} u' \tag{1.9}$$

$$\hat{T}' = \frac{-iN^2}{g\omega} w' \tag{1.10}$$

$$\frac{\mathrm{p}'}{\rho_0} = \frac{\omega^2 - f^2}{k\omega + ilf} u' \tag{1.11}$$

$$\frac{\rho'}{\rho_0} = -\hat{T}' \tag{1.12}$$

where p', ρ', u', v' and w' are the fluctuation components of p, ρ, u, v and w respectively, $\hat{T}' = T'/\overline{T}$ is called the normalized temperature fluctuation, $\overline{T}$ is the basic state temperature, ρ_0 is the basic state density and T' is the fluctuation component of temperature. It is often advantageous to consider normalized temperature fluctuations in gravity wave studies (rather than simply temperature fluctuations) for reasons that will become apparent later. Polarization equations under various different approximation strategies are described elsewhere [e.g., *Hines*, 1960; *Gossard and Hooke*, 1975; *Gill*, 1982; *Holton*, 1992].

Equation (1.4) and equations (1.8) to (1.12) are generally regarded as being good approximations to the characteristics of many real (and essentially non-linear) gravity waves that propagate within the Earth's atmosphere. They are utilized by *Fritts and VanZandt* [1993], *Fritts and Lu* [1993] and *Lu and Fritts* [1993] in their gravity wave parameterization schemes and also by *Eckermann et al.* [1996] in their attempt to estimate gravity wave momentum fluxes[8]. It should be noted, however, that (1.4) and (1.8) to (1.12) are only valid if the linearization assumptions are valid. If these assumptions do not hold true to good approximation then the gravity wave motions are said to be non-linear.

It is apparent from (1.4) that three-dimensional, vertically propagating, wave solutions (called internal gravity waves) must have intrinsic frequencies that lie between the inertial frequency, f, and the Väisälä-Brunt frequency, N, given that N is typically very much larger than f throughout the lower and middle atmospheres. The inertial frequency is the oscillation frequency of a horizontally displaced air parcel in a resting atmosphere when Coriolis and centrifugal forces are in balance [*Holton*, 1992]. The Väisälä-Brunt frequency (or buoyancy frequency), N, is the oscillation frequency of a vertically and adiabatically displaced air

[8]The divergence of gravity wave momentum flux determines the influence of these waves on the background flow.

parcel in a stably-stratified atmosphere when pressure gradient and gravitational forces are in balance [*Holton*, 1992]. Both are fundamental to gravity wave theory.

An interesting property of gravity waves (one that follows from the dispersion equation) is that the vertical component of group velocity is in the opposite direction to the vertical component of phase velocity [e.g., *Gossard and Hooke*, 1975; *Gill*, 1982]. This means that downward progression of phase corresponds to upward propagation of wave energy and vice versa. In fact the group velocity is parallel to the lines of constant phase and perpendicular to the phase velocity (which is, of course, parallel to the wavenumber vector). Particle motions are confined to the plane perpendicular to the wavenumber vector [e.g., *Gill*, 1982] and thus gravity waves are transverse wave motions. These features have been demonstrated using stratified fluids within the laboratory by, for example, *Mowbray and Rarity* [1967] and are often illustrated by means of diagrams such as Figures 1.4 and 1.5 [e.g., *Lindzen*, 1971; *Gill*, 1982 and others].

Figure 1.4 provides a physical picture of internal gravity wave motions and their three-dimensional oscillation structures while Figure 1.5 depicts the wave-induced particle motions in the plane perpendicular to the wavenumber vector. The examples shown are for inertio-gravity waves which are elliptically polarized due to the significant influence of the Coriolis force. However, for waves with $\omega \gg f$, Coriolis effects are negligible and the waves become linearly polarized. In this case, the velocity components of Figure 1.4 that are both into and out of the page become negligible while in Figure 1.5 the particle motions occur along the ellipse semi-major axis $\overline{\mathrm{AXB}}$. It is also true from equation (1.4) that the angle between the wavenumber vector $\vec{K}$ and the horizontal plane (labelled ϕ' in Figure 1.5) is related to the wave intrinsic frequency according to the following equation [e.g., *Gossard and Hooke*, 1975; *Gill*, 1982]

$$\tan^2 \phi' = \frac{N^2 - \omega^2}{\omega^2 - f^2} \tag{1.13}$$

where $\tan \phi' = m/K_h$. Therefore, elliptically-polarized inertio-gravity wave oscillations occur in near-horizontal planes (ϕ' close to 90°) whereas linearly-polarized internal gravity wave oscillations occur at larger angles to the vertical (smaller ϕ'). Pure inertial oscillations occur in the horizontal plane and are circularly polarized. Gravity waves with different intrinsic frequencies propagate in different directions (and at different phase speeds) and thus gravity waves are said to be dispersive [e.g., *Holton*, 1992].

The diagrams of Figures 1.4 and 1.5 have been drawn for the case of zonally propagating gravity waves ($l = 0$). This may be done without loss of generality since the horizontal

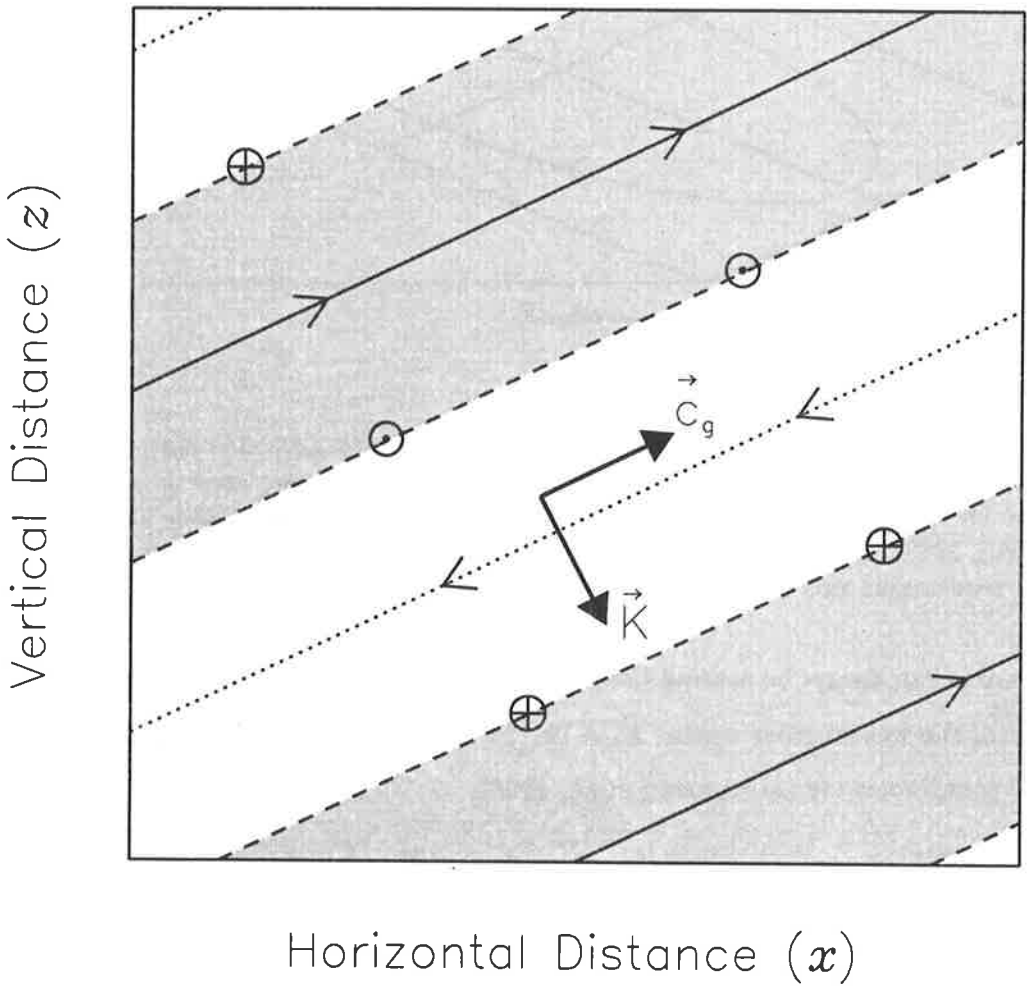

Figure 1.4: Schematic illustration of velocity fluctuations in the x–z plane for a zonally propagating ($l = 0$) inertio-gravity wave under the Boussinesq approximation [adapted from *Gill*, 1982; *Andrews et al.*, 1987; *Eckermann*, 1990a]. Solid lines are contours of maximum perturbation velocity (in the plane of the page) while dotted lines are contours of minimum perturbation velocity. Dashed lines are zero perturbation contours in the plane of the page. Arrows, including those into (denoted by $\oplus$) and out of (denoted by $\odot$) the page, which are northward and southward pointing arrows, respectively, indicate the directions of the perturbation velocity vectors (u', v', w') in each case. These directions are for the southern hemisphere ($f < 0$) situation only. The relationship between the group velocity vector, $\vec{c}_g$, and the wavenumber vector, $\vec{K}$, is illustrated. Phase progression occurs in the direction of the wavenumber vector.

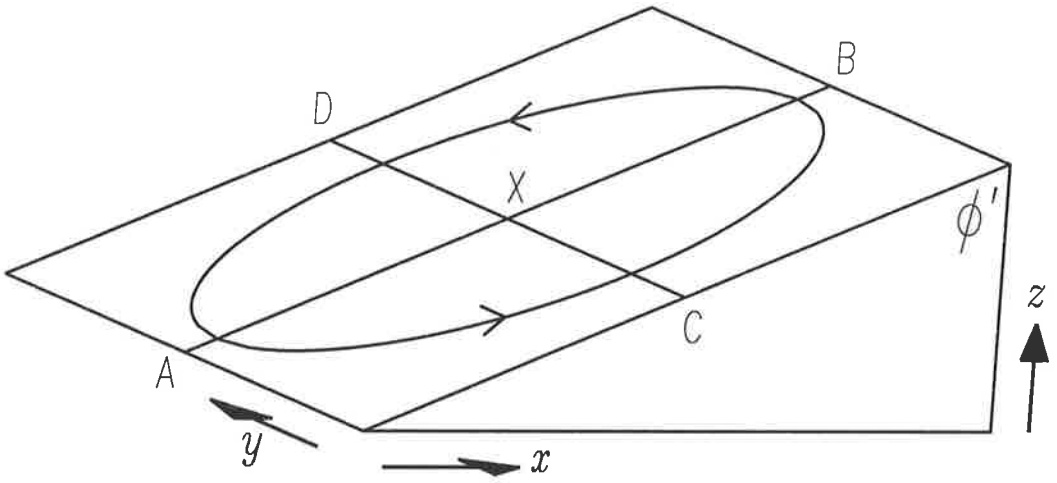

Figure 1.5: Inertio-gravity wave particle motions in the plane perpendicular to the wavenumber vector [after *Gill*, 1982]. Rotation is in the anticlockwise sense in the southern hemisphere for $m < 0$. The vector addition of Coriolis and buoyancy forces is always toward point X [*Gill*, 1982]. The horizontal phase velocity is parallel to the horizontal projection of the ellipse semi-major axis $\overline{\text{AXB}}$.

coordinate axes can always be rotated such that the new x-axis is in line with the horizontal component of the wavenumber vector, $\vec{K}_h = (k, l, 0)$. The horizontal perturbation velocities in the new coordinates are [*Eckermann et al.*, 1996]

$$u'_{||} = u' \cos\phi + v' \sin\phi \tag{1.14}$$

$$u'_{\perp} = -u' \sin\phi + v' \cos\phi \tag{1.15}$$

where $u'_{||}$ is the perturbation velocity component parallel to $\vec{K}_h$, $u'_{\perp}$ is the perturbation velocity component perpendicular to $\vec{K}_h$ and ϕ is the azimuth angle of the wavenumber vector, that is $\phi = \arctan(l/k)$. The polarization equations are simplified in the new coordinates by setting $l = 0$ and replacing u' and v' by $u'_{||}$ and $u'_{\perp}$, respectively, in (1.8) to (1.12).

The theory discussed so far is appropriate for a Lagrangian frame of reference and is essentially derived under the assumption (which was unstated until now) that the basic state winds are constant. The simplest approximation in this case is to set $\overline{u} = \overline{v} = \overline{w} = 0$ and thus the ground-based (Eulerian) and Lagrangian reference frames are equivalent. However, the observed horizontal winds[9] of the Earth's atmosphere are neither zero nor constant with height (as evidenced by Figure 1.3) and the presence of horizontal wind shear serves to

[9]The basic state vertical winds are generally small and are well approximated by $\overline{w} = 0$.

complicate the basic framework presented thus far. In fact the interaction between the basic state winds and gravity waves is a two-way process [*Andrews et al.,* 1987]. Not only do gravity waves significantly alter the mean flow but also the mean flow can have significant influence on gravity wave propagation [e.g., *Andrews et al.,* 1987].

When the basic state horizontal wind $\vec{U}_0 = (\overline{u}, \overline{v}, 0)$, N^2, or ρ are height dependent, as indeed they are in the Earth's atmosphere, the linearized equations of motion become more difficult to solve. They require different solution strategies and Liouville-Green (or WKBJ) analysis is typically used. This technique provides approximate (ray-tracing) solutions which describe how waves "refract" as they propagate vertically within the atmosphere. The technique assumes that $\vec{U}_0$, N^2 and ρ vary slowly with height and also that the dispersion and polarization equations, which were stated earlier, are valid at any given height[10] [e.g., *Andrews et al.,* 1987]. The basic state conditions are further assumed to be independent of horizontal distance and time so that the horizontal wavenumber, $\vec{K}_h$, and horizontal ground-based phase speed, c_h, are constant following a wave group[11]. Therefore both ω and m depend only upon the height-variable properties of the medium through which the wave propagates. This dependence is described by the following "Doppler-shifting" equations [e.g., *Fritts and VanZandt,* 1987; *Eckermann et al.,* 1995],

$$\omega = K_h(c_h - \overline{U}\cos\xi) \tag{1.16}$$

$$m = \frac{N}{|c_h - \overline{U}\cos\xi|}\,(\gamma/\delta_-)^{1/2} \tag{1.17}$$

where $\overline{U} = |\vec{U}_0|$, $\gamma = (1-\omega^2/N^2)$, $\delta_- = (1-f^2/\omega^2)$ and ξ is the angle between $\vec{K}_h$ and $\vec{U}_0$[12]. The height dependence of wave amplitude is defined by the conservation of total wave action [*Bretherton and Garrett,* 1968] where the wave action density is defined by $A = E_0/\omega$ for a gravity wave with energy density E_0. For more details of the ray tracing theory described here see, for example, *Lighthill* [1978] or *Andrews et al.* [1987].

Equation (1.17) is not strictly a Doppler-shifting equation since the vertical wavenumber is independent of the frame of observation. However, a height-variable vertical wavelength due to wind shear is often said to be Doppler-shifted [e.g., *Hines,* 1991b; *Eckermann,* 1995] since this follows from the Doppler shifting of wave frequency through the dispersion equation. Such changes will be referred to hereinafter as Doppler-shifting effects even though wave refraction might be considered as a more appropriate description.

[10] Significant changes to the polarization equations must be made in certain circumstances.
[11] This approximation is not necessary to obtain a ray-tracing solution but it does simplify such a solution.
[12] The use of the functions γ and δ_- follows the notation of *Fritts and VanZandt* [1993].

It is evident from (1.16) that while ω must be bound by f and N, the same need not be true of the observed frequency, $\sigma = c_h K_h$, in the ground-based frame of reference. Furthermore, a wave with an intrinsic frequency, ω, which lies between f and N, may be Doppler shifted such that it equals either f or N at some later height. Clearly, something significant must occur at these heights. It is understood, in the context of Liouville-Green theory [e.g., *Gossard and Hooke*, 1975; *Phillips*, 1977], that wave reflection occurs as ω approaches N while wave absorption occurs as ω approaches f. Both situations have been demonstrated in the laboratory by *Koop* [1981].

One experiment undertaken by *Koop* [1981] took place in a non-rotating ($f = 0$), stratified fluid with a steady background shear flow where constant-frequency gravity waves were generated by an oscillating cylinder at the bottom of the fluid. The observed wave disturbance is illustrated schematically in Figure 1.6 which has been adapted from the diagrams of *Koop* [1981] by *Murphy* [1990]. Photographic evidence of the results are given by *Koop* [1981] where lines of constant phase where made visible in the experiment by shadowgraph techniques. These exploit wave-induced variations of fluid refractive index to highlight lines of constant phase.

Waves were generated at constant frequency by the oscillating cylinder and propagated upward (phase progression occurred downward) at an angle to the horizontal defined by (1.13) where $f = 0$ in this case. Note in particular that waves with both positive and negative horizontal phase speeds, with respect to a stationary observer, were generated. Once the waves encountered the region of background wind shear their intrinsic frequencies were affected according (1.16), as were their propagation directions as a consequence. Waves propagating against the flow had their intrinsic frequencies shifted toward N and their group velocity vectors became orientated closer to the vertical. Waves propagating with the flow had their intrinsic frequencies shifted toward zero and their group velocity vectors became orientated closer to the horizontal. A turning level existed for waves moving against the flow at a height, z_t, which was defined by

$$\omega_i + \overline{U}(z = z_t)K_h = N \tag{1.18}$$

where ω_i was the intrinsic frequency of the waves immediately upon generation [*Koop*, 1981]. In contrast a so-called critical level was approached by waves moving with the flow at a height, z_c, [*Koop*, 1981] which was defined by

$$\overline{U}(z = z_c)K_h = \omega_i \tag{1.19}$$

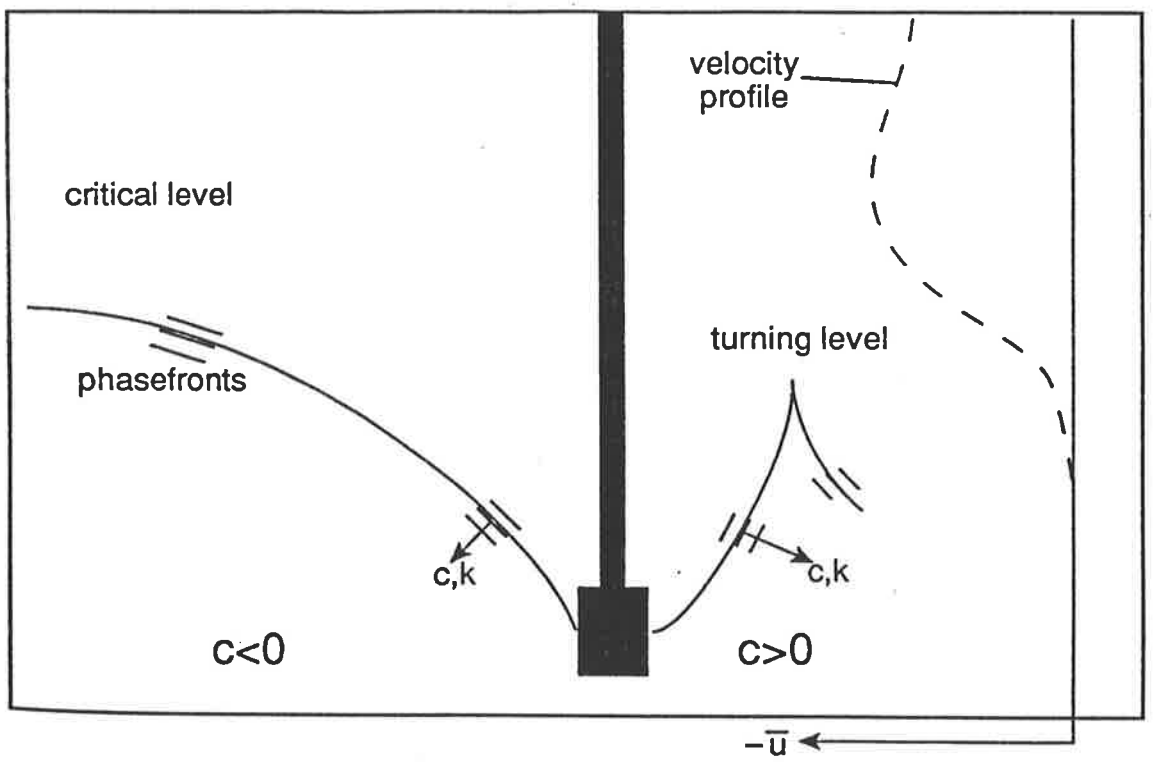

Figure 1.6: Schematic illustration of an experiment by *Koop* [1981] demonstrating gravity waves propagating into turning and critical levels due to background wind shear. This figure has been adapted from the diagrams of *Koop* [1981] by *Murphy* [1990].

The experimental results presented by *Koop* [1981] were in good agreement with linear gravity wave theory.

The critical level of an atmospheric gravity wave is defined as the height at which the ground-based horizontal phase speed of the wave and the basic-state horizontal wind, in the direction of $\vec{K}_h$, are equal. Mathematical treatment of wave characteristics near a critical level is difficult since the linearized wave equations become singular. Early studies by, for example, *Bretherton* [1966], *Booker and Bretherton* [1967] and *Jones* [1967] have explored this problem while experimental studies by *Koop* [1981] and *Thorpe* [1981] have provided some confirmation of the theoretical expectations. It is now understood that waves degenerate into turbulence as they approach their critical levels and that above this height (assuming upward wave propagation) the waves either cease to exist or, at the very least, are significantly reduced in amplitude. Waves with different horizontal phase velocities have different critical levels.

Critical level interactions are of particular importance to atmospheric gravity wave theory since they provide a mechanism for momentum transfer to the mean flow. Furthermore, such interactions may selectively remove particular waves from a vertically propagating spectrum of gravity waves, thus leaving a filtered and azimuthally anisotropic spectrum at greater heights. This selective filtering process is an important component of mesospheric wave breaking hypotheses [e.g., *Lindzen*, 1981]. In addition, critical level interactions are crucial to the Doppler-shifting wave saturation theory of *Hines* [1991b] which will be considered later.

Wave reflection processes, such as the process illustrated in Figure 1.6, have been used to explain the longevity of wave disturbances at or near ground level which are observed under certain meteorological conditions [e.g., *Uccellini and Koch*, 1987]. Waves are said to be ducted in these cases and behaviour of the atmosphere becomes analogous to that of an optical waveguide. The Australian Morning Glory [e.g., *Clarke*, 1972; *Crook*, 1988; *Clarke*, 1989] is one particularly spectacular example of this and has, as a consequence, been well studied. While possibly important in a meteorological context [e.g., *Uccellini*, 1975], ducted wave motions are not thought to be significant in influencing large scale atmospheric motions.

The total energy density (kinetic plus potential) per unit mass of a propagating gravity wave is defined by

$$E_0 = \frac{1}{2}\left[\overline{u'^2} + \overline{v'^2} + \overline{w'^2} + \frac{g^2\overline{\hat{T}'^2}}{N^2}\right] \tag{1.20}$$

where the overbar in each case represents a mean over one wavelength [e.g., *Gill*, 1982; *Sidi et al.*, 1988]. This definition follows naturally from the fluid-dynamical equations of motion under the Boussinesq approximation. The wave energy is equally partitioned between kinetic and potential energy components in most cases although this is not true for waves with intrinsic frequencies near f, the inertial frequency [e.g., *Gill*, 1982]. It is also the case that wave energy need not be conserved if the wave propagates within a medium that is time dependent and/or nonuniformly moving [*Bretherton and Garrett*, 1968]. Under Liouville-Green approximations, and also more generally, it is the total wave action that is conserved moving with a wave group[13] [*Bretherton and Garrett*, 1968; *Andrews and McIntyre*, 1978b]. Indeed, *Andrews and McIntyre* [1978b] have demonstrated that this is true without using linearization or Liouville-Green approximations. The conservation of total wave action appears to be

[13] *Bretherton and Garrett* [1968] point out that the principle of wave action conservation is analogous to similar conservation principles for simple oscillators which are subject to slow changes in their defining characteristics. They suggest the example of a pendulum which consists of a bob on a string of slowly varying length [*Bretherton and Garrett*, 1968].

a fundamental property of the wave motion.

Propagating gravity waves do not possess a uniquely defined non-zero momentum density since the net momentum flux of wave-induced particle motions is zero when averaged over one wave cycle [e.g., *McIntyre*, 1981]. Generally speaking, displaced air parcels are returned to their equilibrium or basic state positions once a wave packet has propagated through a particular region of the atmosphere. However, when wave amplitudes become large (for example when waves approach critical levels) material contours may be deformed irreversibly[14] due to various possible instabilities in the motion. Momentum is effectively transferred from the wave source to the atmosphere at the altitude of wave breaking without affecting the mean motions of the intermediate atmosphere. This picture of wave breaking has been proposed and is discussed by *McIntyre and Palmer* [1983, 1984, 1985], and the most appropriate analogy is with breaking surf on an ocean beach [e.g., *Andrews et al.*, 1987] as has been described earlier. It is worth noting that the momentum source may be external to the atmosphere as is the case for topographically generated gravity waves [*Fritts*, 1984].

Mathematically, the effect of wave breaking and momentum transfer is described by the so-called Reynolds stress tensor [e.g., *Bretherton*, 1969]. The divergence of this tensor appears as a force term in the equation of Eulerian-mean motion under linearization approximations and represents the forcing of the mean flow due to eddy motions. When wave forcing is non-zero the atmosphere must adjust in order that momentum, mass and thermal balance be maintained. Residual vertical and meridional circulations can be generated and have been used to explain the reversal of meridional temperature gradients near the mesopause. Adjustments to the mean flow must occur at time scales that are distinct from those of the waves themselves.

For gravity waves, the most dynamically important Reynolds stress term is thought to be the vertical flux of zonal momentum. This is defined by $\rho_0\overline{u'w'}$ for $f \ll \omega$ where the overbar represents a mean over one wave cycle. Other stress terms are potentially important also. The zonal mean flow acceleration, $\overline{u}_t$, that results from a vertical flux of zonal momentum is [e.g., *Fritts*, 1984]

$$\overline{u}_t = -\frac{1}{\rho_0}\frac{d}{dz}\left(\rho_0\overline{u'w'}\right) \tag{1.21}$$

and is zero in the absence of wave damping, critical levels and local thermal forcing [e.g., *Lindzen* 1990]. This latter point is a statement of the so-called Eliassen-Palm theorem[15]

[14] *McIntyre and Palmer* [1983, 1984] have suggested a general criterion for the onset of wave breaking which, they propose, occurs at the transition between reversible and irreversible deformation of material contours.

[15] Generalizations of the Eliassen-Palm theorem have been reported in more recent studies by *Andrews and*

which is named after the authors of an early theoretical study [*Eliassen and Palm*, 1961]. The measurement of wave momentum flux is an important goal of experimental research into atmospheric gravity wave motions. This point is stated in various review papers [e.g., *Fritts et al.*, 1984; *Andrews*, 1987].

Atmospheric gravity wave sources are potentially many and varied. Any physical mechanism capable of exciting air parcel oscillations with intrinsic frequencies between f and N is a potential source mechanism [e.g., *Lindzen*, 1971]. Proposed wave generation mechanisms include air flow over topography, squall lines, frontal systems, penetrative convection, wave-wave interactions, geostrophic adjustment and shear instability[16] [*Gossard and Hooke*, 1975]. Different source mechanisms are likely to be important over different regions of the Earth's surface. It is also understood that most atmospheric gravity waves are likely to be of tropospheric origin.

The theoretical framework presented in this section is by no means an exhaustive one. Rather, certain concepts have been described (properly referenced) which will be drawn upon in later chapters and are frequently drawn upon within the literature. A wide variety of texts treat these concepts in a rigorous manner [e.g., *Gossard and Hooke*, 1975; *Phillips*, 1977; *Lighthill*, 1978; *Gill*, 1982; *Andrews et al.*, 1987; *Lindzen*, 1990]. It should be noted that the theoretical framework presented here describes monochromatic waves whereas, in general, a broad spectrum of such waves exists. This point was recognized in some of the earliest studies of atmospheric gravity waves [see *Hines*, 1963] and has necessitated the more recent development of gravity wave spectral models. Such models are reviewed in Chapter 2.

Gravity waves are known to be present in oceans and a broad understanding of research in this cognate field is of relevance. In particular, some important publications of the atmospheric literature have already drawn from ideas first presented in an oceanic context. Notable examples include *VanZandt* [1982] who referenced the successful oceanic studies of *Garrett and Munk* [1972, 1975] and also *Dewan and Good* [1986] who referenced analogous concepts proposed by *Phillips* [1977]. More recently, the Doppler-shifting wave saturation theory proposed by *Hines* [1991b] appears to be an atmospheric analog of an oceanic study by *Allen and Joseph* [1989]. The ideas presented by these authors were arrived at independently and from different perspectives. The following section of this introductory chapter provides a brief review of the cognate research field of gravity waves in oceans.

McIntyre [1976, 1978a].

[16] Topographic forcing of gravity waves is the most well understood of the various proposed generation mechanisms and *Smith* [1979] provides an extensive review of theory and observations.

1.3 Gravity Waves and Oceans

Internal gravity waves are found everywhere in the ocean and are believed to account for a large fraction of ocean variability [*Müller et al.,* 1986]. As *Munk* [1981] puts it, no interior calm has ever been reported. These waves manifest themselves on the surface as alternate bands of roughened and smoothed water [*Hughes*, 1978] and are distinct from two-dimensional surface waves which cause significant variability at the ocean surface. Typical displacement amplitudes are of the order of 10 m while typical scales are of the order of kilometres and hours [e.g., *Munk*, 1981]. Internal oceanic gravity waves provide a link in the presumed energy cascade from large to small scales [*Müller et al.,* 1986].

The defining characteristics of gravity waves in oceans are significantly different to those of the Earth's atmosphere. Firstly, the ocean is more weakly stratified and typical values of the Väisälä-Brunt frequency are an order of magnitude smaller than those of the lower or middle atmospheres, especially within the deeper ocean [e.g., *Holloway and Müller*, 1990]. Secondly, the basic state currents of the ocean are weak in comparison to basic state winds in the atmosphere and so critical level filtering and basic-state wind shear effects may not be as important here [*VanZandt*, 1982]. Thirdly, the ocean is a bounded system which, on average, is only a few kilometres deep whereas the atmosphere is unbounded and of considerably larger vertical extent. Upwardly propagating gravity waves in the atmosphere must be dissipated[17] at some greater height by, for example, critical level interaction or by molecular diffusion above the turbopause. In contrast, gravity waves in oceans can suffer several reflections from (or near) the ocean surface and floor[18], are not dissipated through critical level interactions in any great number, and are therefore likely to be longer lived.

As in the atmosphere, there is a wide variety of possible oceanic gravity wave sources. Since the upper layer of the ocean contains the highest density of energy, this is where the most important wave sources are likely to be [*Thorpe*, 1975]. Proposed generation mechanisms at (or near) the ocean surface include travelling pressure fields, travelling buoyancy fluxes, travelling wind stress fields, corrugations at the base of the surface mixed layer and the non-linear interaction between surface waves of nearly equal frequency and wavenumber [e.g., *Thorpe*, 1975; *Garrett and Munk*, 1979]. Fluid motion over ocean floor topography is also a plausible generation mechanism while generation due to resonant wave-wave interactions may be important within the ocean interior [e.g., *Thorpe*, 1975; *Garrett and Munk*,

[17] Assuming that atypical reflection processes can be ignored.
[18] Since multiple reflections are possible, particular standing wave modes may exist.

1979]. In the latter case a cascade of gravity wave energy is envisaged.

Gravity wave fluctuations in oceans have been measured using several different observational techniques which measure field variables such as fluid velocity and temperature as functions horizontal distance, vertical distance and time [e.g., *Garrett and Munk*, 1979; *Munk*, 1981]. These have indicated that the spectral distributions of internal wave energy as functions of frequency, horizontal wavenumber and vertical wavenumber are approximately invariant[19], that is, they are approximately independent of geographic position and season. *Garrett and Munk* [1972, 1975] have proposed a "universal" model spectrum which describes this invariant spectral distribution of gravity waves in oceans (hereinafter referred to as the GM75 model). It is a heuristic model which assumes that the waves of the spectrum are linear, horizontally isotropic and satisfy gravity wave dispersion and polarization equations.

The "universal" nature of the observed fluctuation spectra could be indicative of some saturation (wave breaking) phenomenon [*Garrett and Munk*, 1975] or, as *Munk* [1981] puts it, the interior equivalent of whitecaps. Other possible explanations include constancy of forcing, nonlinear resonant cascades, or the effects of large-scale shear [*Wunsch*, 1975]. A consensus on the exact cause of the approximate invariance of gravity wave spectra has not yet been achieved [see the review by *Müller et al.*, 1986]. This is also true for the atmospheric case where observed spectra are found to display a similar "universal" character. It appears that recent work by *Allen and Joseph* [1989] and *Hines* [1991b] may be the start of converging ideas on this issue. It is also worth noting that wave source spectra are not expected to be invariant since many of the proposed generation mechanisms show significant variability with season and geographic location (e.g. wind stress at the ocean surface).

It has been pointed out by *Wunsch* [1975] that knowledge of where wave spectra differ from the GM75 model is important since this should be indicative of wave sources and sinks. However, a subsequent and extensive study by *Wunsch* [1976] showed that observed spectra from diverse deep-ocean regions of the western North Atlantic were in close agreement with the GM75 model. The largest deviation occurred near the Muir Seamount, indicating that topographic sources are likely to be significant, but the spectra rapidly recovered their equilibrium forms [*Wunsch*, 1976]. A further study by *Wunsch and Webb* [1979] has supported this conclusion. It appears that the equilibrium GM75 spectrum occupies a large portion

[19] A similar invariance of observed gravity wave spectra in the atmosphere is also found [*VanZandt*, 1982]. However, more recent experimental studies have indicated that significant deviations from the universal form can occur in certain situations. These may be related to the large basic-state winds and wind shears that can exist in the atmosphere [e.g., *Eckermann*, 1995] but are not present in oceans.

of the ocean [e.g., *Wunsch and Webb*, 1979] and therefore gravity waves are not likely to be as important in influencing the large scale motions as they are in the atmosphere. Wave energy sinks are most likely to occur near the ocean surface or floor, for example in submarine canyons [e.g., *Wunsch and Webb*, 1979]. However, more recent studies suggest that topographically generated gravity waves may have some role to play in forcing large-scale ocean currents such as the Antarctic Circumpolar Current [see the report of *Holloway and Müller*, 1990].

1.4 Summary

In summary, gravity waves are believed to play an important role in determining the large-scale circulation structures of the atmosphere. The exact nature of this role must be carefully studied if a comprehensive understanding of atmospheric dynamics is to be achieved. Gravity waves are also important in oceans and oceanic gravity wave characteristics have been extensively researched. This is a cognate research field and concepts that were first proposed in the oceanic literature have since been utilized in an atmospheric context. Nevertheless, the defining characteristics of gravity waves are significantly different in oceans, as are the important interactions between waves and the mean flow.

The basic theory of monochromatic gravity waves has been well documented for quite some time. Furthermore, the predicted characteristics of such waves have been verified experimentally under ideal laboratory conditions. However, a broad superposition of many waves is believed to exist in the atmosphere (and in oceans) and this has resulted in more recent studies which have focused upon their spectral characteristics. Indeed, the most recent attempts to parameterize the effects of gravity waves upon the mean flow have utilized a spectral description of the wave field. In the following chapter, a brief review of recent literature is presented and the research goals of this thesis are stated.

Chapter 2

Gravity Wave Spectra: A Brief Review

2.1 Introduction

Atmospheric gravity waves have been studied using radars, lidars, radiosondes and rocketsondes which measure field variables such as wind velocity and temperature. In the troposphere and lower stratosphere, wind-profiling radars supply the majority of information although instrumented aircraft and radiosondes also supply valuable contributions. However, at higher altitudes, radars, rocketsondes and more recently lidars are the prominent sources of information. These, together with measurements from other sources (airglow imagers for example), have supplied a growing body of knowledge about gravity waves in the lower and middle atmospheres. Yet, despite the large number of observations, the construction of a detailed climatology of gravity wave activity is hampered by the sparse geographic distribution of research radars and lidars, while rocketsonde observations of the middle atmosphere are largely confined to the northern hemisphere. In addition, there are certain theoretical questions that have not been answered by the current experimental information.

Initially, the debate was centered upon the relative importance of gravity waves and two-dimensional turbulence in forming the mesoscale fluctuations that were observed in the atmosphere. *Dewan* [1979] and *VanZandt* [1982] argued for a gravity wave interpretation, suggesting that mesoscale fluctuations are the direct result of a superposition of many gravity waves. However, *Gage* [1979], *Lilly* [1983], and *Gage and Nastrom* [1985] argued that two-dimensional turbulence is the main cause of mesoscale fluctuations. It is likely that both

waves and stratified turbulence are present in the atmosphere, but it is now widely accepted that gravity wave motions are dominant [e.g., *Vincent and Eckermann*, 1990]. The aim of this thesis is not so much to provide supporting evidence for the gravity wave interpretation, but rather to contribute additional information to a comprehensive climatology of atmospheric gravity wave activity.

More recently, the debate has focused upon the physical processes that are apparently acting to limit wave amplitude growth with height. A common feature of many experimental studies is the approximately invariant forms of the vertical wavenumber and frequency power spectra, despite the exponential decrease of density with height, and regardless of season and geographic location. This feature was first recognized by *VanZandt* [1982] who proposed, by analogy with the GM75 spectrum in oceans, that there exists a "universal" spectrum of atmospheric gravity waves based on published spectra from the troposphere and lower stratosphere. Several wave saturation theories have since been suggested [*Dewan and Good*, 1986; *Smith et al.*, 1987; *Weinstock*, 1990; *Hines*, 1991b; *Dewan*, 1994; *Gardner*, 1994; *Zhu*, 1994].

Each theory proposes a physical mechanism thought to be responsible for limiting wave amplitude growth and each predicts, approximately, the "saturated" vertical wavenumber power spectrum amplitudes that should be observed. However, due to theoretical uncertainties in the various proposed mechanisms, it has proven difficult to distinguish between them on the basis of spectral amplitude calculations alone. The question of which physical mechanism is acting to limit wave amplitudes is still, very much, an open one. It seems likely that the successful theory will best account for some of the more unexpected experimental results which show observed spectra that are significantly different from the "universal" form [*Hines*, 1993a].

VanZandt [1990, p. 113] has noted that it is useful to document, not only the mean wave field characteristics, but also the departures from the mean field since "much of the interesting physics and useful applications of the gravity wave field depend upon these departures". Clearly, this is an important experimental goal as was earlier noted by *Wunsch* [1975] for the cognate research field of oceanic physics. In the following section, a brief review of experimental studies is presented and the current knowledge regarding the mean spectrum is discussed. The review will concentrate upon the gravity wave power spectra determined from radar, lidar, radiosonde and rocketsonde observations.

2.2 Observations of Saturated Gravity Wave Power Spectra

The earliest studies of mesoscale fluctuation spectra utilized balloon measurements of the troposphere and lower stratosphere and radar measurements of the troposphere and mesosphere. Balloon measurements were best suited for the determination of vertical wavenumber power spectra, because of their poor temporal resolution, while radar measurements were best suited for the determination of frequency spectra, because of their poor vertical resolution. For example, *Endlich et al.* [1969] used several Jimsphere balloon soundings to determine the vertical wavenumber spectral distributions of horizontal winds between 500 m and approximately 16 km over Cape Kennedy, Florida. On the other hand, *Balsley and Carter* [1982] used MST radar measurements from Poker Flat, Alaska, to determine the frequency spectra of radial winds in the troposphere and mesosphere. Subsequent radar studies by, among others, *Vincent* [1984], *Balsley and Garello* [1985], *Smith et al.* [1985] and *Meek et al.* [1985] have provided additional information. *Dewan et al.* [1984] were able to determine vertical wavenumber spectra in the middle stratosphere by spectrally analyzing horizontal wind velocity fluctuations derived from rocket-laid vertical smoke trails.

A broad experimental description of the wave field, in the lower and middle atmospheres, was first presented by *VanZandt* [1985] who combined the published spectra from various sources. *VanZandt* [1985, Figure 4, p. 155] noted that the vertical wavenumber spectra of horizontal wind speed fluctuations had amplitudes that increased more slowly with altitude than did the frequency spectra of horizontal winds, at least for the vertical scales that were being considered. The vertical wavenumber spectra were of the form $F(m) \propto m^{-t}$, where t was somewhere between 2 and 3, while the ground-based frequency spectra were of the form $F(\sigma) \propto \sigma^{-p}$, where p was somewhere between 1.5 and 2.0. Observations of horizontal wavenumber spectra [from *Nastrom and Gage*, 1985] and frequency spectra of vertical velocity fluctuations [from, among others, *Ecklund et al.*, 1983] were also presented.

Figure 2.1 illustrates vertical wavenumber power spectra of horizontal wind fluctuations which have been compiled from some of the earlier publications by *Smith et al.* [1987]. The vertical wavenumber spectra from the troposphere, stratosphere and mesosphere are from *Endlich et al.* [1969], *Dewan et al.* [1984] and *Smith et al.* [1985], respectively, while the thermospheric spectrum was attributed to a private communication. Further details about these spectra, which span the altitude range from the troposphere to the lower thermosphere, are provided by *Smith et al.* [1987]. Note that the tropospheric and thermospheric spectra

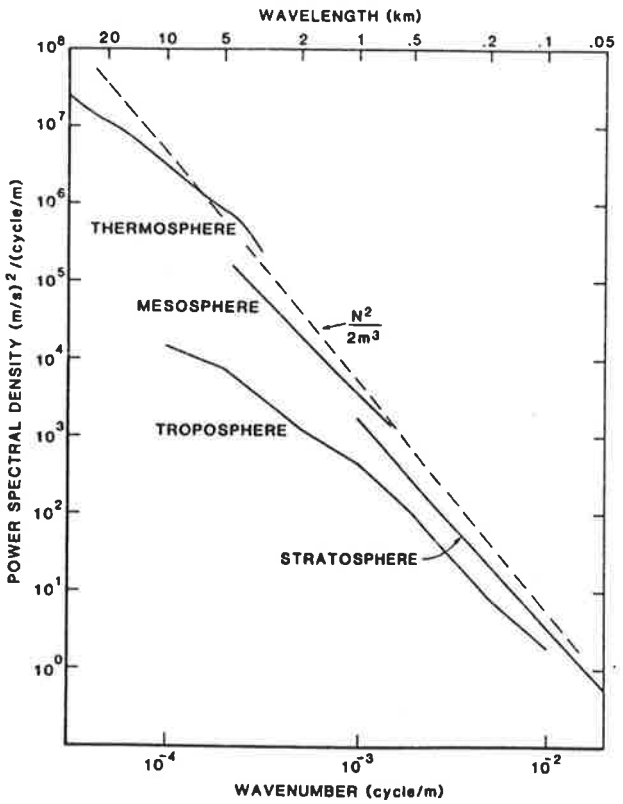

Figure 2.1: Vertical wavenumber power spectra of horizontal wind velocity fluctuations observed within different altitude regions of the atmosphere [from *Smith et al.*, 1987]. All spectra have been scaled to a common value of N^2.

have been scaled to a common value of N^2 [*Smith et al.*, 1987].

It is evident that the vertical wavenumber spectral amplitudes in Figure 2.1, at high vertical wavenumbers, are roughly consistent. They appear to be bounded by the dashed line in each case and this general observation led to the idea that the wave field might be saturated throughout the atmosphere, based on similar speculation concerning the spectrum of oceanic gravity waves. Subsequent theoretical studies have attempted to define spectral amplitude saturation limits for the gravity wave field. The dashed line in Figure 2.1 is based upon the limits proposed by *Dewan and Good* [1986].

Dewan and Good [1986] argued that the theoretical saturation limit at any given wavenumber is defined by the monochromatic wave amplitude needed for marginal convective or dynamic instability. They demonstrated that if individual wave packets saturate, and if the bandwidths of such packets are $\delta m \propto m$, then the spectral amplitude saturation limit is proportional to N^2/m^3 for horizontal wind velocity fluctuations. If it can be assumed that the

turbulence generated by the instability of waves is sufficient to maintain wave amplitudes at the threshold of instability, then the observed spectral amplitudes of saturated waves should display an N^2/m^3 dependence. This agrees well with the observed spectra presented in Figure 2.1. As noted above, the tropospheric and thermospheric spectra have been scaled to a common value of N^2, thus confirming the N^2 dependence of saturated spectral amplitudes. Similarly, the m^{-3} dependence is well approximated by the observed spectra at large vertical wavenumbers.

Of course, not all waves in the spectrum need to be saturated. Given the m^{-3} dependence of the theoretical saturation limit, it would be reasonable to expect that there exists a high-wavenumber saturated region of the spectrum and a low-wavenumber unsaturated region. The amplitudes of waves in the unsaturated region are likely to depend on either the source spectrum of waves or on nonlinear wave-wave interactions [*Dewan and Good*, 1986]. Note that each spectrum of Figure 2.1 displays saturated amplitudes, approximately, with the exception of the low-wavenumber region of the tropospheric spectrum.

Smith et al. [1987] extended the theory of *Dewan and Good* [1986] to accommodate the effects of a random superposition of unsaturated gravity waves. They argued that the fluctuations resulting from a superposition of many waves with less than saturation amplitudes can contain convectively unstable lapse rates at some heights [*Smith et al.*, 1987]. Thus the observed spectra should have saturation amplitudes that are smaller than those inferred by assuming that individual wave packets saturate in isolation. *Smith et al.* [1987] assumed that the vertical wavenumber power spectrum was of the form,

$$F(\mu) \propto \frac{\mu^s}{1+\mu^{s+t}} \tag{2.1}$$

where $\mu = m/m_*$, m_* is a constant, $s = 0$ and $t = 3$. A theoretical saturation limit was derived by integrating the contributions to the total saturated variance which was defined by the criterion for the onset of convective instability [e.g., *Fritts*, 1984]. This theoretical saturation limit, for $m \gg m_*$ was found to be,

$$E_{U'}(m) \approx \frac{N^2}{6m^3} \tag{2.2}$$

where $E_{U'}(m)$ is the vertical wavenumber power spectral density of horizontal wind velocity fluctuations and m_* is called the characteristic vertical wavenumber[1] [*Smith et al.*, 1987].

[1]In the derivation of (2.2), it was assumed that the intrinsic frequency spectrum of gravity waves, $B(\omega)$, was given by $B(\omega) \propto \omega^{-p}$ where $p = 5/3$. The m^{-3} dependence was also assumed based on the dimensional analysis of *Dewan and Good* [1986].

Note that $E_{U'}(m)$ is strictly the sum of the vertical wavenumber power spectra of zonal and meridional wind velocity fluctuations.

The model spectral form, proposed by *Smith et al.* [1987] for the vertical wavenumber power spectrum of horizontal wind velocity fluctuations, is divided into two regions which are separated by the characteristic vertical wavenumber, m_*. At high vertical wavenumbers ($m > m_*$), the power spectral densities are constrained by (2.2). However, at low vertical wavenumbers ($m < m_*$), the waves are proposed to be unsaturated and free to increase their amplitudes as the spectrum propagates vertically into regions of less dense air. Thus it is the growth at small vertical wavenumbers that accounts for the increase in total wave energy [*Smith et al.*, 1987]. This increase is known to occur from the comparisons of tropospheric and mesospheric frequency spectra [e.g., *Balsley and Carter*, 1982] and the characteristic vertical wavenumber is anticipated to decrease with altitude as more and more waves approach their monochromatic amplitude limits.

Figure 2.2 illustrates the model gravity wave power spectrum, as a function of vertical wavenumber, that was first introduced by *VanZandt and Fritts* [1989]. This is called the modified-Desaubies spectrum and is defined[2] by (2.1) with $s = 1$ and $t = 3$. It has been updated from the model spectrum used by *Smith et al.* [1987] since this earlier model ($s = 0$ and $t = 3$) leads to unrealistic vertical fluxes of wave energy [*VanZandt and Fritts*, 1989]. The amplitudes and characteristic vertical wavenumbers of the illustrated spectra were chosen to be representative of the observed vertical wavenumber power spectra of horizontal wind velocity fluctuations in the troposphere, stratosphere and mesosphere. Figure 2.2 highlights the proposed increase of spectral amplitudes at low vertical wavenumbers together with the proposed decrease of the characteristic vertical wavenumber, with increasing altitude. In fact the variation of m_* with altitude is controlled by the variation of wave variance [*Smith et al.*, 1987]. Note that the spectra from different altitude regions should be viewed as having been scaled to a common value of N^2.

Recent experimental studies using radars and radiosondes [*Fritts et al.*, 1988; *Tsuda et al.*, 1989; *Tsuda et al.*, 1991] have provided additional evidence in support of the theoretical saturation limits proposed by *Smith et al.* [1987]. Perhaps the most compelling evidence was provided by *Tsuda et al.* [1989] who analyzed radar winds observed in the troposphere, lower stratosphere and mesosphere over the MU radar in Japan. Their data were observed

[2]The choice of the parameter s is arbitrary since little is known about the low-wavenumber region of the spectrum.

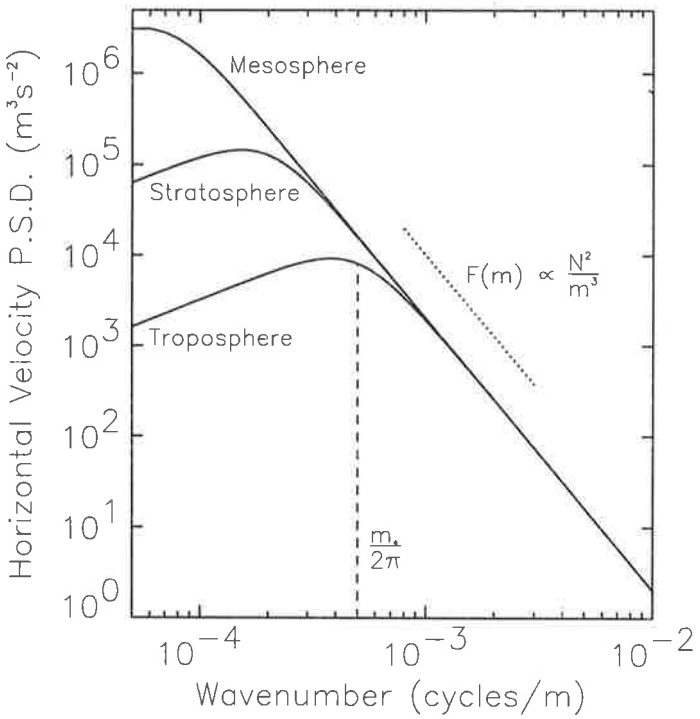

Figure 2.2: The modified-Desaubies spectrum of horizontal wind velocity fluctuations in different regions of the atmosphere [after *Smith et al.*, 1987].

simultaneously in each atmospheric region using the same radar technique and all data were analyzed using very similar methods. Reasonable agreement was found[3], in all three regions of the atmosphere, with the theoretical saturation limits proposed by *Smith et al.* [1987].

Very recently, research lidars have been used to probe the temperature fluctuation fields of the stratosphere and mesosphere including those regions of the upper stratosphere and lower mesosphere, between approximately 30 and 60 km, that cannot be probed using present radar technology. Indeed, *Tsuda et al.* [1989], using the MU radar in Japan, were unable to determine the vertical wavenumber power spectra of horizontal winds between heights of 21 and 65 km. *Dewan et al.* [1984] analyzed high-vertical-resolution rocketsonde measurements between approximately 20 and 40 km, but their results were based on only a few soundings. In contrast, lidars can provide valuable climatological information about the mesoscale structure of temperature fluctuations induced by gravity waves throughout the stratosphere and mesosphere. Note that the theoretical amplitude limits of horizontal

[3]It must be noted that *Tsuda et al.* [1989] compared the spectra of zonal and meridional wind velocity, rather than the spectrum of total horizontal wind velocity, with the proposed saturation limits. Thus the agreement is to within only a factor of approximately 2. Furthermore, the tropospheric component spectra appeared to be more energetic, in comparison with the theoretical saturation limits, than did the spectra from the lower stratosphere and mesosphere.

wind velocity fluctuations are related to those of normalized temperature fluctuations by the polarization equations of gravity waves. It is appropriate to consider power spectra of normalized temperature fluctuations, rather than of temperature fluctuations, since the saturation limits for these spectra are stationary if N is constant.

The first results using lidars [e.g., *Wilson et al.,* 1991; *Beatty et al.,* 1992; *Senft et al.,* 1993] indicate that the vertical wavenumber power spectra of normalized temperature fluctuations in the upper stratosphere and lower mesosphere have amplitudes, at high vertical wavenumbers, that are significantly smaller than the saturation limits proposed by *Smith et al.* [1987]. However, the mesospheric spectra determined above approximately 60 km do display saturated amplitudes in accordance with the radar results at comparable heights. These lidar results are of particular interest since they challenge the notion that the wave field is saturated throughout the middle atmosphere. Nevertheless, recent theoretical studies by *Kuo and Lue* [1994] and *Eckermann* [1995] have attempted to explain the lidar spectra within the context of the gravity wave saturation theories. These studies are discussed in section 4.6.

The observations that have been reviewed in this section provide a broad understanding of the nature and shape of the vertical wavenumber and frequency power spectra of mesoscale fluctuations in the middle atmosphere. Generally speaking, the vertical wavenumber power spectra of horizontal winds and normalized temperatures are represented by the modified-Desaubies form while the frequency spectra are represented by $F(\sigma) \propto \sigma^{-p}$ where p is between 1.5 and 2.0. It is now accepted that these spectra are caused by gravity waves and a gravity wave interpretation is assumed, and in some places reinforced, throughout this thesis. Note, however, that the review of observations presented here is not an exhaustive one. In particular, there have been no discussions regarding the frequency spectra of vertical winds or the horizontal wavenumber spectra of horizontal winds and temperatures. These important spectral distributions are described elsewhere [e.g., *Nastrom and Gage*, 1985; *Ecklund et al.,* 1986] and are broadly explained within a gravity wave framework [*Fritts and VanZandt,* 1987; *Gardner et al.,* 1993a].

In the following section, the recent attempts to explain the observed gravity wave power spectra are briefly reviewed. These include the simple models proposed by *Dewan and Good* [1986] and *Smith et al.* [1987] which have already been discussed. In addition, there have been two recent attempts to parameterize the effects of an upward propagating spectrum of gravity waves on the mean flow. Such parameterization schemes are of importance since they link the

research of theorists, who model large-scale motions in the lower and middle atmospheres, and experimentalists, who use convenient analytical tools including power spectrum analysis. These two proposed schemes will be discussed in the next section.

2.3 The Spectral Theory of Gravity Waves

Several authors have put forward theoretical explanations of the observed vertical wavenumber power spectra of mesoscale fluctuations in the middle atmosphere. According to *Hines* [1993a], these explanations can be divided into three main theories. The first is based on the idea that spectral amplitudes, at high vertical wavenumbers, are determined by the linear instability of either individual waves or the superposed wave field as a whole [*Dewan and Good*, 1986; *Smith et al.*, 1987]. The second suggests that the observed spectra are caused by wave dissipation due to off-resonant wave-wave interactions [*Weinstock*, 1990] while the third argues that individual waves suffer Doppler-spreading due to the fluctuating winds of the entire spectrum [*Hines*, 1991b]. Each theory predicts that the observed spectral amplitudes of horizontal winds, at high vertical wavenumbers, should be at least approximately proportional to N^2/m^3 which is taken to be the mean observed form based on earlier compilations of mesoscale fluctuation spectra. At present, these competing theories are on equal terms in their correspondence with observations [*Hines*, 1993a][4].

Weinstock [1990] argued that the contribution of all waves in a spectrum to the dissipation of a given wave must be important in determining the universal form of the observed vertical wavenumber power spectra. By assuming that wave dissipation was due to off-resonant wave-wave interactions only, and that this dissipation could be approximately accounted for using a diffusion term, *Weinstock* [1990] solved the wave equation for the saturated portion of the spectrum. The saturated spectrum was defined to be invariant with height and, using this definition, the vertical wavenumber power spectrum of saturated gravity waves was shown to be proportional to N^2/m^3 in accordance with observations and the earlier theories based on linear instability criteria. Thus dissipation by nonlinear wave-wave interactions may explain the observed spectral form.

[4] In fact *Hines* [1993a] argues that the recent lidar results from the stratopause region are compatible with his theory of Doppler spreading and incompatible with the other two competing theories. However, this compatibility relies on assumptions about the source spectrum of waves that have no firm theoretical basis. The study by *Hines* [1993a] highlights the extent of wave spectrum variability that is allowed for under the Doppler-spreading model, rather than the success of a critical prediction of the model. Indeed, *Hines* [1993a] acknowledges that there may be some debate about the validity of the recent lidar data.

A different theory was put forward by *Hines* [1991b,c] although this was based on the same notion that the individual waves of the spectrum must interact nonlinearly with the superposed wave field as a whole. However, *Hines* [1991b] argued that individual waves are smeared throughout vertical wavenumber space as a consequence of Doppler shifting caused by the random winds of the entire spectrum and that waves with large vertical wavenumbers are more susceptible to Doppler shifting than waves with small vertical wavenumbers[5]. Thus gravity waves with large vertical wavenumbers are much more likely to encounter critical levels and to be removed from the spectrum. This obliteration of some waves, together with the smearing of the remaining waves, was demonstrated to result in a horizontal wind velocity spectrum that was proportional to approximately N^2/m^3 at vertical wavenumbers[6] larger than $m_C \approx N/(2\mathcal{U}_{\mathrm{RMS}})$ where $\mathcal{U}_{\mathrm{RMS}}$ is the root-mean-square of the horizontal wind velocity fluctuations. It was further demonstrated that as horizontal wind velocity variance increases with height, more waves become obliterated and the low-wavenumber source-dependent region of the spectrum gradually erodes (m_C decreases). Given that as individual waves approach their critical levels they degenerate into turbulence (at some vertical wavenumber $m_M \gg m_C$), a more or less regular, but not continuous, production of turbulence was envisaged for an upward propagating spectrum of waves. Note that this turbulent dissipation of wave energy is very different from the dissipation envisaged by *Weinstock* [1990] since it is the large-scale waves that control the dissipation of the small or medium-scale waves. In contrast, the dissipation of a given wave due to off-resonant wave-wave interactions was supposed to occur at the hands of other waves with smaller vertical scales [*Weinstock*, 1990][7].

More recently, some additional explanations of the observed vertical wavenumber power spectra have been put forward [*Dewan*, 1994; *Zhu*, 1994; *Gardner*, 1994]. These are either extensions to, or reworkings of, some of the earlier theories. For example, *Zhu* [1994] has extended the theory of *Weinstock* [1990] by including the effects of dissipation due to scale-dependent radiative damping which was neglected in the earlier study as a first approximation. Similarly, *Dewan* [1994] has extended the linear instability theory by assuming

[5]Gravity waves with small vertical wavenumbers have small horizontal phase speeds (for zero mean winds) that are comparable to the root-mean-square of the random horizontal winds of the superposed wave field. This is evident from (1.4) with $f \ll \omega \ll N$.

[6]Gravity waves of the source spectrum with m near m_C were assumed to be quickly obliterated by critical level interaction. Thus the high-wavenumber region of the observed spectrum was assumed to be caused by the smearing of waves with m near m_C.

[7]*Hines* [1993b] acknowledges that both Doppler spreading and dissipation due to off-resonant wave-wave interaction may occur simultaneously. Indeed, various aspects of Hines' Doppler-spreading theory and Weinstock's nonlinear diffusion approach have been combined in a recent theoretical study by *Medvedev and Klaassen* [1995].

that the observed spectra are defined by simultaneous saturation and cascade properties. On the other hand, *Gardner* [1994] has proposed a new model, similar to Weinstock's model, in which wave amplitudes are assumed to be controlled by nonlinear wave-wave interactions and to be reasonably modelled as a diffusion process. However, unlike in Weinstock's formulation, *Gardner* [1994] has modelled the effects of diffusion as a filtering process. All three theories predict that the observed vertical wavenumber power spectra of horizontal wind velocity fluctuations can be proportional to N^2/m^3 at high vertical wavenumbers. Yet the theories proposed by *Gardner* [1994] and *Zhu* [1994] do allow for some variability of the spectral form depending on various assumptions including assumptions regarding the source spectrum of gravity waves.

At present, there is no consensus about which physical mechanism is causing the observed invariance of gravity wave power spectra at high vertical wavenumbers. Indeed, the issue appears to be a contentious one [e.g., *Hines*, 1991a]. Each theory predicts, under favourable conditions and assumptions, an N^2/m^3 dependence which has been established[8] as the typical observed form of horizontal wind velocity spectra as a function of vertical wavenumber. Yet there are no critical predictions of the various theories that might reasonably be used to distinguish between them on the basis of comparison with observed spectra. Nevertheless, it must be important to document departures from the typical form, if such departures exist in the lower and middle atmospheres[9], since ultimately the successful theory must account for all observations obtained from the various different measurement systems including both radars and lidars. *Hines* [1993a], *Zhu* [1994] and *Gardner* [1994] have already attempted to explain some of these departures[10].

Despite the lack of consensus, some recent studies have attempted to parameterize the effects of gravity waves on the mean flow based on earlier theories of wave field saturation. For example, *Fritts and Lu* [1993] and *Lu and Fritts* [1993] have developed a parameterization scheme which assumes various constraints on the growth of wave energy that are based largely on the linear instability theory of gravity wave saturation. This scheme uses a spectral formulation devised by *Fritts and VanZandt* [1993] which is in good agreement with observed spectra and which satisfies gravity wave dispersion and polarization equations under the Boussinesq approximation (allowing for nonhydrostatic and rotational effects). On the other

[8] In fact a recent interpretation of radiosonde observations by *Nastrom et al.* [1996] has even questioned this point.

[9] The observed spectra are likely to depart from the typical form, near wave sources at least.

[10] Additional explanations have been put forward by *Kuo and Lue* [1994] and *Eckermann* [1995] which may be independent of the physical mechanism that is responsible for the saturation of the gravity wave field.

hand, *Hines* [1996a,b] has devised a different parameterization scheme which is based on the Doppler-spreading theory of the saturated gravity wave field. Both schemes represent an important step forward towards the goal of understanding and modelling the effects of a broad spectrum of gravity waves on the large scale structures of the atmosphere.

Fritts and VanZandt [1993] presented a model three-dimensional gravity wave power spectrum which makes use of functional forms of the one-dimensional vertical wavenumber and frequency power spectra that are in good agreement with experimental findings. They assumed a total energy spectrum that is separable in vertical wavenumber, m, intrinsic frequency, ω, and azimuthal direction of propagation, ϕ, and is given by

$$E(\mu,\omega,\phi) = E_0 A(\mu) B(\omega) \Phi(\phi) \tag{2.3}$$

where

$$A(\mu) = A_0 \frac{\mu^s}{1+\mu^{s+t}} \tag{2.4}$$

$$B(\omega) = B_0 \omega^{-p} \tag{2.5}$$

and where $\mu = m/m_*$, $m = 2\pi/\lambda_z$, λ_z is the vertical wavelength, m_* is the characteristic vertical wavenumber (in units of radians per metre), E_0 is the total gravity wave energy per unit mass (energy density) and the parameters s, t, and p are to be determined by comparison with the slopes of observed power spectra. The functions $A(\mu)$, $B(\omega)$ and $\Phi(\phi)$ are defined to be normalized to unity when integrated over all possible μ, ω and ϕ, respectively. These normalization constraints in turn define the constants A_0 and B_0 as described by *Fritts and VanZandt* [1993].

The model spectral distributions of u', v', w' and $\hat{T}'$ are related to the model energy spectrum according to the polarization equations of gravity waves. These distributions are given by

$$E_{u'}(\mu,\omega,\phi) = E_0 A(\mu) B(\omega) \Phi(\phi) \left[\cos^2\phi + \frac{f^2}{\omega^2}\sin^2\phi\right] \gamma(\omega) \tag{2.6}$$

$$E_{v'}(\mu,\omega,\phi) = E_0 A(\mu) B(\omega) \Phi(\phi) \left[\sin^2\phi + \frac{f^2}{\omega^2}\cos^2\phi\right] \gamma(\omega) \tag{2.7}$$

$$\begin{aligned} E_{U'}(\mu,\omega,\phi) &= E_{u'}(\mu,\omega,\phi) + E_{v'}(\mu,\omega,\phi) \\ &= E_0 A(\mu) B(\omega) \Phi(\phi) \delta_+(\omega) \gamma(\omega) \end{aligned} \tag{2.8}$$

$$E_{w'}(\mu,\omega,\phi) = \frac{\omega^2}{N^2} E_0 A(\mu) B(\omega) \Phi(\phi) \delta_-(\omega) \tag{2.9}$$

$$E_{\hat{T}'}(\mu,\omega,\phi) = \frac{N^2}{g^2} E_0 A(\mu) B(\omega) \Phi(\phi) \delta_-(\omega) \tag{2.10}$$

where E represents power spectral density, $\gamma(\omega) = (1-\omega^2/N^2)$, $\delta_{\pm}(\omega) = (1 \pm f^2/\omega^2)$, $\delta_{-}(N)$ is assumed to be unity, and E_0 is the total energy density defined by (1.20) [*Fritts and VanZandt*, 1993]. Each equation follows from (1.8), (1.9), (1.10) and (1.20) after lengthy but straightforward manipulation[11], as discussed by *Sidi et al.* [1988]. Note, however, that (2.10) was chosen to replace equation (8) from *Fritts and VanZandt* [1993] since normalized temperature fluctuations, rather than vertical displacement fluctuations, are analyzed in the present study. The normalized temperature and vertical displacement fluctuations of monochromatic gravity waves are related by

$$\hat{T}' = -\frac{N^2}{g}\,\zeta' \tag{2.11}$$

where $\zeta' = -i\omega w'$ is the vertical displacement fluctuation and where air parcel displacements are assumed to occur adiabatically [e.g., *Gill*, 1982; *Sidi et al.*, 1988].

Using equations (2.3) to (2.9), *Fritts and VanZandt* [1993] were able to determine the important spectral distributions of the vertical fluxes of zonal and meridional momentum (per unit mass). These were integrated over all possible values of μ, ω and ϕ in order to define the net vertical fluxes of zonal and meridional momentum as functions of only a few parameters that might be determined experimentally. By choosing reasonable values[12] for the parameters p, f and N, the net momentum fluxes were shown to be given by

$$(F_{P_x}, F_{P_y}) \approx (b_x, b_y)\, E_0/22 \tag{2.12}$$

where

$$(b_x, b_y) = \int_0^{2\pi} \Phi(\phi)\,(\cos\phi, \sin\phi)\; d\phi \tag{2.13}$$

and where F_{P_x} and F_{P_y} denote the net vertical fluxes of zonal and meridional momentum (per unit mass), respectively [*Fritts and VanZandt*, 1993]. Thus the momentum flux at any given height is determined by the total energy of the wave field and the parameters b_x and b_y which are defined by the degree of wave field anisotropy, assuming that f and N are known and that p is reasonably defined from experimental evidence.

The spectral formulation presented by *Fritts and VanZandt* [1993], and summarized briefly here, provides a basis for a gravity wave parameterization scheme which has been tested in steady [*Fritts and Lu*, 1993] and transient [*Lu and Fritts*, 1993] flow conditions. However, this formulation also highlights some important aspects of the wave field that

[11] Recall that $\phi = \arctan(l/k)$.

[12] The parameters p and f/N were chosen to be 5/3 and 1/200, respectively.

might be determined experimentally. Clearly, the most important parameters that must be estimated, aside from the spectral parameters s, t and p, are the total wave energy density and the anisotropy parameters, b_x and b_y. Such measurements can either provide initial conditions for atmospheric models at low altitudes or constraints for them at higher altitudes [*Fritts and Lu*, 1993; *Lu and Fritts*, 1993]. Of course experimentalists must also seek to verify the various assumptions of these models. Is the form of the vertical wavenumber power spectrum independent of altitude? How does the total gravity wave energy respond to changes in N, $\overline{\rho}$ and $\overline{U}$? Is the wave field truly separable in m, ω and ϕ? Answers to these questions and estimates of E_0, b_x and b_y are of importance if a comprehensive understanding of the effects of a gravity wave spectrum on the mean flow is to be achieved.

The more recent parameterization scheme proposed by *Hines* [1996a,b] is based on a different understanding of the manner in which the gravity wave field is constrained. Nevertheless, this new spectral formulation assumes that the wave field is separable in K_h and m, and that the waves of the spectrum obey simplified dispersion and polarization equations. However, it is the horizontal wind velocity variance and its azimuthal distribution that is fundamental to the new approach. Momentum deposition occurs when a gravity wave propagating in a given azimuth is obliterated due to severe Doppler spreading caused by the total wind variance in that azimuth[13]. The azimuthal distribution of the remaining waves defines the net vertical flux of horizontal momentum while the altitude variations of momentum flux define the inferred mean flow accelerations. *Mengel et al.* [1995] have already successfully modelled the mean zonal winds and temperatures of the middle atmosphere by using this approach, including the quasi-biennial oscillation of the equatorial lower stratosphere and the semi-annual oscillations of the equatorial upper stratosphere and mesosphere[14].

The further testing and refining of the parameterization schemes proposed by *Fritts and Lu* [1993] and *Hines* [1996a,b] promises to be a fertile field of scientific research. Experimental studies should also contribute by providing the initial conditions and constraints for atmospheric models. It is worth noting that, despite fundamental theoretical differences, both parameterization schemes begin with similar formulations. The wave field is assumed to be separable, at least to some extent, and the waves of the spectrum obey simplified dispersion and polarization equations, as defined by, for example, equations (2.6) to (2.10) although the model spectral forms may differ. In addition, the degree of wave field anisotropy is of

[13] The background winds can act to either accentuate or halt the dissipation of waves in a given azimuth.

[14] *Mengel et al.* [1995] conclude that gravity waves may significantly contribute to both the quasi-biennial oscillation and the semi-annual oscillations.

crucial importance to both schemes and is parameterized in some way. Clearly, experimental observations of the extent of wave field anisotropy is very important in the absence of direct measurements of momentum fluxes at all heights.

2.4 Summary and Research Goals

The theoretical study of atmospheric gravity waves has progressed to the stage of furnishing detailed parameterization schemes which describe the influence of a broad spectrum of gravity waves on the mean flow and which depend on only a few parameters. These schemes are based on, and constrained by, a large number of gravity wave observations in the lower and middle atmospheres. Yet there still exists considerable debate about which physical process is acting to limit the growth of gravity wave energy with increasing altitude. Furthermore, the current experimental description of the wave field is based largely on observations from only a small number of locations which are mostly in the northern hemisphere. Consequently, a detailed climatology of gravity wave activity, which describes the seasonal and geographic variability in both hemispheres, has not yet been compiled. Such a compilation is vital if the effects of gravity waves are to be fully understood and modelled.

The research goals of this thesis are twofold. The first broad goal is to contribute information to a detailed climatology of gravity wave activity in the southern hemisphere. In particular, the aim is to document departures from the mean spectral form, if such departures exist, and to provide evidence that might be used to distinguish between the various competing saturation theories. The second broad goal is to provide climatological information, using conventional data that is readily available, which might be of direct relevance to the recent gravity wave parameterization schemes. Such information should include estimates of the total gravity wave energy density (or the horizontal wind velocity variance) and the degree of wave field anisotropy. The data to be considered are conventional radiosonde (meteorological balloon) measurements which are obtained on a daily basis by many meteorological services around the world. This study is the first to attempt gravity wave analyses of high-vertical-resolution radiosonde data from a network of stations in the southern hemisphere. Conventional radiosondes can measure atmospheric temperature, and in some cases horizontal wind velocity, up to maximum altitudes of approximately 30 km.

Strictly speaking, measurements of three component wind velocity and temperature are required to define completely the total energy per unit mass, E_0. However, it is possible to

estimate this parameter from temperature measurements alone using the appropriate gravity wave polarization equation and the three-dimensional model spectrum of *Fritts and VanZandt* [1993]. By integrating (2.10) on both sides with respect to μ, ω, and ϕ using (2.3), (2.4), (2.5) and the normalization condition for $\Phi(\phi)$, namely, $\int_0^{2\pi} \Phi(\phi)d\phi = 1$, the following equation is derived relating the energy density E_0 to the total normalized temperature variance,

$$E_0 = \frac{g^2}{N^2} \frac{1}{B_0 C_{In}} \overline{\hat{T}'^2} \tag{2.14}$$

where

$$C_{In} = \frac{f^{1-p}}{1-\tilde{f}^2} \left[\frac{1-\tilde{f}^{p-1}}{p-1} - \frac{1-\tilde{f}^{p+1}}{p+1} \right] \tag{2.15}$$

and where $\tilde{f} = f/N$ and p is the slope of the one-dimensional intrinsic frequency spectrum[15]. The total normalized temperature variance is easily determined from radiosonde measurements and (2.14) will be used in a later chapter to estimate E_0. Note that the value of p most commonly used in the literature [e.g., *Smith et al.*, 1987; *Weinstock*, 1990] is 5/3. This value is based on the observed spectral distributions of horizontal wind velocity and temperature.

The vertical wavenumber power spectra that are presented in this thesis will be compared against the theoretical saturation limits proposed by *Smith et al.* [1987]. Since the various competing theories usually provide approximate estimates of the saturated spectral amplitudes at high vertical wavenumbers, and since these estimates are very similar given their uncertainty, the theoretical saturation limits proposed by *Smith et al.* [1987] will be used as a convenient reference only. However, (2.2) describes the saturation limits of the one-dimensional vertical wavenumber power spectrum of total horizontal wind velocity whereas temperature measurements are mainly considered here. The theoretical saturation limits of normalized temperature fluctuations due to *Smith et al.* [1987], as a function of inverse vertical wavelength, are

$$E_{\hat{T}'}(1/\lambda_z) \approx \frac{N^4}{6g^2} \frac{1}{p} \frac{1}{(2\pi)^2} \frac{1}{(1/\lambda_z)^3} \tag{2.16}$$

where λ_z is vertical wavelength and $E_{\hat{T}'}$ is normalized temperature power spectral density. This follows from (2.2) and the appropriate polarization equation if it can be assumed that the one-dimensional frequency spectrum is given by $B(\omega) \propto \omega^{-p}$ [see *Fritts et al.*, 1988]. Note that, although p appears in (2.16), this saturation limit is actually independent of p since the constant of proportionality in (2.2) was determined by assuming that $p = 5/3$. Thus

[15] In obtaining (2.14), three assumptions have been made: first, the three-dimensional energy spectrum is assumed to be separable in m, ω, and ϕ; second, the one-dimensional frequency spectrum is assumed to be of the form $B(\omega) \propto \omega^{-p}$; third, the Boussinesq approximation (allowing for nonhydrostatic and rotational effects) is assumed to be valid.

the saturated normalized temperature variance due to *Smith et al.* [1987] is independent of the intrinsic frequency distribution of gravity waves whereas the saturated horizontal wind velocity variance depends upon the proportion of wave variance with intrinsic frequencies near f, the inertial frequency.

A description of the radiosonde data and analysis techniques that are used in this thesis is presented in the following chapter. Some of these analysis techniques are based on several studies of meteorological rocket data [*Hirota*, 1984; *Eckermann and Vincent*, 1989; *Hamilton*, 1991; *Eckermann et al.*, 1995] which were not reviewed in section 2.2 since the data considered were of such coarse resolution (of the order of 1 km) that the saturated regions of the gravity wave power spectra were not adequately resolved. Nevertheless, the analysis of meteorological rocket data has provided valuable climatological information about the most energetic gravity waves in the stratosphere and lower mesosphere. These analyses will be discussed later when appropriate.

Chapter 3

Radiosonde Data and Analysis Techniques

3.1 Introduction

The experimental data that were utilized in this thesis comprise radiosonde soundings from 22 stations which cover the Australian sector of the southern hemisphere. All data were supplied by the Australian Bureau of Meteorology. The locations of the various stations are illustrated in Figures 3.1 and 3.2 while further details, including the time intervals over which data were available, are provided in Table 3.1. The purpose of choosing these particular stations was to provide sufficient geographic coverage so as to allow a climatology of wave activity to be obtained. In particular radiosonde stations were chosen so that observations from a range of different longitudes could be combined into relatively narrow latitude bands. This allows a climatology to be built up which is not biased by possible localized source effects. A further 13 radiosonde stations are operated by the Australian Bureau of Meteorology but were not used in the present study.

Meteorologists often report radiosonde measurements at standard pressure levels (which are typically separated by between 1 and 3 km) even though the raw measurements are obtained at much greater vertical resolution. Therefore standard level measurements will not resolve the most dominant gravity waves of the troposphere and lower stratosphere as reported by, for example, *Fritts and Chou* [1987] and *Fritts et al.* [1988]. Recently, however, the Australian Bureau of Meteorology began routinely recording and archiving the high resolution measurements of radiosondes. These data are the subject of investigation in this

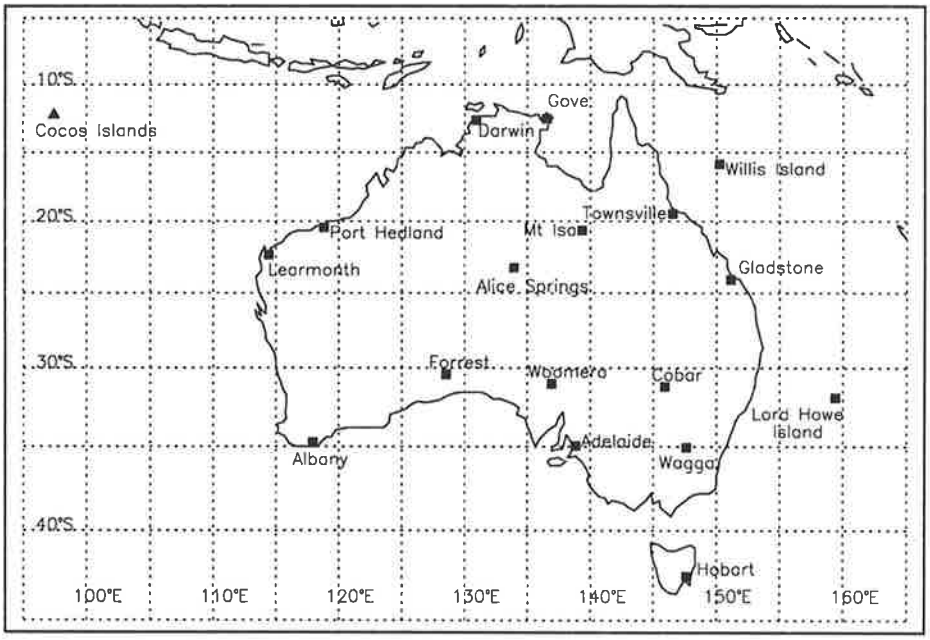

Figure 3.1: Map showing the locations of Australian radiosonde stations. Solid triangles indicate those stations which measure Digicora winds (see section 3.2 for further details).

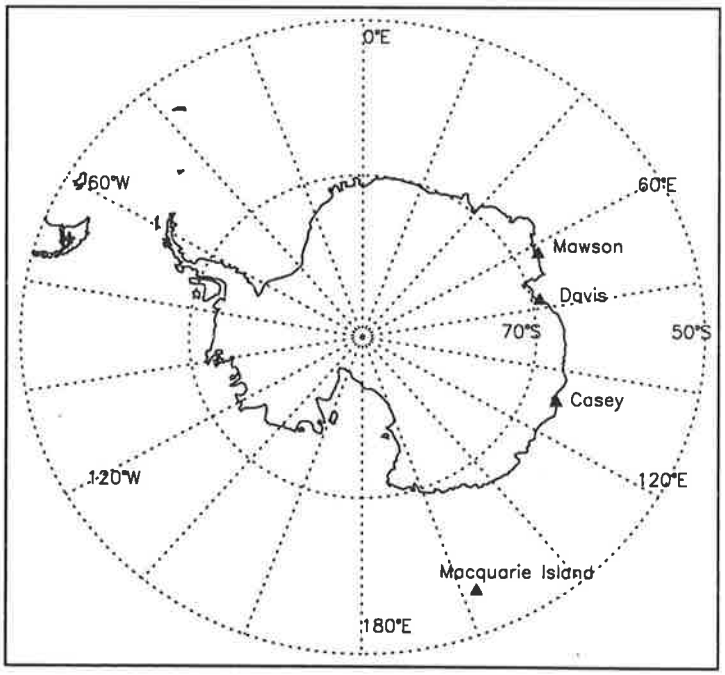

Figure 3.2: Map showing the locations of Australian radiosonde stations in the Antarctic and sub-Antarctic. Solid triangles indicate those stations which measure Digicora winds (see section 3.2 for further details).

Station Name	WMO Station Number	Location deg South, deg East	Time Intervals
Adelaide	94672	35, 139	May 1991 – Feb 1993
Albany	94802	35, 118	Mar 1991 – May 1992
Alice Springs	94326	23, 134	May 1991 – May 1992
Casey	89611	66, 111	Apr 1993 – Apr 1995
Cobar	94711	31, 146	Apr 1991 – May 1992
Cocos Islands	96996	12, 97	Sep 1992 – Dec 1993
Darwin	94120	12, 131	Jun 1991 – May 1992
Davis	89571	69, 78	Jul 1992 – Apr 1995
Forrest	94646	31, 129	Apr 1991 – May 1992
Gladstone	94380	24, 151	Jun 1991 – May 1992
Gove	94150	12, 137	Jun 1991 – May 1992
Hobart	94975	43, 147	Apr 1991 – May 1992
Learmonth	94302	22, 114	Jun 1991 – May 1992
Lord Howe Island	94995	32, 159	Jun 1991 – May 1992
Macquarie Island	94998	55, 159	Apr 1993 – Apr 1995
Mawson	89568	68, 63	May 1993 – Apr 1995
Mount Isa	94332	20, 139	Apr 1991 – May 1992
Port Hedland	94312	20, 118	Nov 1990 – May 1992
Townsville	94292	19, 147	Jun 1991 – May 1992
Wagga	94910	35, 147	May 1991 – May 1992
Willis Island	94299	16, 150	Aug 1991 – May 1992
Woomera	94659	31, 137	Apr 1991 – May 1992

Table 3.1: Information regarding the radiosonde stations that were studied in this thesis. The final column indicates the time intervals over which data were analyzed.

thesis and are of sufficient resolution to define a large portion of the gravity wave spectrum, including the dominant waves. Nevertheless, since meteorological radiosonde data are not gathered for research purposes, their use in gravity wave studies must be carefully justified. Important issues to consider in this context include measurement accuracy, measurement sensor response times and the observational geometry of radiosonde soundings. These issues will be reviewed here accordingly.

Radiosonde data from each station were not studied over the same time intervals (see Table 3.1) although data from all stations, with the exception of Willis Island, were studied over at least a one-year period. The exact time range of the studied data depended on when these were first archived at high resolution by the Australian Bureau of Meteorology. Note, however, that continuous high-resolution radiosonde data were available from all stations

between August 1991 and May 1992 with the exceptions of Mawson, Casey, Davis, Macquarie Island and the Cocos Islands[1]. Future studies might consider a larger data set where all measurements are from the same time period.

Previous radiosonde studies of gravity wave motions in the troposphere and lower stratosphere have utilized either single soundings [e.g., *Cot and Barat*, 1990; *Barat and Cot*, 1992; *De la Torre et al.*, 1994 and, inter alia, *Sidi et al.*, 1988] or many closely separated soundings from an observational campaign [e.g., *Thompson*, 1978; *Cadet and Teitelbaum*, 1979; *Tsuda et al.*, 1994b and, inter alia, *Fritts et al.*, 1988]. *Tsuda et al.* [1991] analyzed high resolution radiosonde data from more than two years of observation over a single northern hemisphere location while *Kitamura and Hirota* [1989] analyzed operational rawinsonde data from a network of stations in and around Japan. In the latter study only standard pressure levels and significant levels were utilized and so vertical resolution, although sufficient for observing the dominant waves, was poorer than in other studies. The temperature data analyzed in this thesis are comparable in quality and vertical resolution to those analyzed by *Tsuda et al.* [1991]. The results presented in Chapter 4 may be considered as an extension of their study to a network of southern hemisphere radiosonde stations. In addition to temperature measurements, horizontal wind speed measurements of sufficient quality and vertical resolution to delineate gravity wave characteristics were available from two of the Australian radiosonde stations. These are of comparable quality to those data analyzed by *Tsuda et al.* [1994b].

3.2 Horizontal Wind and Temperature Measurement

Vaisala RS80–15 radiosondes[2] were used at each meteorological station of Table 3.1 during the times stated[3]. These measure pressure, temperature and relative humidity in the atmosphere at approximately 2-s intervals but the measurements pass through quality control and smoothing algorithms and so 10-s "filtered" data are finally reported. Since standard meteorological sondes have vertical speeds of approximately 5 m s^{-1}, the vertical resolution of measurements is approximately 50 m.

[1] Radiosonde measurements from Casey, Davis, Mawson and Macquarie Island were provided on a weekly basis, via the internet, and the help of staff at these stations is gratefully acknowledged.

[2] The term radiosonde is used here to describe instrumented balloons which measure either thermodynamic parameters or horizontal winds, or both [following *Lally*, 1985]. However, the term rawinsonde is sometimes used elsewhere to describe instrumented balloons which measure both thermodynamic parameters and horizontal winds.

[3] Vaisala is a company based in Finland that specializes in the manufacture of meteorological instruments.

In addition to measurements of pressure, temperature and relative humidity, measurements of horizontal wind velocity are also made at each radiosonde station. These are obtained (in most cases) by attaching a reflective target to the sondes and monitoring their progress by radar. Standard measurements obtained in this manner are reported with poor vertical resolution and are inadequate for use in gravity wave studies [*Thompson*, 1978]. However, some stations now use a newer system where the sonde's position, and hence velocity, is determined by using radio transmitters of the OMEGA and Russian VLF NAVAID networks [*Lange*, 1985; *Karhunen*, 1991]. This system, called the Digicora system, has been developed by Vaisala. Horizontal winds are reported at 10-s intervals, although the measurements are effectively oversampled (see the discussion later in this section), and are of sufficient quality for use in gravity wave studies. The Australian radiosonde stations which use this system (at present) are those at Casey, Davis, Mawson, Macquarie Island and the Cocos Islands. Thus the data studied here consists of temperature measurements from all 22 stations that are listed in Table 3.1 and also simultaneous horizontal wind speed measurements from 5 of those stations. Pressure measurements are also used[4] but are not studied for gravity wave fluctuations while relative humidity measurements are not considered.

The capacitive temperature sensor used by the Vaisala RS80–15 radiosonde is believed to have a resolution of ± 0.1°C rms [see *Ivanov et al.*, 1991]. This is the nominal value stated by the company[5]. Figure 3.3 illustrates some examples of temperature profiles observed by radiosonde over Macquarie Island. Also plotted are temperature fluctuation profiles within both the troposphere and lower stratosphere where the shaded regions indicate the anticipated root-mean-square random measurement error based on claims by the manufacturer. The fluctuation profiles are obtained by subtracting fitted third-order polynomials. It is apparent that small vertical scale fluctuations on single profiles are geophysical and are not caused by random measurements errors.

The temperature measurements reported at each station have passed through quality control algorithms that were developed by Vaisala. These involve removing suspect measurements and replacing them by linear interpolation. Measurements are deemed to be suspect if they do not satisfy certain rejection criteria based on known physical constraints. In addition, the raw measurements, made at approximately 2-s intervals, are smoothed in

[4] Pressure measurements are used to estimate the radiosonde temperature sensor response time within the lower stratosphere. This is discussed in detail in appendix A.

[5] Radiosondes manufactured by Vaisala have been rigorously tested in international radiosonde comparison experiments [*Nash and Schmidlin*, 1987; *Schmidlin*, 1988; *Ivanov et al.*, 1991]).

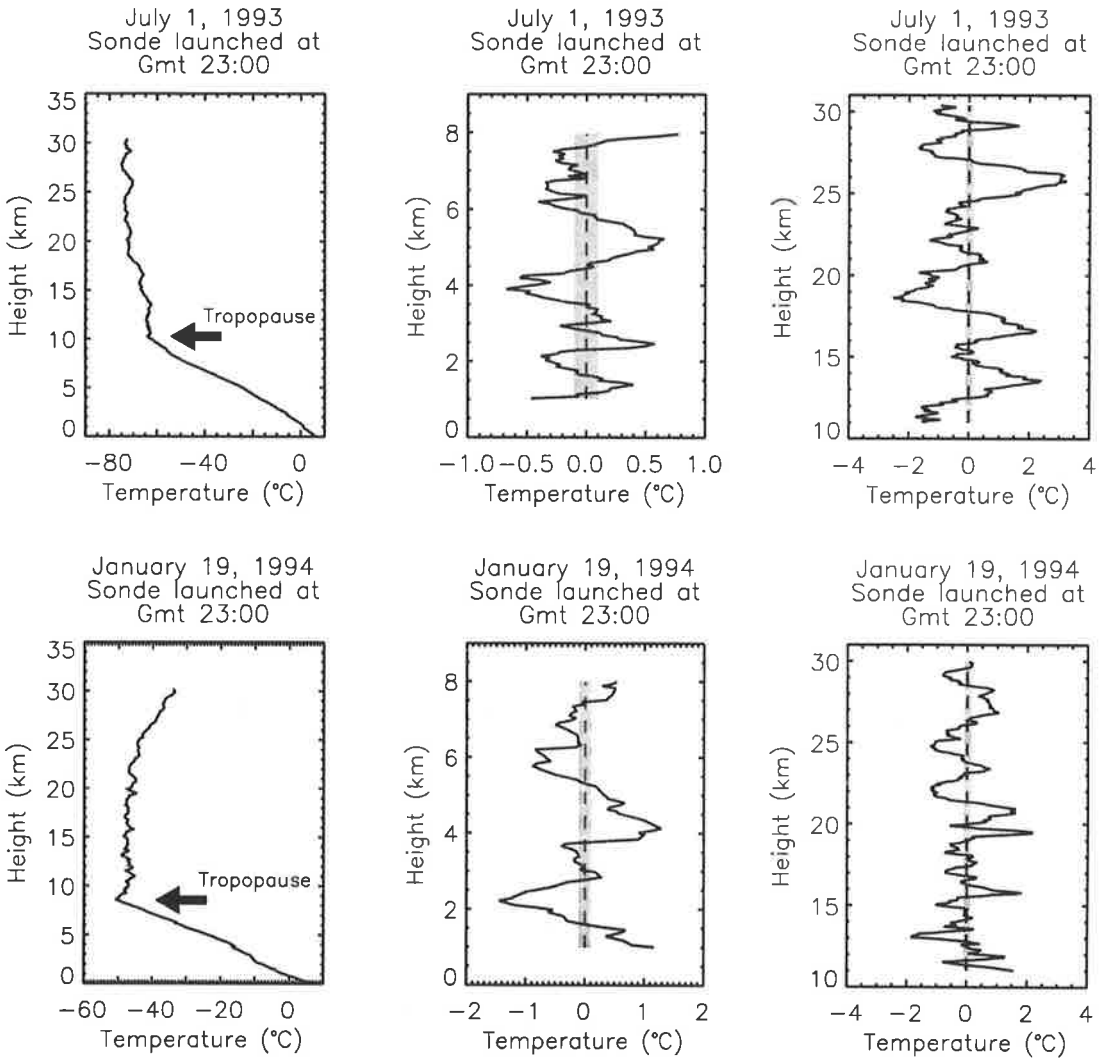

Figure 3.3: Temperature and temperature fluctuation profiles observed by radiosonde over Macquarie Island on July 1, 1993, and on January 19, 1994. Temperature fluctuation profiles are obtained by fitting and then subtracting a third-order polynomial over the altitude range of interest. The plots are organized in rows such that, from left to right, the first plot shows the observed temperature profile, the second shows the fluctuation profile between 1 and 8 km (troposphere), and the third shows the fluctuation profile between 11 and 30 km (lower stratosphere). The location of the tropopause in each case is given while the shaded regions indicate the anticipated root-mean-square random measurement error. Gmt stands for Greenwich mean time.

order to obtain the 10-s "filtered" data that are used here.

Horizontal wind speed measurements are also reported at 10-s intervals and pass through similar quality control algorithms. Stray winds that fail to satisfy the so-called Grubbs criterion [*MET Program Manual*, 1989] are replaced by cubic-spline interpolation and, following this, the winds are smoothed. However, the smoothed data are reported at the same resolution as the raw data, that is at 10-s intervals, and so are effectively oversampled. A cubic spline smoothing algorithm, within a running window of either 130-s or 250-s extent, is used. This corresponds, approximately, to vertical lengths of 650 m and 1250 m, respectively. A determination of the transfer function for the smoothing procedure is not attempted in this thesis. It is clear, however, that fluctuation amplitudes at vertical scales that are smaller than twice the smoothing window length will be attenuated in some manner. This attenuation will be discussed further where appropriate.

Horizontal winds obtained using NAVAID radio transmitters are generally of good quality. However, measurements made at the Antarctic stations of Davis, Mawson and Casey appear to be adversely affected by poor reception of the radio transmissions at these particular locations. Poor reception is caused by heavy attenuation of VLF radio signals as they travel over large regions of surface ice and also by ionospheric disturbances due to sunspot activity and at the day/night boundary [*Lange*, 1985; *B. Gunn*, private communication, 1993]. Also, most of the radio transmitters of the two NAVAID networks are located in the northern hemisphere and one particular transmitter in Liberia has been operating intermittently due to recent civil war in that country. Radio signals from at least three different locations are required to determine horizontal winds [e.g., *Lange*, 1985].

Radiosondes released at Davis rarely receive signals of sufficient clarity from three separate transmitters and so horizontal winds are generally not reported at this location. There appears to be little hope of studying Digicora wind fluctuations from Davis. In contrast, Digicora winds are regularly reported up to stratospheric heights from Mawson and Casey. However, comparisons with simultaneous radar wind measurements [*B. Gunn*, private communication, 1993] indicate significant standard vector deviations of the order of 4 or 5 m s^{-1}. Therefore Digicora winds are considered to be unreliable at these locations[6]. As a consequence, the winds observed from Casey and Mawson (and also the few reports from Davis) are not analyzed in this thesis. Only those winds observed from Macquarie Island and the

[6]It is worth noting that the standard vector deviations of winds observed over Mawson are improved when the OMEGA network transmitter in Liberia is operating [*B. Gunn*, private communication, 1993].

Cocos Islands are considered since there are no serious problems with signal reception at these locations.

The random error of Digicora zonal and meridional winds, assuming reasonable signal reception, is less than or equal to 1 m s^{-1} rms between 700 and 200 hPa [*Ivanov et al.*, 1991]. Figure 3.4 illustrates examples of zonal and meridional wind speed and wind speed fluctuation profiles observed over Macquarie Island. As in Figure 3.3, the shaded regions indicate the probable extent of the root-mean-square random measurement error which is taken to be approximately 0.5 m s^{-1} based on the results of *Ivanov et al.* [1991]. It is apparent, in the stratosphere at least, that fluctuations on single wind component profiles are geophysical.

Given that reported Digicora winds are both smoothed and also subject to relatively large random measurement errors, the prospect of studying small-amplitude or small-vertical-scale gravity waves in these data is poor. Temperature measurements are more appropriate for such analysis. However, Digicora wind measurements are able to resolve the dominant gravity waves and can therefore provide valuable information about such waves. Several important gravity wave characteristics can be determined when simultaneous measurements of horizontal wind and temperature are available. Nevertheless, other instrumental properties, aside from measurement accuracy, may affect the interpretation of wave characteristics and these will now be discussed.

3.3 Radiosonde Observation Geometry

The interpretation of radiosonde observations of gravity waves is complicated by the geometry of these observations. Instrumented balloons rise slowly in the vertical at speeds of approximately 5 m s^{-1} and also drift horizontally with the background winds. As a consequence, observed horizontal wind and temperature profiles are not strictly vertical profiles since the measurements are not made along a vertical line from the point of the balloon's release. Furthermore, successive measurements are taken at 10-s intervals and so the observed profiles are not instantaneous "snapshots" of the atmosphere. Therefore, the observed vertical scales of the wave are not necessarily the true vertical scales since observations may be influenced by horizontal and temporal variations of the wave field.

Both *Sidi et al.* [1988] and *Gardner and Gardner* [1993] have studied the above problem, although *Sidi et al.* [1988] consider only the effects of a finite balloon ascent velocity. To

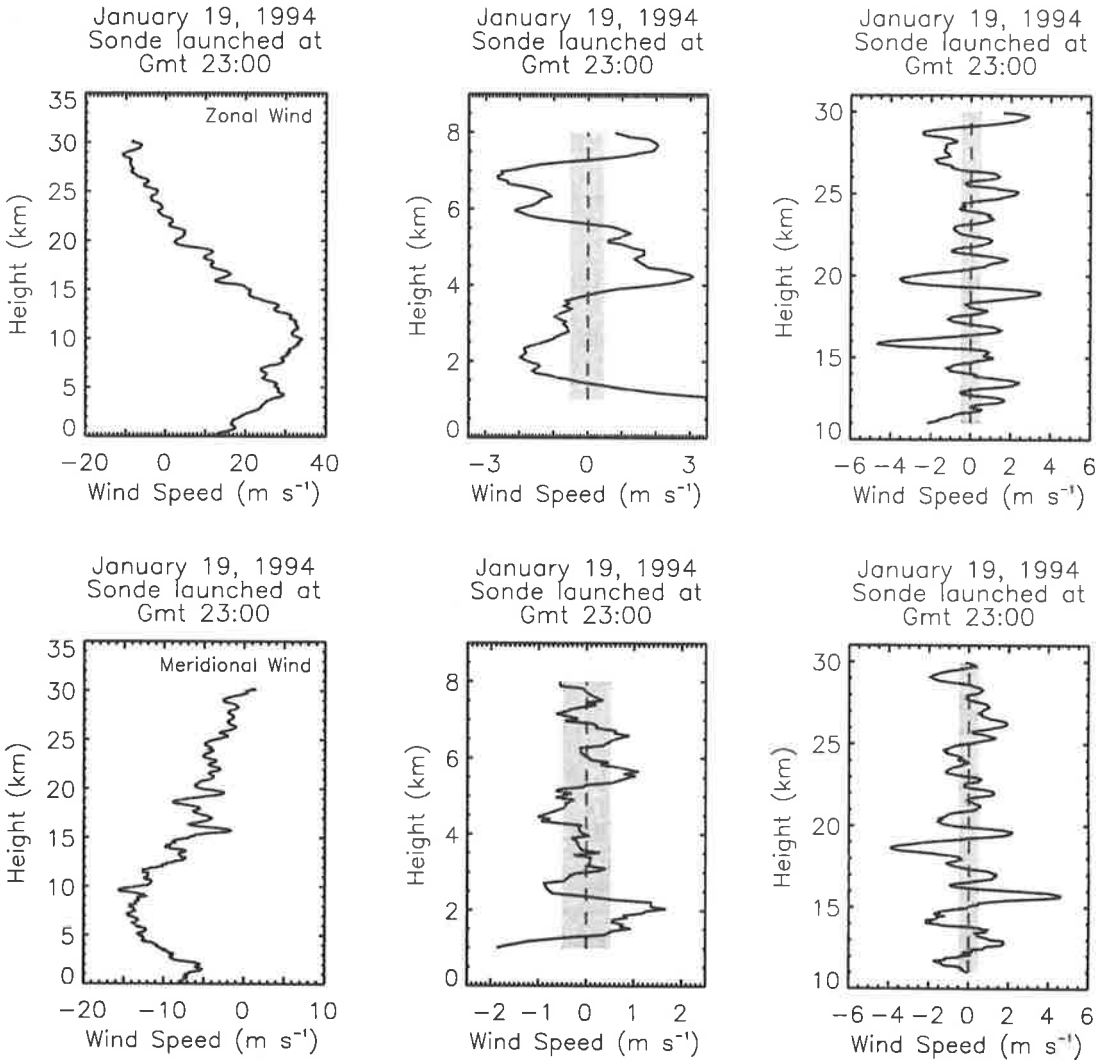

Figure 3.4: Zonal and meridional wind speed and wind speed fluctuation profiles observed by radiosonde over Macquarie Island on January 19, 1994. Wind speed fluctuation profiles are obtained by fitting and then subtracting a third-order polynomial over the altitude range of interest. The plots are organized in rows such that the first row illustrates zonal winds while the second row illustrates meridional winds. Each row illustrates, firstly, the observed wind profile, secondly, the fluctuation profile between 1 and 8 km (troposphere), and thirdly, the fluctuation profile between 11 and 30 km (lower stratosphere). The troposphere is located at 8.5 km (see Figure 3.3) and the shaded regions indicate the anticipated root-mean-square random measurement error. Gmt stands for Greenwich mean time.

illustrate how the observed vertical wavenumber may be affected, consider, after *Sidi et al.* [1988], the following scenario. Suppose a sonde measures a monochromatic gravity wave with wavenumber $\vec{K} = (k, l, m)$ and intrinsic frequency ω. Suppose also that the sonde ascends with finite vertical velocity V_0 and has a constant horizontal drift in the zonal direction $\overline{u}$. The variation of the wave's phase (denoted here by φ), over a short time interval δt and along any trajectory is given by,

$$\delta\varphi = -\omega\delta t + k\delta x + l\delta y + m\delta z \tag{3.1}$$

However, along the sonde trajectory it is true that $\delta z = V_0\delta t$, $\delta x = \overline{u}\,\delta z/V_0$ and $\delta y = 0$. Therefore, the observed vertical wavenumber ($m' = \frac{d\varphi}{dz}$) is given by

$$m' = m\left[1 + \frac{k\overline{u}}{mV_0} - \frac{\omega}{mV_0}\right] \tag{3.2}$$

and depends upon both the temporal and horizontal scales of the wave.

The second term in the square brackets of (3.2) describes the effects of the sonde's drift on the observed vertical wavenumber. This term is negligible provided that $\lambda_x/\lambda_z \gg \overline{u}/V_0$. The third term in the square brackets of (3.2) describes the effect of the finite sonde ascent velocity on the observed vertical wavenumber. This term is negligible provided that $c_z = \omega/m \ll V_0$. Essentially these two conditions require that the sonde traverses the wave cycle during a time interval that is much smaller than the wave's period while drifting horizontally over a distance that is much smaller than the wave's horizontal wavelength.

Typical vertical scales of gravity waves in the upper troposphere and lower stratosphere are of the order of 2.5 km [e.g., *Fritts et al.,* 1988] and typical horizontal scales are of the order of a hundred kilometres or more [e.g., *Nastrom et al.,* 1987]. The intrinsic frequency spectrum is believed to be a red noise spectrum and so typical intrinsic periods should be closer to the inertial period than to the buoyancy period. From (3.2) it is clear that the radiosonde observation geometry has negligible effect on the observed vertical wavenumber at these typical scales assuming $V_0 \approx 5$ m s^{-1} and using reasonable values of $\overline{u}$ from Figure 1.3. However, it is the high-wavenumber tail region of the one-dimensional vertical wavenumber power spectrum that is of particular interest when comparing saturation theories with experimental observations. Therefore it is important to ascertain the effects of observation geometry on this portion of the spectrum.

Gardner and Gardner [1993] modelled the distortion of vertical wavenumber power spectra of normalized temperature fluctuations derived from radiosonde observations, where the

radiosonde has finite ascent velocity and drifts horizontally at a constant rate. The canonical model spectrum that was used is not reported here[7]. However, the results are reproduced in Figure 3.5 for different choices of the parameters V_0 and $\overline{u}$. Note that the effects due to finite ascent velocity and horizontal drift were considered separately. This was achieved by setting $\overline{u} = 0$ in the former case and by setting V_0 to be large but finite in the latter case. The true (undistorted) vertical wavenumber power spectrum is denoted by $F_T(m)$ in each plot where m is in units of cycles per metre.

The sondes studied in this thesis have typical ascent velocities between 4 and 6 m s^{-1}. Figure 3.5 indicates that there is negligible distortion of the observed vertical wavenumber spectrum due to sonde ascent effects at these velocities. Similarly, spectral distortion due to the sonde's horizontal drift appears to be insignificant when $\overline{u} \leq 10V_0$ or, using the nominal value of $V_0 = 5$ m s^{-1}, when $\overline{u} \leq 50$ m s^{-1}. This is approximately the largest value of the climatological-mean horizontal winds that are found in the troposphere and lower stratosphere of the southern hemisphere (see, for example, Figure 1.3). However, *Gardner and Gardner* [1993] conclude that nonnegligible distortion is possible, especially at small vertical wavenumbers, when horizontal winds reach 60 m s^{-1} or larger. Winds of this magnitude can occur in the lower stratosphere at high latitudes, particularly in the vicinity of the southern hemisphere polar vortex, and a small degree of spectral distortion is therefore possible at such high-latitude sites.

Spectral distortion due to finite sonde ascent velocity and horizontal drift is not believed to be a serious problem in this study based on the results of *Sidi et al.* [1988] and *Gardner and Gardner* [1993]. Even under those conditions where nonnegligible distortion may occur, the proposed spectral distortion[8] is small when compared with the more serious distortion caused by the slow response of the radiosondes' temperature sensors at stratospheric heights. The response time is peculiar to the type of sensor used[9] and, if large enough, will prevent the radiosonde from accurately measuring rapid changes in temperature as the balloon moves vertically. The spectral distortion that arises may be corrected, however, and this correction procedure will now be discussed.

[7]The model spectrum is similar to that proposed by *Fritts and VanZandt* [1993] and is based on experimental results.

[8]From Figure 3.5, shallower spectral slopes are anticipated.

[9]The radiosondes that are studied here have relatively slow response times.

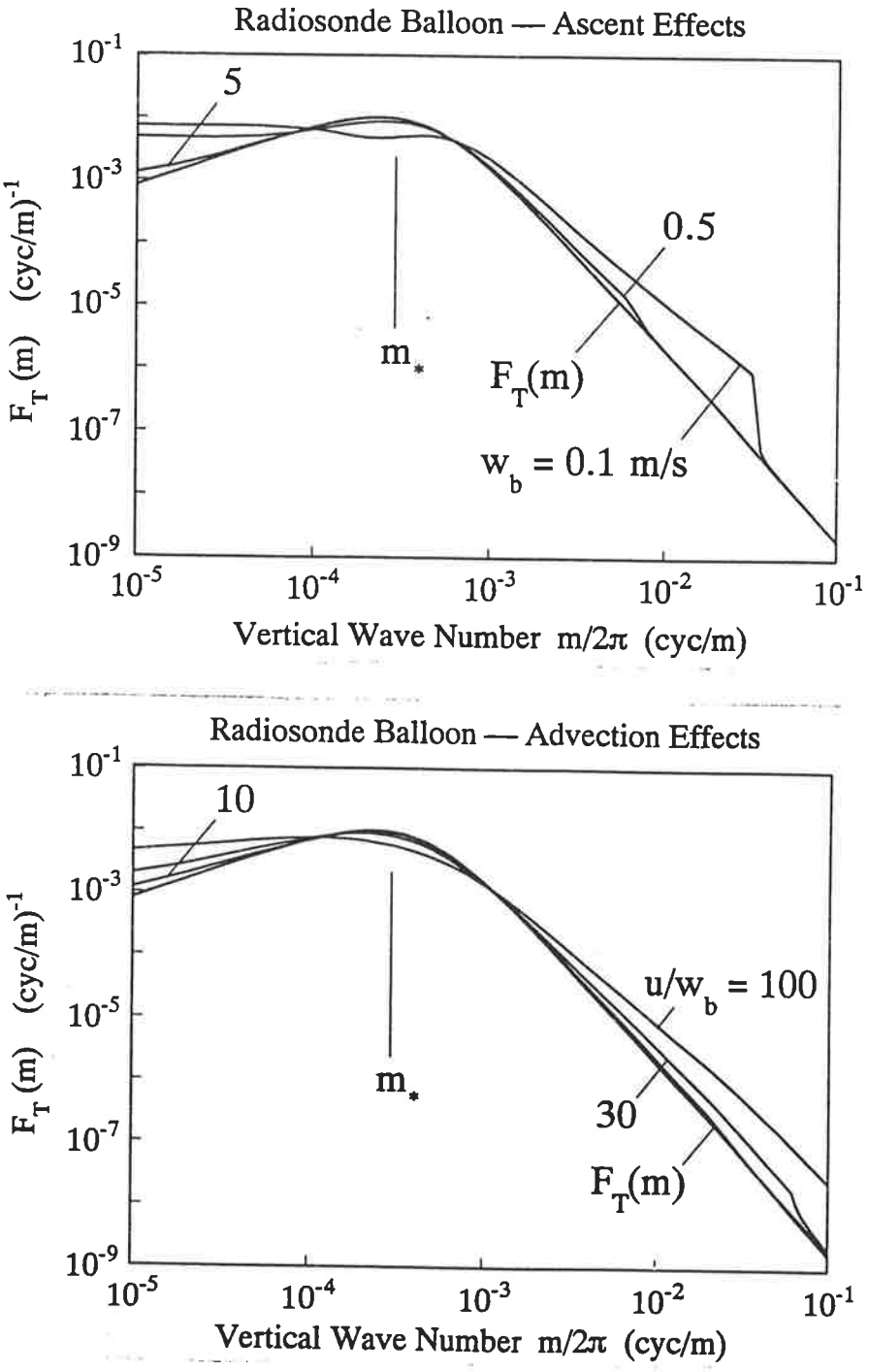

Figure 3.5: The theoretical distortion of a model vertical wavenumber power spectrum of normalized temperature fluctuations near the tropopause, denoted by $F_T(m)$ in the diagram, due to the finite ascent ascent velocity, w_b, and horizontal drift, u, of radiosondes [from *Gardner and Gardner*, 1993]. In the top diagram, u is set to zero, while in the bottom diagram, w_b is set to be large but finite. The notation used for the radiosonde ascent velocity, w_b, differs from the notation used in the text.

3.4 Temperature Sensor Response

The effect of temperature sensor response time on gravity wave fluctuations observed by radiosondes is generally not considered in the literature since many experimental radiosondes use fast response temperature sensors. For example, *Shutts et al.* [1988], *Sidi et al.* [1988] and *Cot and Barat* [1989] use temperature sensors with fast response times in their radiosonde packages. However, the capacitive temperature sensors used by Vaisala RS80–15 radiosondes have relatively slow response times [*Nash and Schmidlin*, 1987, p. 22] which may be of the order of 10 s at stratospheric heights[10]. Therefore, the present observed normalized temperature spectral amplitudes at high vertical wavenumbers may be significantly attenuated while no attenuation of published spectra appears to occur. The purpose of this section is to describe a spectral correction technique which will be utilized in later chapters.

It is well known that a temperature sensor will behave in such a way that the rate of change of the sensor's temperature is proportional to the difference between the temperature of the sensor and that of its surrounding environment [*Fritschen and Gay*, 1979]. Mathematically, this may be expressed as

$$\frac{dT_s}{dt} = -\frac{1}{\tau}\left[T_s - T\right] \tag{3.3}$$

where T_s is the sensor temperature, T is the environment temperature and τ is defined as the response time constant. The value of τ is peculiar to the type of sensor used and to the environment in which it is placed.

The response of a given temperature sensor to any time-varying environment temperature $T(t)$ is completely defined by (3.3). The steady state response to a sinusoidally varying environment is of particular importance, however, since this describes a filter function, $I(\omega)$, which relates the environment or input spectrum $X(\omega)$ to the measured spectrum $X_s(\omega)$ according to $X_s(\omega) = I(\omega)X(\omega)$ at each angular frequency ω [e.g., *Bath*, 1974]. Here $X(\omega)$ and $X_s(\omega)$ refer to the Fourier transforms of $T_s(t)$ and $T(t)$, respectively, rather than their power spectral densities. If $I(\omega)$ is known then the environment spectrum can be recovered from the observed spectrum since $X(\omega) = X_s(\omega)/I(\omega)$.

Consider the case of a balloon which rises at constant vertical velocity V_0 and carries a temperature sensor with known response time τ. Suppose also that the sensor is measuring a background or environment temperature profile that is sinusoidally dependent upon height

[10] Response times of this magnitude, generally, present no problem in a meteorological context.

z but is independent of time, that is, $T(z) = A\exp[i(mz + \varphi)]$ where $m = 2\pi/\lambda_z$ and where the complex notation has its usual meaning. Equation (3.3) is therefore given by

$$\frac{dT_s}{dz} + \frac{1}{\beta}T_s = \frac{1}{\beta}T \tag{3.4}$$

where $\beta = V_0\tau$. The "steady state" solution of this new equation for constant β is readily calculated,

$$T_s(z) = \frac{A}{1 + im\beta}\exp[i(mz + \varphi)] \tag{3.5}$$

and thus defines a filter function $I(m) = 1/[1+im\beta]$, analogous to the function $I(\omega)$ discussed earlier, which relates the Fourier transform of $T_s(z)$ to that of $T(z)$ at each spatial frequency or wavenumber m. Since power spectral density is proportional to the absolute value squared of a Fourier transform it follows that the observed vertical wavenumber power spectrum is related to the true or environment power spectrum according to the following equation

$$E_{T_s}(m) = \frac{1}{1 + (m\beta)^2}E_T(m) \tag{3.6}$$

where $E_{T_s}(m)$ and $E_T(m)$ are vertical wavenumber power spectra of $T_s(z)$ and $T(z)$ fluctuations respectively. Equation (12) can therefore be used to correct observed vertical wavenumber power spectra of temperature fluctuations and to recover their true forms provided that V_0 and τ are known and are constants. Furthermore, the relation is also valid for vertical wavenumber power spectra of normalized temperature fluctuations provided that $\overline{T_s}(z)$ does not differ significantly from $\overline{T}(z)$. This would appear to be a reasonable assumption.

Figure 3.6 displays the measurement distortion of a modified-Desaubies vertical wavenumber power spectrum with $m_*/2\pi = 5 \times 10^{-4}$ cycles per metre (cpm) and with spectral amplitudes chosen to represent typical observations of normalized temperature fluctuations. The parameter β was assigned the value of 40 m. This corresponds to the typical balloon ascent velocity ($V_0 = 5$ m s^{-1}) and to estimates of response times ($\tau = 8$ s) within the altitude range 17–24 km. Notice that the spectral distortion is only significant at high vertical wavenumbers. Notice also that the total observed variance is not significantly reduced since the shaded area of Figure 3.6 comprises just 4% of the total area under the modified-Desaubies spectrum.

Estimating the radiosonde's temperature sensor response time poses a difficult problem since τ depends upon air temperature and air density. A broad discussion of how these estimates can be obtained and to what extent they are reliable is given in appendix A. The discussion is based on experimental results presented in two Vaisala test reports. However, it

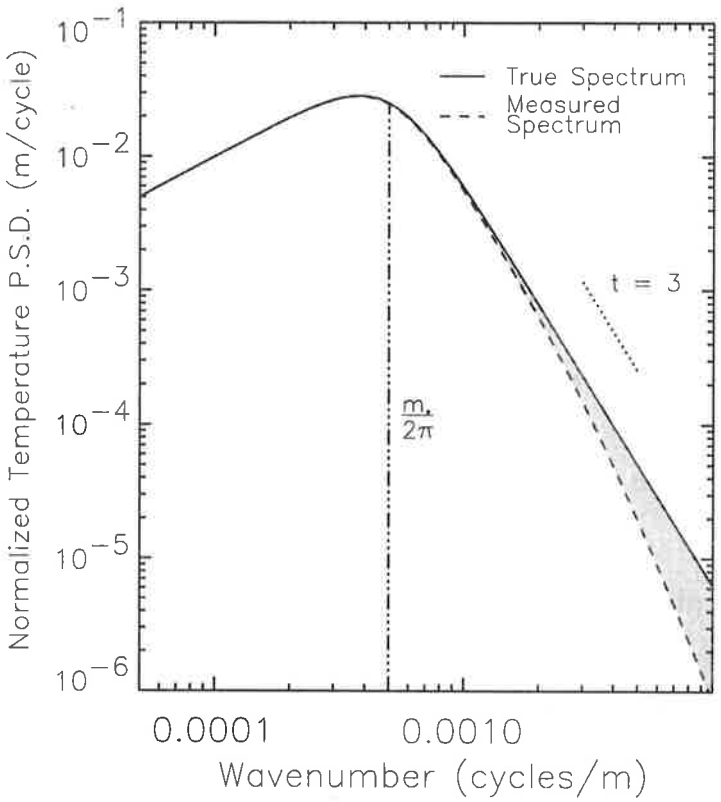

Figure 3.6: The theoretical distortion of a modified-Desaubies vertical wavenumber power spectrum measured by a radiosonde with temperature sensor response time $\tau = 8$ s and with vertical ascent velocity $V_0 = 5$ m s^{-1}. The shaded region comprises 4% of the total area under the modified Desaubies spectrum.

should be noted here that there is some uncertainty as to the correct value for the response time τ. This may result in a bias for the spectral parameter, t, of corrected power spectra, although estimates of both the characteristic wavenumber and the total wave variance will not be significantly affected. More details are provided in appendix A.

The height-averaged response times were found to lie between 7 and 8 s within the 17 to 24-km altitude range and between 1 and 2 s within the 2 to 9-km altitude range. The response times were not constant within these ranges but may be considered as constants to good approximation. This point is discussed further in appendix A and is not believed to result in serious errors, despite the fact that τ was assumed to be constant in the derivation of (3.6). Since the response time is small within the troposphere, the correction to the observed power spectrum, for the wavenumber range that is being investigated here, is marginal. As a result the correction technique that is described by (3.6) need only be applied to the calculation of stratospheric power spectra.

3.5 Power Spectrum Analysis

The vertical wavenumber power spectra of normalized temperature fluctuations that are presented in this thesis were (in most cases) calculated using the Blackman-Tukey algorithm with a 90% lag Bartlett window where the data were first prewhitened by differencing. This technique follows *Dewan et al.* [1984, 1988] who used the same algorithm to analyze horizontal wind velocity fluctuations derived from rocket-laid vertical smoke trails. The various steps of the calculation procedure are described in detail by *Dewan et al.* [1988] and these are followed here. Normalized temperature fluctuations, $\hat{T}'$, were calculated by estimating $\overline{T}$ with a fitted second-order polynomial over the particular height interval being investigated.

The purpose of prewhitening data before spectral analysis is to reduce the effects of spectral leakage [e.g., *Blackman and Tukey,* 1958]. Prewhitening by differencing is useful when the spectrum to be calculated is a red noise type spectrum, that is when $F(m) \propto m^{-t}$ where $F(m)$ is power spectral density and where t is positive. It is therefore useful in this study since accurate estimates of spectral amplitudes within the high-wavenumber tail region of a modified-Desaubies type spectrum are required. However, when $F(m) \propto m^{s}$, where s is positive, the calculated spectral amplitudes may be significantly biased if differenced data are considered. Therefore differenced data should not be used when attempting to determine the spectral parameter s of a modified-Desaubies type spectrum. This point will be discussed again in chapter 4.

A possible source of error in the spectral analysis procedure arises due to the fact that radiosonde observations are unequally spaced in altitude. Although successive measurements were recorded at 10-s intervals, the corresponding altitudes traversed by the sonde tended to vary; typical height intervals were found to be between 40 and 60 m. Strictly speaking the Blackman-Tukey algorithm cannot be applied to unequally spaced data such as this.

The approach used here was to interpolate the measurements at 50-m intervals using cubic spline interpolation and to assume that the calculated power spectrum was not significantly different from the spectrum that would be found were the original data points equally spaced. In order to be confident of this, however, a comparison was made between vertical wavenumber power spectra of normalized temperature fluctuations calculated with both the Blackman-Tukey algorithm and with a particular discrete Fourier transform proposed by *Ferraz-Mello* [1981]. This latter technique was devised specifically for the purpose

of making accurate estimates of power spectral density from unequally spaced data. The comparison was found to be favourable (see the results presented in chapter 4) and so the Blackman-Tukey algorithm appears to have valid application in this case.

In contrast to the above finding, however, *Moore et al.* [1988] concluded that equispaced analysis techniques may obscure oceanic gravity wave spectral structure at high vertical wavenumbers if the observed data are not equally spaced. Ocean profiles may be unequally spaced in depth, as are radiosonde profiles in height, due to variations in instrument lowering rate caused by, for example, ship heave [*Moore et al.*, 1988]. Therefore both oceanic and atmospheric problems are, in broad terms, the same although the wave spectra in each case need not be. *Moore et al.* [1988] analyzed two temperature profiles between 750 m and 1200 m depth which were observed at approximately 500 and 300 km, respectively, off the east coast of Australia. A comparison was made between spectra calculated using irregularly-spaced techniques proposed by *Brillinger* [1972, 1983] and spectra calculated using equispaced techniques which involved cubic spline interpolation of the observed data. The comparison was unfavourable at vertical wavenumbers larger than, approximately, 0.05 cycles per metre which corresponds to wavelengths smaller than, approximately, 20 m. The equispaced analysis techniques gave spectra that were in good agreement with the canonical GM75 model spectrum whereas the irregularly-spaced techniques, at large vertical wavenumbers, did not.

Despite the conclusions of *Moore et al.* [1988], the Blackman-Tukey algorithm is considered to be valid in this study based on comparisons with the algorithm proposed by *Ferraz-Mello* [1981]. It is acknowledged that some difficulties can arise but, it is argued, these are not significant for the radiosonde data used here which are of coarser resolution and which are closer to being equally spaced. However, no attempt is made to critically compare the irregularly-spaced spectral techniques used by *Moore et al.* [1988], that is the algorithms proposed by *Brillinger* [1972, 1983], and the technique that was used here (which was proposed by *Ferraz-Mello* [1981]). Such a comparison is beyond the scope of the present study.

Another possible source of difficulty arises if the observed data are nonstationary with altitude. It is important in this context to consider only those segments of data which, based on theoretical understanding, might be anticipated to yield stationary spectra. For example, from (2.16), the vertical wavenumber power spectrum of normalized temperature fluctuations is anticipated to be dependent upon N^4. Since significant increases in buoyancy

frequency occur near the tropopause, any data segments containing a tropopause should not be spectrally analyzed. Similarly, it is prudent to study normalized temperature fluctuations, rather than simply temperature fluctuations, since these data are anticipated to be stationary when N is constant (again see equation 2.16).

There is, however, inherent nonstationarity of the modified-Desaubies gravity wave spectrum which cannot be avoided. This arises since those waves in the source-dependent region of the spectrum will have amplitudes that increase with height in accordance with wave action conservation and with decreasing atmosphere density[11]. Therefore the observed spectrum, which must be calculated over a given height interval, cannot represent the true spectrum at any given height. *Eckermann* [1990b] has studied this problem by numerical simulation and has concluded that limited distortion of the calculated gravity wave spectrum can arise. However, since gravity wave amplitudes increase slowly, although exponentially, with height[12], the proposed distortion is generally not large. Indeed the numerical simulations presented by *Eckermann* [1990b] considered gravity wave fluctuations over a 44.8 km altitude range whereas the spectra studied in this thesis are calculated over altitude ranges of the order of 10 km. Therefore this particular form of spectral nonstationarity is not thought to have significant consequences for the data studied here.

One goal of spectral analysis is to define the dominant vertical scales of gravity waves. *Zangvil* [1977] has demonstrated that the so-called area preserving spectrum correctly defines the true periodicity of a localized disturbance. The area preserving spectrum, $\hat{F}(m)$, is defined by $\hat{F}(m) = mF(m)$, where $F(m)$ is a conventionally defined power spectrum, and is plotted as a function of $\log m$. The variance in a small logarithmic interval $\delta(\log m)$ is given by $\hat{F}(m)\delta(\log m)$, which is equivalent to $F(m)\delta m$, and hence the name area preserving. These spectra have been utilized by, for example, *Fritts et al.* [1988] and *Ogino et al.* [1995] to determine the dominant vertical scales of atmospheric gravity waves. Figure 3.7 illustrates the modified-Desaubies spectrum in both conventional logarithmic and area preserving forms. Notice that the spectrum peaks at different wavenumbers in each case.

The material presented in this section summarizes the spectral analysis techniques that are utilized at various stages in later chapters. The exact techniques that are used in each instance will be described where appropriate. Spectral analysis techniques may also be extended to vector quantities such as the horizontal wind velocities which are observed at

[11]The characteristic vertical wavenumber decreases as a consequence.

[12]The scale height of unsaturated gravity wave energy is thought to be twice the density scale height [e.g., *Fritts and VanZandt*, 1993].

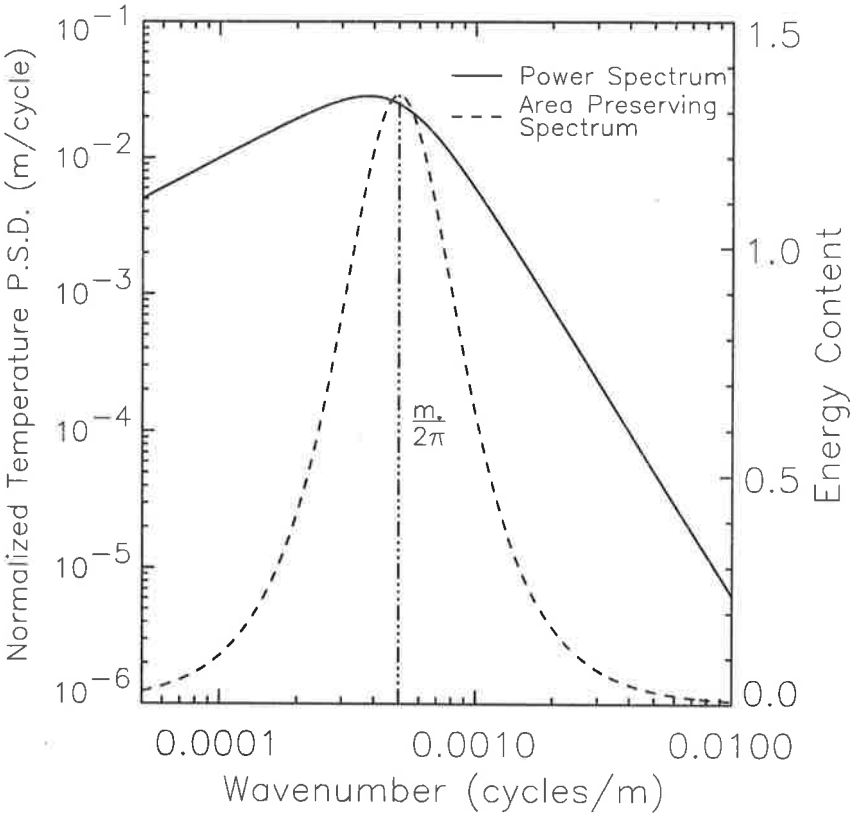

Figure 3.7: The modified-Desaubies spectrum in conventional logarithmic and area preserving forms. Spectral amplitudes were chosen to represent typical observations of normalized temperature fluctuations within the lower stratosphere while m_* was chosen such that $m_*/2\pi = 5 \times 10^{-4}$ cpm. The area preserving spectrum has been multiplied by a factor of 10^5 for convenience.

Macquarie Island and the Cocos Islands. The so-called rotary component spectra can provide important information about gravity waves and these are discussed in the following section.

3.6 Rotary Spectrum Analysis

Fluctuations of horizontal wind velocity vectors can be decomposed into circular-clockwise and circular-anticlockwise rotating components by means of rotary spectrum analysis [e.g., *Gonella*, 1972; *O'Brien and Pillsbury*, 1974]. Upward propagating inertio-gravity waves induce anticlockwise rotating wind fluctuation vectors in the southern hemisphere whereas downward propagating inertio-gravity waves induce clockwise rotating wind fluctuation vectors (see the polarization equations presented in chapter 1 and also Figures 1.4 and 1.5). Therefore rotary spectrum analysis can potentially determine the proportion of total gravity wave energy that is upward propagating. In this chapter, and in following chapters, it

is intended that the prefix "upward propagating" implies (unless otherwise stated) upward propagation of wave energy as distinct from upward phase propagation. More specifically, it is intended to imply that the vertical component of the group velocity is positive.

Rotary spectrum analysis has been used to analyze horizontal wind vector fluctuations in various regions of the middle atmosphere by, for example, *Thompson* [1978], *Vincent* [1984], *Eckermann and Vincent* [1989] and *Barat and Cot* [1992]. These studies, among others, provide evidence for the notion that gravity wave sources occur predominantly in the troposphere and that observed waves in the middle atmosphere are predominantly upward propagating. Rotary spectrum analysis has also been applied successfully in oceanic studies by, for example, *Gonella* [1972] and *Leaman and Sanford* [1975]. The latter study provided evidence for the notion that energy sources of inertio-gravity waves in the ocean occur at or near the ocean surface.

Rotary component spectra, as functions of vertical wavenumber, are constructed by taking the Fourier transform of the horizontal wind velocity vector which is expressed as

$$r(z) = u(z) + iv(z) \tag{3.7}$$

where, as before, u and v are the zonal and meridional components of horizontal wind velocity, respectively [e.g., *Leaman and Sanford*, 1975; *Vincent*, 1984]. If $\mathcal{R}(m)$ is the Fourier transform of $r(z)$ then the clockwise-rotating component spectrum $RS_{CL}(m)$ and anticlockwise-rotating component spectrum $RS_{ACL}(m)$ are

$$RS_{CL}(m) \propto \mathcal{R}_{-m}\mathcal{R}^*_{-m} \tag{3.8}$$

$$RS_{ACL}(m) \propto \mathcal{R}_{+m}\mathcal{R}^*_{+m} \tag{3.9}$$

where $\mathcal{R}_{+m}$ and $\mathcal{R}_{-m}$ are the complex values of $\mathcal{R}$ at wavenumbers $+m$ and $-m$, respectively, and where the asterisk indicates a complex conjugate[13] [e.g., *Vincent*, 1984]. The sum of $RS_{CL}(m)$ and $RS_{ACL}(m)$ is equal to the vertical wavenumber power spectrum of total horizontal wind speed [e.g., *Barat and Cot*, 1992].

The rationale behind rotary spectrum analysis, after *Leaman and Sanford* [1975], is as follows. Spectral decomposition defines sinusoidal waves for both u and v at vertical wavenumber m. When taken together these define a helix which is (in general) elliptically polarized and which may be represented by

$$u_m + iv_m = u_+ \exp(imz) + u_- \exp(-imz) \tag{3.10}$$

[13]The notation $RS_{CL}(m)$ and $RS_{ACL}(m)$ follows *Barat and Cot* [1992].

where u_+ and u_- are complex [*Leaman and Sanford*, 1975]. Therefore the clockwise and anticlockwise components of variance, in a small wavenumber band δm about m, may be defined by

$$\delta m\ RS_{CL}(m) = \frac{1}{2} u_-^* u_- \tag{3.11}$$

$$\delta m\ RS_{ACL}(m) = \frac{1}{2} u_+^* u_+ \tag{3.12}$$

where $RS_{CL}(m) + RS_{ACL}(m)$ is equal to $E_u(m) + E_v(m)$ [e.g., *O'Brien and Pillsbury*, 1974; *Leaman and Sanford*, 1975].

Consider the scenario where $u_m = A \cos mz$ and $v_m = B \sin mz$[14]. In this example the horizontal wind velocity vector rotates in an anticlockwise manner with height while the tip of the vector traces a helix as illustrated in Figure 3.8. The component amplitudes u_+ and u_- are given by

$$u_+ = \frac{1}{2}(A + B) \tag{3.13}$$

$$u_- = \frac{1}{2}(A - B) \tag{3.14}$$

and so spectral power will appear in both clockwise and anticlockwise component spectra for $A \neq B$ (see Figure 3.8). However, a gravity wave which might induce such a vector oscillation with height would be upward propagating in the southern hemisphere and thus the variance of an upward propagating gravity wave does not appear, in general, in the anticlockwise component only. Indeed linearly polarized gravity wave variance (e.g. the case where $B = 0$) will appear equally in both clockwise and anticlockwise component spectra. Nevertheless it is true in general, from (3.13) and (3.14), that the majority of upward propagating gravity wave energy will appear in the anticlockwise component whereas, by analogy, the majority of downward propagating gravity wave energy will appear in the clockwise component (in the southern hemisphere).

Rotary component spectra can provide useful information about mean vertical directions of gravity wave energy propagation. However, further information about gravity wave polarization and about horizontal wave propagation directions can be obtained by studying the so-called Stokes parameters of the wave motion. In fact *Eckermann* [1990a] has pointed out that the rotary component power spectra are related to the Stokes parameters in the Fourier domain. The utility of Stokes parameter analysis in gravity wave studies is discussed in the following section.

[14]The choice of a 90° phase difference between u_m and v_m can be made without loss of generality since the horizontal coordinate axes can always be rotated such that this is the case.

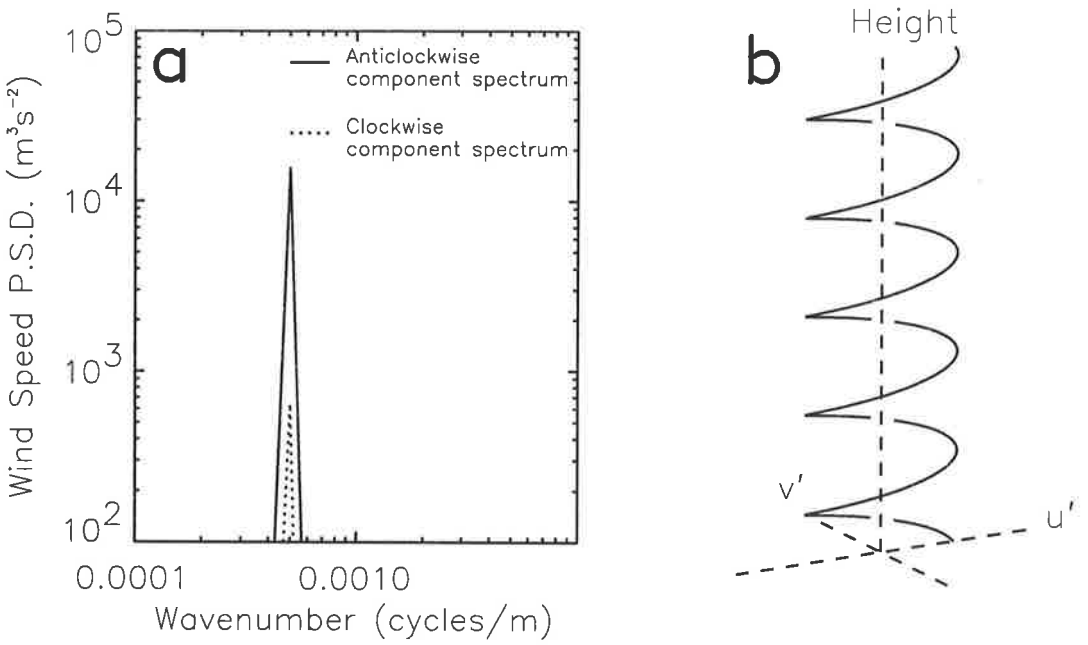

Figure 3.8: (a) The rotary component spectra of an elliptically-polarized monochromatic gravity wave which has $\lambda_z = 2$ km, is sampled at 50-m intervals over 10 km, and has zonal and meridional fluctuation components given by $u_m = 1.5 \cos mz$ and $v_m = 1.0 \sin mz$, respectively. (b) Schematic illustration of the wind vector fluctuations used to calculate the rotary spectra in (a). Each point indicates the tip of the horizontal wind velocity vector at a given height while gaps in the curve show that the velocity vector is passing behind the vertical axis [after *Leaman and Sanford*, 1975].

3.7 Stokes Parameter Analysis

The polarization of atmospheric gravity waves was first studied using Stokes parameters by *Vincent and Fritts* [1987] who based their technique on the Stokes parameter description of partially-polarized quasi-monochromatic electromagnetic (EM) waves. The Stokes parameters of an EM wave, with orthogonal instantaneous electric field amplitudes $E_x(t)$ and $E_y(t)$, are defined by

$$I = \left\langle E_x^2 \right\rangle + \left\langle E_y^2 \right\rangle \tag{3.15}$$

$$D = \left\langle E_x^2 \right\rangle - \left\langle E_y^2 \right\rangle \tag{3.16}$$

$$P = 2 \left\langle E_x E_y \cos \epsilon \right\rangle \tag{3.17}$$

$$Q = 2 \left\langle E_x E_y \sin \epsilon \right\rangle \tag{3.18}$$

where ϵ is the phase difference between the x and y components of the electric field vector, and where the $\langle\ \rangle$ brackets indicate time averages [e.g., *Hecht*, 1987; *Vincent and Fritts*,

1987]. These parameters can be determined from simple experiments [e.g., *Born and Wolf*, 1970] and provide a statistical measure of the degree of polarization of a partially polarized wave.

The first parameter, I, is proportional to the total irradiance while the other three parameters specify the state of polarization [e.g., *Hecht*, 1987]. Stokes parameter D indicates an excess of linearly polarized irradiance along the x or y axes as does Stokes parameter P along axes at 45° and 135° azimuth. Stokes parameter Q indicates an excess of either right-hand circularly polarized irradiance or left-hand circularly polarized irradiance. For a more detailed discussion about these parameters see, for example, *Kraus* [1966], *Born and Wolf* [1970] or *Hecht* [1987].

A completely polarized wave has Stokes parameters such that $I^2 = D^2 + P^2 + Q^2$ whereas a completely unpolarized wave has Stokes parameters such that $D = P = Q = 0$ [e.g., *Kraus*, 1966]. The ratio of polarized irradiance to total irradiance is given by

$$d = \left(D^2 + P^2 + Q^2\right)^{1/2} / I \tag{3.19}$$

where d is called the degree of polarization [e.g., *Born and Wolf*, 1970]. Each Stokes parameter, and the degree of polarization parameter d, may be determined experimentally by appropriate use of polaroid filters [e.g., *Hecht*, 1987].

Vincent and Fritts [1987] considered the instantaneous zonal and meridional perturbation velocities of a partially polarized gravity wave and defined, by analogy, the Stokes parameters of such a wave to be

$$I = \overline{u_0'^2} + \overline{v_0'^2} \tag{3.20}$$

$$D = \overline{u_0'^2} - \overline{v_0'^2} \tag{3.21}$$

$$P = 2\,\overline{u_0' v_0' \cos\epsilon} \tag{3.22}$$

$$Q = 2\,\overline{u_0' v_0' \sin\epsilon} \tag{3.23}$$

where, as before, ϵ is the phase difference between the zonal and meridional components, and where u_0' and v_0' are the peak amplitudes of u' and v', respectively. While *Vincent and Fritts* [1987] considered time series data, *Eckermann and Vincent* [1989] extended the Stokes parameter concept to vertical profiles of horizontal wind velocity measured by rocket-borne falling sphere. Furthermore, these authors calculated Stokes parameters in the Fourier domain since the gravity wave field is, in general, polychromatic. However, as pointed out by *Eckermann and Vincent* [1989], any Stokes parameter determined at a given wavenumber

has little significance since a single wave event is typically smeared throughout wavenumber space due to changes in the basic state atmosphere with height.

If $u'(z)$ and $v'(z)$ have Fourier transforms $\mathcal{U}_R(m) + i\,\mathcal{U}_I(m)$ and $\mathcal{V}_R(m) + i\,\mathcal{V}_I(m)$, respectively, then the Stokes parameters are defined by

$$I(m) = C\left\{\mathcal{U}_R^2(m) + \mathcal{U}_I^2(m) + \mathcal{V}_R^2(m) + \mathcal{V}_I^2(m)\right\} \tag{3.24}$$

$$D(m) = C\left\{\mathcal{U}_R^2(m) + \mathcal{U}_I^2(m) - \mathcal{V}_R^2(m) - \mathcal{V}_I^2(m)\right\} \tag{3.25}$$

$$P(m) = 2C\left\{\mathcal{U}_R(m)\mathcal{V}_R(m) + \mathcal{U}_I(m)\mathcal{V}_I(m)\right\} \tag{3.26}$$

$$Q(m) = 2C\left\{\mathcal{U}_R(m)\mathcal{V}_I(m) - \mathcal{U}_I(m)\mathcal{V}_R(m)\right\} \tag{3.27}$$

where C is some constant [*Eckermann and Vincent*, 1989]. The value of C may be chosen such that each Stokes parameter is in units of power spectral density or such that the total variance is normalized to a value of 1 $m^2\ s^{-2}$. It is also worth noting that the rotary component spectra are related to the Stokes parameters according to $RS_{CL} = (I - Q)/2$ and $RS_{ACL} = (I + Q)/2$ where the rotary spectra are defined as in the previous section [*Eckermann*, 1990a, p. 249].

The dominant sense of horizontal alignment of a gravity wave field may be objectively determined by using Stokes parameters. If $\overline{\phi}$ is the mean horizontal alignment then

$$\overline{\phi} = \frac{1}{2}\arctan\left(\frac{P}{D}\right) \tag{3.28}$$

and is given in units of degrees anticlockwise from east [*Vincent and Fritts*, 1987]. For a linearly-polarized monochromatic gravity wave this defines the alignment of horizontal particle motion whereas for an elliptically-polarized wave it defines the semi-major axis of the motion ellipse. For a partially polarized wave motion it defines the preferred sense of alignment of the polarized component. This concept breaks down, however, when both P and D approach zero at which point either circularly-polarized inertial wave motions are being considered[15] or the wave motion is completely unpolarized. A horizontally isotropic wave field should result in completely unpolarized particle motions since u' and v' are statistically independent in this case.

Equation (3.28) limits the direction of horizontal phase propagation of an ideal, completely-polarized monochromatic wave to two possible values since $\vec{K}_h = (k, l, 0)$ must lie along the semi-major axis of the motion ellipse[16]. Figure 3.9 illustrates this situation with the

[15] A pure inertial wave has no horizontal component to the wavenumber vector

[16] Although gravity wave motions are transverse in three dimensions, the major oscillations are parallel to the wavenumber vector in the horizontal plane (see Figures 1.4 and 1.5).

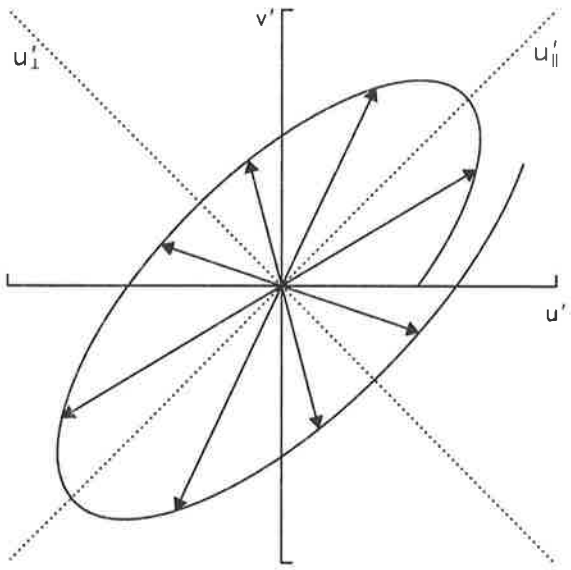

Figure 3.9: The hodograph of an ideal elliptically-polarized inertio-gravity wave that is upward propagating in the southern hemisphere and has an amplitude that increases with height. The $u'_{\parallel}$ and $u'_{\perp}$ axes are orientated along the motion ellipse major and minor axes, respectively [after *Hamilton*, 1991].

hodograph of an ideal elliptically-polarized inertio-gravity wave that is upward propagating on the southern hemisphere. While $\overline{\phi}$ defines the $u'_{\parallel}$ axis, it does not indicate whether $\vec{K}_h$ is directed along the positive or negative sections of this axis. Further information is required to resolve this ambiguity.

Kitamura and Hirota [1989] and *Hamilton* [1991] have pointed out that the direction of horizontal phase propagation may be resolved by considering the variations of both $u'_{\parallel}$ and $\hat{T}'$. For an ideal monochromatic wave these fluctuation quantities are 90° out of phase[17]. If the positive $u'_{\parallel}$ axis is chosen arbitrarily, the sign of $\overline{u'_{\parallel}\hat{T}'_{+90}}$ determines whether the intrinsic phase velocity vector is parallel to or antiparallel to this axis [see *Hamilton*, 1991], where $\hat{T}'_{+90} = i\hat{T}'$[18]. Equations (1.9) and (1.10) may be rearranged and combined such that

$$\overline{u'_{\parallel}\hat{T}'_{+90}} = \frac{-N^2}{g\omega}\frac{K_h}{m}\overline{u'^2_{\parallel}} \tag{3.29}$$

and so clearly the sign of $\overline{u'_{\parallel}\hat{T}'_{+90}}$ defines the sign of $c_h^{\text{int}} = \omega/K_h$ given that the sign of m is known. Therefore, the ambiguity in horizontal phase propagation direction is resolved when simultaneous wind and temperature measurements are available. For a partially polarized

[17]The temperature fluctuation either lags or leads the parallel-component wind velocity fluctuation depending on the sign of m which may be determined experimentally from the wind fluctuation hodograph.

[18]This quantity may be obtained by the application of a Hilbert transform [*Eckermann et al.*, 1996].

wave motion, the horizontal direction defined by (3.28) and (3.29) has been interpreted to define the dominant direction of horizontal phase propagation by *Hamilton* [1991].

The dominant intrinsic frequency of a gravity wave field (if such a dominant signal exists) may also be estimated by using Stokes parameters. For a monochromatic inertio-gravity wave, the intrinsic frequency is defined by the eccentricity of the motion ellipse. In terms of the Stokes parameters this is given by

$$AR = \cot\left\{\frac{1}{2}\arcsin\left(\frac{Q}{dI}\right)\right\} \tag{3.30}$$

where $AR = \omega/f$ is the axial ratio [*Eckermann and Vincent*, 1989]. However, when a superposition of many gravity waves exists, the interpretation of (3.30) is somehow more complicated. *Eckermann and Hocking* [1989] argue that AR may be a function of azimuthal directionality, rather than some dominant intrinsic frequency, in this case. Therefore, estimates of ω obtained from axial ratio calculations must be treated with caution.

The Stokes parameters are useful analytic tools which can describe the polarization state of an atmospheric gravity wave field. They have been utilized in the literature by *Vincent and Fritts* [1987], *Eckermann and Vincent* [1989], *Vincent and Eckermann* [1990] and *Eckermann et al.* [1995]. Furthermore, analogous analytic techniques have been utilized by *Hamilton* [1991] and *Tsuda et al.* [1994b]. They are used here to study the observed horizontal wind velocity fluctuations over Macquarie Island and the Cocos Islands.

3.8 Summary

The material presented in this chapter describes the experimental data that are utilized and the analysis techniques that are employed in later chapters. Radiosonde temperature measurements of sufficient vertical resolution and precision to study the spectral distribution of gravity waves are available from all stations of Table 3.1. However, simultaneous horizontal wind velocity measurements of sufficient vertical resolution, precision and accuracy are only available from Macquarie Island and the Cocos Islands. Since temperature measurements are obtained using the same radiosonde systems in each case, any inferred differences between stations are not due to differing measurement techniques. The same is also true of the wind velocity measurements from Macquarie Island and the Cocos Islands.

The interpretation of vertical wavenumber power spectra of normalized temperature fluctuations is complicated by such issues as the sonde's horizontal drift, the sonde's finite ascent

velocity and the uneven vertical spacing of observations. However, it is the temperature sensor response time, especially within the lower stratosphere, that is of greatest concern. This may be as large as 10 s at stratospheric heights and will probably cause significant attenuation of spectral amplitudes at high vertical wavenumbers. A correction technique has been developed to deal with the problem.

When simultaneous measurements of temperature and horizontal wind velocity are available, more information about gravity waves may be obtained than is the case with temperature measurements alone. Most notably, the dominant directions of vertical and horizontal phase propagation may be determined by using rotary spectrum and Stokes parameter analysis techniques. The dominant directions inferred from several soundings, when considered together, provide a qualitative picture of the degree of wave field anisotropy over a given time interval [e.g., *Hamilton*, 1991; *Tsuda et al.*, 1994b; *Eckermann et al.*, 1995]. Yet the recent gravity wave model proposed by *Fritts and VanZandt* [1993] suggests that the net vertical flux of zonal and meridional momentum depends on wave energy density and on some measure of horizontal wave field anisotropy. It would therefore seem reasonable to expect that estimates of net vertical momentum flux might be made from simultaneous measurements of horizontal wind and temperature. A technique for doing this is reviewed in chapter 7 and is based on ideas proposed by *Eckermann and Vincent* [private communication, 1994].

The following chapter presents an analysis of temperature fluctuation measurements from all stations listed in Table 3.1 This is a study of the variance characteristics of gravity waves in the southern hemisphere troposphere and lower stratosphere. Some of these results also appear in *Allen and Vincent* [1995]. The analysis of simultaneous wind and temperature measurements from Macquarie Island and the Cocos Islands are presented in chapters 5 and 6, respectively. These data are from very different geographic locations and provide further information about gravity waves over near-equatorial and midlatitude locations. In chapter 7, estimates of the net vertical flux of zonal and meridional momentum are presented and discussed while the conclusions of this study are summarized in chapter 8.

Chapter 4

Variance Characteristics of Gravity Waves

4.1 Introduction

The main purpose of this chapter is to study seasonal and geographical variations of gravity wave temperature variance. At present the extent of these variations is not well understood, especially within the southern hemisphere, and the available data set of high-resolution radiosonde measurements may be used to address the problem. Furthermore, it is possible to compare the gravity wave saturation theories of *Smith et al.* [1987], *Hines* [1991b] and others with observed spectral amplitudes. However, due to various theoretical and experimental uncertainties, it is difficult to distinguish between these theories on the basis of spectral amplitude calculations alone. Nevertheless, a discussion is provided in section 4.5.

The results that are presented provide climatological information about the atmospheric gravity wave field in the troposphere and lower stratosphere, and this is the intent of the analysis undertaken. Climatological variations of wave activity, in a given altitude range, may reflect variations in the strength of wave sources or the effects of wave interactions with the mean flow. However, the temporal and horizontal resolution of the available radiosonde measurements[1] is generally too poor to resolve the temporal and horizontal scales of gravity waves[2]. It is therefore difficult to isolate particular wave sources and, at best, it is only possible to provide circumstantial evidence of the dominant sources of climatological-mean

[1] Successive radiosonde soundings are typically separated by either 12 or 24 hours while the various stations are separated by many hundreds of kilometres (see Figures 3.1 and 3.2).

[2] Some gravity wave frequencies may be resolved at low latitude stations where f approaches zero.

Station Name	Time Intervals	Station Name	Time Intervals
Adelaide	May 1991 – Feb 1993	Hobart	Apr 1991 – May 1992
Albany	Mar 1991 – May 1992	Learmonth	Jun 1991 – May 1992
Alice Springs	May 1991 – May 1992	Lord Howe	Jun 1991 – May 1992
Cobar	Apr 1991 – May 1992	Mount Isa	Apr 1991 – May 1992
Darwin	Jun 1991 – May 1992	Port Hedland	Nov 1990 – May 1992
Davis	Jul 1992 – Apr 1993	Townsville	Jun 1991 – May 1992
Forrest	Apr 1991 – May 1992	Wagga	May 1991 – May 1992
Gladstone	Jun 1991 – May 1992	Willis Island	Aug 1991 – May 1992
Gove	Jun 1991 – May 1992	Woomera	Apr 1991 – May 1992

Table 4.1: The radiosonde data considered by *Allen and Vincent* [1995].

wave energy. Other studies [e.g., *Eckermann and Vincent*, 1993; *Pfister et al.*, 1993a,b; *Sato et al.*, 1995], which use data from various observational campaigns, can better delineate gravity wave source mechanisms.

Some of the results presented in this chapter also appear in *Allen and Vincent* [1995] where a smaller data set was considered. At the time of that analysis, much of the data from the Antarctic and sub-Antarctic stations, and all of the data from the Cocos Islands were not yet available. Details of the data considered by *Allen and Vincent* [1995] are presented in Table 4.1. Notice that only 10 months of data from Davis were analyzed. In fact more data were available at the time but many soundings after April 1993 did not reach higher than 20 km due to shortages of hydrogen at that particular station. The stratospheric data record from Davis, between April 1993 and January 1994, is comparatively poor as a consequence.

The results discussed here follow those of *Allen and Vincent* [1995] although additional results from Mawson, Casey, Macquarie Island and the Cocos Islands are considered where appropriate. The basic data set described in Table 4.1 was analyzed consistently by applying the same analysis techniques in all cases. However, the additional data were not always analyzed in exactly the same manner for various reasons. While this may cause some difficulties, the basic conclusions of *Allen and Vincent* [1995] do not change when the additional results are considered.

4.2 The Background Atmosphere

The characteristics of the basic state atmosphere varies from station to station and from season to season. An understanding of these characteristics is of importance since the characteristics of gravity waves can be significantly influenced by changes in the basic state atmosphere. The purpose of this section is to describe the mean conditions of the troposphere and lower stratosphere over the meteorological stations given in Table 3.1.

The basic structure of the background temperature profile in the lower regions of the atmosphere is well represented by the structure illustrated in Figure 1.1. However, the height of the tropopause does show significant variation with latitude. This may be as high as 18 km at equatorial locations or as low as 8 km over the poles. The latitude dependence of tropopause height is illustrated schematically in Figure 1.3.

Time-height contours of basic-state temperature and Väisälä-Brunt frequency squared derived from radiosonde observations at Gove, Adelaide and Davis are illustrated in Figures 4.1, 4.2 and 4.3, respectively. These stations were chosen to be representative of low, middle and high-latitude sites. Each diagram was constructed by averaging data, from all soundings that reached altitudes of 24 km or greater, into 4 km by 1 month bins. Also, the raw data were bilinearly interpolated such that smoother contour patterns were produced. Values of Väisälä-Brunt frequency squared were calculated from temperature measurements by using (1.5).

The examples from Gove and Davis (Figures 4.1 and 4.3, respectively) are extremes in the sense that the typical tropopause height at other stations (e.g., Figure 4.2) tend to fall between the typical tropopause heights found at these sites. The typical position of the tropopause is best represented by the contours of Väisälä-Brunt frequency squared and is clearly defined at Gove, and at Davis during summer, where steplike increases in Väisälä-Brunt frequency squared are observed. However, at Adelaide, and at Davis during winter, the tropopause height is less clearly defined. It is not uncommon for there to exist more than one height at which the meteorological definition of a tropopause is satisfied at these sites. Nevertheless, for the purposes of gravity wave studies, it is the regions where N^2 is approximately constant that are of interest and such regions are clearly defined in Figures 4.1, 4.2 and 4.3.

The mean winds over all stations, with the exceptions of Macquarie Island, the Cocos

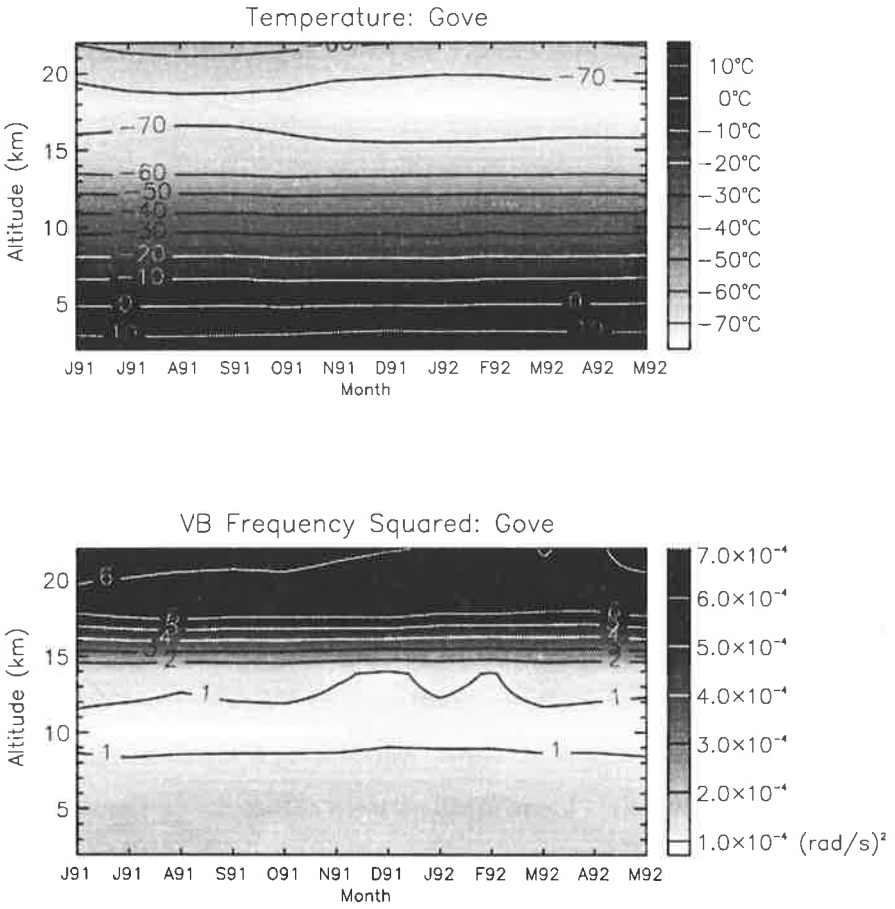

Figure 4.1: Time-height contours of temperature and Väisälä-Brunt frequency squared observed at Gove between June 1991 and May 1992. The raw data have been interpolated to produce a smoother contour pattern.

Islands, Mawson and Casey[3], are not known from the available data. It is therefore necessary to consider reference atmosphere winds for information of this nature. Figure 1.3 illustrates latitude-height contours of zonal-mean zonal winds based on reference atmosphere data. The salient features of interest here are, firstly, the winter wind maximum at high latitudes in the lower stratosphere (the polar vortex), and secondly, the winter wind maximum near the tropopause at 30°S (the sub-tropical jet stream). It is clear that the Antarctic and sub-Antarctic stations will experience the strongest upper-level winds although there is significant seasonal variation in the strength of these winds. For more details regarding the characteristics of reference atmosphere winds see *Marks* [1989].

[3]The Digicora wind measurements from Mawson and Casey are thought to be of poorer accuracy than those from Macquarie Island and the Cocos Islands. Some Digicora mean winds are presented in later chapters.

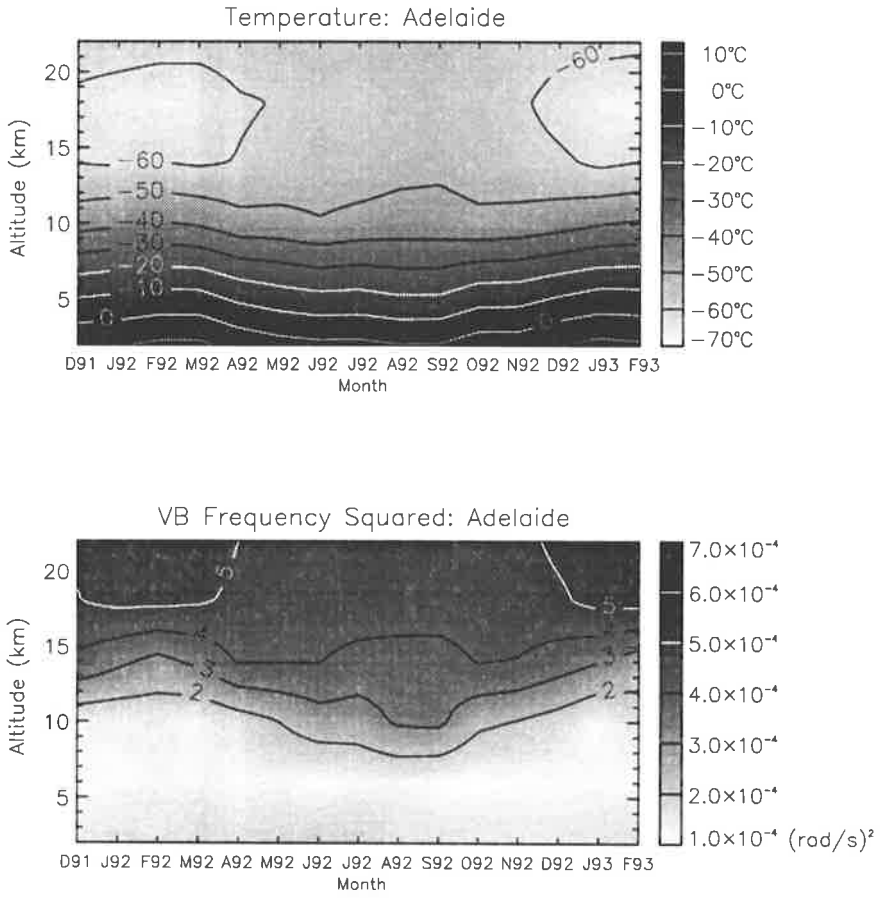

Figure 4.2: As in Figure 4.1, but for data obtained at Adelaide between December 1991 and February 1993.

4.3 Gravity Wave Power Spectra

Radiosonde profiles of normalized temperature fluctuations, $\hat{T}'(z)$, were spectrally analyzed in two altitude intervals, usually between 2.0 and 9.0 km in the troposphere and between 17.0 and 24.0 km in the lower stratosphere. However, at some stations slightly different altitude intervals were used and these are given in Table 4.2. The principal reason for choosing each interval was to ensure a stationary spectrum since, as discussed earlier, the vertical wavenumber power spectrum of normalized temperature fluctuations is anticipated to be dependent upon N^4. Figures 4.1, 4.2 and 4.3 may be used as a guide to determine which are the most appropriate altitude intervals to use.

Examples of radiosonde temperature profiles observed from Gove, Adelaide, and Davis during southern-hemisphere summer and winter months are illustrated in Figures 4.4, 4.5 and 4.6. Successive profiles, which usually correspond to either a 12-hour or 1-day delay between

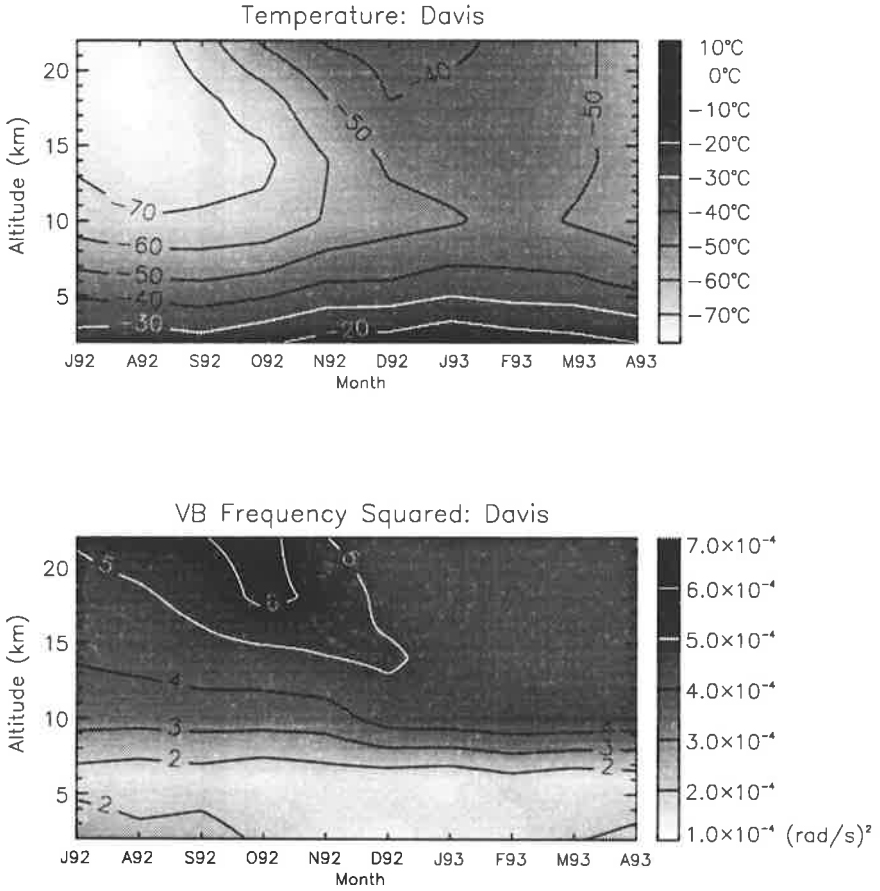

Figure 4.3: As in Figure 4.1, but for data obtained at Davis between July 1992 and April 1993.

soundings, are displaced by 10°C or 20°C, respectively. The altitude intervals used for power spectrum analysis are illustrated by the shaded regions in each plot. These correspond to the altitude intervals that are given in Table 4.2.

Data segments for which continuous measurements were unavailable throughout the entire height interval of interest or for which a tropopause was found within this interval were not included in the power spectrum analysis. The former condition often arose when the sonde did not reach the maximum height required for a given station as defined in Table 4.2. The latter condition also arose from time to time and the relevant profiles were excluded to ensure a constant background Väisälä-Brunt frequency squared profile. Approximately 30% of all available stratospheric data segments were rejected in this manner. This figure, however, was much smaller for tropospheric data. The particular height ranges that were employed at each station were chosen in order to minimize the number of profiles rejected. The number of profiles that were finally analyzed, in both the troposphere and lower stratosphere,

Station Name	Height Intervals for Data Analysis, km		Number of Available Soundings	Number of Soundings Analyzed	
	Troposphere	Stratosphere		Troposphere	Stratosphere
Adelaide	2.0–9.0	17.0–24.0	1344	1224	909
Albany	2.0–9.0	17.0–24.0	519	481	364
Alice Springs	2.0–9.0	17.0–24.0	366	336	244
Cobar	2.0–9.0	17.0–24.0	528	498	373
Darwin	2.0–9.0	17.5–23.5	730	655	453
Davis	1.0–8.0	16.0–23.0	556	481	435
Forrest	2.0–9.0	17.0–24.0	421	402	343
Gladstone	2.0–9.0	17.0–24.0	435	408	263
Gove	2.0–9.0	17.5–24.5	457	431	313
Hobart	2.0–9.0	16.0–23.0	852	799	452
Learmonth	2.0–9.0	17.0–24.0	348	339	239
Lord Howe	2.0–9.0	17.0–24.0	444	401	287
Mount Isa	2.0–9.0	17.0–24.0	575	520	350
Port Hedland	2.0–9.0	18.0–25.0	531	519	474
Townsville	2.0–9.0	17.0–24.0	341	334	234
Wagga	2.0–9.0	17.0–24.0	485	447	331
Willis Island	2.0–9.0	17.5–24.5	304	286	249
Woomera	2.0–9.0	17.0–24.0	544	505	393

Table 4.2: The height intervals and number of soundings used for power spectrum analysis. The data listed are those studied by *Allen and Vincent* [1995].

are provided in Table 4.2.

Vertical wavenumber power spectra calculated from individual temperature profiles were averaged in order to improve the confidence limits of spectral amplitude estimates. Following the suggestion of *T. E. VanZandt* [private communication, 1992], normalized individual power spectra were averaged, that is, each spectrum was divided by its total variance before averaging. The purpose of this technique was to ensure that all spectra contribute equally to the shape of the mean spectrum. Once calculated, the mean spectrum was renormalized by multiplying by the averaged total variance[4].

Examples of mean vertical wavenumber power spectra of normalized temperature fluctuations observed at Adelaide during both summer and winter months within the altitude ranges of 2.0–9.0 km (troposphere) and 17.0–24.0 km (lower stratosphere) are illustrated in

[4]Mean spectra were calculated over 1-month periods and then stored to disk. However, for the purpose of economy, the spectra presented in this chapter are 3-month averages. These were obtained by taking a weighted arithmetic mean of 1-month average spectra where the weighting was proportional to the number of temperature profiles analyzed during each month.

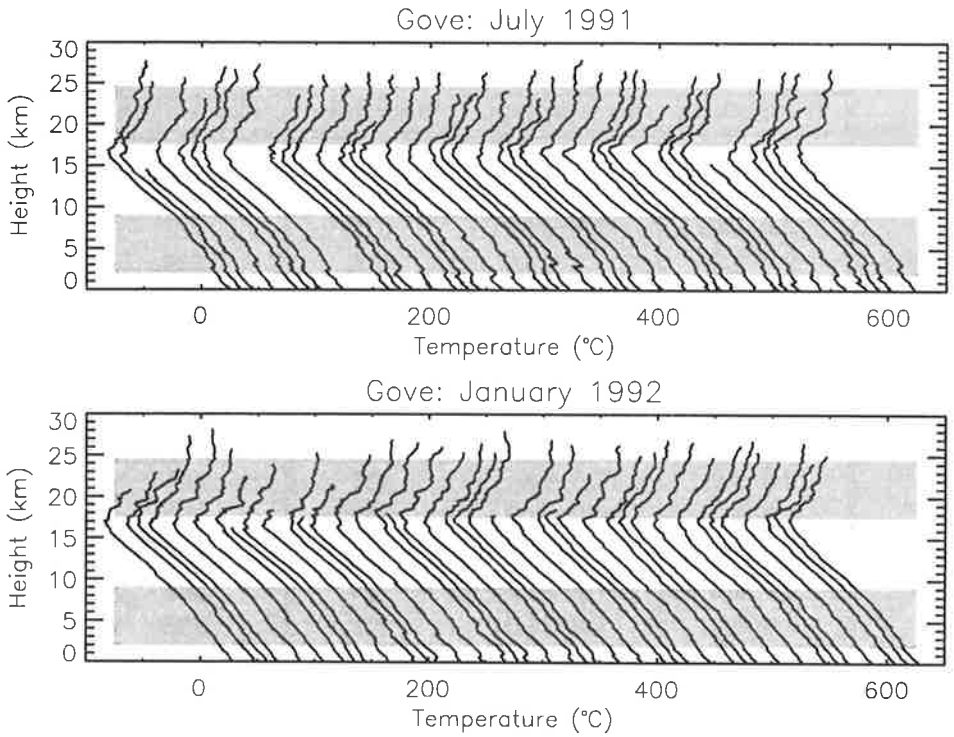

Figure 4.4: Examples of temperature profiles observed at Gove (12°S, 137°E) during the months of January and July. Successive profiles are displaced by 10°C per 12-hour delay between soundings. Shaded areas indicate the height intervals over which temperature profiles were spectrally analyzed.

Figure 4.7. Also plotted, for the case of stratospheric spectra, are the response-time corrected power spectra. These are related to the observed spectra according to (3.6) where τ was obtained using the technique described in appendix A and where an averaged V_0 was used since the balloon ascent velocity is known for each individual temperature profile. In this thesis it is the response-time corrected spectrum that is believed to provide the best estimate of the true normalized temperature power spectral density and all of the stratospheric power spectra presented hereinafter (with the exception of those in Figure 4.10) will have undergone this correction procedure. Recall, however, that tropospheric power spectra do not require correction to good approximation. Figure 4.7 also illustrates the same spectra in area preserving forms.

Each power spectrum in Figure 4.7 has been presented with a maximum wavenumber of 8.0×10^{-3} cycles per metre (cpm). However, the Nyquist spatial frequency for data interpolated at 50-m altitude intervals is 0.01 cpm. The cutoff wavenumber was chosen since the mean separation of adjacent points for a given temperature profile was found to vary about 50 m. As a consequence, spectral amplitudes at the very highest wavenumbers may

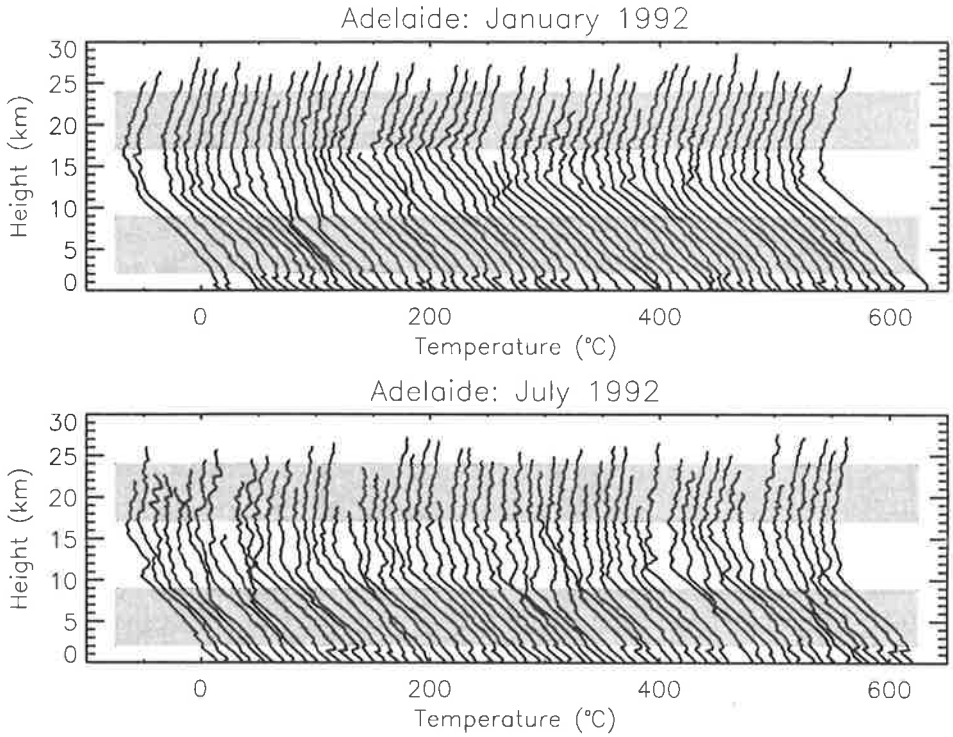

Figure 4.5: As in Figure 4.4, but for temperature profiles observed at Adelaide (35°S, 139°E) during the months of January and July.

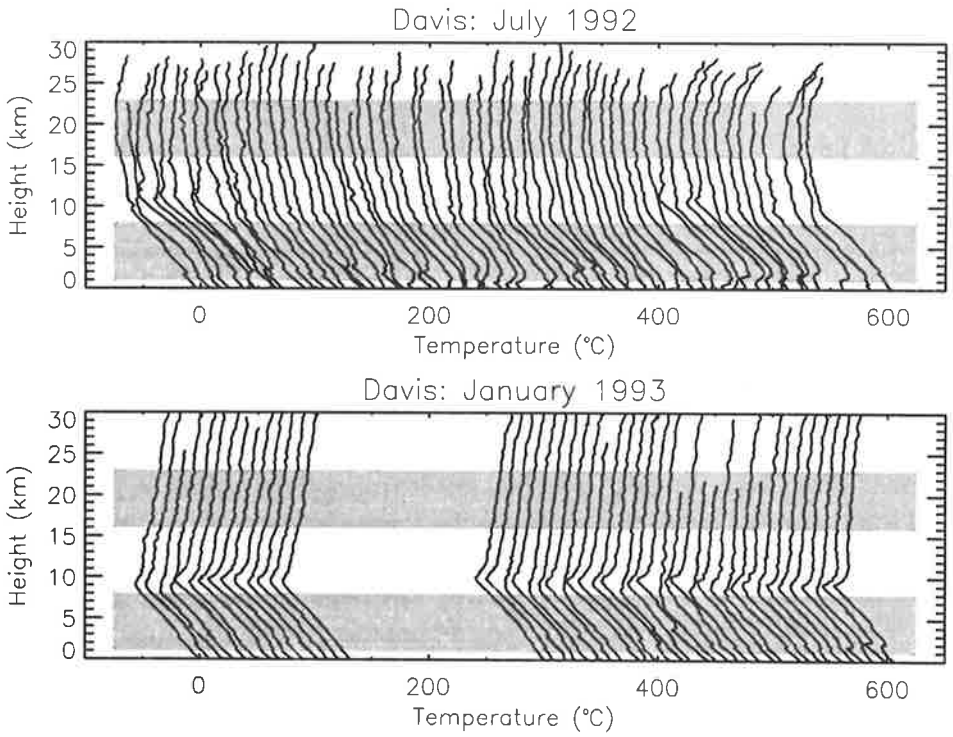

Figure 4.6: As in Figure 4.4, but for temperature profiles observed at Davis (69°S, 78°E) during the months of January and July.

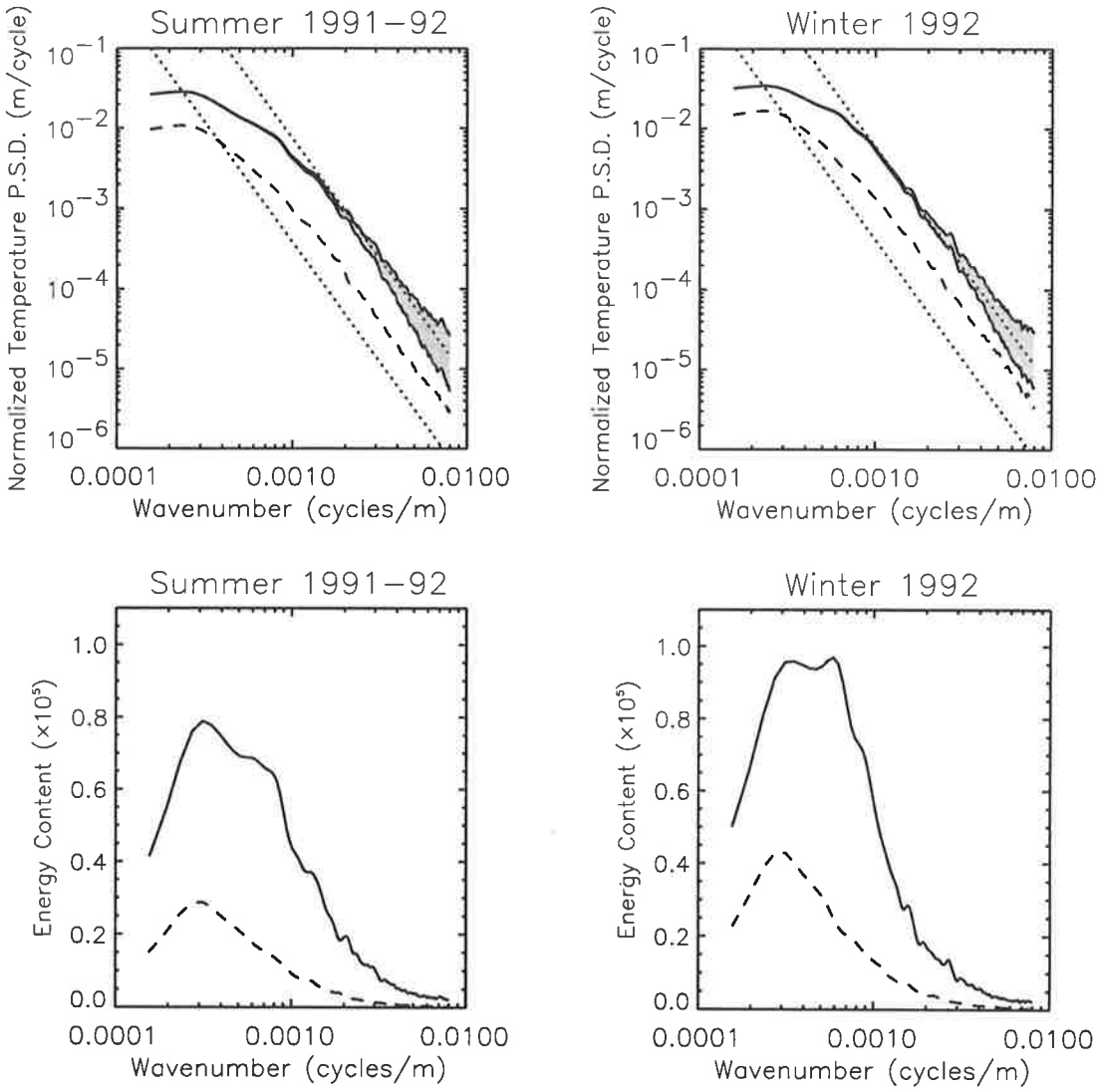

Figure 4.7: The mean vertical wavenumber power and area preserving spectra of normalized temperature fluctuations observed at Adelaide during summer (December, January, February) and winter (June, July, August) months. Both tropospheric (dashed lines) and stratospheric (solid lines) spectra are displayed as are the theoretical saturation limits due to *Smith et al.* [1987] (dotted lines). For stratospheric observations, the corrected and uncorrected power spectra are illustrated where the correction technique is described in section 3.4 and appendix A. The shaded regions comprise approximately 5% of the total area under each corrected power spectrum. Stratospheric area preserving spectra have been corrected for response time distortion.

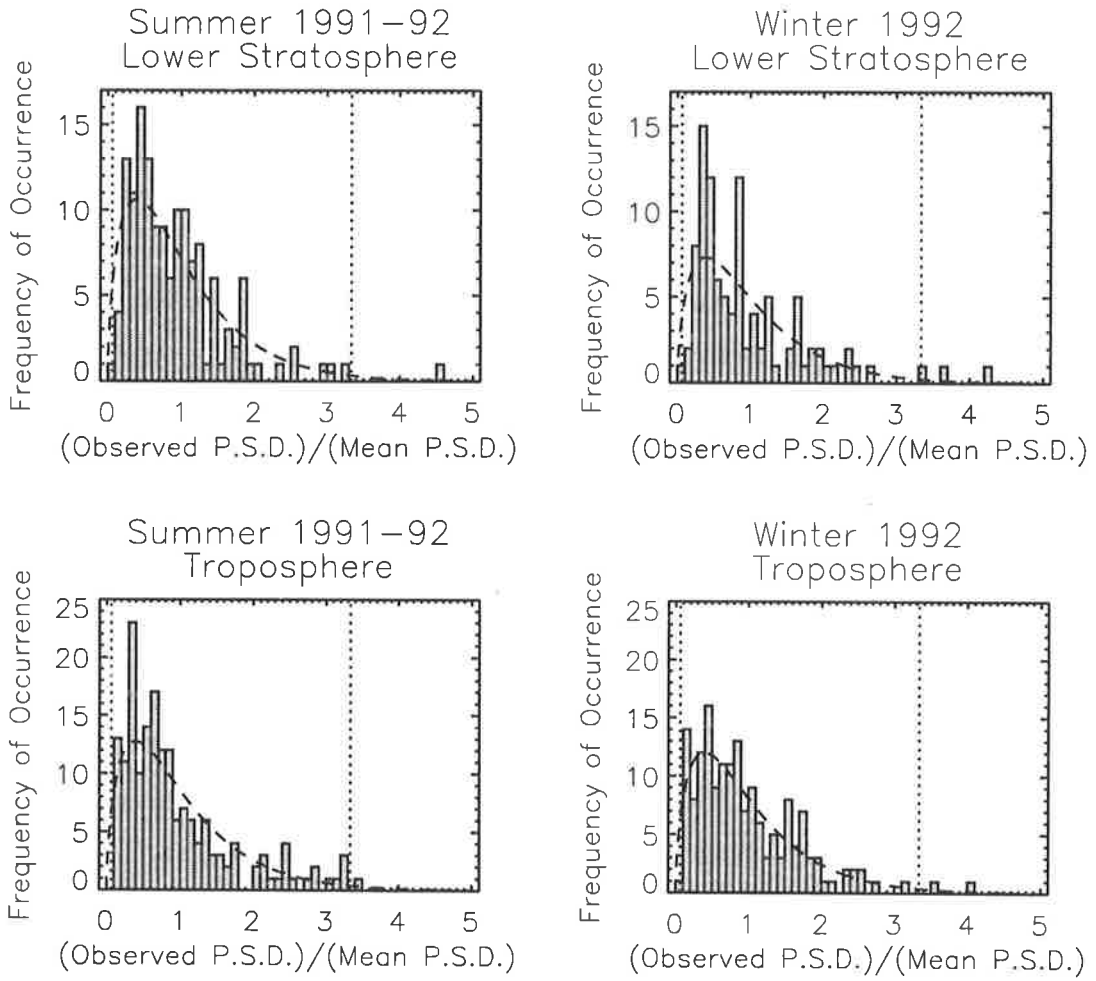

Figure 4.8: Statistical distributions of $E_{\hat{T}'}(m/2\pi = 2 \times 10^{-3}$ cpm) divided by the arithmetic mean value during both summer and winter months at Adelaide (as in Figure 4.7). The probability distribution function $P\left(\chi^2_\nu/\nu\right)$, for $\nu = 3.3$, is also plotted in each case (dashed lines) where 96% of the area under $P\left(\chi^2_\nu/\nu\right)$ is found between the dotted lines. Both tropospheric and stratospheric spectral amplitudes are considered.

be biased due to aliasing.

The procedure of averaging spectra may potentially obscure short-time-scale variations of gravity wave spectral form. To demonstrate that this is not the case consider Figure 4.8. In this diagram statistical distributions of observed power spectral density, at vertical wavenumber $m/2\pi = 2 \times 10^{-3}$ cpm, are illustrated. The individual power spectra used to generate each plot were the same as those used to determine the mean spectra in Figure 4.7.

If $F(m)$ is power spectral density then the statistical distribution of $F(m)/\overline{F(m)}$ is approximated by χ^2_ν/ν where χ^2_ν is the so-called chi-square random variable [*Jenkins and Watts*,

1968]. The probability distribution function of χ^2_ν is given by

$$P\left(\chi^2_\nu\right) = \frac{1}{2^{\nu/2}\Gamma(\nu/2)} \left(\chi^2_\nu\right)^{(\nu-2)/2} \exp\left(-\chi^2_\nu/2\right) \tag{4.1}$$

where Γ is the gamma function and ν is the number of degrees of freedom [e.g., *Bevington*, 1969]. The usual definition of a probability distribution function applies here in that the integral of $P\left(\chi^2_\nu\right)$ between $\chi^2_\nu = a$ and $\chi^2_\nu = b$ is the probability that χ^2_ν lies between a and b. For spectra calculated using the Blackman-Tukey algorithm with a 90% lag Bartlett window the number of degrees of freedom is $\nu = 3.3$ [*Jenkins and Watts*, 1968].

Figure 4.8 illustrates the distribution of $E_{\hat{T}'}(m/2\pi = 2 \times 10^{-3}$ cpm) divided by the arithmetic mean value for both tropospheric and stratospheric spectra during summer and winter months at Adelaide. Also plotted is the probability distribution function $P\left(\chi^2_\nu/\nu\right)$ which has been scaled in each case such that the area is equivalent to that of the observed distribution. If the observed spectra are time invariant during the three-month periods considered here then Figure 4.8 should illustrate sample distributions of a parent population defined by χ^2_ν/ν. This does appear to be the case by inspection[5]. Furthermore, similar results are found at other wavenumbers although these are not reported here.

It is evident from Figure 4.8 that short-time-scale geophysical variations of power spectral density are not resolved in the data and that some form of averaging is required to study temporal variations in spectral form. This may be achieved either by averaging in wavenumber space or in time. The latter possibility is chosen here so that information regarding the fine structure of spectra is maintained.

One interesting feature of Figure 4.7 is that the tropospheric power spectra have spectral amplitudes, at high vertical wavenumbers, that are significantly larger than the theoretical saturation limits proposed by *Smith et al.* [1987]. Similar results were also reported by *Tsuda et al.* [1991] for tropospheric spectra calculated from radiosonde observations obtained at Shigaraki, Japan (35°N, 136°E). In contrast, the stratospheric power spectra of Figure 4.7 are, more or less, consistent with the theoretical saturation limits of *Smith et al.* [1987]. Again, a similar result was also reported by *Tsuda et al.* [1991].

The interpretation of tropospheric spectra is difficult since the troposphere is also believed to be the dominant source of gravity wave energy. Recall that *Wunsch* [1976] found oceanic

[5] An analogous result is reported by *Nastrom et al.* [1996] who used a logarithmic x-axis to demonstrate that the distribution of the logarithm of spectral amplitudes, at a given vertical wavenumber, is roughly normally distributed.

spectral amplitudes[6] that were larger than usual near the Muir Seamount of the western North Atlantic ocean. *Wunsch* [1976] argued that this provided prima facie evidence of an oceanic gravity wave source since the wave spectrum near a source would require some time before reaching its equilibrium state. By analogy, the large spectral amplitudes in the troposphere may be indicative of the troposphere's role as the dominant source of atmospheric gravity wave energy.

However, this simple interpretation belies the complicated processes that may be occurring in the lower atmosphere which are distinct from those of the deep ocean. Convection is an important dynamical process in the troposphere, especially at equatorial latitudes or in the atmospheric boundary layer, and a convectively unstable atmosphere cannot support gravity wave motions. Furthermore, not only is convection a plausible source of gravity waves [e.g., *Pfister et al.*, 1993a; *Sato et al.*, 1995], but it is also possible that gravity wave displacements may trigger convection [e.g., *Uccellini and Koch*, 1987]. Therefore, a complex interaction between these very different dynamical processes may be occurring.

To investigate the possibility that convective layers are prominent in the troposphere over Adelaide, the fluctuations of N^2 are considered following *Tsuda et al.* [1991]. Figure 4.9 illustrates the occurrence frequency of N^2, averaged over 500-m intervals, within the altitude ranges of 2.0 to 9.0 km (troposphere) and 17.0 to 24.0 km (lower stratosphere) over Adelaide. These are the same altitude ranges used to determine the power spectra presented in Figure 4.7 and observations during both summer and winter months are considered as before.

The histograms of N^2 in the lower stratosphere are approximately fitted by a Gaussian distribution with N^2 never falling below zero. Therefore large convectively unstable layers are not present in the stratosphere over Adelaide, as was also found by *Tsuda et al.* [1991] over Shigaraki, Japan. However, the histograms of N^2 in the troposphere indicate that N^2 occasionally falls below zero and that convectively unstable layers may be present there. Nevertheless, the observed distribution appears to be clipped at $N^2 = 0$ and in the vast majority of cases N^2 is greater than zero. *Tsuda et al.* [1991] interpreted a similar result to be caused by gravity-wave-induced fluctuations of N^2 about some positive background value N_b^2 where, on occasion, the wave amplitudes were such that convective overturning

[6]The observed spectral amplitudes were found to be significantly larger than those of the canonical GM75 model.

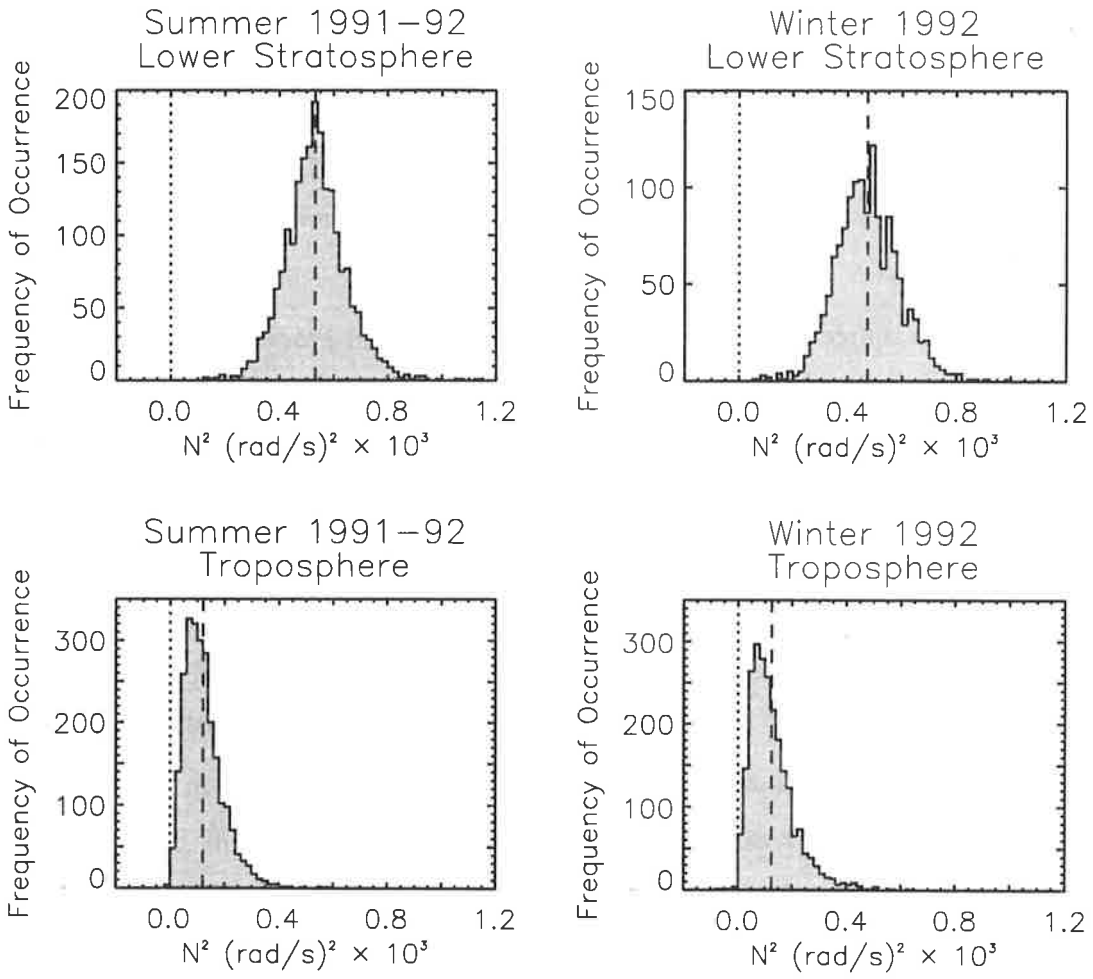

Figure 4.9: The distribution of N^2, averaged over 500-m altitude intervals, within the troposphere (2.0–9.0 km) and lower stratosphere (17.0–24.0 km) over Adelaide. The same observations were used as in Figure 4.7 while the mean values in each case are indicated by dashed lines.

occurred. Convective overturning acts to reduce the amplitudes of perturbations and therefore the observed N^2 distribution was clipped and asymmetric [see *Tsuda et al.*, 1991]. This interpretation is followed here such that the variance characteristics of the observed perturbations are interpretated to be those of gravity waves that are commonly supported, not only in the lower stratosphere, but in the troposphere over Adelaide also.

As discussed in chapter 3, the uneven vertical spacing of measurements may lead to erroneous power spectral density estimates if equispaced analysis algorithms are used. In this section a comparison is made between three different algorithms using stratospheric data obtained over Adelaide during summer months. The three algorithms considered are, firstly, the Blackman-Tukey algorithm [see *Dewan et al.*, 1988], secondly, the fast Fourier

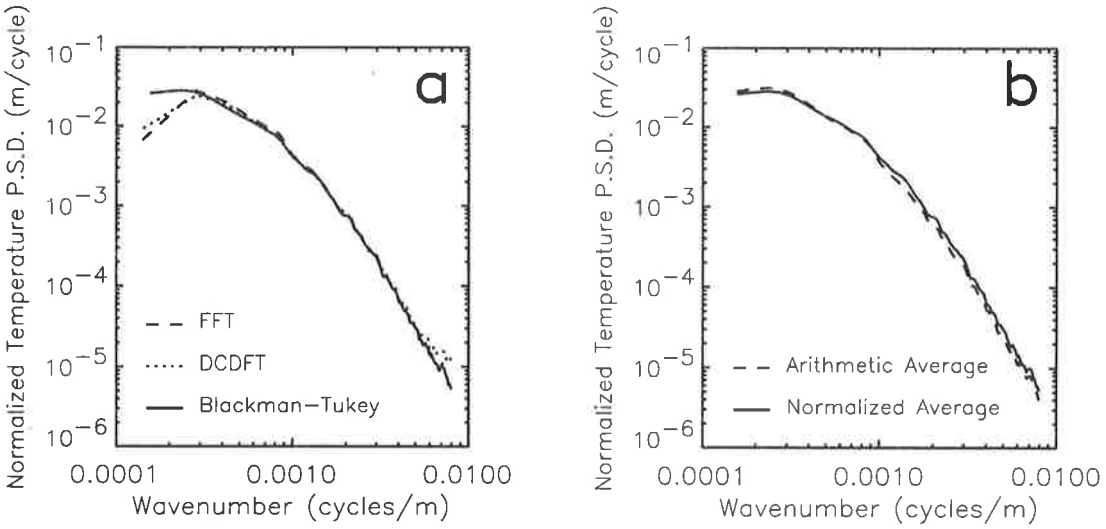

Figure 4.10: (a) The mean summer spectrum (1991-92) in the lower stratosphere over Adelaide calculated using the Blackman-Tukey (solid line), FFT (dashed line) and DCDFT (dotted line) algorithms. (b) The mean summer spectrum in the lower stratosphere over Adelaide (1991-92) calculated by arithmetic average (dashed line) and by arithmetic average of normalized individual spectra (solid line). See text for more details.

transform (FFT) algorithm, and thirdly, the so-called date-compensated discrete Fourier transform (DCDFT) algorithm proposed by *Ferraz-Mello* [1981]. In the latter two cases the power spectra were obtained by taking the modulus squared of the transformed data and then multiplying by a suitable constant. The purpose of comparison, following the recommendation of *Moore et al.* [1988], is to justify the use of equispaced algorithms by comparison with more appropriate (but possibly more computer intensive) methods such as the one due to *Ferraz-Mello* [1981].

Figure 4.10a illustrates the mean stratospheric power spectra derived from radiosonde data obtained over Adelaide during the months of summer 1991–92 using the Blackman-Tukey, FFT and DCDFT algorithms. For the two equispaced techniques the observed data were interpolated at 50-m intervals using cubic spline interpolation while, for the FFT and DCDFT algorithms, $\overline{T}$ was removed by fitting and then subtracting a cubic polynomial[7]. The results indicate broad agreement between all three techniques and so the Blackman-Tukey algorithm, after interpolation of data, appears to be valid in this instance.

There are some differences between the three spectra presented in Figure 4.10a. Firstly,

[7]For the Blackman-Tukey algorithm that is used here, $\overline{T}$ is estimated using a second-order polynomial. However, a cubic polynomial is removed after the normalized data are prewhitened [see *Dewan et al.*, 1988]. Therefore, cubic polynomials are used for the other algorithms in order to be consistent.

the amplitudes of the Blackman-Tukey spectrum do not match those of the other spectra at the lowest vertical wavenumbers. This is due to spectral leakage and will be discussed in more detail shortly[8]. Secondly, the DCDFT spectrum has slightly larger amplitudes at the highest vertical wavenumbers. This is probably caused by either aliasing or spectral leakage. Note, however, that there is no additional structure in the spectrum as was found by *Moore et al.* [1988] who used algorithms proposed by *Brillinger* [1972, 1983].

The mean spectra presented in Figure 4.10a were obtained by using the averaging technique described earlier in the section which involved normalizing each individual spectrum before arithmetic averaging. The purpose of this technique is to better estimate the mean spectral shape by allowing all individual spectra to contribute equally. If a simple arithmetic average is considered then the shape of the mean spectrum will most closely resemble the shapes of those individual spectra that happen to have larger spectral amplitudes [*T. E. VanZandt*, private communication, 1992]. Considerable importance must be attached to the mean shape of the spectrum since this is often used in comparison with various proposed gravity wave saturation theories.

Figure 4.10b compares mean spectra calculated using an arithmetic average of both individual spectra and normalized individual spectra. The individual spectra considered were from Adelaide during summer 1991-92 (as in Figure 4.10a) and the Blackman-Tukey algorithm was used in each case. This diagram illustrates that the choice of averaging technique has little bearing on the final result since the mean spectra calculated using both techniques are very similar. Nevertheless, the technique of averaging normalized individual spectra is chosen here and is applied consistently throughout this chapter.

It is apparent that the high-wavenumber spectral slope, t, is well defined by power spectral density calculations using radiosonde observations of temperature. However, the low-wavenumber, positive spectral slope, s, is not resolved in the spectra presented thus far. In fact little is known about the behaviour of the gravity wave spectrum at low vertical wavenumbers which is likely to be source dependent and need not have some fixed form. *VanZandt and Fritts* [1989] argue that s must be greater than zero otherwise unrealistic vertical fluxes of wave action or energy are obtained. Nevertheless, this parameter is yet to be determined experimentally.

Observations of gravity wave fluctuations in the lower regions of the atmosphere provide the best opportunity of defining s since m_* is thought to decrease with altitude. In

[8]The total areas under each spectrum of Figure 4.14a are approximately the same.

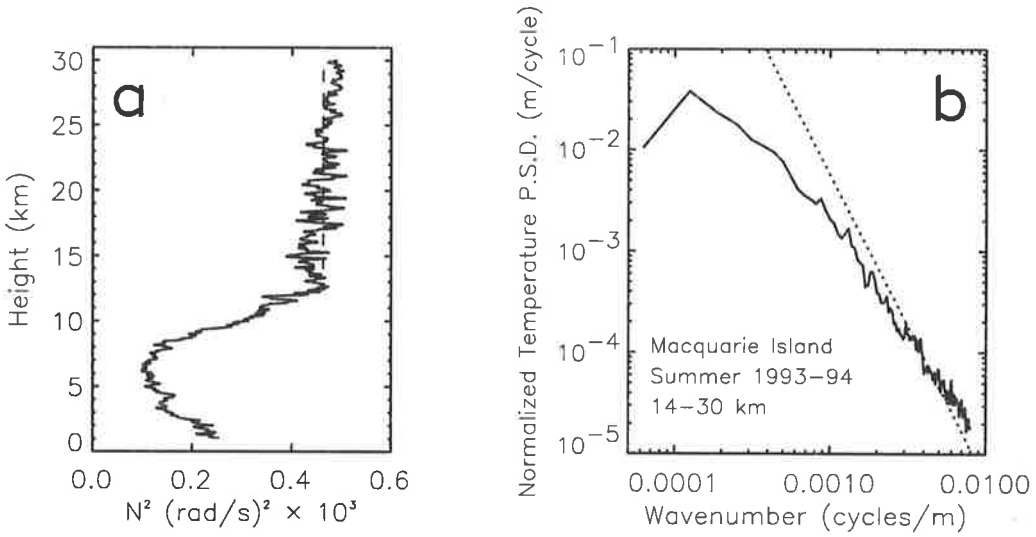

Figure 4.11: (a) The mean Väisälä-Brunt frequency squared profile observed at Macquarie Island during summer 1993-94. A dashed line indicates the height-averaged value between 14 and 30 km. (b) The mean spectrum in the lower stratosphere over Macquarie Island during summer 1993–94. The mean spectrum was calculated using an FFT algorithm between 14 and 30 km while the saturation limits due to *Smith et al.* [1987] are also plotted (dotted line).

this section an attempt is made to determine s from experimental observation. Data from Macquarie Island are considered since a large altitude range is available from this site over which the basic state N^2 profile is approximately constant. It should be noted, however, that problems caused by spectral nonstationarity, as discussed by *Eckermann* [1990b], may be significant in this instance.

Figure 4.11b illustrates the mean vertical wavenumber power spectrum of normalized temperature fluctuations calculated from observations made at Macquarie Island during summer months. The data considered were from altitudes between 14 and 30 km which is in the lower stratosphere over Macquarie Island. Only those soundings that reached 30 km or higher and had no meteorologically-defined tropopauses between 14 and 30 km were analyzed. The basic state Väisälä-Brunt frequency squared is approximately constant within this altitude range (see Figure 4.11a).

As was pointed out in the preceding chapter, the technique of prewhitening by differencing should not be used for the determination of s. In fact for $F(m) \propto m^s$, where $F(m)$ is power spectral density and s is positive, first differencing acts to "precolour", rather than "prewhiten", the observed data. Therefore significant spectral leakage may occur at low

vertical wavenumbers ($m \ll m_*$) if gravity wave fluctuation data are treated by differencing[9]. The mean spectrum presented in Figure 4.11b has been calculated using the FFT algorithm[10] where the effects of spectral leakage are minimized by application of a Welch window [e.g., *Press et al.,* 1988]. Also, the basic state temperatures were obtained by fitting third-order polynomials in each case. The FFT algorithm, rather than the Blackman-Tukey algorithm, was chosen since the resultant mean spectrum is not oversampled in spatial frequency. As such, this spectrum is more illustrative as will become apparent shortly.

The spectral amplitudes in Figure 4.11b, with the exception of the first spectral ordinate, decrease monotonically with increasing vertical wavenumber (or at least their trends do). Therefore, any determination of s must rely on only two independent points[11]. Furthermore, the first ordinate cannot be known to great accuracy unless $\overline{T}(z)$ is exactly given by a third-order polynomial in each case and is therefore adequately removed. As a consequence, it must be concluded that s cannot be determined with reliability from the illustrated spectrum.

The problem of estimating s is linked to that of removing $\overline{T}(z)$ from the observed temperature profiles. In Figure 4.11, $\overline{T}(z)$ was removed by fitting, and then subtracting, a third-order polynomial. However, other plausible techniques can be used. For example, a fitted polynomial of different order might be considered[12] or, alternatively, a monthly mean profile might be removed from individual profiles. However, in the latter case, fluctuations which have temporal scales that are distinct from those of gravity waves may not be adequately removed. Another technique was applied by *Tsuda et al.* [1994b] who analyzed 100 radiosonde soundings which were obtained at approximately 6-hour intervals during an observational campaign in Indonesia. These authors high-pass filtered their data in time[13] before studying fluctuation profiles of horizontal wind velocity. However, a similar technique cannot be applied here since the radiosonde soundings are typically of poorer temporal resolution and are often unevenly spaced in time.

[9]It must be noted that *Tsuda et al.* [1989] arrive at a different conclusion regarding the effects of prewhitening. They conclude that prewhitening preserves the spectral form at small vertical wavenumbers [*Tsuda et al.,* 1989, p. 2443]. However, their results were not reproduced with the Blackman-Tukey algorithm that was used here, which is the same as the technique used by *Dewan et al.* [1984, 1988]. Furthermore, when the raw data of Figure 4.10a were not prewhitened, the Blackman-Tukey algorithm provided spectral amplitudes at small vertical wavenumbers that were in good agreement with the spectral amplitudes produced by the other two techniques. This is consistent with the notion that differencing causes spectral leakage towards vertical wavenumbers $m \ll m_*$.

[10]This is the only instance in chapter 4 where the Blackman-Tukey algorithm is not used.

[11]More points are available if the Blackman-Tukey algorithm is used but the resultant spectra are oversampled and successive spectral ordinates are not independent.

[12]Note that a third-order polynomial may have two turning points and so can potentially remove significant power from the first spectral ordinate.

[13]The cutoff period was near to, but slightly larger than, the inertial period

The standard altitude range that is used for the calculation of power spectra is chosen to be 7 km in most cases (see Table 4.2). This is usually sufficient to resolve the dominant vertical scales as illustrated by area preserving spectra in the following section. However, it is insufficient for a reliable determination of s and no attempt is made to determine accurately the spectral amplitudes for $m \ll m_*$. Similarly, no attempt was made by *Tsuda et al.* [1991] who high-pass filtered their temperature profiles using a cutoff wavelength at 3.6 km. Spectral amplitudes at the lowest vertical wavenumbers were reduced as a consequence. In contrast, the spectra presented here display more gradual bends as m approaches m_*. This is likely to be caused by spectral leakage of variance from the characteristic wavenumber toward smaller vertical scales which is accentuated when treating gravity wave fluctuation profiles by differencing.

In summary, the material presented in this section describes the analysis techniques used to determine fluctuation power spectra. Specific examples were provided where appropriate using observations from Gove, Adelaide and Macquarie Island. The purpose of the following section is to apply these techniques to the entire data set described in Table 4.1. In particular, it is the seasonal and geographic variations of both gravity wave spectral form and also total gravity wave variance that are investigated.

4.4 Seasonal and Latitudinal Variations

Seasonal variations of gravity wave spectral form are studied using seasonal-mean spectra from four representative stations. These are Gove, Adelaide, Hobart and Davis, and the mean spectra are displayed in Figures 4.12, 4.13, 4.14 and 4.15, respectively. Mean spectra from other stations are presented in appendix B.

Significant seasonal variations of spectral form are not found at any of the four stations, at least to within a factor of approximately two or three. Small variations are evident but appear to be greatest within the low-wavenumber, source-dependent region of the spectrum, as might be expected. For example, the winter months at Adelaide and Hobart are characterized by an increase in frontal activity at ground level. Since cold fronts are known gravity wave sources [e.g., *Eckermann and Vincent*, 1993], it is plausible to suppose that the source-dependent region of the spectrum will display larger amplitudes during winter than during summer. Also *Kitamura and Hirota* [1989] have suggested a relationship between wave disturbances and the subtropical jet at the tropopause level which peaks during winter months. Larger

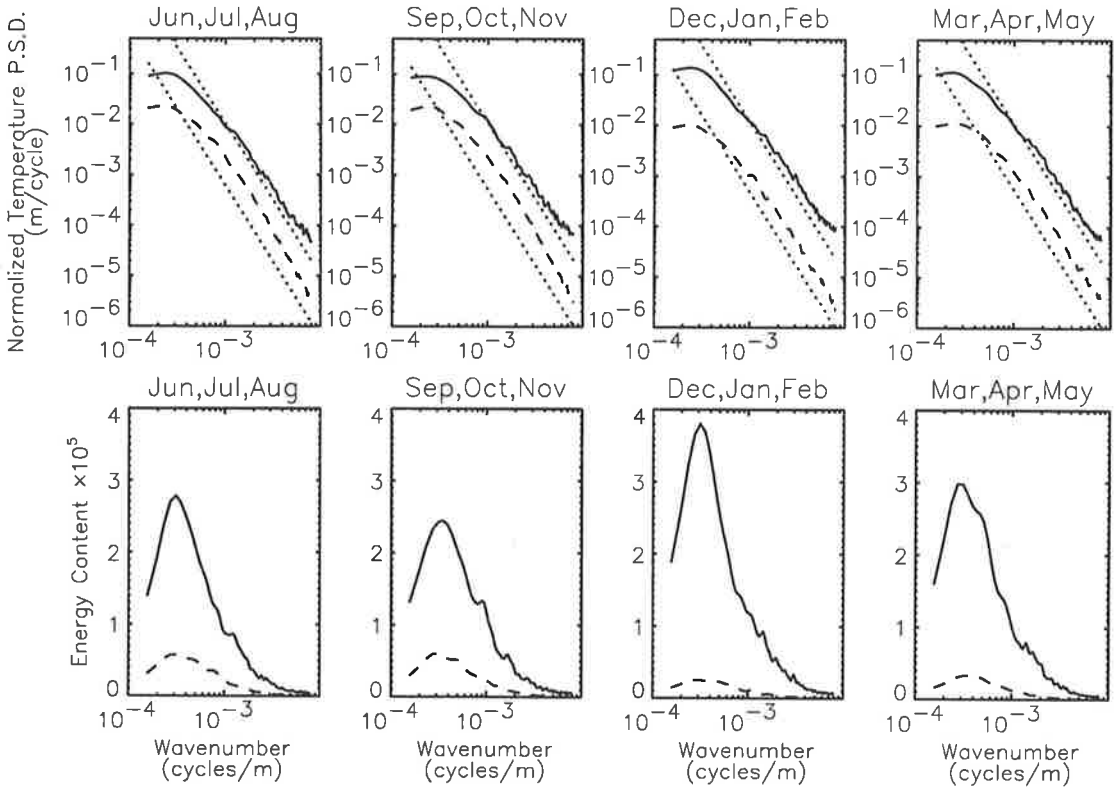

Figure 4.12: Vertical wavenumber power spectra and area preserving spectra of normalized temperature fluctuations observed at Gove (12°S, 137°E). Solid lines indicate stratospheric spectra while dashed lines indicate tropospheric spectra. Each spectrum is a 3-month average and the saturation limits due to *Smith et al.* [1987] are plotted for comparison purposes (dotted lines). The 95% confidence limits are approximately given by 0.85 and 1.15 multiplied by the spectral amplitude at each wavenumber.

spectral amplitudes are observed during winter and within the low-wavenumber region of the spectrum at both tropospheric and stratospheric heights over Adelaide and Hobart.

In contrast, the observed stratospheric spectra at Gove display larger amplitudes during the so-called monsoon season (December to February) than they do during other months. Convection is thought to be an important source mechanism at equatorial and near-equatorial locations [e.g., *Pfister et al.*, 1993a; *Tsuda et al.*, 1994b; *Karoly et al.*, 1996] and is much more prominent and widely spread during the monsoon season [e.g., *May et al.*, 1995]. Therefore, increased source activity is likely to be responsible for the large spectral amplitudes. However, tropospheric spectra at Gove appear to display larger spectral amplitudes during the months of June through to November than they do during the monsoon season. This apparently puzzling result will be considered in detail later.

The spectra observed at Davis are particularly interesting since the stratospheric spectra

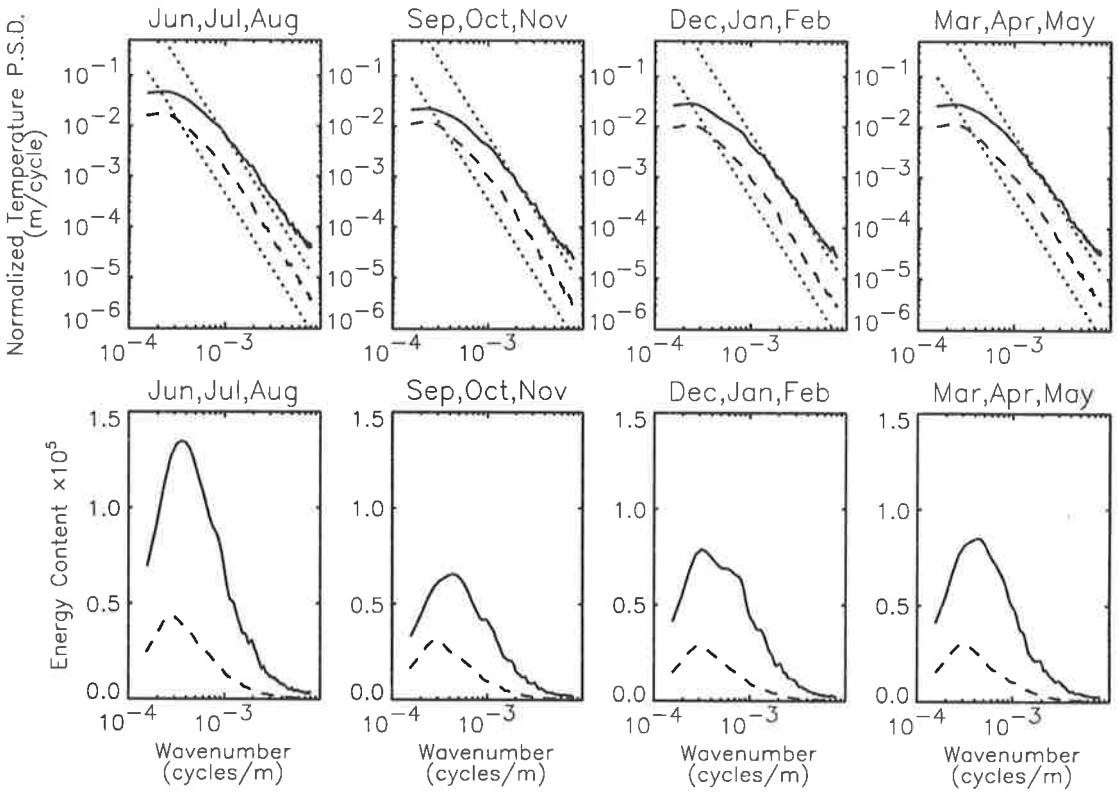

Figure 4.13: As in Figure 4.12, but for data observed at Adelaide (35°S, 139°E) between June 1991 and May 1992.

are significantly attenuated in comparison with the stratospheric spectra observed at low-latitude and midlatitude sites. In contrast, the spectral amplitudes within the troposphere are consistent with, or greater than, those found elsewhere. Therefore, assuming tropospheric spectra are indicative of wave sources, the attenuated spectra in the stratosphere are not caused by weak source activity. The seasonal variations at Davis are not particularly large[14] and so there exists considerable variability of the gravity wave spectral form between high and low latitudes.

Latitudinal variations of spectral form are studied by averaging spectra from various stations into eight latitude bands as is described in Table 4.3. These are time and, where possible, zonally averaged spectra, and are illustrated in both conventional logarithmic and area preserving forms in Figures 4.16 and 4.17, respectively. Note that not all available data have been used to generate these figures. The spectra considered were essentially those presented by *Allen and Vincent* [1995] with additional results from Macquarie Island,

[14]The seasonal variations in the lower stratosphere appear to be out of phase with those in the troposphere.

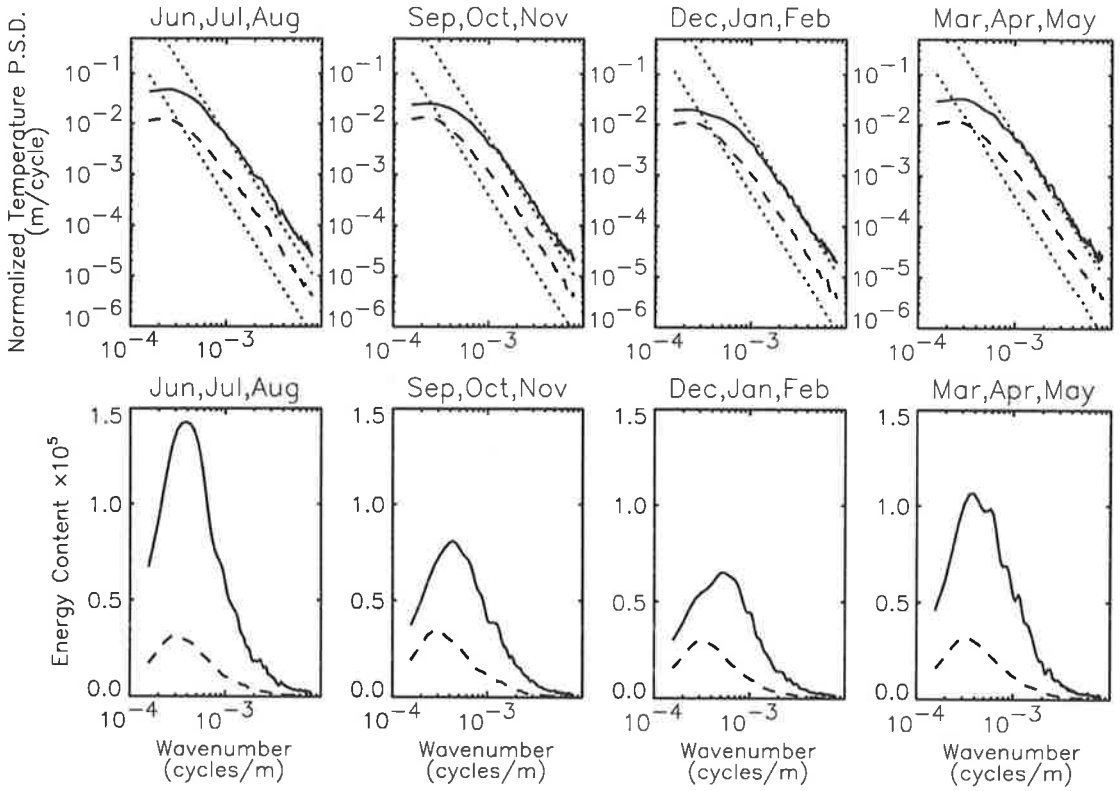

Figure 4.14: As in Figure 4.12, but for data observed at Hobart (43°S, 147°E) between June 1991 and May 1992.

between April 1993 and March 1994, also included[15].

Figures 4.16 and 4.17 demonstrate that spectral amplitudes and total variance decline with increasing latitude in the lower stratosphere of the southern hemisphere (Australian sector). For low-latitude and midlatitude sites, latitudinal variations occur predominantly within the low-wavenumber region of the spectrum. However, observed spectra at high-latitude sites appear to be significantly attenuated, in comparison with the saturation limits due to *Smith et al.* [1987], at all but the very highest wavenumbers. In contrast, there exists no corresponding variation of the tropospheric spectral form. Although data from Mawson and Casey have not contributed to Figures 4.16 and 4.17, the results from these stations are well represented by those from Davis (see appendix B). Similarly, observed spectra from the Cocos Islands are well represented by those obtained from Darwin and Gove.

The spectra that have been presented indicate that there exists some seasonal variation of gravity wave activity in the lower stratosphere which is superimposed upon a general decrease of wave activity with increasing latitude. The seasonal variations at low latitudes

[15]Data from Macquarie Island were spectrally analyzed over the same altitude intervals as those from Davis.

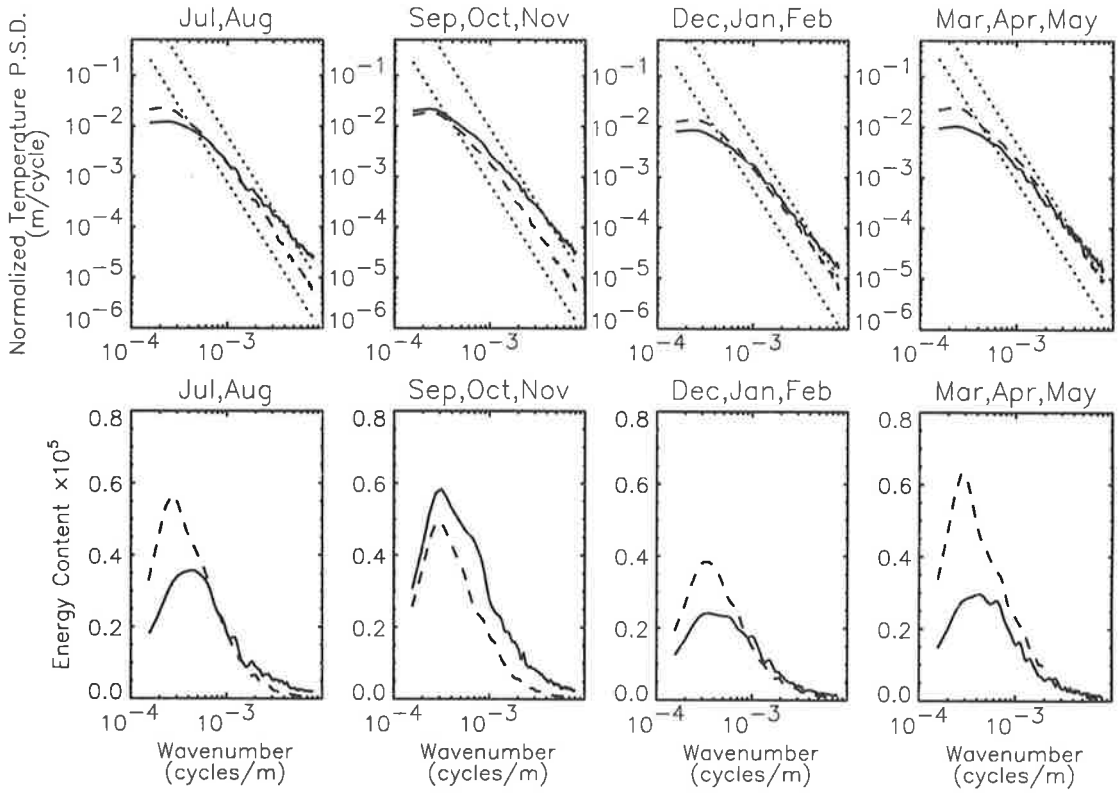

Figure 4.15: As in Figure 4.12, but for data observed at Davis (69°S, 78°E) between July 1992 and May 1993.

are out of phase with those at middle and high latitudes. Variations of tropospheric spectral form are more difficult to delineate and will be discussed later in section 4.7. Although the relevant results are not reported here, there appears to be little longitudinal variation of gravity wave activity. For example, there is little bias between results from the west and east coasts of Australia.

Figure 4.18 highlights the seasonal and latitudinal variations of gravity wave activity at low-latitude and midlatitude sites. This diagram illustrates contours of total gravity wave energy density, E_0, as a function of time and latitude within both the troposphere and lower stratosphere. All stations of Table 4.1, with the exceptions of Davis and Willis Island, were utilized while E_0 was obtained from observations of normalized temperature variance using (2.14) with $p = 5/3$. Contours were calculated after averaging data into 1-month bins using six of the seven latitude bands that were described in Table 4.3. Since the various latitude bands are unequally spaced, raw data were first interpolated at equal (and smaller) intervals using Delaunay triangulation.

Seasonal variations of stratospheric wave activity are easily recognized in Figure 4.18.

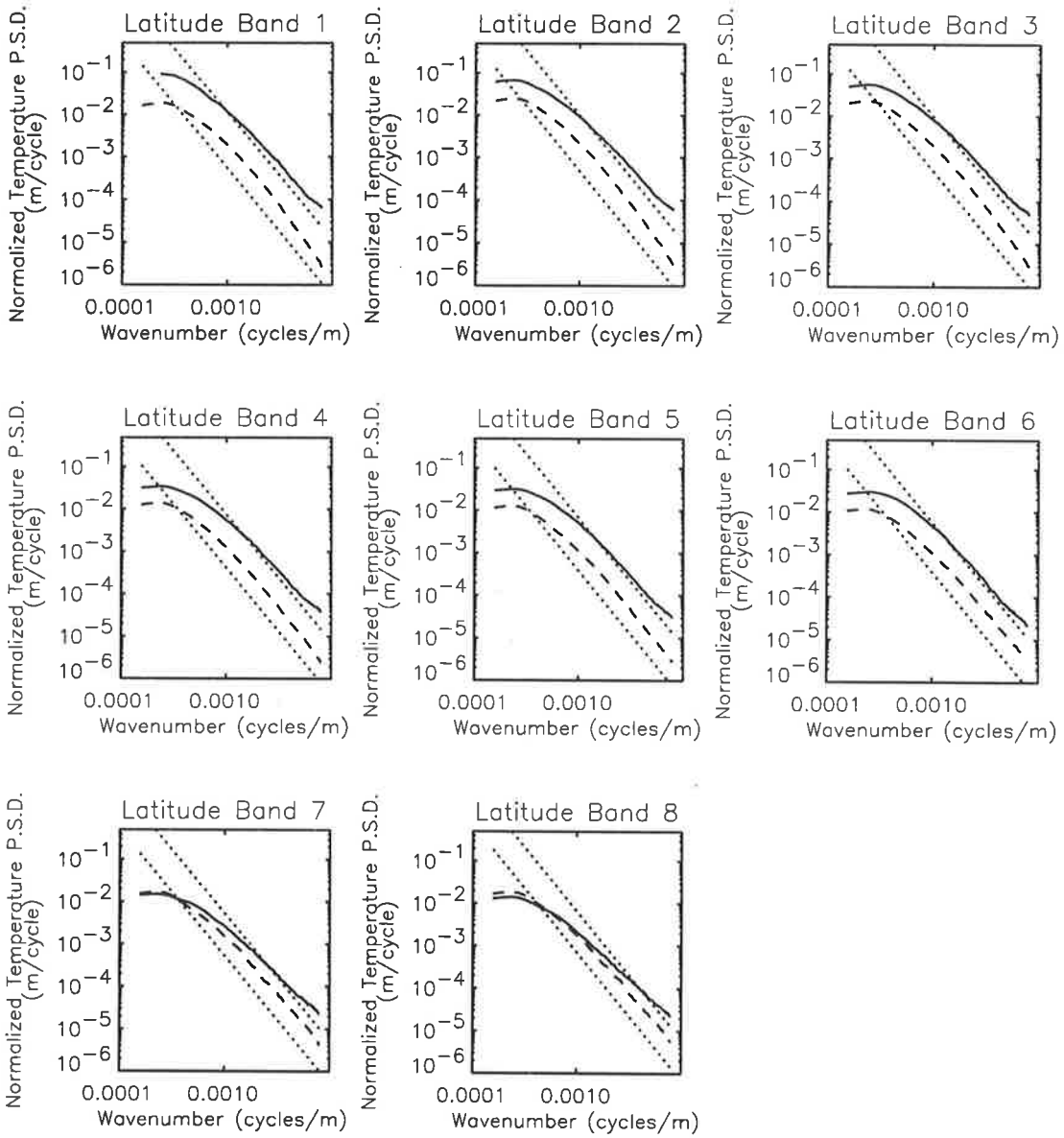

Figure 4.16: Vertical wavenumber power spectra of normalized temperature fluctuations for the troposphere (dashed lines) and lower stratosphere (solid lines). The theoretical saturation limits of *Smith et al.* [1987] are also plotted for comparison purposes (dotted lines). Each spectrum is the result of averaging individual power spectra into seven latitude bands as described in Table 4.3. The 95% confidence limits are approximately given by 0.95 and 1.05 multiplied by the spectral amplitude at each wavenumber.

Latitude Band	Radiosonde Stations	No. of Profiles Analyzed	
		Stratosphere	Troposphere
1	Gove, Darwin	766	1086
2	Mt. Isa, Townsville, Port Hedland	1058	1373
3	Gladstone, Learmonth, Alice Springs	746	1083
4	Forrest, Woomera, Cobar, Lord Howe Island	1396	1806
5	Wagga, Albany, Adelaide	1252	1660
6	Hobart	452	799
7	Macquarie Island	457	584
8	Davis	435	481

Table 4.3: The division of stations into eight latitude bands.

These confirm the seasonal trends described above which were inferred from the variations of spectral form. At low latitudes (10°S to 20°S) a clear annual variation is observed with wave energy peaking during the monsoon months of December to February. However, at middle latitudes (30°S to 40°S) a maximum is seen during the winter months when cold fronts sweep across southern Australia. A transition between these two regimes occurs at intermediate latitudes (20°S to 30°S) where a semiannual variation is observed.

The seasonal variations of tropospheric wave activity are, surprisingly, not well correlated with those in the stratosphere. At middle latitudes (30°S to 40°S) a small peak in wave activity is seen during winter months but the variation is smaller than that observed in the lower stratosphere. However, at lower latitudes (10°S to 30°S) a strong peak in energy density is observed between July and November which is in contrast with the stratospheric case where the maximum is found between December and February. The sudden increase in tropospheric variance cannot be associated with any one geographic feature since the maximum is found at a number of different stations including Port Hedland, Alice Springs, Townsville and Willis Island. A discussion of this result is provided in section 4.7.

Table 4.4 presents estimates of the spectral parameters E_0, t, m_* and $c_* = N/m_*$ which are all defined within the model formulation of *Fritts and VanZandt* [1993]. These are determined from the shape and spectral amplitudes of the observed spectra at each station. The estimates of E_0 were obtained using (2.14) where $\overline{\hat{T}'^2}$ is simply the area under the relevant power spectrum and where an averaged Väisälä-Brunt frequency, N, was used. Estimates of t and $m_*/2\pi$, and hence c_* also, were found using the Levenberg-Marquardt least squares

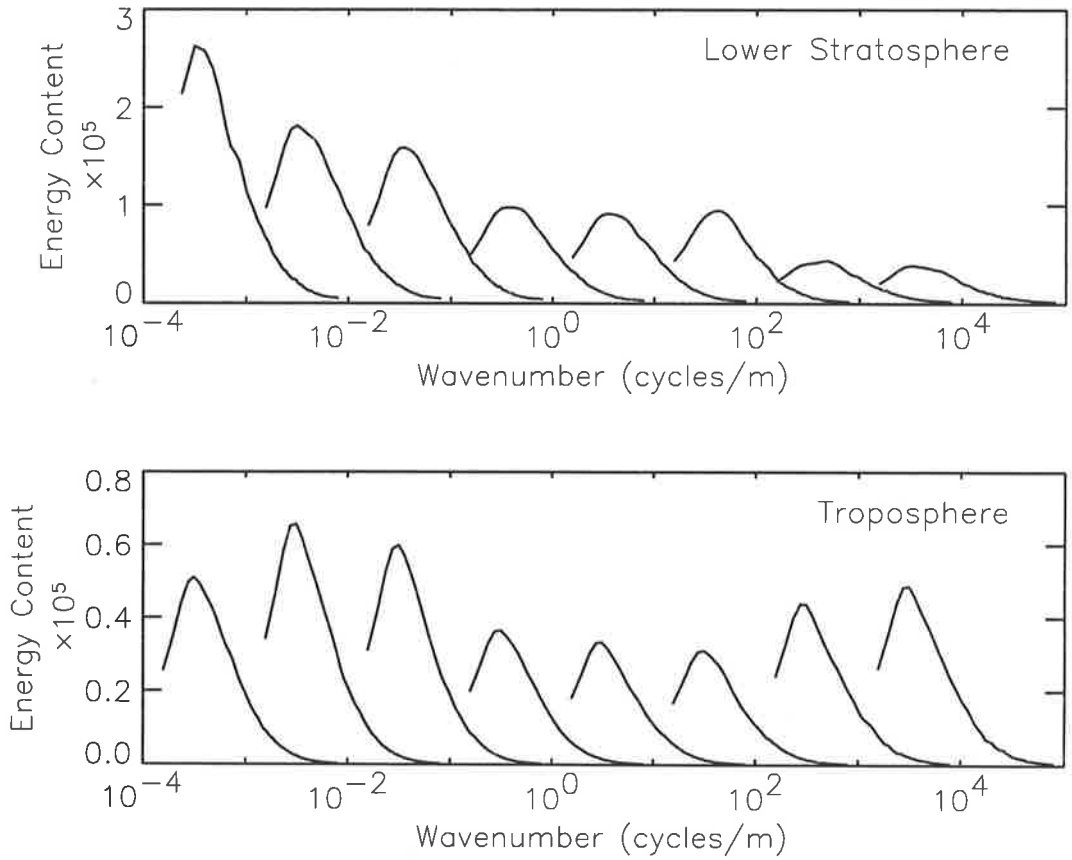

Figure 4.17: Vertical wavenumber area preserving spectra of normalized temperature fluctuations for the troposphere (bottom plot) and lower stratosphere (top plot). These are the same as in Figure 4.16 but are plotted in area preserving forms. Successive spectra are displaced horizontally by a factor of 10 and, from left to right, correspond to latitude bands 1 through to 8 (see Table 4.3).

curve-fitting algorithm with a fitting function given below.

$$F(m) = F_0 \frac{m/m_*}{1 + (m/m_*)^{t+1}} \tag{4.2}$$

The three unknown parameters, F_0, m_* and t, were obtained by fitting to monthly mean spectra and then averaging these estimates over time. Table 4.4 provides a description, at least to a certain extent, of the mean behaviour of the gravity wave field at each station. Note, however, that the degree of wave field anisotropy cannot be estimated from temperature measurements alone. The parameterization of wave field anisotropy is an important component of the model proposed by *Fritts and VanZandt* [1993].

The spectral parameter t for stratospheric power spectra was found to be consistently smaller than 3, the expected value from linear saturation theory. However, this parameter

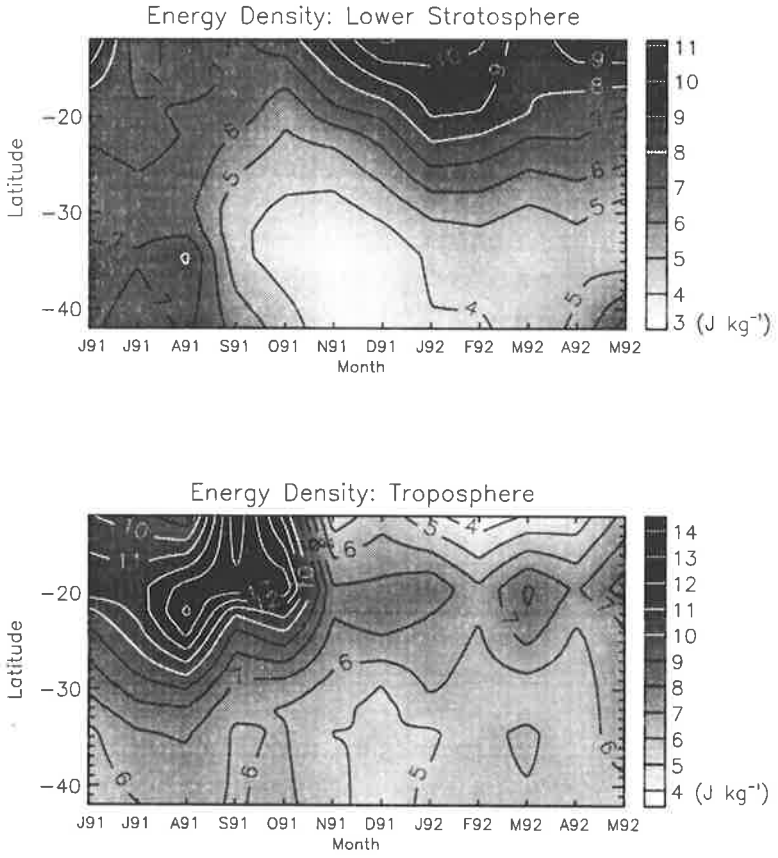

Figure 4.18: Time-latitude contours of total gravity wave energy density, E_0, for the troposphere and lower stratosphere. The energy density was obtained using (2.14) where the normalized temperature variance was calculated within the height intervals described in Table 4.2.

for tropospheric power spectra was found to be very close to 3 at most stations. Recall that each stratospheric power spectrum has been corrected for spectral distortion that is believed to be associated with the radiosonde's temperature sensor response time. The tropospheric power spectra have not undergone this correction procedure, however, since the response time is small at tropospheric heights. It is possible that estimates of t within the stratosphere are biased since there is some uncertainty as to the correct value for τ. As a consequence, all values within the appropriate column of Table 4.4 should be treated with some caution. More details about this problem are provided in appendix A, but it should be noted that estimates of other spectral parameters will not be affected.

The characteristic vertical wavelength, $2\pi/m_*$, was found to be close to 2.5 km within both the troposphere and lower stratosphere. It was sometimes slightly smaller in the stratosphere than in the troposphere but more often the reverse was true. Also there exists little

Station	t		$m_*/2\pi$ (cpm)		c_* (m s^{-1})		E_0 (J kg^{-1})	
	Trop.	Strat.	Trop.	Strat.	Trop.	Strat.	Trop.	Strat.
Adelaide	2.8	2.5	3.8×10^{-4}	4.0×10^{-4}	4.7	9.0	5.7	4.5
Albany	2.8	2.6	3.8×10^{-4}	4.0×10^{-4}	4.7	9.0	6.0	4.5
Alice Springs	3.1	2.5	4.2×10^{-4}	3.7×10^{-4}	4.5	10.5	9.1	6.4
Cobar	3.0	2.5	4.1×10^{-4}	3.7×10^{-4}	4.4	9.9	6.5	4.9
Darwin	3.1	2.6	4.8×10^{-4}	4.2×10^{-4}	4.0	9.9	7.7	8.1
Davis	2.7	2.2	3.6×10^{-4}	3.3×10^{-4}	5.8	10.8	6.3	2.0
Forrest	3.0	2.4	4.3×10^{-4}	3.8×10^{-4}	4.2	9.7	6.5	4.6
Gladstone	3.0	2.5	4.0×10^{-4}	3.6×10^{-4}	4.8	10.9	8.0	6.4
Gove	3.0	2.5	4.5×10^{-4}	3.3×10^{-4}	4.3	12.5	6.6	9.8
Hobart	2.7	2.6	3.5×10^{-4}	4.1×10^{-4}	5.0	8.7	5.5	5.1
Learmonth	3.1	2.5	4.4×10^{-4}	3.9×10^{-4}	4.2	10.3	8.6	6.9
Lord Howe	2.9	2.4	4.2×10^{-4}	3.9×10^{-4}	4.3	9.5	5.6	3.9
Mount Isa	3.0	2.5	4.3×10^{-4}	3.7×10^{-4}	4.4	11.8	9.5	7.5
Port Hedland	3.1	2.5	4.6×10^{-4}	3.5×10^{-4}	3.9	11.4	10.5	7.1
Townsville	3.0	2.5	4.2×10^{-4}	4.0×10^{-4}	4.6	10.5	9.3	7.5
Wagga	2.8	2.5	3.7×10^{-4}	3.9×10^{-4}	4.7	9.3	5.8	5.0
Willis Island	3.0	2.5	4.5×10^{-4}	3.3×10^{-4}	4.3	12.3	7.2	8.4
Woomera	2.8	2.5	3.7×10^{-4}	3.9×10^{-4}	4.8	9.5	6.1	5.3

Table 4.4: Estimates of spectral parameters for the troposphere and lower stratosphere.

seasonal or latitudinal variation of this parameter. However, the characteristic wavelength is less clearly defined in the lower stratosphere at high latitudes since the peaks in area preserving spectra are somewhat broader there.

The yearly-averaged energy density, E_0, was typically found to decrease with increasing latitude in the lower stratosphere. The most notable exception was at Lord Howe Island which had a comparatively small energy density for its latitude band. In the troposphere, the yearly-averaged energy density was largest in latitude bands 2 and 3, as was also evident in Figures 4.17 and 4.18. Of course, when estimating E_0 it is assumed that all observed temperature variance is due to gravity waves. *Fritts et al.* [1988] recognized convection as a possible source of contamination at tropospheric heights while temperature inversions can also cause fluctuations on single profiles that are difficult to remove as part of the basic state profile. These issues will be discussed in section 4.7.

The variation of gravity wave energy density with height and time can be examined using the radiosonde data from each station. Time-height contours of normalized temperature variance and total energy density at Gove, Adelaide and Davis were presented by *Allen and*

Vincent [1995]. These diagrams indicated that the largest variances typically occurred near the tropopause, especially when there existed large vertical gradients in atmosphere stability. However, the sharp gradients of temperature at the tropopause are difficult to adequately model and therefore remove as part of the basic state temperature profile. This problem is discussed by *Allen and Vincent* [1995] and their results do need to be treated with some caution as a consequence.

Here a similar analysis is undertaken but, following *Tsuda et al.* [1991], the variance is calculated within a small wavenumber band which includes only gravity waves that are thought to be "saturated". Therefore, the observed variance may be compared with the theoretical expectation within given height intervals. This form of analysis can potentially reveal those heights at which proposed saturation limits are valid.

The power spectral density at large vertical wavenumbers ($m \gg m_*$) due to *Smith et al.* [1987] is given by (2.16). Therefore, the normalized temperature variance between vertical wavenumbers m_1 and m_2, which is obtained by integration, is given by

$$\overline{\hat{T}'^2_{\text{SFV}}} = \frac{1}{48\pi^2 pg^2} N^4 \left(\lambda_1^2 - \lambda_2^2\right) \tag{4.3}$$

where $m_* \ll m_1 < m_2$ and $m = 2\pi/\lambda$. However, for the radiosonde data considered here, the observed spectral amplitudes at high vertical wavenumbers are attenuated according to (3.6). Thus the model variance is given by $\overline{\hat{T}'^2_{\text{MOD}}} = \overline{\hat{T}'^2_{\text{SFV}}} - C$ where C represents the relevant shaded area of Figure 3.5 and can be obtained numerically provided that β is known.

Figure 4.19 illustrates variance profiles from Gove, Adelaide and Davis which were calculated from radiosonde measurements obtained over three-month periods. The observed temperature profiles were first high-pass filtered using cutoff wavelengths at $\lambda_1 = 500$ m and $\lambda_2 = 125$ m, and following this the variance profiles were calculated using 500-m box-car windows. The final profiles illustrate the observed variance divided by the model variance where β was obtained at each height using the technique described in appendix A. Thus if the normalized variance equals one, then there exists good agreement with the model due to *Smith et al.* [1987] within a given altitude range. This analysis technique follows *Tsuda et al.* [1991] and for more details see their study[16]. Note, however, that *Tsuda et al.* [1991] also include a multiplication factor that takes account the actual passband characteristics of the filter used. This factor is not used here and it is assumed, essentially, that the filter is ideal

[16] Following *Tsuda et al.* [1991], N was calculated within 1-km intervals so as to better estimate its background value.

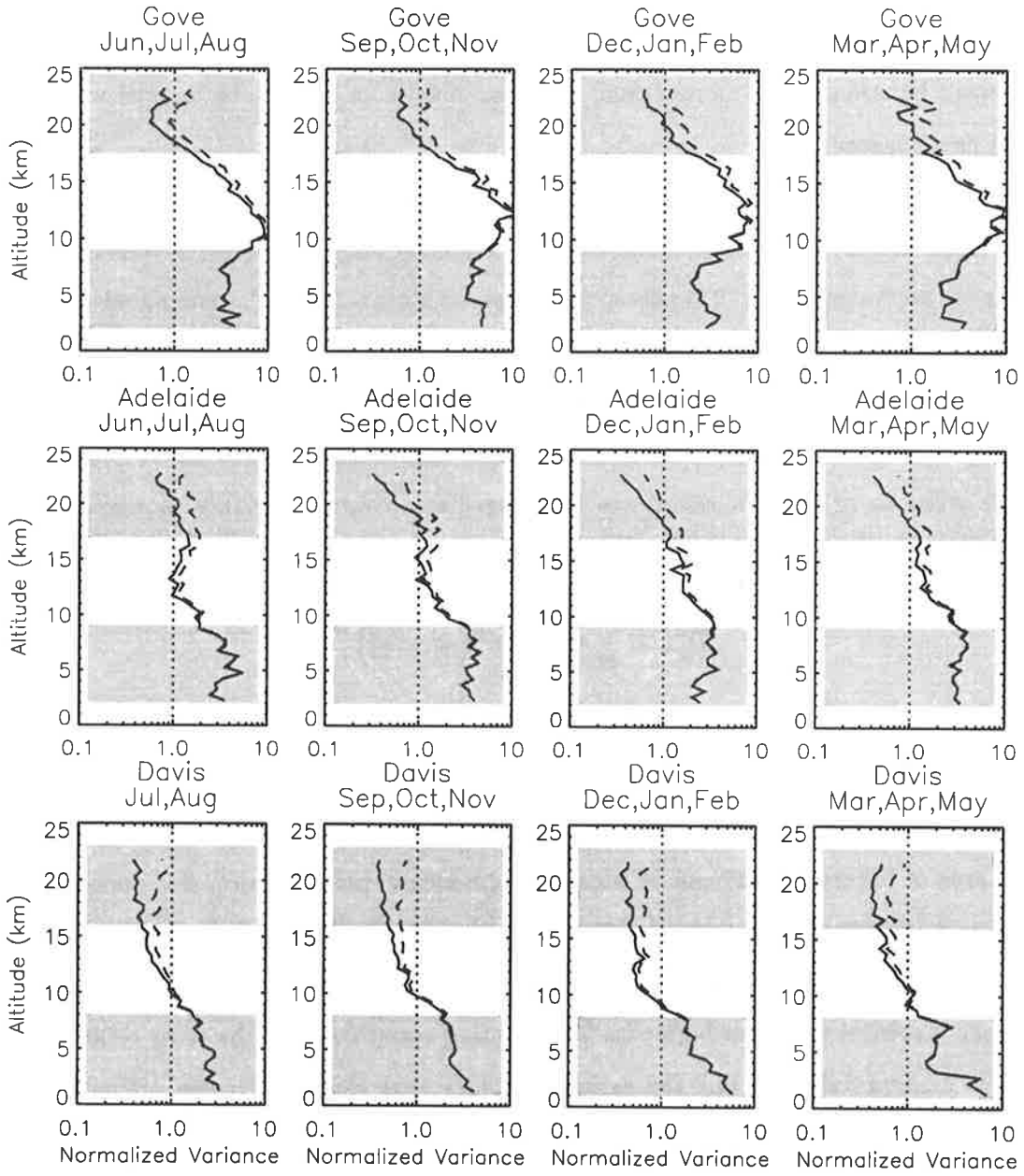

Figure 4.19: Vertical profiles of normalized variance calculated from observations obtained at Gove, Adelaide and Davis. The same data were used as in Figures 4.12, 4.13 and 4.15, and shaded areas indicate the altitude ranges that were used in those analyses. Solid lines correspond to observed variances that have been normalized by equation (4.3). Dashed lines correspond to observed variances that have been normalized after inclusion of the response time correction factor, C. Further details are provided in the text.

and there exists no spectral leakage. Since the multiplication factor is constant its exclusion will have no affect upon conclusions regarding the height dependence of variance.

The high-pass-filtered variance profiles from Gove and Adelaide indicate values that are larger than those of the model in the troposphere and values that are approximately consistent with those of the model in the lower stratosphere. In contrast, the profiles from Davis indicate significant attenuation of variance in the lower stratosphere. These results are consistent with the vertical wavenumber power spectra presented earlier.

There appears to be no enhancement of saturated wave variance at the tropopause as suggested *VanZandt and Fritts* [1989]. The most significant enhancement was found at Gove but the variance maximum occurred below the typical tropopause height. A similar result was also reported by *Tsuda et al.* [1994b] who analyzed radiosonde observations from Watukosek, Indonesia (7.57°S, 112.68°E). The enhancement may be the result of noise contamination, rather than gravity wave supersaturation, and this possibility will be discussed further in chapter 6.

In summary, this section presents analyses of the variance characteristics of gravity waves which are determined from radiosonde measurements of temperature. In some cases representative examples were presented for the purposes of economy and additional power spectra are presented in appendix B. A discussion of various aspects of these results is provided in the following sections.

4.5 Saturation Theory Comparison

The power spectra presented in Figures 4.12, 4.13, 4.14 and 4.15 have been compared with the theoretical saturation limits proposed by *Smith et al.* [1987]. These limits were chosen as a convenient reference since they are often considered in the literature. The predictions of other theories [e.g., *Weinstock*, 1990; *Hines*, 1991b; *Dewan*, 1994; *Gardner*, 1994; *Zhu*, 1994], within the limits of theoretical approximation and uncertainty, are very similar. It has proven difficult to distinguish between these theories on the basis of spectral amplitude calculation and comparison.

The observed power spectra within the stratosphere are discussed in this section since tropospheric spectra may not have a pure gravity wave interpretation (see section 4.7). Furthermore, tropospheric spectra may not have reached an equilibrium state since they are obtained near to, or within, the source region itself. In contrast, stratospheric spectra have

a relatively clear gravity wave interpretation and observed spectral amplitudes, with some exceptions, are within the general range predicted by recent theories.

The high-wavenumber spectral slopes, t, of stratospheric power spectra are typically shallower, to a small degree, than the theoretical expectation due to *Smith et al.* [1987] which is $t = 3$. Other theories [e.g., *Weinstock*, 1990; *Hines*, 1991b; *Zhu*, 1994] allow for some variability although $t = 3$ is usually considered to be the nominal value. The shallower slopes observed here may result from a bias in estimates of temperature sensor response time as discussed in appendix A, or from aliasing due to high spatial frequency noise. Furthermore, the sonde's horizontal drift may result in some distortion of the vertical wavenumber power spectra which are expected to have shallower slopes as a consequence [*Gardner and Gardner*, 1993]. All of these factors may be contributing to the spectral slope that is observed and so estimates of t (see Table 4.4) should not be regarded as inconsistent with the predicted value $t = 3$ within the stratosphere.

The problems described above highlight the difficulties in saturation theory comparison with any one spectrum due to experimental uncertainty. However, variations of spectral form should be geophysical (at least to within the stated 95% confidence limits) since any experimental bias is anticipated to be the same for each spectrum[17]. Therefore, the significant attenuation of stratospheric spectral amplitudes at high latitude sites must be explained within a wave saturation framework.

The Doppler-shifting theory proposed by *Hines* [1991b] allows for some height variability of spectral amplitudes at "saturated" wavenumbers while similar variability is allowed within the theoretical frameworks proposed by *Weinstock* [1990], *Gardner* [1994] and *Zhu* [1994]. *Hines* [1993a] has suggested Doppler-shifting theory as a possible explanation for some attenuated spectra observed by lidar in the stratosphere [*Wilson et al.*, 1991; *Beatty et al.*, 1992; *Senft et al.*, 1993]. However, the proposed height variability depends upon certain characteristics of the source spectrum of gravity waves. The source spectrum is not known from the data available here.

Alternatively, *Fritts and Lu* [1993], *Kuo and Lue* [1994] and *Eckermann* [1995] have argued that attenuated spectra may arise when there exists a vertical shear in the basic state winds. The proposed attenuation due to *Eckermann* [1995] appears to occur independently of the physical mechanism that is responsible for constraining wave amplitudes at high vertical

[17] Distortion due to the sonde's horizontal drift is one possible exception. However, as was noted in chapter 3, this distortion is small even for the largest mean winds.

wavenumbers. Thus the presence of attenuated spectra is not necessarily indicative of any one particular mechanism. It must be concluded that the results presented here cannot be used to distinguish between the various competing wave saturation theories.

4.6 Wind-Shifting Theory Comparison

The qualitative behaviour of gravity wave power spectra in various regions of the atmosphere has been discussed by *Kuo and Lue* [1994] and *Eckermann* [1995]. *Kuo and Lu* [1994] argue that certain aspects of observed spectra can be explained by a simple analytic model of wave-shear interaction which was derived by *Kuo et al.* [1992] under a first order approximation of the Navier-Stokes equation. According to this picture, the horizontal wind velocity saturation limit[18] is universally $N^2/2m^3$ and is typically reached in the troposphere and middle mesosphere [*Kuo and Lue*, 1994]. However, in the stratosphere and lower mesosphere the saturation limit is not reached since the dominant waves in these regions lose energy to the zonal mean flow due to its vertical shear. Seasonal variations of spectral form are attributed to seasonal changes in the strength and sign of the shear.

A similar picture has been proposed by *Eckermann* [1995] and this picture will be considered here. *Eckermann* [1995] argues that attenuated spectra arise due to changes in background wind speeds which can refract waves such that they have smaller vertical wavenumbers and also smaller total shear variance[19]. This model differs from that of *Kuo and Lue* [1994] in that the wind shear does not play a direct role in modifying wave characteristics through the equations of motion [*Eckermann*, 1995]. Rather, discrete changes in basic state horizontal wind speeds alter wave characteristics under the Liouville-Green approximation that was discussed in chapter 1. The refraction processes envisaged by *Eckermann* [1995] follow from the model frameworks presented by *Lindzen* [1981] and *Fritts and Lu* [1993].

The so-called "wind-shifting" theory of *Eckermann* [1995] predicts that gravity waves are either "upshifted" or "downshifted" depending upon the sign of $\hat{\beta}$ where

$$\hat{\beta} = \mathrm{sgn}\left[\frac{\frac{d}{dz}\overline{U}}{c_h^{\mathrm{int}}}\right] \tag{4.4}$$

[18] This is the saturation limit for horizontal velocity power spectral density that is attributed to *Dewan and Good* [1986].

[19] An increase or reduction of variance is necessary in order that wave action be conserved.

and where c_h^{int} is the intrinsic horizontal phase speed. When $\hat{\beta} = -1$, wave action conservation yields downshifted waves with smaller amplitudes and vertical wavenumbers. Conversely, when $\hat{\beta} = +1$, wave action conservation yields upshifted waves with larger amplitudes and vertical wavenumbers[20]. Attenuated spectra are predicted when the dominant waves of a given spectrum are downshifted while saturated spectra are predicted when the reverse is true. According to *Eckermann* [1995], the model is sufficiently robust in nature that similar spectral responses occur regardless of the physical mechanism responsible for saturating gravity waves.

Eckermann [1995] applied wind-shifting theory to various observations in the literature, including those of *Allen and Vincent* [1995], and was able to predict, retrospectively, the presence of attenuated spectra in some instances. The application of wind-shifting theory to the results of *Allen and Vincent* [1995] is of particular interest here and the following discussion is based on the relevant section of *Eckermann* [1995]. Also, additional results from Antarctic stations other than Davis are considered in the discussion.

Following *Eckermann* [1995], the spectra from the lower stratosphere are considered[21]. From Figure 4.16, these may be divided into two groups. Stratospheric power spectra from within latitude bands 1 though to 6 (including Willis Island and the Cocos Islands) have spectral amplitudes, at large vertical wavenumbers ($m \geq 10^{-3}$ cpm), that are either equal to or larger than the theoretical saturation limits due to *Smith et al.* [1987]. These are saturated, unattenuated spectra that should be dominated by $\hat{\beta} = +1$ waves under the wind-shifting model of *Eckermann* [1995]. Conversely, stratospheric power spectra from Macquarie Island and the Antarctic stations have spectral amplitudes, at large vertical wavenumbers, that are often smaller than the theoretical saturation limits due to *Smith et al.* [1987]. Furthermore, these spectra have amplitudes that are significantly smaller than those found at other sites. Such spectra should be dominated by $\hat{\beta} = -1$ waves under the wind-shifting model of *Eckermann* [1995].

The classification of spectra into two groups is clearly an oversimplification since there exists a gradual trend toward "attenuated" spectra at high latitudes (see Figure 4.17). Also there exists subtle variations of spectral form with season which can differ between spectra of the same group. The following discussion is an attempt to explain the apparent attenuation

[20] Wave amplitudes are upshifted or downshifted relative to the exponential increase caused by the atmosphere's density structure. See *Eckermann* [1995] for further details.

[21] *Eckermann* [1995] argued that comparison between wind-shifting theory and tropospheric observations is not practicable since the troposphere is the source region of most waves.

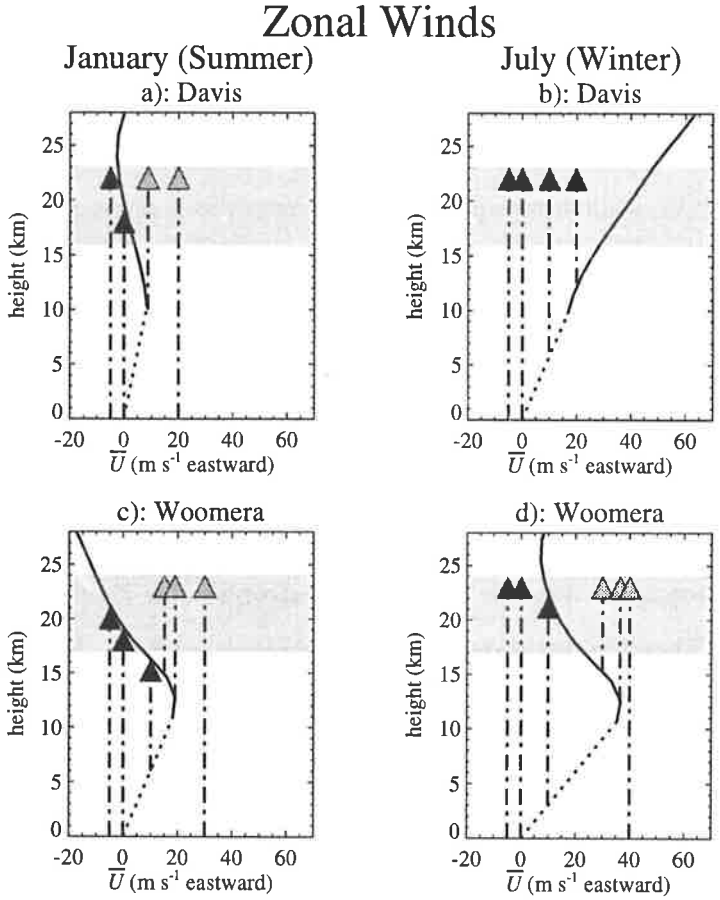

Figure 4.20: Climatological CIRA zonal winds (solid lines) during summer and winter over Davis, Antarctica, and Woomera, Australia [reproduced from *Eckermann*, 1995]. The shaded regions indicate the height intervals used for spectral analysis while open and closed arrows denote gravity waves with $c_h > \overline{u}$ and $c_h < \overline{u}$, respectively. For further details see *Eckermann* [1995].

of stratospheric spectra at high latitude sites.

Figure 4.20 illustrates zonal-mean zonal wind profiles over Davis and Woomera[22] during both summer and winter months. This diagram has been reproduced from *Eckermann* [1995] and the winds are based on data from *CIRA* [1986]. Upward propagating gravity waves are indicated in the diagram by open and closed arrows which appear at the ground-based horizontal phase speeds, c_h, of these waves [*Eckermann*, 1995]. Values of c_h are assumed to be of the order of $\overline{u}$ in the troposphere (following *Lindzen* [1981]) while shaded areas indicate the altitude intervals that were used for spectral analysis.

Consider, firstly, the winter winds at both Davis and Woomera (Figures 4.20b and 4.20d,

[22]The mean wind conditions over Woomera were chosen by *Eckermann* [1995] so as to be representative of mean conditions at other midlatitude sites. Similarly, the mean winds at Davis are representative of those at Mawson, Casey and Macquarie Island.

respectively). The important difference between these profiles is that the zonal winds continue to increase with altitude within the lower stratosphere over Davis whereas they decrease with altitude within the same region over Woomera. Thus, the hypothesised gravity waves are downshifted at Davis while both upshifted and downshifted waves propagate through the lower stratosphere at Woomera. Wind-shifting theory therefore predicts attenuated spectra at high latitude sites and saturated spectra at midlatitude sites, as is observed.

Now consider the summer winds at Davis and Woomera (Figures 4.20a and 4.20c, respectively). Firstly, at Woomera, the zonal mean winds are such that upshifted gravity waves are filtered from the spectrum either before or within the height interval used for spectral analysis. Therefore attenuated spectra are predicted in this case. In contrast, upshifted gravity waves can propagate through the lower stratosphere at Davis and the wind shear itself is quite weak. Therefore saturated spectra are predicted here. However, the observed summer spectrum at Davis appears to be attenuated, as it is in winter, while the summer spectrum at Woomera appears to be saturated. Thus wind-shifting theory does not predict the qualitative results in these instances[23].

Eckermann [1995] argued that the interpretation of summertime spectra, within the framework of wind-shifting theory, was made difficult by a lack of detailed knowledge concerning source climatologies in the southern hemisphere. For example, it is not yet clear whether topographic forcing is as important in the southern hemisphere as it has been found to be in the northern hemisphere by, among others, *Nastrom and Fritts* [1992]. Meteorological sources [e.g., *Eckermann and Vincent*, 1993] may be relatively more important although *Bacmeister et al.* [1990] have reported evidence of mountain wave activity over Antarctica. More knowledge about wave sources may be needed but, at this stage at least, the qualitative results described in section 4.4 appear to be inconsistent with the predictions of wind-shifting theory during summer months.

4.7 Discussion

The material presented in this chapter details the variance characteristics of gravity waves in the troposphere and lower stratosphere. These were delineated from high-vertical-resolution radiosonde measurements which were obtained from the Australian sector of the southern

[23] Figure 4.19 indicates that the saturated wave variance observed at Adelaide during summer begins to attenuate above, approximately, 20 km. This is qualitatively consistent with the removal of upshifted gravity waves by the background flow, as is illustrated in Figure 4.20c.

hemisphere. The main results are listed below.

1. The vertical wavenumber power spectra have spectral slopes that are close to -3 at most stations, especially within the troposphere.

2. There are definite seasonal variations of wave variance within the lower stratosphere where the time of maximum variance changes from low latitudes to midlatitudes. In contrast, seasonal variations of normalized temperature variance in the troposphere are more difficult to interpret.

3. Spectral amplitudes within the troposphere are consistently larger than the theoretical saturation limits proposed by *Smith et al.* [1987], often by as much as a factor of 3.

4. Spectral amplitudes within the lower stratosphere are approximately consistent with the theoretical saturation limits proposed by *Smith et al.* [1987], although there is a gradual trend toward smaller amplitudes at high latitude sites.

5. The characteristic vertical wavelength is of the order of 2.5 km within both the troposphere and the lower stratosphere, although is typically smaller in the troposphere.

6. The largest gravity wave variances tend to be found at low-latitude stations.

It has been assumed throughout chapter 4 that all fluctuations with vertical scales between about 7 km and at least the Nyquist wavelength[24] are caused by gravity waves. Although observed spectral amplitudes are within the general range predicted by recent gravity wave theories, this assumption needs to be carefully examined. For example, processes such as convection and inversions may cause fluctuations on single profiles that are either difficult to distinguish from gravity wave activity or difficult to remove as part of the basic state temperature profile. Furthermore, equatorial waves can have vertical scales and amplitudes that are comparable to those of dominant gravity waves [e.g., *Wallace*, 1973]. Therefore, these waves may be responsible for a significant portion of the observed variance at near-equatorial stations.

The possibility that convection may be prominent throughout the troposphere was discussed in section 4.3. There it was argued that convection is not prominent over Adelaide based on N^2 distributions within both the troposphere and lower stratosphere. Similar N^2 distributions were found at representative stations elsewhere. Convection is anticipated to

[24]The Nyquist wavelength is approximately 100 m for the data studied here.

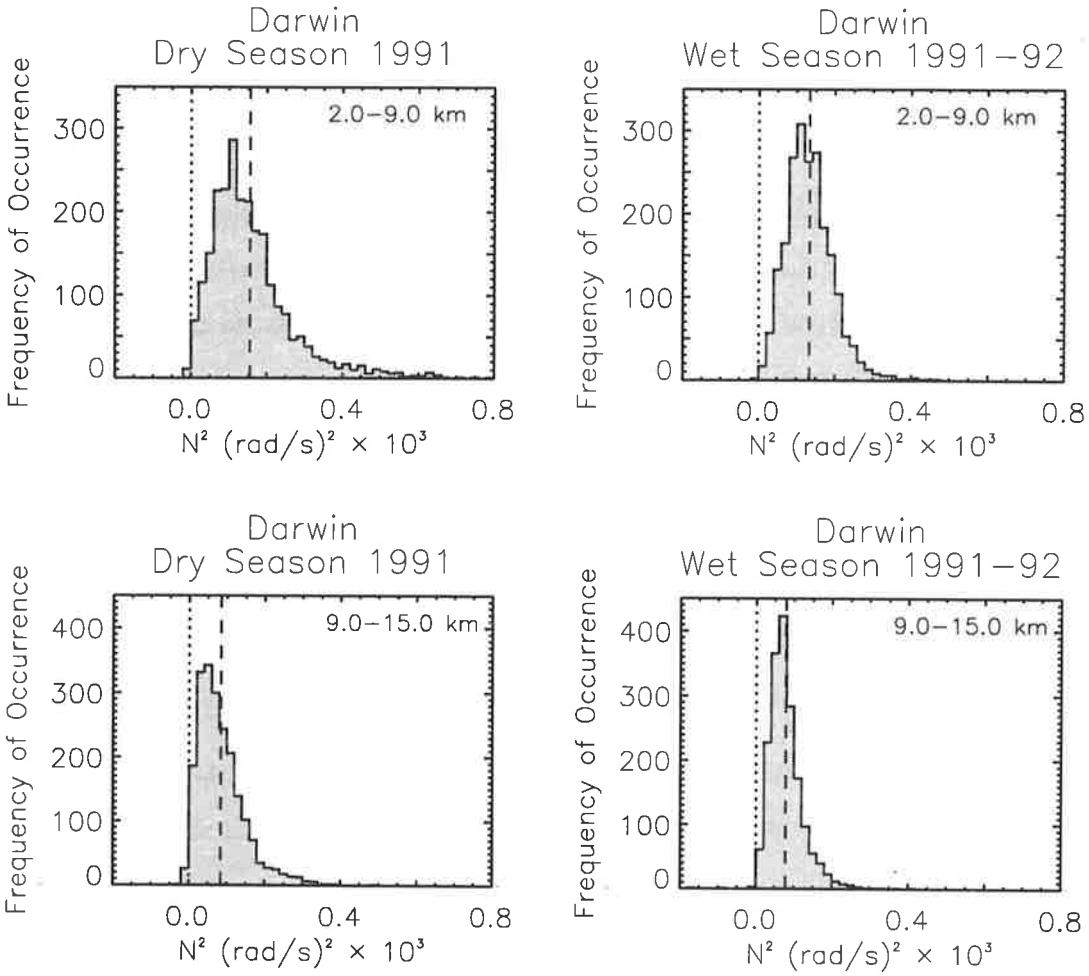

Figure 4.21: The distribution of N^2, averaged over 500-m altitude intervals, within the lower troposphere (2.0–9.0 km) and upper troposphere (9.0–15.0 km) over Darwin. Observations from wet season (December, January and February) and dry season months (June, July and August) were considered. Dashed lines indicate the mean values in each plot.

be most important within the troposphere at near-equatorial sites, especially during the wet season. Figure 4.21 illustrates N^2 distributions[25] from Darwin during both wet season and dry season months. These distributions are similar to those of Figure 4.9 and gravity waves do appear to be commonly supported within the troposphere over Darwin, as was also found within the troposphere over Adelaide[26].

The possibility that equatorial waves may have contributed a significant portion of the observed variance at the near-equatorial stations is discussed in chapter 6. There it is

[25]The Väisälä-Brunt frequency squared was calculated in each case using the dry adiabatic lapse rate.

[26]It is worth noting that during dry season months there exists an increased occurrence of large N^2 values, of the order of 4.0×10^{-4} $(\text{rad/s})^2$, between 2.0 and 9.0 km at Darwin. This is likely to be indicative of an increased occurrence of temperature inversions during these months.

argued (for the lower stratosphere over the Cocos Islands at least) that most of the observed variance occurs at temporal scales that are consistent with those expected of gravity waves. Furthermore, simple linear models of equatorially trapped waves [e.g., *Gill*, 1982; *Andrews et al.*, 1987] suggest that equatorial wave amplitudes decrease by a factor of approximately e^{-1} at 12 degrees of latitude. Therefore, for the near-equatorial stations studied here, the observed variance is not thought to be contaminated (at least not significantly) by equatorial wave motions.

Temperature inversions can cause fluctuations on individual profiles within the troposphere that are of larger magnitude than those due to gravity waves over small height intervals. These fluctuations are caused by radiative rather than dynamical processes but are difficult to filter from observed profiles. Thus inversions may contaminate gravity wave observations in the troposphere. For example, Figure 4.22 illustrates temperature profiles observed from Townsville during August 1991 and February 1992. Large inversions are evident in the lower troposphere during August. These structures are often long-lived, lasting for periods of several days or more[27], and might therefore be removed by time filtering. However, as has been discussed elsewhere, time filtering is not practicable for the majority of data studied here.

The large increase of temperature variance within the low-latitude troposphere between July and November (Figure 4.18) may be caused by the presence of large temperature inversions during these months[28]. For example, Figure 4.22 illustrates low-altitude temperature inversions at Townsville which appear to be much more common during August than they are during February. These inversions must contribute to the observed normalized temperature variance between 2.0 and 9.0 km and similar inversions are found at other low-latitude stations[29]. As a consequence, the total gravity wave energy density between 2.0 and 9.0 km will be overestimated at these stations during dry season months. Whether or not this is sufficient to explain the large increase described in Figure 4.18 is not known.

The latitudinal variations of tropospheric area preserving spectra, which are illustrated in Figure 4.17, are also likely to be contaminated by temperature inversions. Inversions are common at polar latitudes, particularly at the south pole (see appendix C), and the large variances found at latitude bands 7 and 8 are likely to be affected by inversions[30].

[27] At least they appear at the same time of day for periods of several days or more

[28] The variance in Figure 4.18 was interpreted as being due to gravity waves.

[29] For further examples see Figure 4.4 and also Figure 2 of *Allen and Vincent* [1995].

[30] Note that tropospheric data from latitude bands 7 and 8 were spectrally analyzed between 1.0 and 8.0 km whereas data from other stations were spectrally analyzed between 2.0 and 9.0 km. The former height range

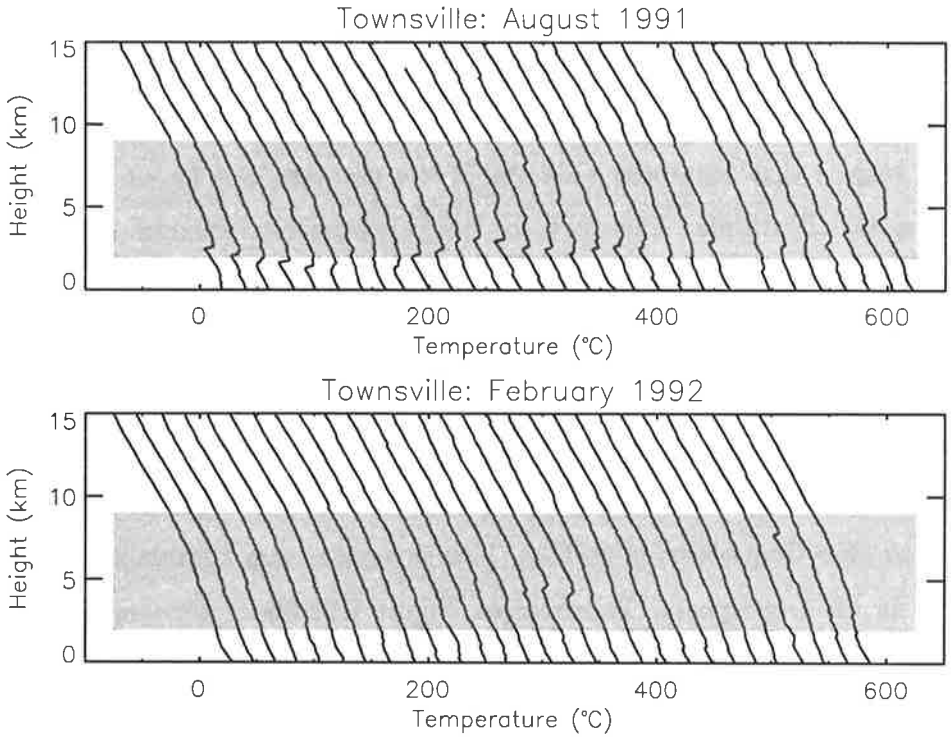

Figure 4.22: Examples of tropospheric temperature profiles observed at Townsville (19°S, 147°E) during the months of August and February. Successive profiles are displaced by 20°C and correspond to a 24-hour delay between soundings. The shaded area indicates the height interval used for power spectrum analysis.

Similarly, area preserving spectra from latitude bands 1, 2 and 3 are likely to be affected as was discussed above. Inversions are also common at midlatitude stations but often appear below 2 km (see, for example, Figure 4.5). Therefore, tropospheric spectra are not thought to be significantly contaminated by inversions at midlatitudes. More specialized analysis (for example, time filter analysis[31]) is needed to determine the quantitative effect of inversions upon the tropospheric results presented here.

The choice of altitude range for tropospheric spectral analysis at low latitudes is not ideal. While there exists little choice at high and middle latitudes, larger altitudes might be chosen at low latitudes since the tropopause is typically higher at such sites. Nevertheless, Figure 4.19 demonstrates that high-wavenumber variances are consistently larger than those due to *Smith et al.* [1987] at all altitudes throughout the troposphere over Gove[32]. Examples of tropospheric spectra from the Cocos Islands, calculated between altitudes of 7 and 14 km,

was necessary since typical tropopause heights are of the order of 9.0 km at the Antarctic and sub-Antarctic stations.

[31] Inversions do tend to be long-lived by inspection but need not be in general.

[32] Indeed the normalized variance is largest between 9 and 15 km where inversions are, at best, rare.

are presented in chapter 6.

It is more certain that temperature fluctuations within the lower stratosphere are caused by gravity waves. For example, *Sidi et al.* [1988] and *Fritts et al.* [1988] have found that temperature and horizontal wind velocity fluctuations within the lower stratosphere are roughly consistent with gravity wave polarization equations. This is also demonstrated in chapters 5 and 6 using temperature and horizontal wind fluctuations observed from Macquarie Island and the Cocos Islands. Furthermore, the spectra presented here have amplitudes and slopes that are approximately consistent with recent gravity wave saturation theories. The majority of evidence in the literature, and also in this chapter, supports a gravity wave interpretation of mesoscale temperature fluctuations within the lower stratosphere[33].

The spectral amplitudes found in the lower stratosphere over Davis, Mawson, Casey and Macquarie Island are interesting since they are smaller, especially at the lowest vertical wavenumbers, than those found at other stations. The spectral slopes are also more shallow than those at other stations. In contrast, spectral amplitudes and slopes within the troposphere are approximately consistent with those found elsewhere. Therefore, assuming tropospheric spectra are indicative of wave sources, weak wave source activity is not responsible for the attenuation of stratospheric spectra over Antarctic and sub-Antarctic stations.

An alternative possibility is that the wave spectrum is influenced in some way by the strong background winds that are found over the high-latitude stations studied here (e.g., as proposed by *Fritts and Lu* [1993]). This possibility was discussed in section 4.6. However, the main difficulty with this scenario is that the attenuated spectra show little seasonal variation whereas the basic state winds vary considerably with season (e.g., Figure 4.20). The mean zonal winds in the lower stratosphere are particularly strong during winter but are comparable with zonal winds found elsewhere during summer. Nevertheless, the calculated spectra show little seasonal variability and spectral amplitudes are actually largest during the months of July to November (Figure 4.15) when the mean zonal winds are strong. Clearly these findings require further investigation.

Figure 4.23 summarizes the seasonal and latitudinal variations of normalized temperature variance and E_0 within the lower stratosphere. This diagram is the same as Figure 14 of *Allen and Vincent* [1995] except that additional results from Macquarie Island, between April 1993 and March 1994, are also included. Error bars indicate, approximately, the 95%

[33] Results presented by *Cot and Barat* [1990] provide one possible exception.

confidence limits of estimates from each latitude band. This diagram, together with Figure 4.18, emphasizes the annual cycle of wave activity at low latitudes which is out-of-phase with wave activity at midlatitudes. In all seasons, but especially in summer, there is a strong equatorward gradient of energy density, with E_0 increasing by a factor of approximately 5 from polar to equatorial latitudes.

The above results agree well with other studies in the northern hemisphere. *Kitamura and Hirota* [1989] found that wave activity in the midlatitude lower stratosphere over Japan maximized in winter, and that wave activity increased toward the equator. Lidar studies at altitudes of 35 km over western Europe also show an annual cycle of temperature variance with a winter maximum and an equatorward gradient [*Souprayen*, 1993].

It should be noted that E_0 is the measure of wave activity used in the *Fritts and VanZandt* [1993] parameterization scheme. However, other schemes may use different indicators of wave activity. In some cases these parameters can still be estimated from the figures and tables presented here. For example, *Hines* [1996a,b] has developed a scheme which uses the root-mean-square of the horizontal wind perturbation as the input parameter. This may be estimated from normalized temperature variance measurements using the following equation,

$$\overline{U'^2} = \overline{u'^2} + \overline{v'^2} \approx \frac{pg^2}{N^2}\overline{\hat{T}'^2} \tag{4.5}$$

where U' is the first-order perturbation of total horizontal wind velocity. Equation (4.5) is derived from standard polarization equations[34] by assuming that the spectrum of waves is separable in all variables and that the one-dimensional frequency spectrum is given by $B(\omega) \propto \omega^{-p}$. From Figure 4.23 and using $p = 5/3$ it can be seen that the root-mean-square of U' varies from approximately 1.5 m s^{-1} at Davis to approximately 4.0 m s^{-1} at 12°S.

4.8 Concluding Comments

The advantage of using radiosonde measurements in gravity wave research is their extensive geographic and temporal coverage. This allows estimates of important spectral parameters to be made that are not biased by localized source effects. It also allows seasonal and latitudinal variations of wave activity to be identified. Gravity wave variance characteristics have been described in this chapter using radiosonde data from the Australian sector of the southern hemisphere.

[34]The polarization equation upon which (4.5) is based may be invalid at high vertical wavenumbers, according to *Hines* [1991b], which could be a source of error.

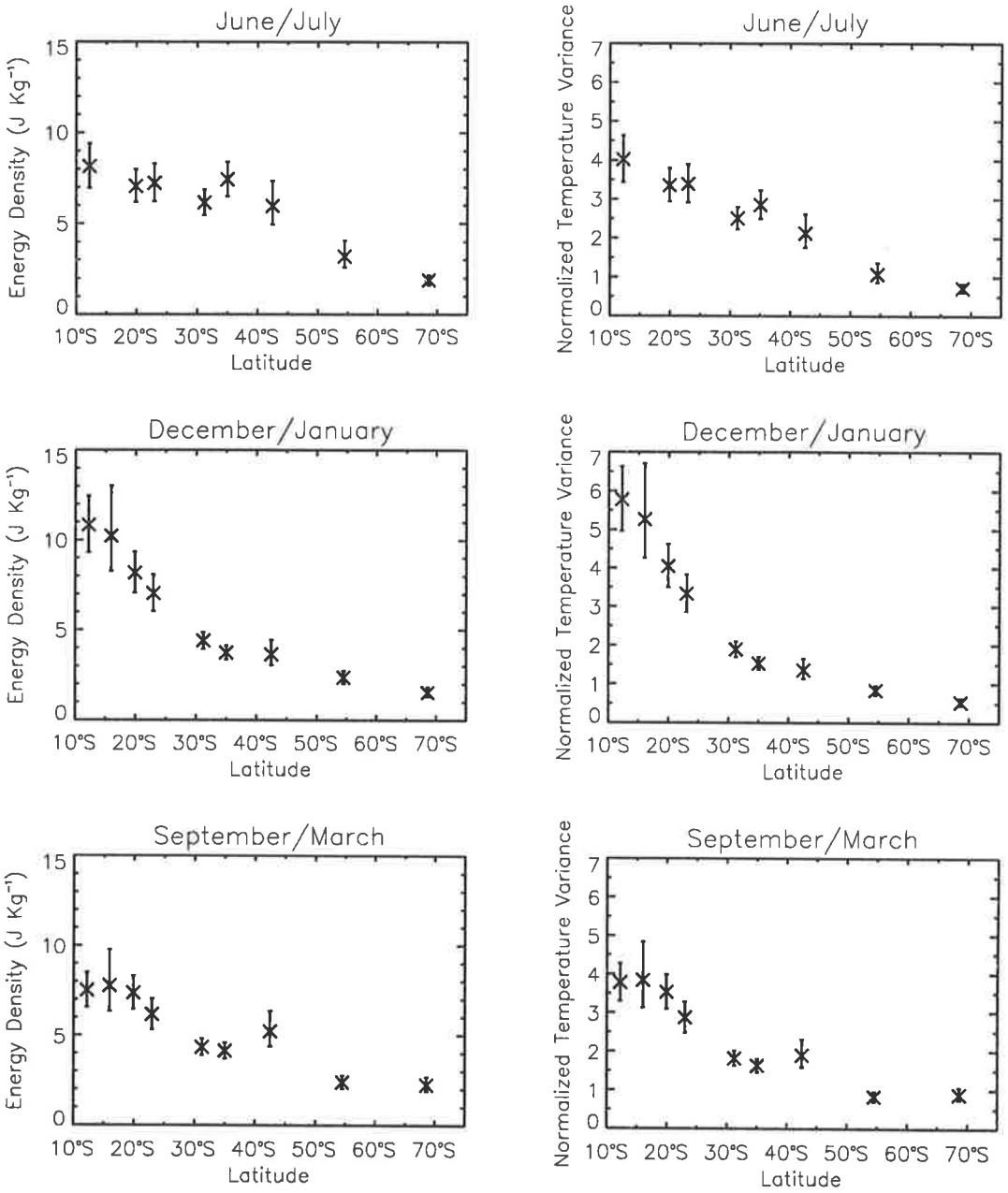

Figure 4.23: The variation of normalized temperature variance and gravity wave energy density as a function of latitude within the lower stratosphere (17.0 to 24.0 km in most cases). Data from the various stations have been averaged into latitude bands as described in Table 4.3 and over 2-month periods in each case. Furthermore, the results from Willis Island are included for the months of December/January and September/March. Normalized temperature variance estimates have been multiplied by a factor of 10^5 and error bars approximate the 95% confidence limits of each estimate. The results from Davis within the June/July plots were calculated from observations during July and August 1992.

Climatological studies of gravity waves are important in defining the extent of wave activity throughout the atmosphere. If theorists and modelers believe that more work of this nature is needed within the troposphere and lower stratosphere then a global-scale study of radiosonde data may provide an important contribution. All that is needed is for certain stations throughout the world, which are already launching radiosondes on a daily basis, to archive their data at high vertical resolution. *Hamilton and Vincent* [1995] report on recent efforts to attempt such a study.

It must be emphasized that temperature measurements alone are not sufficient to fully describe the gravity wave field. In particular, the degree of wave field anisotropy is an important parameter of the *Fritts and VanZandt* [1993] model formulation which requires horizontal wind velocity measurements in order to be estimated. Therefore, simultaneous horizontal wind and temperature measurements are preferable to radiosonde measurements of temperature only. The following chapters discuss additional gravity wave characteristics which can be determined when simultaneous wind and temperature measurements are available. Winds and temperatures from Macquarie Island and the Cocos Islands are considered.

Chapter 5

Macquarie Island: A Case Study

5.1 Introduction

The characteristics of gravity wave motions over Macquarie Island (55°S, 159°E) are investigated in this chapter using radiosonde observations of temperature and horizontal wind velocity. Macquarie Island is located approximately 1500 km south-south-east of Tasmania. It is an elongated (aligned north-south) and rocky island which is 34 km long and 5.5 km wide at its broadest [e.g., *Crohn*, 1986]. Most of the island is a plateau of between 200 and 300 m altitude. However, some isolated peaks rise above the plateau and the largest of these, Mt. Hamilton, is 433 m above sea level [e.g., *Crohn*, 1986]. The Australian Bureau of Meteorology radiosonde station is located on the northern edge of the island and is 7 m above sea level.

The climate of Macquarie Island, as reviewed by *Streten* [1988], is typical of the sub-Antarctic. It is characterized by a high frequency of strong eastward winds, frequent gales and a high number of days with precipitation throughout the year [*Streten*, 1988]. Much of this precipitation is associated with the passage of frontal systems. Indeed, *Streten* [1988] estimates that, on average, a front or depression centre passes the island once every 5 or 6 days. Therefore, fronts may be an important source of gravity waves over Macquarie Island.

Another possible source of waves is the topography of the island itself. Strong eastward winds flowing across a north-south ridge can generate vertically-propagating gravity waves [e.g., *Smith*, 1979]. However, the east-west dimensions of Macquarie Island are such that at least some portion of mountain wave energy is likely to be trapped within the troposphere. This arises since mountain waves with small horizontal scale may be Doppler shifted to

periods less than the buoyancy period [e.g., *Hines*, 1989] and hence reflected downward before reaching the lower stratosphere.

A further possible source of gravity waves over Macquarie Island is the process of geostrophic adjustment. This takes place by means of wave propagation from a region of initial imbalance leaving a steady quasi-geostrophic balanced flow [*Blumen*, 1972]. Geostrophic adjustment is likely to be a strong source of low-frequency wave activity and may explain the observed preponderance of gravity wave energy at near-inertial frequencies [*Fritts and Luo*, 1992]. Both modelling [e.g., *Fritts and Luo*, 1992; *Luo and Fritts*, 1993] and experimental studies [e.g., *Uccellini and Koch*, 1987; *Kitamura and Hirota*, 1989] provide evidence for this assertion.

Macquarie Island is a unique site for observation since comparable studies of gravity waves at similar latitudes in the southern hemisphere are few. *Thompson* [1978] used a series of high spatial and temporal resolution radiosonde flights to demonstrate the existence of gravity waves with near-inertial frequencies over Laverton, Australia (38°S). Other relevant studies include those of *Vincent* [1994], who investigated gravity waves in the polar mesosphere over Mawson[1] (68°S), and *Gary* [1989], who investigated mountain wave activity near 20 km over Antarctica. Macquarie Island is located approximately halfway between Tasmania and Antarctica.

Gravity waves at middle latitudes are most important in the mesosphere where they are thought to have significant influence on the mean flow [e.g., *Lindzen*, 1981]. However, the determination of gravity wave characteristics near the dominant tropospheric sources is necessary if the effects of waves are to be fully understood. The aim of this chapter is to investigate the climatological characteristics of gravity waves in the troposphere and lower stratosphere over Macquarie Island. Radiosonde observations of temperature and horizontal wind velocity are utilized and further details about these data are discussed in the following section. The location of Macquarie Island in relation to Antarctica and Australian radiosonde stations in Antarctica is illustrated in Figure 3.2.

5.2 Radiosonde Data and the Background Atmosphere

The radiosonde data set considered in this chapter contains 24 months of operational radiosonde soundings from Macquarie Island (55°S, 159°E) between April 1993 and March

[1]It is worth noting that *Vincent* [1994] observed wave amplitudes over Mawson that were significantly smaller than those found at comparable northern-hemisphere latitudes.

1995. These data were downloaded on a weekly basis and the assistance of Bureau of Meteorology staff is gratefully acknowledged. The wind and temperature measurements were obtained in the manner described in chapter 3. Sondes were usually launched twice daily and reached typical heights of between 25 and 30 km. Figures 5.1 and 5.2 illustrate examples of temperature, zonal wind velocity and meridional wind velocity profiles observed during June and December 1993, respectively. Successive profiles have been displaced horizontally in each plot while missing winds are attributed to poor reception of VLF radio transmissions.

The typical height of the tropopause over Macquarie Island is of the order of 10 km. However, typical tropopause heights do vary from day to day and are not always clearly defined. Temperature inversions are common below 5 km and are likely to affect power spectral density calculations of normalized temperature fluctuations. Power spectra are determined between 1.0 and 8.0 km in the troposphere due to low tropopause heights.

Zonal wind speeds are typically much larger than meridional wind speeds, especially during June which is the time of the onset of the southern hemisphere polar vortex. This is important because horizontal winds observed using NAVAID techniques are obtained in polar coordinates and so the determination of zonal and meridional wind velocity components may result in undesirable propagation of random measurement errors. For example, if $\overline{u}$ is large and $\overline{v}$ is zero then the experimental error of v is proportional to the total horizontal wind speed. This situation must be monitored to ensure that random measurement error does not exceed geophysical gravity wave signals in the meridional wind component.

Figure 5.3 illustrates the mean wind and temperature profiles observed over Macquarie Island during June and December 1993. These were obtained by averaging data from those radiosondes that made continuous wind and temperature measurements up to at least 27 km. Mean horizontal winds and temperatures during the full 2-year observation period are illustrated in Figure 5.4. This figure depicts time-height contours of monthly-mean temperatures, zonal winds and meridional winds which were determined after raw data had been averaged into 500 m by 1 month bins. The binned data were also interpolated so as to produce a smooth contour pattern.

The basic state temperatures in the lower stratosphere vary with season and are largest during summer. The basic state zonal winds also vary with season and are largest during winter. This is the well known annual oscillation of zonal winds which occurs in response to seasonal changes in the latitudinal distribution of temperature. Basic state meridional winds are typically weak while the mean tropopause height is slightly larger during summer.

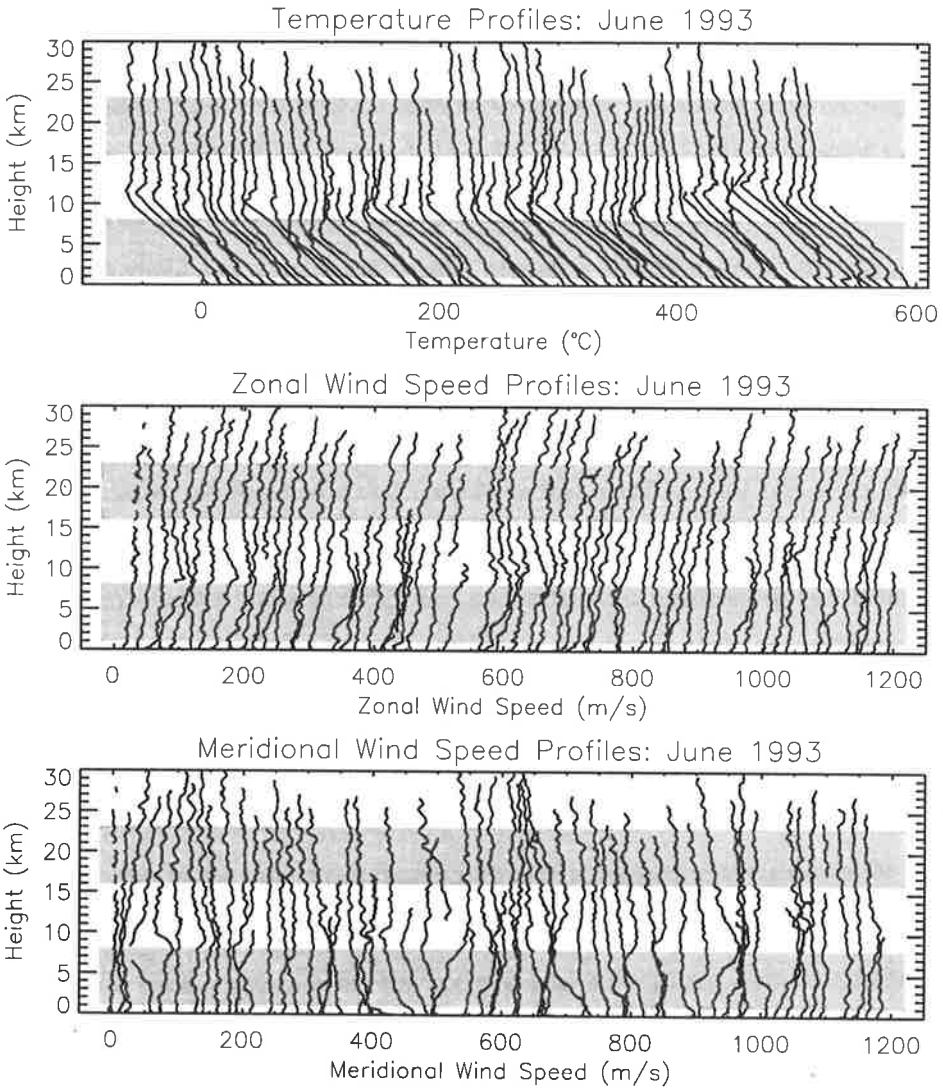

Figure 5.1: Examples of temperature profiles, zonal wind velocity profiles and meridional wind velocity profiles observed over Macquarie Island (55°S, 159°E) during June 1993. Successive temperature profiles are displaced by 10°C and successive wind velocity profiles are displaced by 20 m s^{-1} per 12-hour delay between soundings. Shaded areas indicate the height intervals used for spectral analysis.

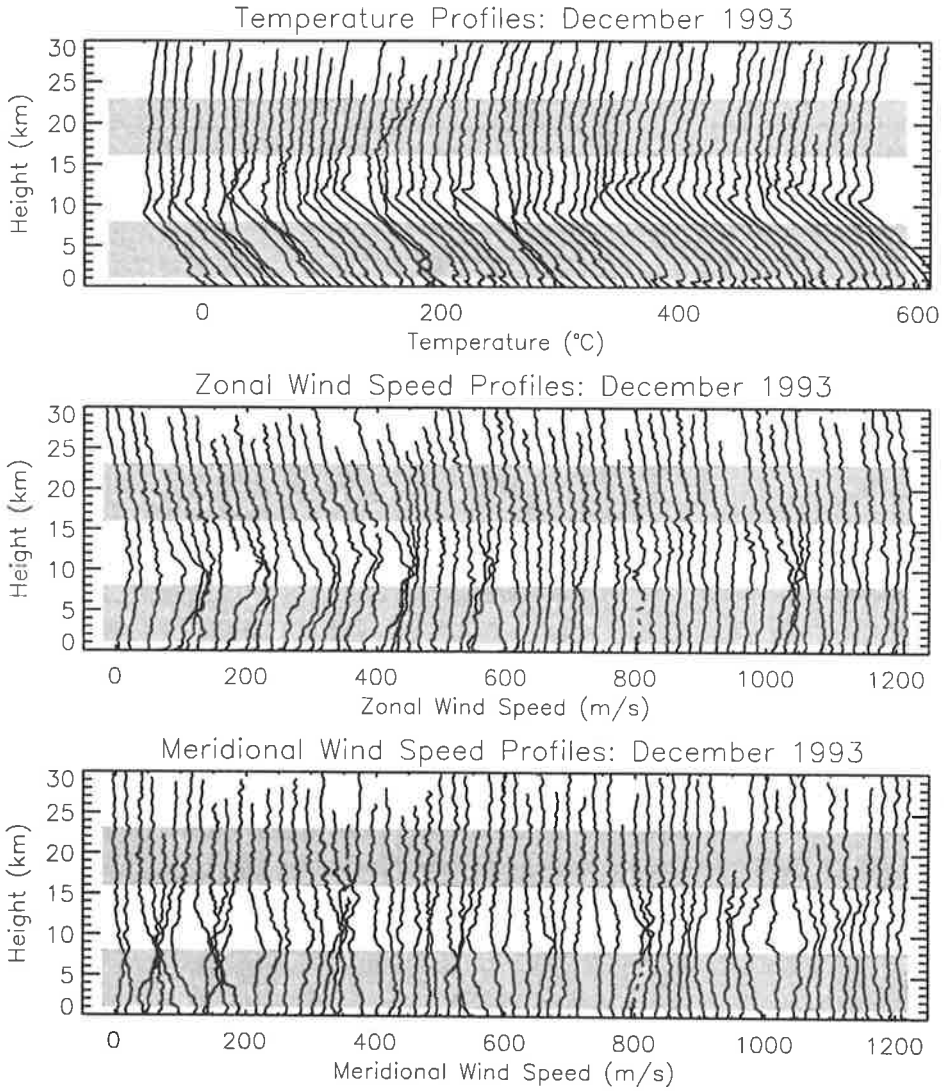

Figure 5.2: As in Figure 5.1, but for temperature profiles, zonal wind velocity profiles and meridional wind velocity profiles observed over Macquarie Island (55°S, 159°E) during December 1993.

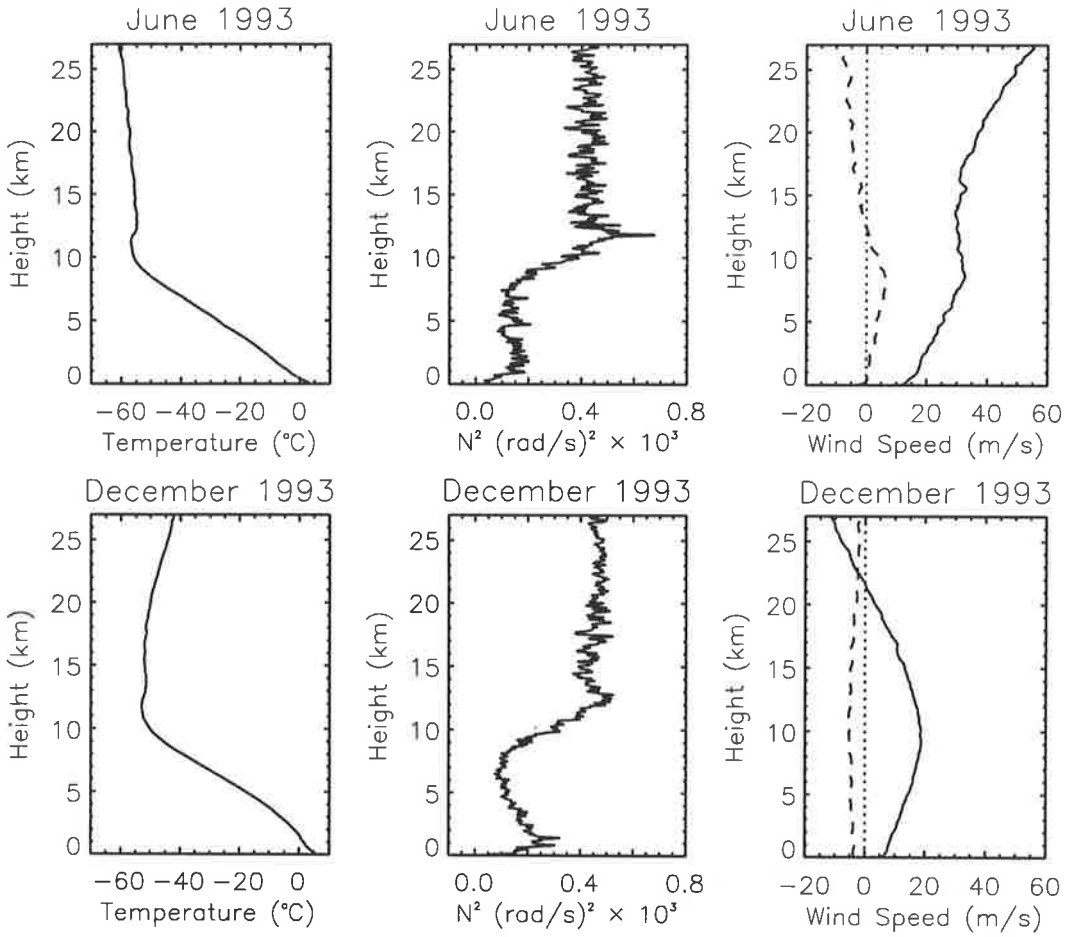

Figure 5.3: Mean vertical profiles of temperature, Väisälä-Brunt frequency squared and horizontal wind velocity components during June 1993 and December 1993 over Macquarie Island. The figure plots are organized in rows such that, from left to right, the first plot illustrates the mean temperature profile, the second illustrates the mean Väisälä-Brunt frequency squared profile and the third illustrates the mean wind velocity component profiles. In the latter case both zonal (solid lines) and meridional (dashed lines) winds are plotted.

The basic state zonal winds are of importance since they are likely to influence the observed characteristics of gravity waves over Macquarie Island. During summer, these winds change sign near 22 km and thus prevent zonally-propagating waves with small or zero ground-based horizontal phase speeds from propagating further into the stratosphere. During winter, strong eastward winds prevail and may affect wave propagation characteristics by refraction processes, as was discussed in chapter 1. In particular, the narrow-band biasing effect described by *Eckermann et al.* [1995] may result in a scarcity of variance in the zonal wind component if this is considered over a small altitude range.

Recall that gravity wave vertical wavelength varies with the basic state horizontal wind

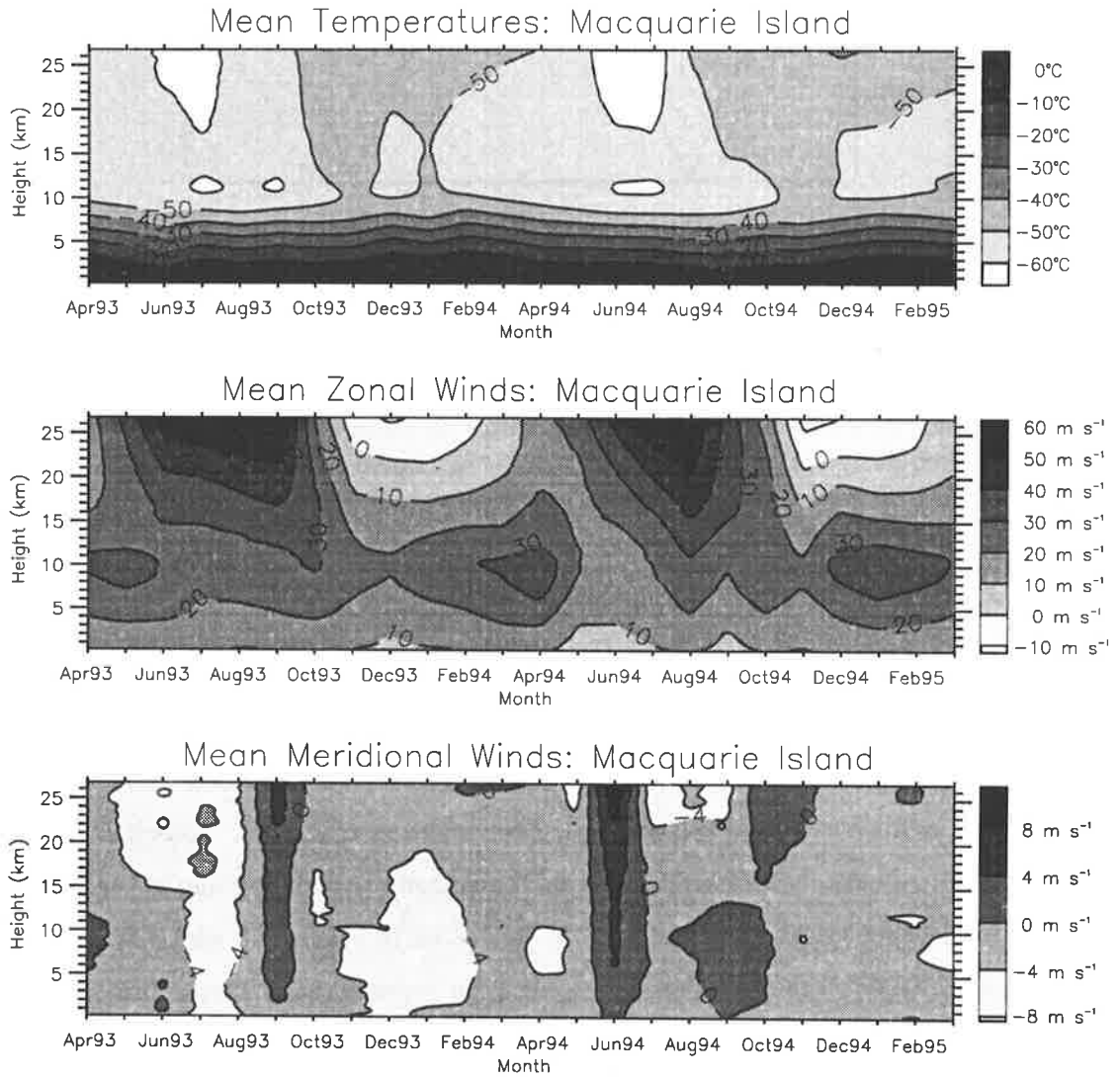

Figure 5.4: Time-height contours of monthly-mean temperature, zonal wind velocity and meridional wind velocity between April 1993 and March 1995 over Macquarie Island. Positive zonal and meridional winds are eastward and northward, respectively.

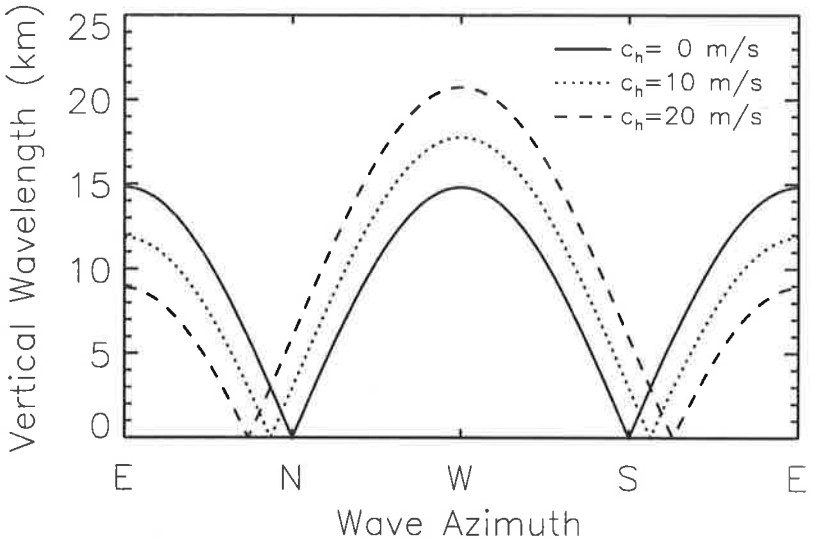

Figure 5.5: The modelled dependence of vertical wavelength as a function of wave azimuth for three different values of ground-based horizontal phase speed [after *Eckermann et al.*, 1995]. The mean horizontal wind velocity was chosen as 50 m s^{-1} and eastward while the Väisälä-Brunt frequency was chosen as 0.021 rad s^{-1}. These values are representative of wintertime conditions in the lower stratosphere over Macquarie Island.

speed, $\overline{U}$, according to

$$\lambda_z = \frac{2\pi \left| c_h - \overline{U} \cos \xi \right|}{N} \frac{(1 - f^2/\omega^2)}{(1 - \omega^2/N^2)} \tag{5.1}$$

where c_h is the ground-based horizontal phase speed and ξ is the azimuth angle between horizontal wind and wavenumber vectors [e.g., *Eckermann et al.*, 1995]. Thus if $\overline{U}$ is large and zonal then λ_z can also be large depending on the magnitude and direction of the ground-based horizontal phase speed. This situation is illustrated in Figure 5.5 which shows, after *Eckermann et al.* [1995], the dependence of λ_z on ξ for representative values of c_h, $\overline{U}$ = 50 m s^{-1} and eastward, $\omega << N$ and $N^2 = 4.5 \times 10^{-4}$ (rad/s)^2. Clearly, the vertical wavelengths of zonally propagating waves can become very large during extreme wind conditions similar to those observed over Macquarie Island in winter. Such waves are not extracted from within narrow altitude intervals since they cannot be distinguished from the mean. This is the narrow band biasing effect of *Eckermann et al.* [1995] and must be taken into consideration when interpreting observed gravity wave characteristics.

Gravity waves propagating against the mean flow may experience reflection, as described in chapter 1, depending on the size of their horizontal wavelength. This is particularly important for mountain waves (c_h = 0 m s^{-1}) generated by small islands, such as Macquarie

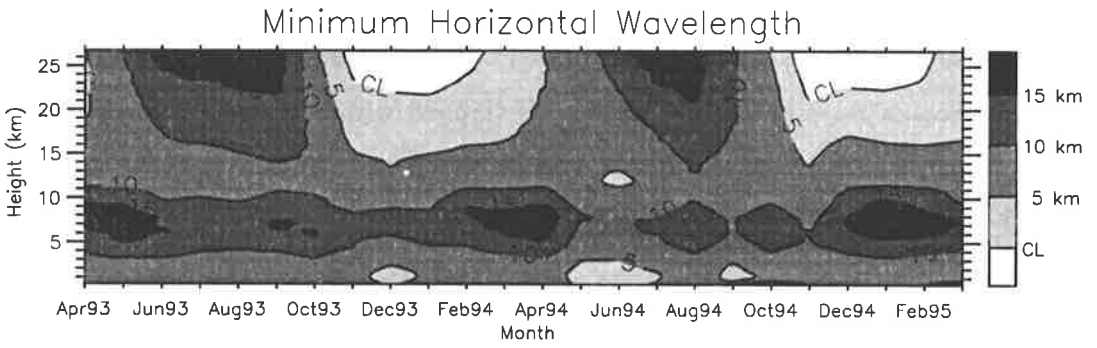

Figure 5.6: Time-height contours of the minimum horizontal wavelength of untrapped, stationary and zonally aligned gravity waves over Macquarie Island. The critical levels of such waves are denoted by "CL" in the diagram.

Island, since they are necessarily of small horizontal scale. The minimum horizontal wavelength of zonally aligned, stationary gravity waves that can propagate upward through a gradually changing profile of zonal wind and N is

$$\lambda_{\min} \approx 2\pi\overline{u}/N \tag{5.2}$$

where $\lambda_{\min}$ is horizontal wavelength [e.g., *Hines*, 1989; *Balsley and Carter*, 1989]. This follows from (1.16) given that wave reflection occurs when ω approaches N.

Figure 5.6 illustrates time-height contours of the minimum horizontal wavelength of untrapped, stationary and zonally aligned gravity waves over Macquarie Island. These were determined, after *Balsley and Carter* [1989], by substituting monthly-mean Väisälä-Brunt frequency and zonal wind velocity profiles into (5.2). Clearly, any zonally aligned mountain wave that reaches the lower stratosphere during summer is not subject to reflection thereafter, although such waves will encounter a critical level in the lower stratosphere near 23 km. In contrast, zonally aligned mountain waves that reach the lower stratosphere during winter can be reflected above about 20 km due to the strong winds of the southern hemisphere polar vortex. The minimum horizontal wavelengths that are anticipated in the lower stratosphere range between approximately 10 and 19 km.

The prevailing, ground level winds over Macquarie Island are known to be eastward [*Streten*, 1988]. However, the east-west scale of Macquarie Island is of the order of 5 km and can only generate gravity waves of very small horizontal scale. For example, the dominant horizontal wavelength of the gravity wave spectrum forced by a bell shaped mountain ridge is $2\pi a$ where a is equivalent mountain half width [*Schoeberl*, 1985]. A reasonable estimate

of half width for Macquarie Island[2] is between 1 and 2 km which means that the dominant horizontal wavelength most probably lies between 6 and 13 km. Therefore, a significant portion of mountain wave energy is likely to be trapped within the troposphere since the dominant horizontal wavelength is of the same order as, or smaller than, the minimum wavelength admitted into the stratosphere.

The extent of mountain wave activity over Macquarie Island is of importance since, if significant, the characteristics of gravity waves determined in this chapter will not be representative of those over the open ocean. Furthermore, the mean winds may not be exactly representative either due to mountain wave drag [*Balsley and Carter*, 1989]. The variance characteristics of gravity waves in the troposphere and lower stratosphere are investigated in the following section.

5.3 Variance Characteristics

The mean vertical wavenumber power spectra of normalized temperature fluctuations over Macquarie Island were presented in Figure 4.16. These spectra were averaged over a 12-month observation period between April 1993 and March 1994. In this chapter, normalized temperature power spectra from Macquarie Island are investigated over the full 24-month observation period. Horizontal wind velocity power spectra are also investigated.

5.3.1 Temperature Variance

Figures 5.7 and 5.8 illustrate mean vertical wavenumber spectra of normalized temperature fluctuations in both conventional logarithmic and area preserving forms, respectively. These were averaged[3] over 3-month periods in most cases and were calculated in the troposphere (1.0–8.0 km) and lower stratosphere (16.0–23.0 km) by applying the same techniques as those used in chapter 4. As before, vertical wavenumber power spectra are plotted against the theoretical saturation limits due to *Smith et al.* [1987] which are used as a convenient reference.

The power spectra determined in the lower stratosphere are similar to those found at Davis (Figure 4.15). They have considerably reduced spectral amplitudes at low vertical

[2]This is taken to be half of the typical east-west spacing of the 200 m contour line.

[3]Note that normalized individual spectra were averaged over 3-month time periods rather than over 1-month time periods as was the case previously. In chapter 4, the 3-month average spectra were in fact weighted arithmetic means of 1-month average spectra.

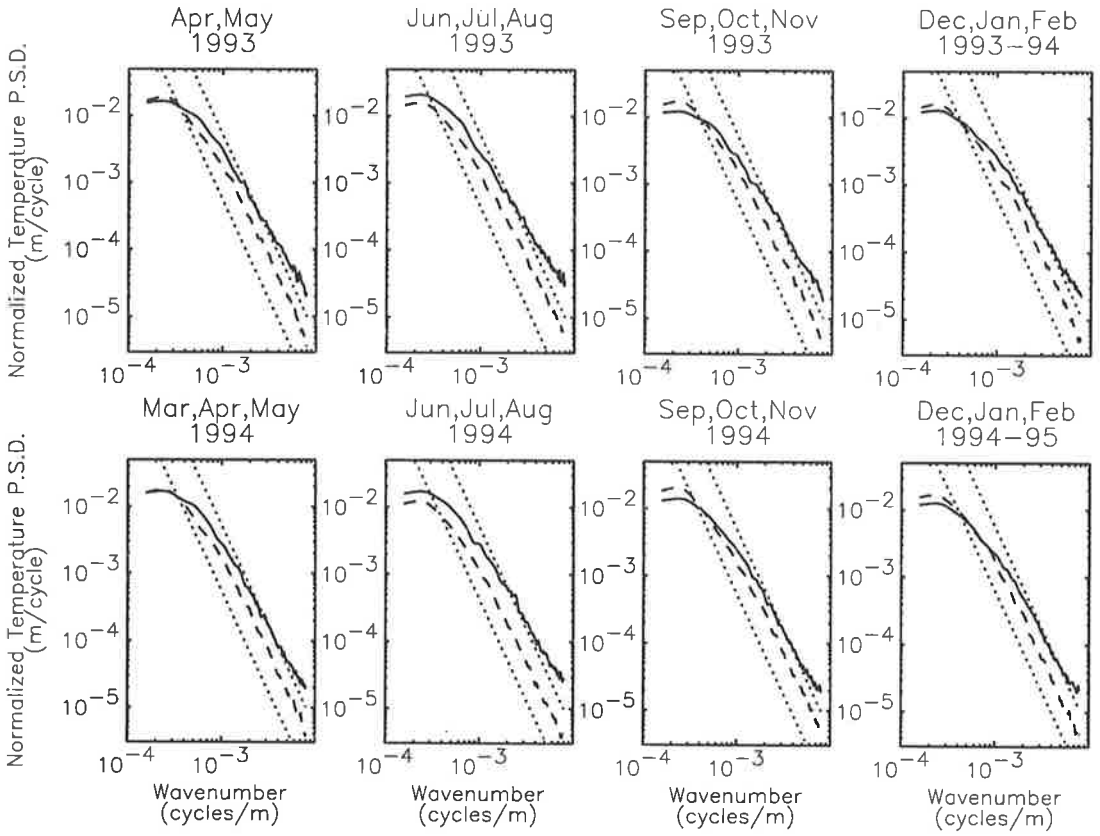

Figure 5.7: Vertical wavenumber power spectra of normalized temperature fluctuations observed at Macquarie Island (55°S, 159°E). Solid lines indicate stratospheric spectra (16.0 to 23.0 km) while dashed lines indicate tropospheric spectra (1.0 to 8.0 km). Each spectrum is either a 2 or 3-month average and the saturation limits due to *Smith et al.* [1987] are plotted for comparison purposes (dotted lines). The 95% confidence limits are approximately given by 0.85 and 1.15 multiplied by the spectral amplitude at each wavenumber.

wavenumbers in comparison to spectra found at low-latitude and midlatitude sites. However, spectral amplitudes at high vertical wavenumbers do approach the theoretical saturation limits proposed by *Smith et al.* [1987]. Area preserving spectra indicate that the largest wave amplitudes occur between March and August while the smallest amplitudes occur during the 3-month period of December, January and February. This is consistent with the seasonal variation of wave energy observed in the lower stratosphere over Hobart (see Figure 4.14).

Tropospheric power spectra have amplitudes that are consistently larger than the theoretical saturation limits due to *Smith et al.* [1987], as is found elsewhere. It is likely that these are affected by temperature inversions, which are not dynamical phenomena, based on inspection of observed temperature profiles such as those displayed in Figures 5.1 and 5.2.

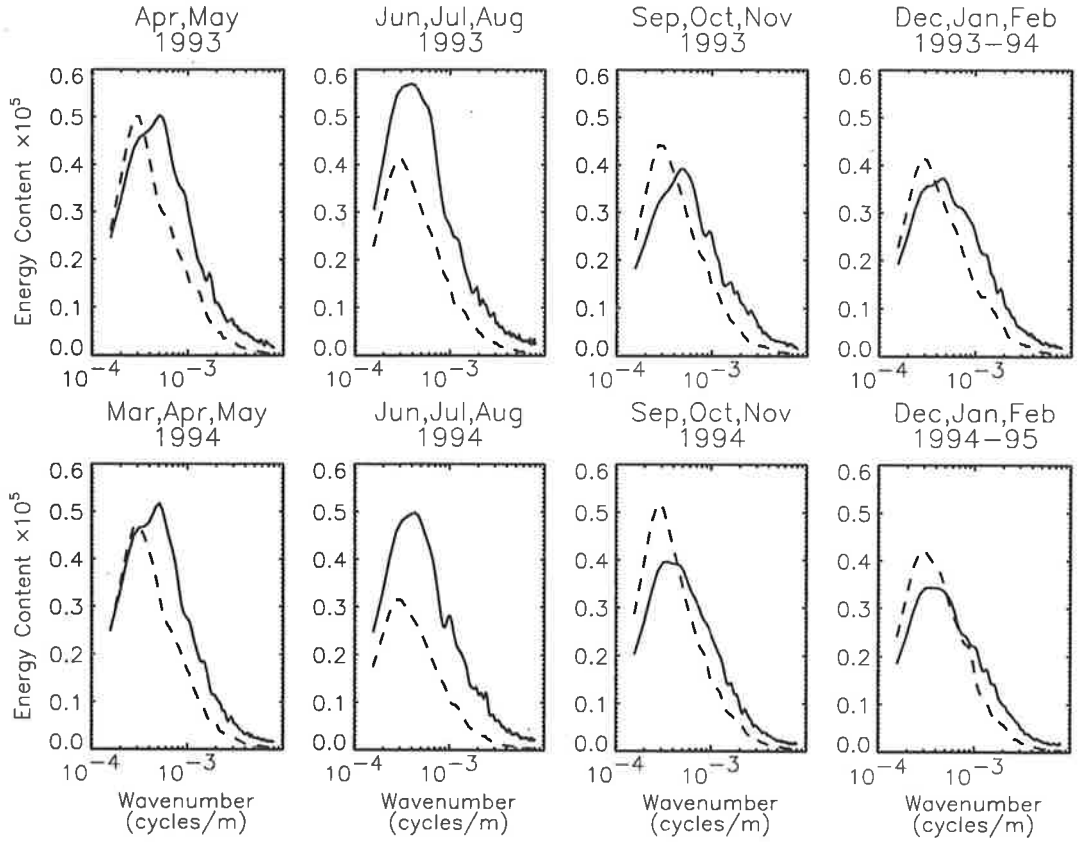

Figure 5.8: As in Figure 5.7, but spectra are presented in area preserving form. Solid lines indicate stratospheric spectra (16.0 to 23.0 km) while dashed lines indicate tropospheric spectra (1.0 to 8.0 km).

The seasonal variation of tropospheric spectral amplitudes is not consistent with the seasonal variation of the lower stratosphere and possibly reflects the occurrence frequency of inversions. Unfortunately, there is little that can be done to remove inversions from the available data.

The dominant vertical wavelength, $2\pi/m_*$, is of the order of 2 or 3 km in both the troposphere and lower stratosphere which is congruous with results found elsewhere. If anything, m_* is consistently smaller for the tropospheric spectra than for the stratospheric spectra. However, m_* is not known to good accuracy since $\overline{T}(z)$ for individual profiles must be estimated by using fitted polynomials. This problem was discussed in chapter 4.

5.3.2 Wind Speed Variance

Figure 5.9 presents mean vertical wavenumber spectra of total horizontal wind velocity fluctuations in both conventional logarithmic and area preserving forms. These spectra are the

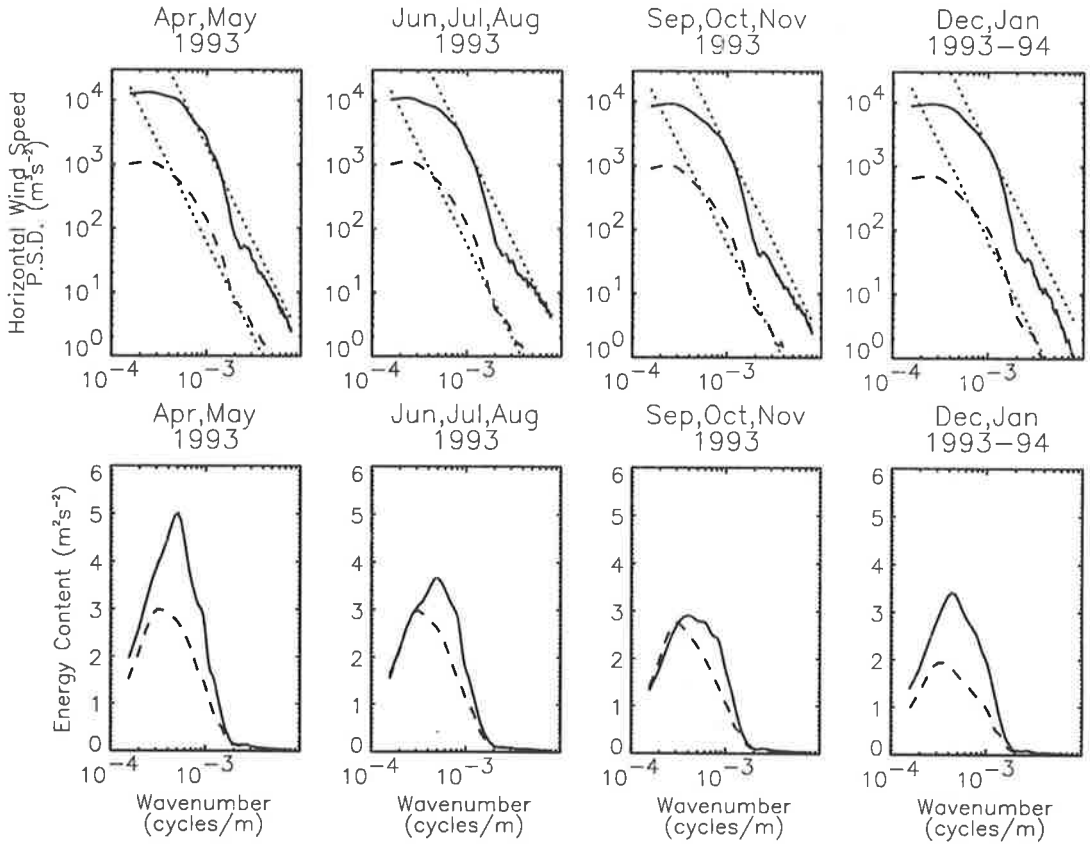

Figure 5.9: Vertical wavenumber power spectra and area preserving spectra of total horizontal wind velocity fluctuations observed at Macquarie Island (55°S, 159°E). Solid lines indicate stratospheric spectra (16.0 to 23.0 km) while dashed lines indicate tropospheric spectra (1.0 to 8.0 km). Each spectrum is either a 2 or 3-month average and the saturation limits due to *Smith et al.* [1987] are plotted for comparison purposes (dotted lines). The 95% confidence limits are approximately given by 0.85 and 1.15 multiplied by the spectral amplitude at each wavenumber. Tropospheric power spectra have been displaced downward by an order of magnitude so as to aid viewing.

sum of zonal and meridional wind component spectra and are plotted against the theoretical saturation limits proposed by *Smith et al.* [1987]. As before, each spectrum was calculated using the Blackman-Tukey algorithm with a 90% lag Bartlett window after the raw data had first been prewhitened by differencing. Only 10 months of horizontal wind velocity measurements, between and including April 1993 and January 1994, were considered.

Recall that all raw wind velocity measurements have been subjected to a cubic spline smoothing algorithm[4] within a running window of either 650-m or 1250-m extent (see section 3.2). At Macquarie Island, the 650-m length smoothing window was used on data obtained before the 24th of January, 1994, while the 1250-m length smoothing window was

[4]This is a data quality control procedure.

used on data obtained thereafter. In the latter case, the calculated power spectra (which are not shown) were found to have considerably attenuated amplitudes and it was clear that a significant portion of gravity wave variance was lost due to severe smoothing. As a consequence, the only wind velocity data to be considered hereinafter will be those that were smoothed within the 650-m length running window.

The observed fluctuation profiles, after smoothing by a cubic spline within a given running window, will have attenuated amplitudes at vertical scales that are smaller than approximately twice the smoothing window length. Consequently, the calculated power spectra are anticipated to have attenuated spectral amplitudes at high vertical wavenumbers. The purpose of data smoothing is to remove any contribution due to random measurement error. From Figure 3.4, this contribution is more important for the component wind velocity profiles, in comparison to temperature profiles, and so requires greater smoothing.

Consider the form of the horizontal wind velocity fluctuation spectra in the lower stratosphere. For vertical wavenumbers $m/2\pi < 10^{-3}$ cpm, the spectral form is generally consistent with the spectral form of normalized temperature power spectra. The dominant vertical wavenumber is of the order of $m_*/2\pi \approx 4 \times 10^{-4}$ cpm and spectral amplitudes converge upon the theoretical saturation limits at larger wavenumbers. This region of the spectrum is thought to represent the true gravity wave spectrum.

At vertical wavenumbers $m/2\pi > 10^{-3}$ cpm, however, lower stratospheric spectral amplitudes become significantly attenuated in comparison to the theoretical saturation limits. This attenuation, presumably, is a direct result of the cubic spline smoothing procedure. Thus all spectral amplitudes at large vertical wavenumbers underestimate their true values. However, an attenuated noise floor, due to random measurement error, is probably present in the high-wavenumber region of the spectrum. In particular, notice the sudden change of spectral slope at $m/2\pi \approx 2 \times 10^{-3}$ cpm which might define the vertical scale at which random noise becomes important. Furthermore, spectral amplitudes for $m/2\pi > 2 \times 10^{-3}$ cpm are approximately the same in both the troposphere and lower stratosphere. This is consistent with a noise floor interpretation since random measurement error is expected to remain independent of altitude.

In section 5.2, it was argued that the random measurement error of the meridional wind component may become larger during conditions of strong zonal wind. This argument is supported by lower stratospheric spectral amplitudes which are clearly larger at high vertical wavenumbers ($m/2\pi > 2 \times 10^{-3}$ cpm) during winter months. Furthermore, much

of the excess variance appears in the meridional wind component spectrum (not shown) as expected. However, the increase in variance is of little significance and the spectra are only affected in the attenuated region. At low vertical wavenumbers ($m/2\pi < 2 \times 10^{-3}$ cpm), the zonal and meridional wind component spectra have similar spectral form during all seasons.

The horizontal wind velocity fluctuation spectra illustrated in Figure 5.9 suggest that the dominant gravity waves of the lower stratosphere are adequately resolved by the data, provided that the 650-m length smoothing window is used. This is also true of the troposphere where spectra have similar form. In contrast, the use of a 1250-m length smoothing window results in a significant reduction of total variance. Therefore, such severely smoothed data are inappropriate for use in gravity wave studies[5].

Area preserving spectra indicate that horizontal wind velocity variance in the lower stratosphere is largest during April and May and smallest between September and January. This is similar to the seasonal variation of normalized temperature variance although the correlation is poorer than might be expected. Note that a strong correlation between total horizontal wind velocity variance and normalized temperature variance is anticipated if the shape of the one-dimensional gravity wave frequency spectrum is time independent. Further details are provided in the following subsection.

5.3.3 Seasonal Variations

Figure 5.10 illustrates monthly-mean gravity wave potential and horizontal kinetic energy estimates (per unit mass) as a function of time, between April 1993 and January 1994, within the troposphere (1.0 and 8.0 km) and lower stratosphere (16.0–23.0 km) over Macquarie Island. From chapter 1, these quantities are given by

$$E_K = \frac{1}{2}\left[\overline{u'^2} + \overline{v'^2}\right] \tag{5.3}$$

$$E_P = \frac{g^2\overline{\hat{T}'^2}}{2N^2} \tag{5.4}$$

where E_P and E_K are potential and horizontal kinetic energy (per unit mass), respectively, and where the variance terms are to be determined from the areas under vertical wavenumber power spectra. Note that the ratio of horizontal kinetic and potential energy is approximately equal to p, the slope of the one-dimensional frequency spectrum. This follows from the polarization equations presented in chapter 2, if it can be assumed that the three-dimensional

[5]It is possible to consider such data provided the significant reduction of total variance is correctly acknowledged.

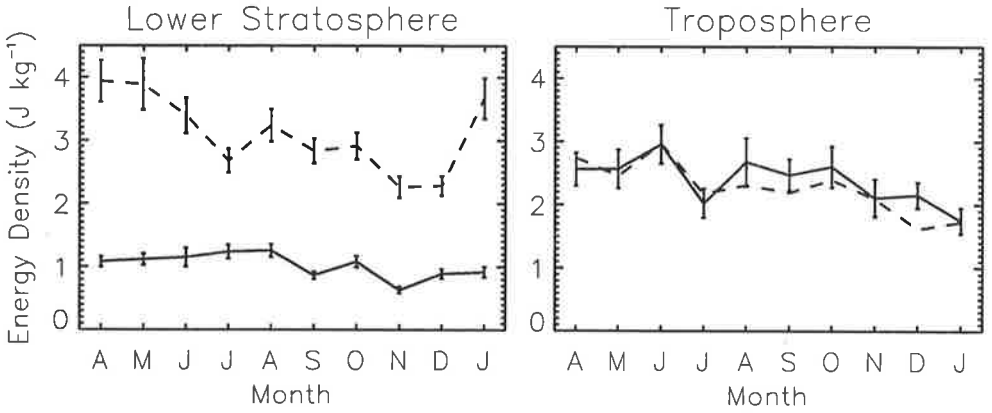

Figure 5.10: Time variations of monthly-mean potential energy per unit mass (solid lines) and horizontal kinetic energy per unit mass (dashed lines) within both the troposphere (1.0–8.0 km) and lower stratosphere (16.0–23.0 km) over Macquarie Island. Error bars describe the standard errors of the means but are not plotted for kinetic energy estimates within the troposphere since these overlay the error bars of potential energy estimates.

energy spectrum is separable and that the one-dimensional frequency spectrum is given by $B(\omega) \propto \omega^{-p}$ where p is approximately greater than 1.1.

In the lower stratosphere, horizontal kinetic energy is consistently larger than potential energy. This is expected of a red-noise frequency spectrum of gravity waves ($p > 1$) since the total energy of waves with ω near f is unequally partitioned between potential and kinetic energy components [e.g., *Gill*, 1982]. The estimate of p most often cited in the literature is $p = 5/3$. However, due to Doppler shifting of observed frequency spectra there remains some uncertainty as to the correct value of p. The mean ratio of lower stratospheric kinetic to potential energy from Figure 5.10 is 3.1 while the standard error of the mean ratio is 0.2. This suggests that the wave field is strongly dominated by low-frequency inertio-gravity waves.

In contrast, tropospheric potential energy is approximately equal to horizontal kinetic energy during all months. This may indicate that the frequency spectrum of gravity waves is quite different within the troposphere, perhaps due to the presence of trapped, small-horizontal-scale mountain waves. However, it is almost certain that temperature inversions will contribute to normalized temperature variance. Therefore, gravity wave potential energy is probably overestimated in the troposphere, at least to some extent. The mean ratio of tropospheric kinetic to potential energy from Figure 5.10 is 0.95 while the standard error of the mean ratio is 0.03.

The comparatively large kinetic energy density in the lower stratosphere suggests that energetic inertio-gravity waves are commonly present. Individual waves might be identified from wind hodographs in some instances [e.g., *Sawyer*, 1961] but a superposition of many different waves is expected in general. Horizontal wind fluctuation hodographs over Macquarie Island are investigated in the following section.

5.4 Hodograph Analysis

The conventional definition of a hodograph is a curve which joins the tips of a particle velocity vector at successive instants in time. However, the hodographs considered in this section describe the tips of horizontal wind vector fluctuations at successive altitudes along a radiosonde trajectory [e.g., *Sawyer*, 1961]. For ideal, monochromatic inertio-gravity waves, this form of hodograph is a spiralling ellipse (see Figure 3.9).

In general, observed wind component profiles are polychromatic and so ideal, elliptical hodographs are not expected in practice. However, on rare occasions, monochromatic wind component fluctuations are found to persist for more than two wave cycles and their hodographs are elliptical figures as expected. Two such examples are illustrated in Figure 5.11. The first is a hodograph of wind vector fluctuations observed on December 19, 1993, while the second was observed on January 22, 1994. Both trace out neat ellipses and were plotted after fitted, third-order polynomials had been removed from the wind velocity component profiles over an 8-km altitude interval. In addition, the wind velocity component profiles were low-pass filtered[6] with a cutoff vertical scale of 500 m.

The two curves of Figure 5.11 display anticlockwise rotation with increasing altitude. Assuming each is the hodograph of a monochromatic inertio-gravity wave[7], then wave energy is upward propagating and the intrinsic frequency is defined by (3.30). Furthermore, the horizontal wavenumber vector is aligned along the semi-major axis[8] which is defined by (3.28). The degree of polarization parameters, for the hodographs of December 19 and January 22, are $d = 0.94$ and $d = 0.88$, respectively.

[6]The purpose of filtering is to produce smoother wind hodographs that are not affected by small amplitude and small vertical scale gravity waves (or noise). Note that the resultant hodographs still represent a broad range of vertical scales, between approximately 8 km and 500 m (or 2 octaves), which includes the dominant vertical scale.

[7]*Eckermann and Hocking* [1989] argue that the appearance of a monochromatic signal over one or two cycles need not imply that the wave field is monochromatic.

[8]Notice that the semi-major axis of the December 19 hodograph does appear to be arbitrary owing to the near-circular nature of this curve.

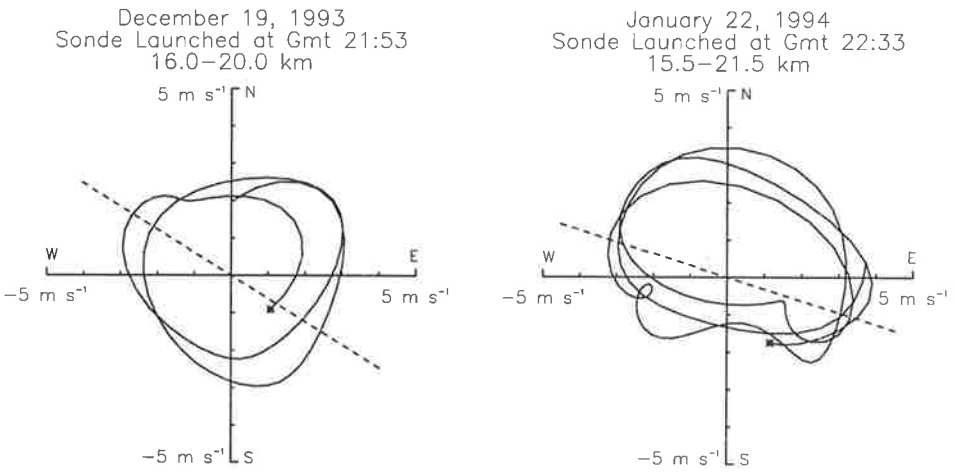

Figure 5.11: Two examples of wind fluctuation hodographs in the lower stratosphere over Macquarie Island. The tip of the wind velocity vector at the lowest altitude is indicated by an asterisk in each case. Dashed lines indicate the preferred sense of alignment of the polarized component which has been determined by Stokes parameter analysis.

More generally, the observed wind hodographs are polychromatic and do not trace neat figures over several wave cycles. However, it is often the case that wind velocity fluctuations appear to have some dominant sense of horizontal alignment. Examples of such hodographs are illustrated in Figure 5.12 where the dashed lines in each case describe the preferred sense of alignment as defined by (3.28). The degree of polarization parameters are $d = 0.84$ and $d = 0.79$ for the December 6 and December 30 hodographs, respectively. Notice that each hodograph displays predominantly anticlockwise wind vector rotation with increasing altitude.

Other hodographs can be found that appear to have no preferred sense of horizontal alignment by inspection. Typically these have small degree of polarization parameters which are of the order of 0.4 or less. A dominant sense of horizontal alignment can be defined in each case but the wave fields are perhaps best described as being unpolarized and azimuthally isotropic. Two examples for which d is less than 0.4 are illustrated in Figure 5.13.

It is evident from inspection of wind hodographs that a dominant sense of vector rotation and a dominant sense of horizontal alignment can be assigned to individual wind hodographs in many instances. Based on the discussions of chapter 3, this implies that dominant directions of horizontal and vertical phase propagation can be determined. Furthermore, the degree of polarization parameter provides an objective measure as to when "dominant" directions are representative of the gravity wave field. Large values of d imply that the wave

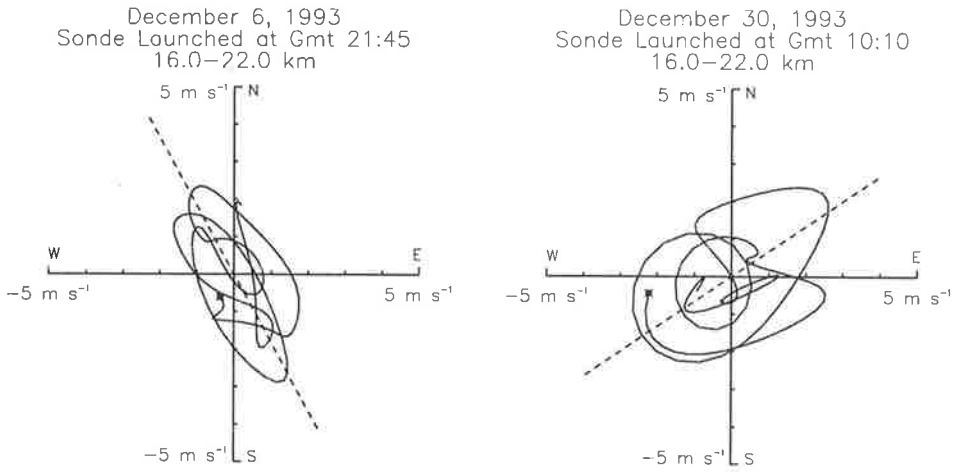

Figure 5.12: As in Figure 5.11, but for wind hodographs which describe a polychromatic wave field. The tip of the wind velocity vector at the lowest altitude is indicated by an asterisk in each case.

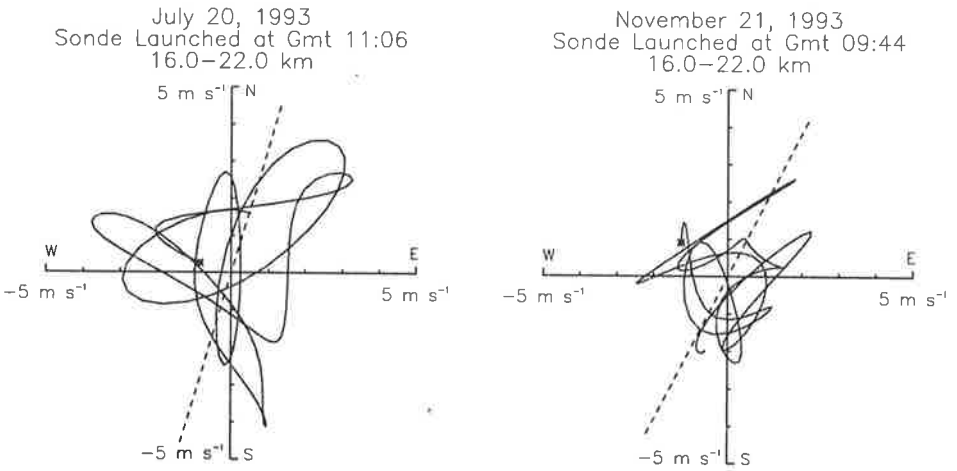

Figure 5.13: As in Figure 5.11, but for wind hodographs which have $d < 0.4$. The tip of the wind velocity vector at the lowest altitude is indicated by an asterisk in each case.

field is strongly polarized while small values imply that the wave field is unpolarized and azimuthally isotropic.

In addition to the above information, it is possible to estimate dominant intrinsic frequencies using (3.30). However, *Eckermann and Hocking* [1989] warn against such practice when the wave field is polychromatic. They argue that the wind hodograph provides information about directionality, rather than intrinsic frequency, in this case. Furthermore, *Hines* [1989] pointed out that a linearly-polarized gravity wave may produce an elliptical hodograph if there exists a background wind shear in the direction transverse to the horizontal wave oscillation. Clearly, any estimate of intrinsic frequency that is obtained using (3.30) must be

treated with some caution.

In this thesis, no attempt is made to estimate dominant intrinsic frequencies from horizontal wind fluctuation hodographs. Rather, the analysis will concentrate upon the dominant directions of horizontal and vertical phase propagation and these are the subject of investigation in the following section. However, *Cho* [1995] has developed a technique for extracting inertio-gravity wave parameters, including the intrinsic frequency, using autospectra and cross spectra of the component horizontal winds[9]. The proposed technique makes allowance for the effects of vertical shear as described by *Hines* [1989]. Thus it may be possible to obtain reasonable estimates of dominant intrinsic frequency from the data considered here while at the same time addressing the concerns of *Hines* [1989] and *Eckermann and Hocking* [1989]. Future studies might attempt such analysis.

5.5 Gravity Wave Propagation Directions

5.5.1 Vertical Propagation

Figure 5.14 illustrates mean rotary power spectra of horizontal wind velocity fluctuations in the troposphere (1.0–8.0 km) and lower stratosphere (13.0–20.0 km and 20.0–27.0 km) over Macquarie Island. Each was calculated using a Fast Fourier Transform (FFT) algorithm in the manner described in chapter 3. The wind velocity fluctuations were determined by subtracting fitted second-order polynomials from the zonal and meridional wind velocity component profiles over the altitude ranges of interest. Individual spectra were averaged arithmetically and the sum of the clockwise and anticlockwise component variances is equal to the total horizontal wind velocity variance.

In the troposphere, the clockwise rotating and anticlockwise rotating component spectra are approximately equal during all seasons. If anything, there is slightly more variance in the clockwise component (approximately 53% of the total variance). This suggests that there is either no preferred direction of vertical propagation or that the wave field is dominated by linearly-polarized waves. The latter may be possible due to the presence of trapped, small-horizontal-scale mountain waves.

In the lower stratosphere, the anticlockwise component spectra are consistently larger than the clockwise component spectra during all seasons. This suggests that gravity wave

[9]Note that the cross spectral method of *Cho* [1995] is related to the Stokes parameter method as described by *Eckermann* [1996].

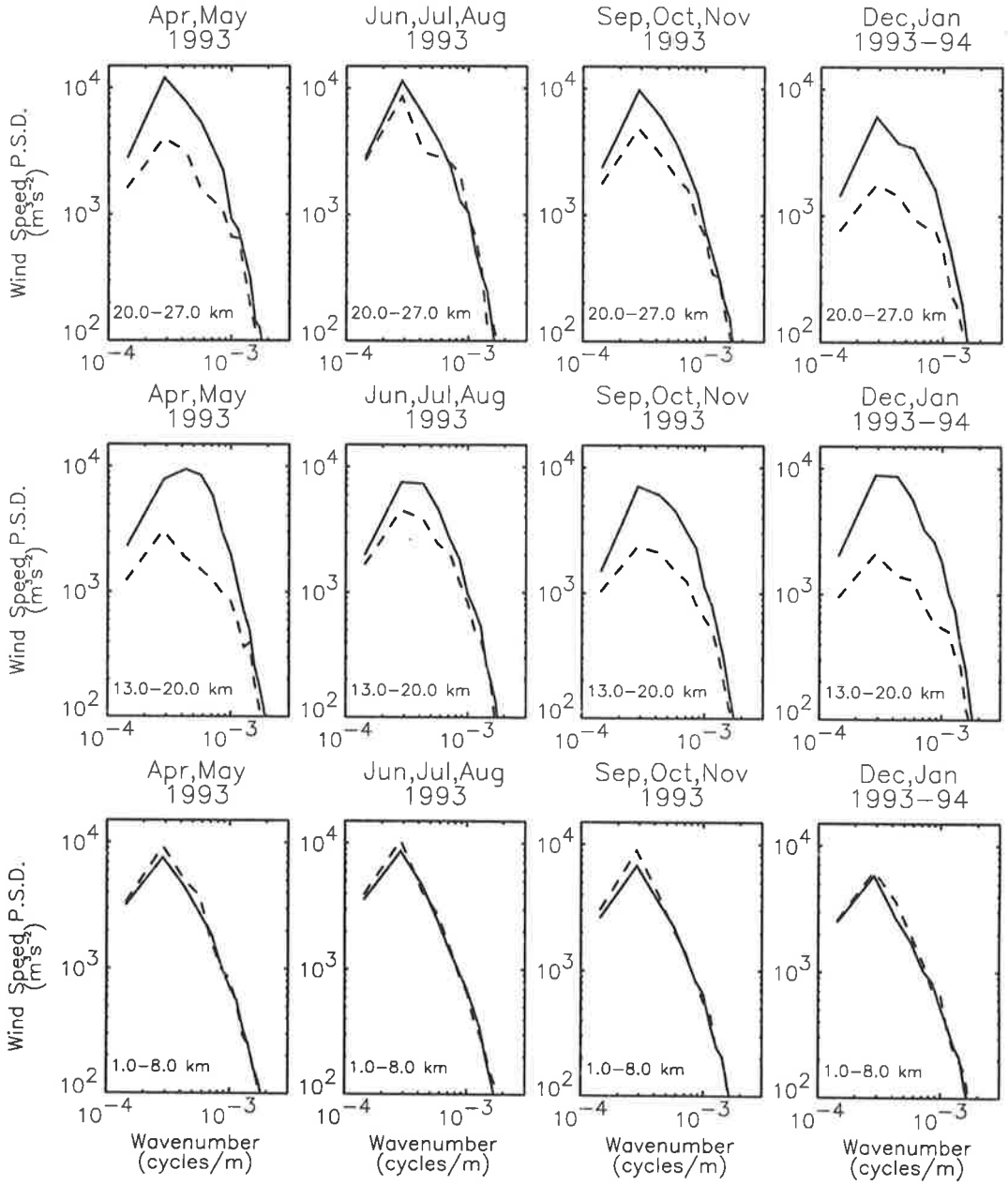

Figure 5.14: Rotary power spectra of horizontal velocity vector fluctuations within the troposphere (1.0–8.0 km) and lower stratosphere (13.0–20.0 km and 20.0–27.0 km) over Macquarie Island. Both clockwise (dashed lines) and anticlockwise (solid lines) component spectra are plotted.

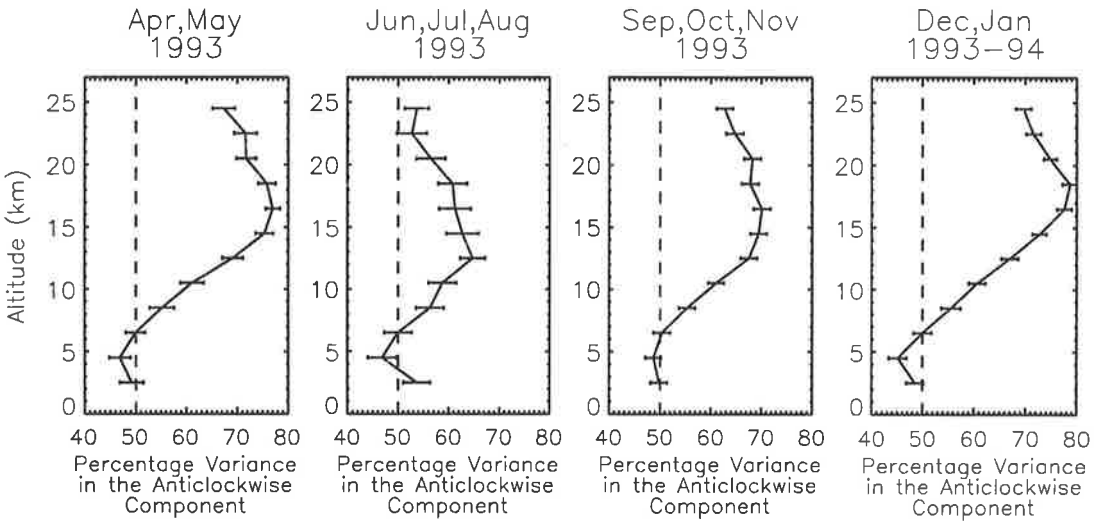

Figure 5.15: The percentage of variance in the anticlockwise rotating component as a function of altitude and averaged within either 2 or 3-month time intervals. Error bars describe the standard errors of the means.

energy is predominantly upward propagating. However, the percentage of variance in the anticlockwise component varies considerably with season and altitude. It is largest during summer and smallest during winter and is always larger between 13.0 and 20.0 km.

To investigate further the seasonal and altitude dependence of rotary component spectra, consider Figure 5.15. This diagram displays the percentage of total horizontal wind velocity variance in the anticlockwise component as a function of altitude. It was constructed by calculating rotary component variances[10] within a 5-km moving window which was shifted vertically in steps of 2 km. Thus the resultant profiles are oversampled in altitude by a factor of 2.5.

The profiles displayed in Figure 5.15 indicate that the percentage of variance in the anticlockwise component maximizes below 20 km in the lower stratosphere. It is clearly larger in summer than in winter where the maxima are 79% and 64%, respectively. During winter, the percentage variance declines to approximately 53% near 25 km compared with values of between 60% and 70% during other seasons. The mean percentage variance is always greater than 50% in the lower stratosphere. Note that the proportion of upward propagating gravity wave energy is probably larger than the percentage of variance in the anticlockwise component, when this is larger than 50%, since elliptically polarized waves have both circular-clockwise and circular-anticlockwise rotating components in general.

[10]These are the areas under rotary component spectra.

The strong seasonal variation of percentage variance in the anticlockwise component is not surprising when compared with similar findings from rocketsonde observations between 20.0 and 60.0 km at several northern hemisphere sites. *Eckermann et al.* [1995] report that a deep minimum in the percentage of clockwise rotations[11] occurs during winter and that a smaller subsidiary minimum occurs during summer at midlatitude sites. Maxima, on the other hand, occur during the equinoxes. With the exception of the subsidiary minimum during summer, these results are consistent with those found between 10.0 and 25.0 km over Macquarie Island.

In their study, *Eckermann et al.* [1995] noted that the seasonal variation of percentage clockwise rotation was well correlated with the seasonal variation in the magnitude of the mean zonal wind between 20.0 and 60.0 km. Strong mean winds, which occurred during the solstices, corresponded to small rotational ratios whereas weak mean winds, which occurred during the equinoxes, corresponded to large rotational ratios. This observation led *Eckermann et al.* [1995] to propose that the percentage clockwise rotation depends upon the mean zonal wind as a consequence of the mean wind's influence on intrinsic frequency (see equation 1.16). During conditions when mean zonal winds are strong and increase with altitude, zonally aligned gravity waves have intrinsic frequencies that are shifted to higher values. Thus their axial ratios are reduced[12] as are their percentage clockwise rotations[13]. During light wind conditions, on the other hand, zonally aligned gravity waves have intrinsic frequencies that are not significantly altered as the waves propagate vertically. As a consequence, such waves will have larger degrees of clockwise rotation than their counterparts during strong wind conditions. According to this picture, changes to the frequency distribution of gravity waves, rather than to the ratio of upward propagating to downward propagating gravity wave energy, are responsible for seasonal changes of the percentage clockwise rotation [*Eckermann et al.*, 1995].

A similar concept may explain the results from Macquarie Island which are illustrated in Figure 5.15. Consider, first, the percentage anticlockwise rotation during winter which is the time of strongest zonal winds in the lower stratosphere. As the mean winds increase from approximately 30 to 50 m s^{-1} between 13.0 and 25.0 km, the percentage anticlockwise

[11] In the northern hemisphere, upward propagating inertio-gravity waves exhibit clockwise rotation of wind velocity vectors with increasing altitude.

[12] The axial ratio of a monochromatic gravity wave is the ratio of fluctuation amplitudes along the major and minor axes of the motion ellipse.

[13] Note that meridionally aligned waves are not subjected to windshifting effects. However, when averaged over all azimuths, the overall effect of windshifting is to reduce the percentage clockwise rotation [*Eckermann et al.*, 1995].

rotation decreases from 64% to 53%. Now if the source spectrum is upward propagating and tropospheric[14], then the zonally aligned gravity waves of the spectrum will have intrinsic frequencies that are shifted to higher values as they propagate vertically through the lower stratosphere. These waves will have hodograph axial ratios that become gradually smaller with increasing altitude which is consistent with the reduction of percentage anticlockwise rotation that is illustrated in Figure 5.15.

During equinox conditions, on the other hand, the mean winds are in transition. Therefore, the shifting of intrinsic frequencies is not as severe as it is during winter conditions which explains the larger percentage anticlockwise rotation. However, during summer, the mean zonal winds peak at approximately 20 m s^{-1} near 10.0 km and decline thereafter, changing direction from eastward to westward near 22.0 km. Consequently, many gravity waves will encounter critical levels in the lower stratosphere and will have intrinsic frequencies that are shifted to lower values. This is consistent with the large values of percentage anticlockwise rotation that are found in Figure 5.15. Note that those gravity waves that survive until the upper stratosphere will have intrinsic frequencies that are shifted to higher values owing to the increasingly strong westward winds within this region (see Figure 1.3). Thus the summertime minimum reported by *Eckermann et al.* [1995] is not necessarily inconsistent with the summertime maximum reported here.

Given that the mean percentage of variance in the anticlockwise component is always greater than 50% and that seasonal variations can be ascribed to seasonal changes in the frequency distribution of waves, then it is reasonable to infer that gravity wave energy is predominantly upward propagating in the lower stratosphere. This is consistent with the current understanding of the gravity wave field and of wave sources. Following *Kitamura and Hirota* [1989] and *Hamilton* [1991], the dominant directions of horizontal phase propagation can now be investigated. The data are divided into what are loosely termed summer (April and November to January) and winter (May to October) months which correspond to the times of smallest and largest mean zonal winds in the lower stratosphere, respectively.

5.5.2 Horizontal Propagation

Firstly, consider the dominant senses of horizontal alignment which are defined by (3.28) and are illustrated by the dashed lines in Figures 5.11, 5.12 and 5.13. Dominant horizontal

[14]It is usual to assume that the source spectrum contains upward propagating gravity waves which have ground-based horizontal phase speeds that are comparable to or smaller than the mean tropospheric winds [e.g., *Lindzen*, 1981].

alignments determined from individual soundings of the lower stratosphere between 16.0 and 23.0 km are illustrated in Figure 5.16. This figure displays the alignments both individually and in polar histogram form. In the former case, each alignment is described by a straight line whose length is proportional to the degree of polarization parameter [after *Vincent*, 1990], while in the latter case, the axis labels describe the number of profiles with a preferred sense of alignment within a given 30° interval. Note that polar histograms treat each horizontal alignment equally, regardless of the degree to which the wave field was polarized.

It is evident from Figure 5.16 that the wave field is preferentially aligned within the north-east and south-west quadrants during winter months. This is also true during summer months although the bias is clearly less severe. The degree of polarization parameter is often larger than 0.5 and can be large for any alignment during summer. If at all, there is a relative scarcity of alignments in the north-west and south-east quadrants (that is, relative to the total number of alignments in these quadrants) which have large values of d during winter.

As was discussed in section 5.4, the degree of polarization parameter provides a useful measure of whether any given alignment is "dominant" or representative of the wave field. Large values of d suggest a strongly-polarized directional wave field whereas small values suggest that the wave field is unpolarized and azimuthally isotropic. It is therefore important to investigate the degree to which the wave field is polarized during summer and winter months. Note that when individual alignments are overlaid such that their lengths are proportional to d, the eye tends to focus on those alignments with large d. When viewed in this manner, the angular distribution of horizontal alignments found during winter appears to be significantly biased when compared with the angular distribution found during summer.

Figure 5.17 illustrates histograms of the degree of polarization parameter, d, determined from individual soundings of the lower stratosphere during summer and winter months. The mean values are given by dashed lines in each case. These are $d = 0.67$ and $d = 0.54$ for summer and winter, respectively. Approximately 5% of soundings during summer and 20% during winter have degree of polarization parameters that are less than 0.4. When these are removed from Figure 5.16, the observed biases of the angular distributions remain unaffected (not shown). Thus when the wave field is polarized and directional, the dominant horizontal alignment is most likely to exist within the north-east and south-west quadrants, especially during winter. However, the wave field is more likely to be polarized during summer.

The horizontal alignments illustrated in Figure 5.16 are now assigned dominant directions

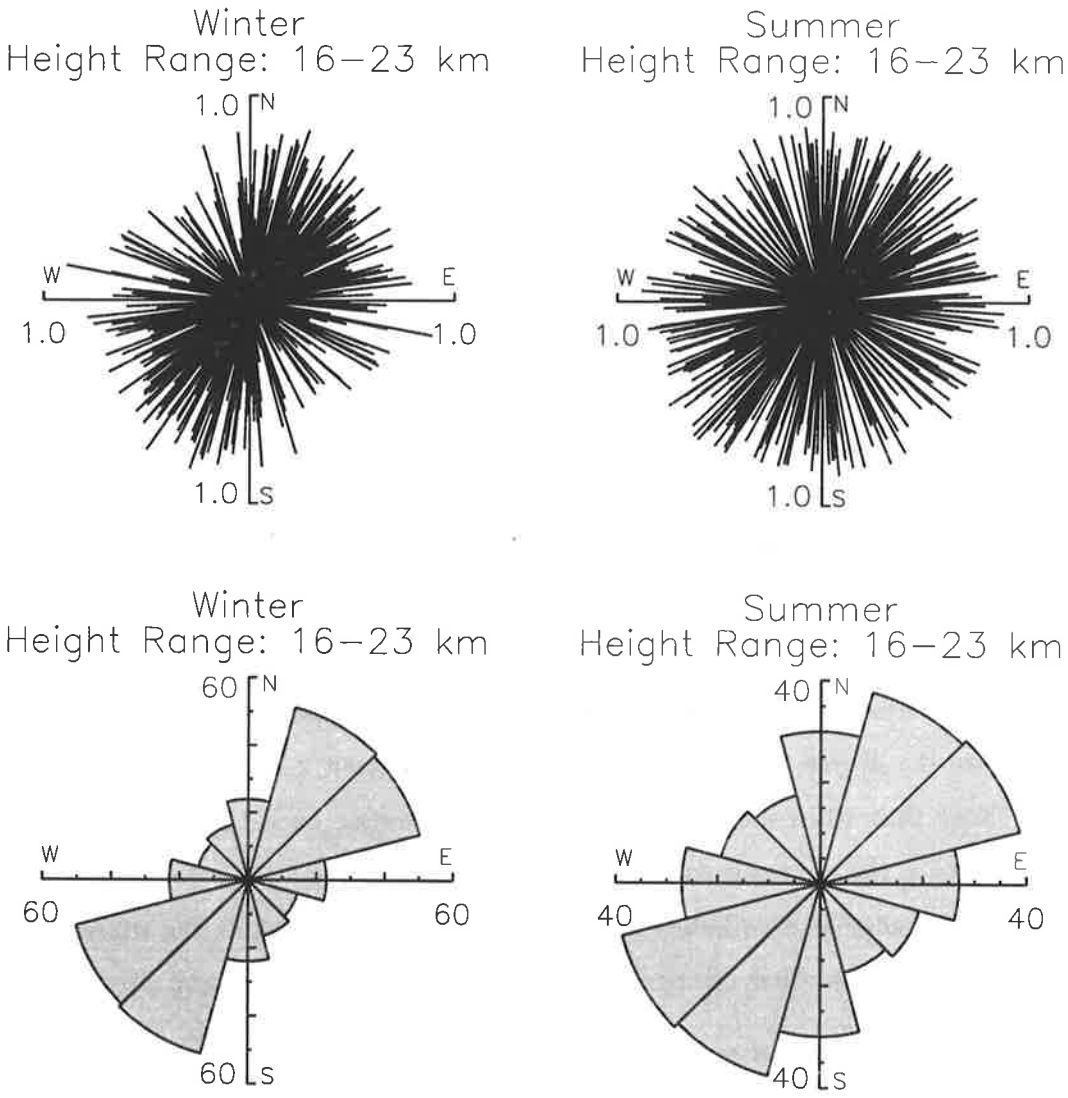

Figure 5.16: The angular distributions of dominant horizontal alignments in the lower stratosphere over Macquarie Island. Data from winter and summer months are considered separately. The two plots of the top row illustrate dominant horizontal alignments inferred from individual soundings where the length of each line is normalized according to the degree of polarization. The two plots of the bottom row illustrate the same distributions in polar histogram form.

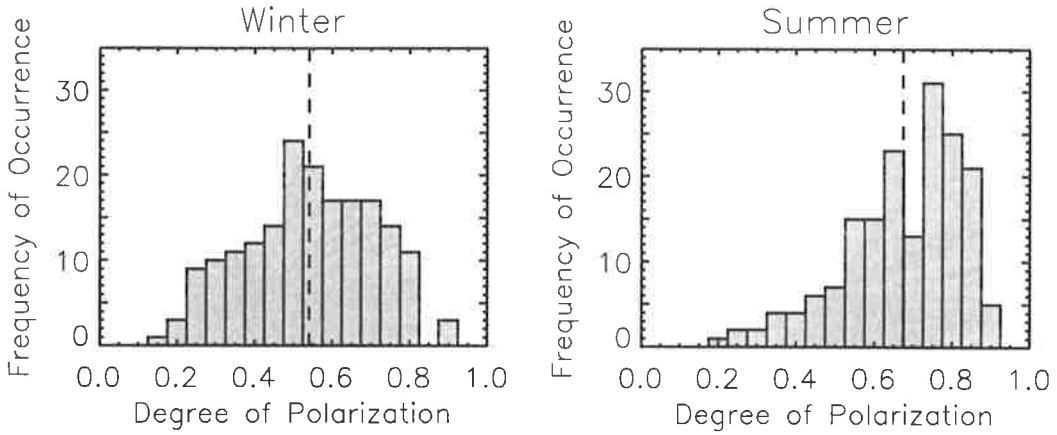

Figure 5.17: The distributions of d from the lower stratosphere (16.0–23.0 km) during winter and summer over Macquarie Island. Dashed lines indicate the mean values in each case.

of horizontal phase propagation[15]. This was achieved by using temperature measurements in the manner described in chapter 3. Firstly, the positive $u'_{||}$ axis was defined arbitrarily such that $-\pi/2 < \overline{\phi} < \pi/2$ where $\overline{\phi}$ is the mean horizontal alignment determined from (3.28). Following this, the parallel component wind fluctuation profile, $u'_{||}$, was determined from (1.14). Finally, the covariance of $u'_{||}$ and $\hat{T}'_{+90}$ was calculated over the altitude range of interest where $\hat{T}'_{+90}$ is the negative Hilbert transform of $\hat{T}'$. The sign of this covariance determines whether the dominant direction of horizontal phase propagation is parallel to or antiparallel to the positive $u'_{||}$ axis, given that the dominant vertical wavenumber is always negative from rotary spectrum analysis.

The above technique for estimating dominant directions of horizontal phase propagation was developed by *Hamilton* [1991]. However, *Hamilton* [1991] considered the covariance of $u'_{||}$ and $\frac{dT'}{dz}$ rather than that of $u'_{||}$ and $\hat{T}'_{+90}$. The Hilbert transform technique, after *Eckermann et al.* [1996], is advantageous since it shifts the phase of all spectral components by 90° without changing their amplitudes. The first derivative shifts the phase of all spectral components by 90° but also accentuates the amplitudes of those components with high spatial frequency. This is a consequence of the Fourier transform derivative theorem [e.g., *Bracewell*, 1986, p. 117].

The angular distributions of dominant directions of horizontal phase propagation in the lower stratosphere (16.0–23.0 km) over Macquarie Island are illustrated in Figure 5.18. This figure is the same as Figure 5.16 except that each horizontal alignment is now reduced to a

[15]These are directions toward a given azimuth.

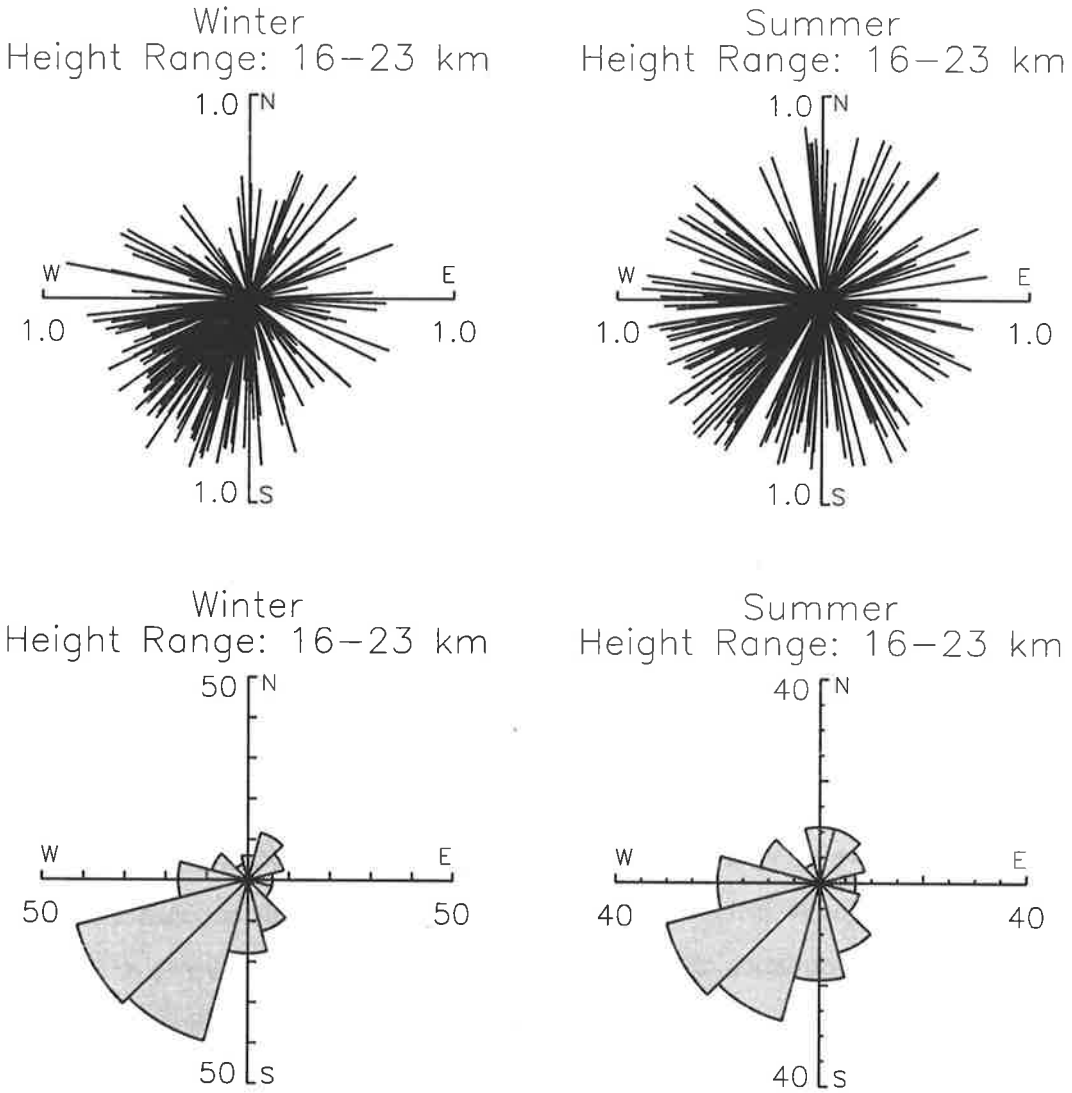

Figure 5.18: As in Figure 5.16, but for dominant directions of horizontal phase propagation. See text for further details.

single propagation direction. As before, the dominant directions are plotted both individually and in polar histogram form. In the former case, the directions are depicted by straight lines whose lengths are scaled according to d, while in the latter case, the axis labels describe the number of profiles with dominant directions within a given 30° interval.

During winter, the dominant propagation directions determined from individual soundings of the lower stratosphere are most commonly found in the south-west quadrant. This is clearly revealed when the angular distribution is plotted in polar histogram form. A similar south-westward bias is found during summer although, in this case, the bias is less severe. Note that the summertime angular distribution does not include data from either February

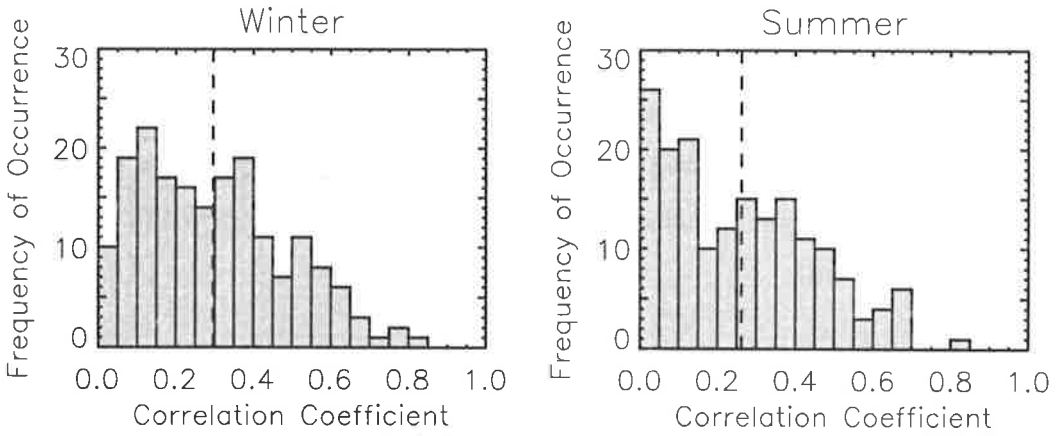

Figure 5.19: The correlation coefficients of $u'_{||}$ and $\hat{T}'_{+90}$ determined from radiosonde observations of the lower stratosphere (16.0–23.0 km) over Macquarie Island. Winter and summer data are considered separately and the dashed lines indicate the mean values in each case.

or March since only 10 months of wind velocity data were available for investigation. Therefore, this distribution may not adequately represent the mean summertime distribution of dominant horizontal phase propagation directions.

Analogous results from the northern hemisphere were reported by *Kitamura and Hirota* [1989] who analyzed radiosonde data from 18 stations in and around Japan. Their study concluded that the dominant wavenumber vector is directed toward the north-west and downward. Furthermore, they suggested that there may be a relation between gravity wave characteristics and the subtropical jet at the tropopause level. The radiosonde stations utilized by *Kitamura and Hirota* [1989] ranged in latitude between approximately 25°N and 45°N.

Following *Hamilton* [1991], the individual propagation directions illustrated in Figure 5.18 are interpreted to be the dominant directions of the wave field. Inspection of wind hodographs and the determination of d suggest that this is a reasonable interpretation in many cases. However, additional evidence is provided by the correlation coefficient of $u'_{||}$ and $\hat{T}'_{+90}$. These fluctuations are expected to be partially correlated in the case of a directional wave field.

Figure 5.19 illustrates the correlation coefficients of $u'_{||}$ and $\hat{T}'_{+90}$ determined from individual soundings of the lower stratosphere (16.0–23.0 km) in histogram form. As before, the data are divided into summer and winter months which correspond to the times of smallest and largest mean winds in the lower stratosphere, respectively. Note that the positive $u'_{||}$ axis was chosen such that the correlation coefficient of $u'_{||}$ and $\hat{T}'_{+90}$ was always positive. The

mean values are 0.26 during summer and 0.30 during winter. Both are larger than 0.2 which, if determined from a random sample of 141 observations, is significant to within approximately 95% confidence [see *Bevington*, 1969, p. 310]. However, 44% of soundings during summer and 37% of soundings during winter had correlation coefficients that were smaller than 0.2. Nevertheless, Figure 5.19 suggests that the wave field is directional in many cases, as has already been noted.

5.6 Summary and Conclusions

The results presented in this chapter describe the characteristics of gravity wave motions in the troposphere and lower stratosphere over Macquarie Island. These were delineated from radiosonde measurements of temperature and horizontal wind velocity which were obtained over 24-month and 10-month observation periods, respectively. The main findings are listed below.

1. Vertical wavenumber power spectra of normalized temperature fluctuations within the lower stratosphere are approximately consistent, at high vertical wavenumbers, with the theoretical saturation limits of *Smith et al.* [1987]. However, these spectra are significantly attenuated in comparison to those found at low-latitude sites, especially within the low-wavenumber region of the spectrum.

2. Spectral amplitudes determined from normalized temperature fluctuations in the troposphere are significantly larger, at high vertical wavenumbers, than the theoretical saturation limits of *Smith et al.* [1987]. This is consistent with tropospheric spectra found elsewhere. These spectra are possibly contaminated by inversions.

3. Vertical wavenumber power spectra of total horizontal wind velocity fluctuations have amplitudes that are consistent with the theoretical saturation limits within the lower stratosphere and amplitudes that are larger than the theoretical saturation limits within the troposphere. However, the spectral amplitudes at high vertical wavenumbers are uncertain owing to random measurement error and to the smoothing of raw data.

4. In the troposphere, potential energy and horizontal kinetic energy are approximately equal, while in the lower stratosphere, horizontal kinetic energy is consistently larger than potential energy.

5. Normalized temperature variance in the lower stratosphere displays an annual oscillation with the maximum occurring during winter. Seasonal variations of horizontal wind velocity variance are less clear, on the other hand, since these data are only available over a 10-month observation period.

6. Rotary power spectra in the lower stratosphere indicate that the majority of variance appears in the anticlockwise rotating component while seasonal variations of the percentage anticlockwise rotation are consistent with predicted seasonal changes in the frequency distribution of gravity waves due to background wind variations [after *Eckermann et al.*, 1995].

7. Rotary power spectra in the troposphere indicate that wave variance is equally partitioned into clockwise and anticlockwise rotating components.

8. The dominant directions of horizontal phase propagation determined from individual soundings of the lower stratosphere are biased toward the south-west during both summer and winter, but especially so during winter.

Wave generation by eastward air flow over Macquarie Island is one potentially important source mechanism. However, as has already been noted (see Figure 5.6), gravity waves that are generated in this manner are likely to be trapped in the troposphere owing to their small horizontal scale and to the strong zonal winds near the tropopause. Indeed, *Mitchell et al.* [1990] report that lee-wave clouds are commonly found in satellite images of cloud structures over Macquarie Island and can extend up to hundreds of kilometres to the east during favourable conditions. Therefore, trapped mountain waves may make a significant contribution to the horizontal wind and temperature variance[16] of the troposphere.

The ratio of horizontal kinetic to potential energy is significantly different in the troposphere, compared with the lower stratosphere, which suggests that the frequency distribution of waves is very different. One possible explanation is the common occurrence of trapped mountain waves which have small horizontal scales and large intrinsic frequencies. If these waves are energetic enough, in a climatological sense, then they may account for the relative strength of normalized temperature variance in the troposphere, as illustrated in Figure 5.10.

[16]Note that radiosondes drift downstream with the mean winds and so can observe mountain waves in principle. However, if the horizontal scales of such waves are small, then the observed vertical wavenumber may be inaccurate due to the sonde's horizontal drift (see equation 3.2).

Alternatively, potential energy estimates may be significantly overestimated due to the presence of temperature inversions between 1.0 and 8.0 km.

In the lower stratosphere, on the other hand, the ratio of horizontal kinetic to potential energy is large. This, together with the inspection of wind hodographs, suggests that the wave field is dominated by low-frequency inertio-gravity waves. One plausible source of such wave activity is geostrophic adjustment [e.g., *Fritts and Luo*, 1992]. However, no concrete evidence is provided in support of this hypothesis.

The most energetic waves detected in the lower stratosphere are typically found to propagate toward the south-west during all seasons. Since the mean zonal winds are considerably different during summer and winter, this suggests that south-westward propagation is a signature of some dominant wave source rather than of wave filtering by the mean flow. Note that when horizontal propagation directions are determined (not shown) over a 14 km altitude range in the lower stratosphere[17], the observed south-westward biases of both summertime and wintertime angular distributions remain the same. Therefore, the narrow band biasing effect described by *Eckermann et al.* [1995] does not appear to affect the wintertime angular distribution of dominant propagation directions. However, it is possible that some gravity wave variance is not detected within the 7-km altitude intervals considered here since south-westward propagating waves can have large vertical wavelengths during conditions of strong eastward winds (see Figure 5.5).

The results presented in this chapter demonstrate that a qualitative picture of the climatological-mean wave field anisotropy can be obtained in the lower stratosphere by using Stokes parameter analysis. These results are thought to be representative of the wave field over the open ocean at 55°S since any mountain waves generated by Macquarie Island are likely to be trapped within the troposphere. The south-westward bias of dominant horizontal propagation directions is analogous to similar results reported by *Kitamura and Hirota* [1989] and *Hamilton* [1991]. These authors found a northward or north-westward bias of dominant horizontal propagation directions in the stratosphere at comparable latitudes of the northern hemisphere. However, *Hamilton* [1991] notes considerably different propagation characteristics at near-equatorial locations. The following chapter investigates the propagation characteristics of gravity waves in the lower stratosphere over one near-equatorial radiosonde station in the southern hemisphere.

[17] In this case there are fewer profiles available for analysis and so the resultant angular distributions are less reliable.

Chapter 6

Cocos Islands: A Case Study

6.1 Introduction

The purpose of this chapter is to study gravity wave characteristics over the Cocos Islands (12°S, 97°E) using radiosonde observations of temperature and horizontal wind velocity. The Cocos (Keeling) Islands are located in the Indian Ocean, approximately 1000 km south-west of Indonesia, and consist of low-lying coral atolls[1] with a total area of 14 square kilometres and with a maximum height of approximately 6 m. This site is particularly interesting since there are no land masses close to the islands and topographic forcing due to the islands themselves is expected to be minimal based on linear wave theory. Other gravity wave sources, particularly convection, are likely to be prominent here.

The basic state circulation structures over equatorial stations such as the Cocos Islands are distinct from those at middle and high latitudes. In the tropical middle atmosphere, the zonal-mean zonal winds display a quasi-biennial oscillation (QBO) in the lower stratosphere, which is symmetric about the equator, and two distinct semi-annual oscillations (SAOs) which are centred on the stratopause (the SSAO) and the mesopause (the MSAO) and are 180° out of phase [e.g., *Wallace*, 1973; *Hirota*, 1980; *Andrews et al.*, 1987]. Superimposed upon these structures are two types of planetary-scale wave motions which can propagate zonally and vertically through the stratosphere [*Wallace*, 1973]. These are the equatorially-trapped Kelvin and mixed Rossby-gravity wave modes which were first identified in the atmosphere by *Wallace and Kousky* [1968] and *Yanai and Maruyama* [1966], respectively. Also present are shorter period gravity waves [e.g., *Cadet and Teitelbaum*, 1979] and these are the subject of investigation in this chapter. Other classes of wave motion, such as tidal

[1]The source of this information is the *Cocos (Keeling) Islands Annual Report 1986–87.*

waves, may also be present.

The QBO of the tropical lower stratosphere is understood to be driven by momentum transfer due to Kelvin and mixed Rossby-gravity waves [*Lindzen and Holton*, 1968; *Holton and Lindzen*, 1972; *Plumb*, 1977; *Plumb and McEwan*, 1978]. Kelvin waves, which are eastward propagating waves, and mixed Rossby-gravity waves, which are westward propagating waves, are believed to force the eastward and westward phases of the QBO respectively. Similarly, eastward and westward propagating gravity waves are thought to drive the MSAO[2], while high-phase-speed Kelvin waves and small-period gravity waves are thought to drive the eastward phase of the SSAO [e.g., *Hitchman and Leovy*, 1988]. Reviews by *Wallace* [1973], *Hirota* [1980] and *Andrews et al.* [1987] provide further details regarding equatorial circulation structures and their proposed driving mechanisms.

It is clear that gravity waves are of importance in the tropical middle atmosphere and the determination of gravity wave characteristics is therefore of considerable interest. Experimental studies by *Fritts et al.* [1992] and *Hitchman et al.* [1992] have already provided some useful information. These authors utilized the MST radar facility at Jicamarca (12°S, 77°W), Peru, to measure gravity wave momentum fluxes during two campaign periods of approximately 10 days duration each. Other radar studies at Arecibo (18°N, 67°W) have delineated inertio-gravity wave characteristics near the equatorial tropopause[3] [*Maekawa et al.*, 1984; *Cornish and Larsen*, 1989; *Cho*, 1995] while the ALOHA-90 and ALOHA-93 campaigns have explored the nature of gravity wave activity over equatorial regions of the mid-Pacific ocean [*Gardner*, 1991; *Gardner*, 1995]. Airborne observations and theoretical analyses by *Pfister et al.* [1993a,b] have also provided important information, as have analyses of meteorological rocketsonde data by, among others, *Hirota* [1984] and *Eckermann et al.* [1995]. The airborne observations provide evidence for the notion that penetrative convection is a prominent source of gravity wave momentum flux at equatorial latitudes.

Radiosonde studies of gravity waves in the tropics are comparatively few although early work by *Madden and Zipser* [1970] and *Cadet and Teitelbaum* [1979] provide evidence of small-period gravity waves at equatorial latitudes. More recently *Tsuda et al.* [1994a,b] have presented extensive analyses of high-vertical-resolution horizontal wind and temperature measurements obtained by radiosonde over Watukosek (8°S, 113°E), Indonesia. These

[2]The proposed mechanism involves the selective transmission of gravity waves by the westward and eastward phases of the SSAO [*Dunkerton*, 1982]. Selective transmission accounts for the phase difference between the SSAO and the MSAO.

[3]The interpretation of observations by *Maekawa et al.* [1984] and *Cornish and Larsen* [1989] has been disputed by *Hines* [1989, 1995].

provide detailed information about both equatorially-trapped and freely-propagating gravity waves at equatorial locations. The radiosonde data studied by *Tsuda et al.* [1994a,b] were from an experimental campaign between February 27 and March 22, 1990.

The aim of this chapter is to extend the analyses of *Tsuda et al.* [1994b] to radiosonde data obtained over a 16-month period. Thus the emphasis is on climatological statistics which cannot be determined from an experimental campaign. However, the data studied here have poorer temporal resolution and poorer height ranges of measurement than those of *Tsuda et al.* [1994a,b] which is a disadvantage. Nevertheless they are of sufficient quality and vertical resolution that important gravity wave characteristics can be determined. More details about the data studied and about the background atmosphere during the observation period are discussed in the following section.

6.2 Radiosonde Data and the Background Atmosphere

The radiosonde data set considered in this chapter contains approximately 16 months of operational radiosonde soundings from the Cocos Islands (12°S, 97°E) between September 1992 and December 1993. These data were supplied by the Australian Bureau of Meteorology. The location of the Cocos Islands in relation to Australia and other Australian radiosonde stations is illustrated in Figure 3.1.

Wind and temperature measurements were obtained in the manner described in chapter 3 and the smoothing window length (see section 3.2) for horizontal winds measured between September 1992 and December 1993 was 130 s. Thus the effective vertical resolution of the horizontal winds considered here is approximately 650 m even though these measurements were reported at 10-s intervals. In contrast, temperature measurements have a vertical resolution of approximately 50 m. Radiosondes were usually launched either once or twice daily and reached typical heights of 25 km.

On the other hand, *Tsuda et al.* [1994a,b] considered radiosonde data obtained over a 25-day period (February 27 to March 22, 1990) from Watukosek (8°S, 113°E), Indonesia[4]. Their sondes were released at approximately 6-hour intervals and reached typical heights, during the daytime at least, of 30 km or more. These provided temperature and horizontal wind velocity measurements of comparable quality to those from the Cocos Islands since the radiosondes used in both cases were the same (RS80–15N). Yet *Tsuda et al.* [1994a,b]

[4]Additional details regarding the experiment of *Tsuda et al.* [1994a,b] are provided by *Tsuda et al.* [1992] including a review of background conditions during the campaign.

report wind velocity measurements with a height resolution of 150 m which is considerably better than the effective resolution of wind velocity measurements from the Cocos Islands. However, the Digicora radiosonde system has various adjustable parameters that can affect the height resolution of wind measurements. It seems likely that *Tsuda et al.* [1994a,b] chose parameters that were different from those used by the Australian Bureau of Meteorology.

Figure 6.1 and 6.2 illustrate examples of temperature, zonal wind velocity and meridional wind velocity profiles observed during October 1992 and April 1993 over the Cocos Islands. Individual profiles have been displaced horizontally in each plot. The data quality and the number of sondes launched during each month tended to vary, with the months of October 1992 and April 1993 providing some of the better examples. Missing winds at certain heights are attributed to poor reception of VLF radio transmissions.

Figure 6.3 illustrates the mean wind and temperature profiles for October 1992 and April 1993. These were obtained by averaging data from those radiosondes which made continuous measurements of wind velocity and temperature up to at least 25 km. Mean winds and temperatures during the full observation period are illustrated in Figure 6.4. This figure depicts time-height contours of monthly-mean temperatures, zonal winds and meridional winds where the contours were calculated from monthly-mean profiles such as those illustrated in Figure 6.3. Raw data were averaged into 500 m by 1 month bins and then interpolated so that smooth contour patterns were produced[5].

The basic state temperatures over the Cocos Islands exhibit little temporal variability and the typical tropopause height is near 16 or 17 km. Similarly, the basic state meridional winds show little temporal variability and are generally weak. The largest values occur immediately below the tropopause and are of the order of 6 m s^{-1} in the poleward direction. Also, an equatorward flow exists in the lowest 1 km of the atmosphere and is of the order of 4 m s^{-1}. In contrast, the basic state zonal winds in the lower stratosphere (18.0 to 25.0 km) exhibit considerable temporal variability. These are westward between September 1992 and March 1993, marginally eastward between April 1993 and July 1993, and westward again between August 1993 and December 1993. The largest observed westward winds are approximately 20 m s^{-1}. Tropospheric zonal winds are typically weak although may be as large 10 m s^{-1} in the upper troposphere.

The zonal circulation structures found over the Cocos Islands are likely to be dominated

[5]During some months, most notably during June 1993, only a few soundings reached 25 km. The accuracy of monthly-mean winds and temperatures in the lower stratosphere during these months may be poor.

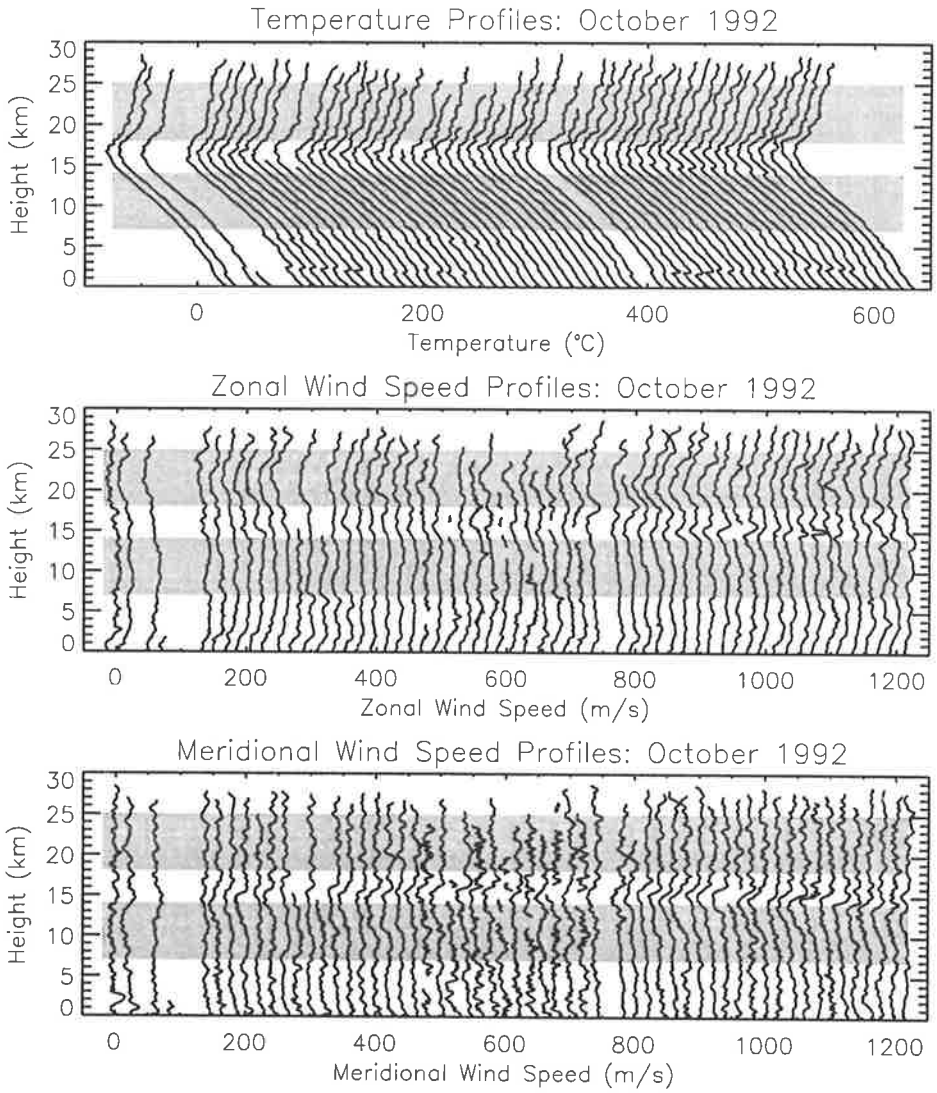

Figure 6.1: Examples of temperature profiles, zonal wind velocity profiles and meridional wind velocity profiles observed over the Cocos Islands (12°S, 97°E) during October 1992. Successive temperature profiles are displaced by 10°C and successive wind velocity profiles are displaced by 20 m s^{-1} per 12-hour delay between soundings. Shaded areas indicate the height intervals used for spectral analysis.

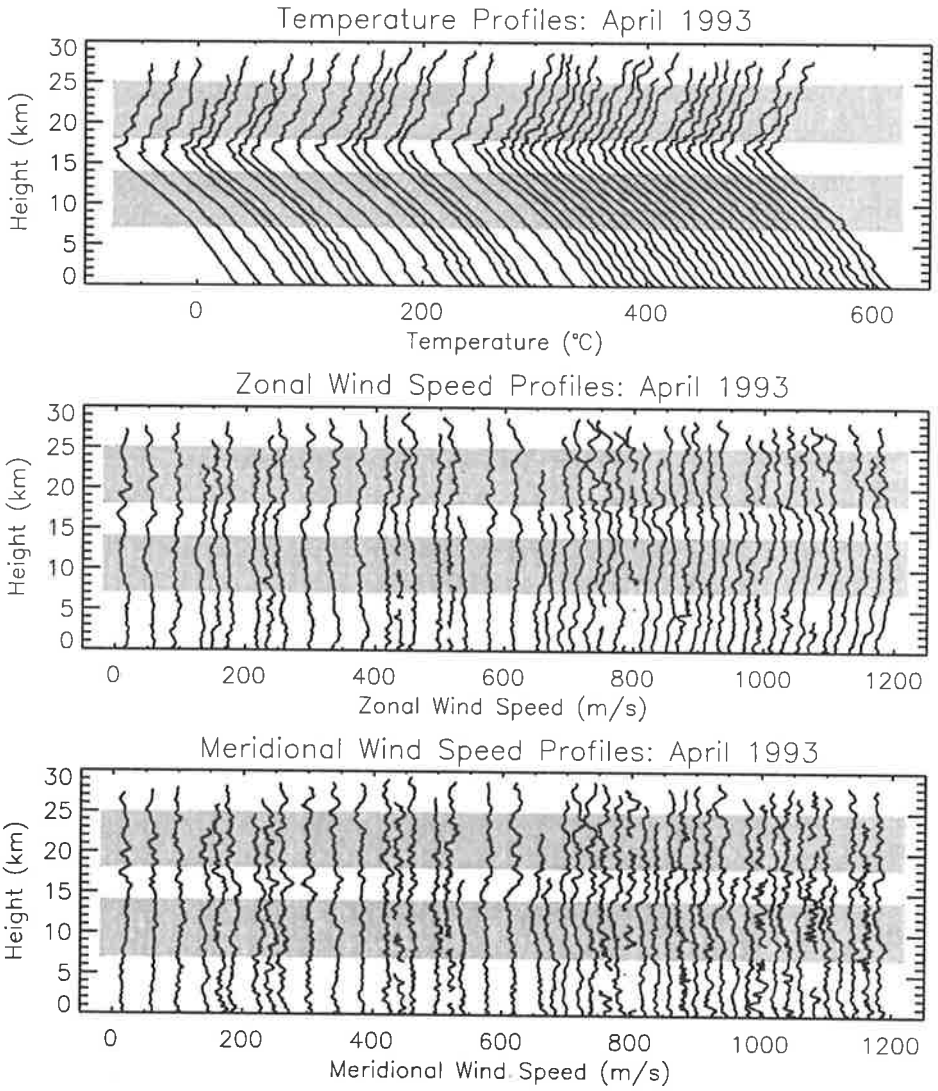

Figure 6.2: As in Figure 6.1, but for temperature profiles, zonal wind velocity profiles and meridional wind velocity profiles observed over the Cocos Islands (12°S, 97°E) during April 1993.

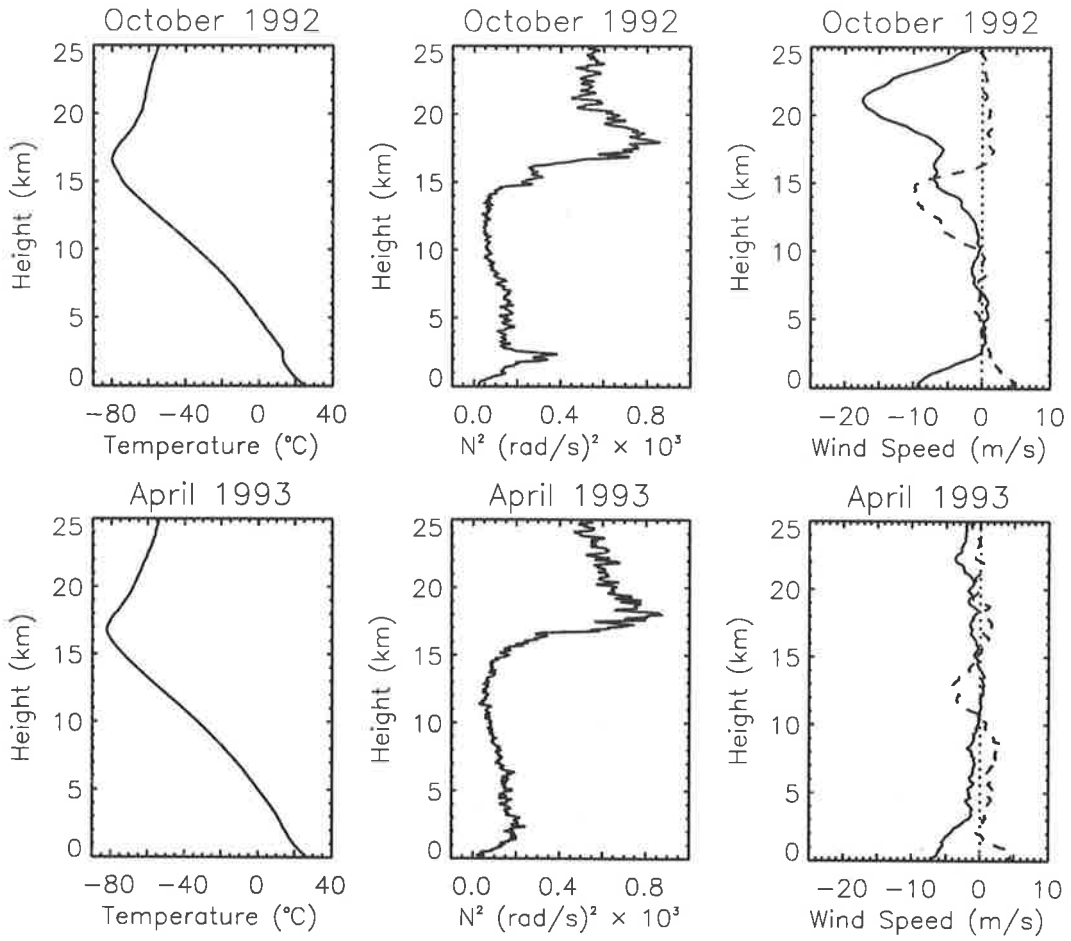

Figure 6.3: Mean vertical profiles of temperature, Väisälä-Brunt frequency squared and horizontal wind velocity components during October 1992 and April 1993 over the Cocos Islands. The plots are organized in rows such that, from left to right, the first plot illustrates the mean temperature profile, the second illustrates the mean Väisälä-Brunt frequency squared profile and the third illustrates the mean wind velocity component profiles. In the latter case both zonal (solid lines) and meridional (dashed lines) winds are plotted.

by the equatorial QBO in the lower stratosphere and monsoon circulation patterns in the troposphere [e.g., *Wallace*, 1973]. The precise characteristics of the stratospheric winds are difficult to determine, however, since the observation period does not extend over one full cycle of the QBO. Therefore, the amplitude of the QBO and the time-mean zonal wind are not known from the available data. These are of only marginal interest in the present study.

Naujokat et al. [1994] report that monthly-mean zonal winds at 22 km over Singapore (1°N, 104°E) were eastward between October 1992 and November 1993. Since the QBO is both zonally symmetric and symmetric about the equator with a latitude independent phase in the southern hemisphere [e.g., *Wallace*, 1973; *Dunkerton and Delisi*, 1985], the

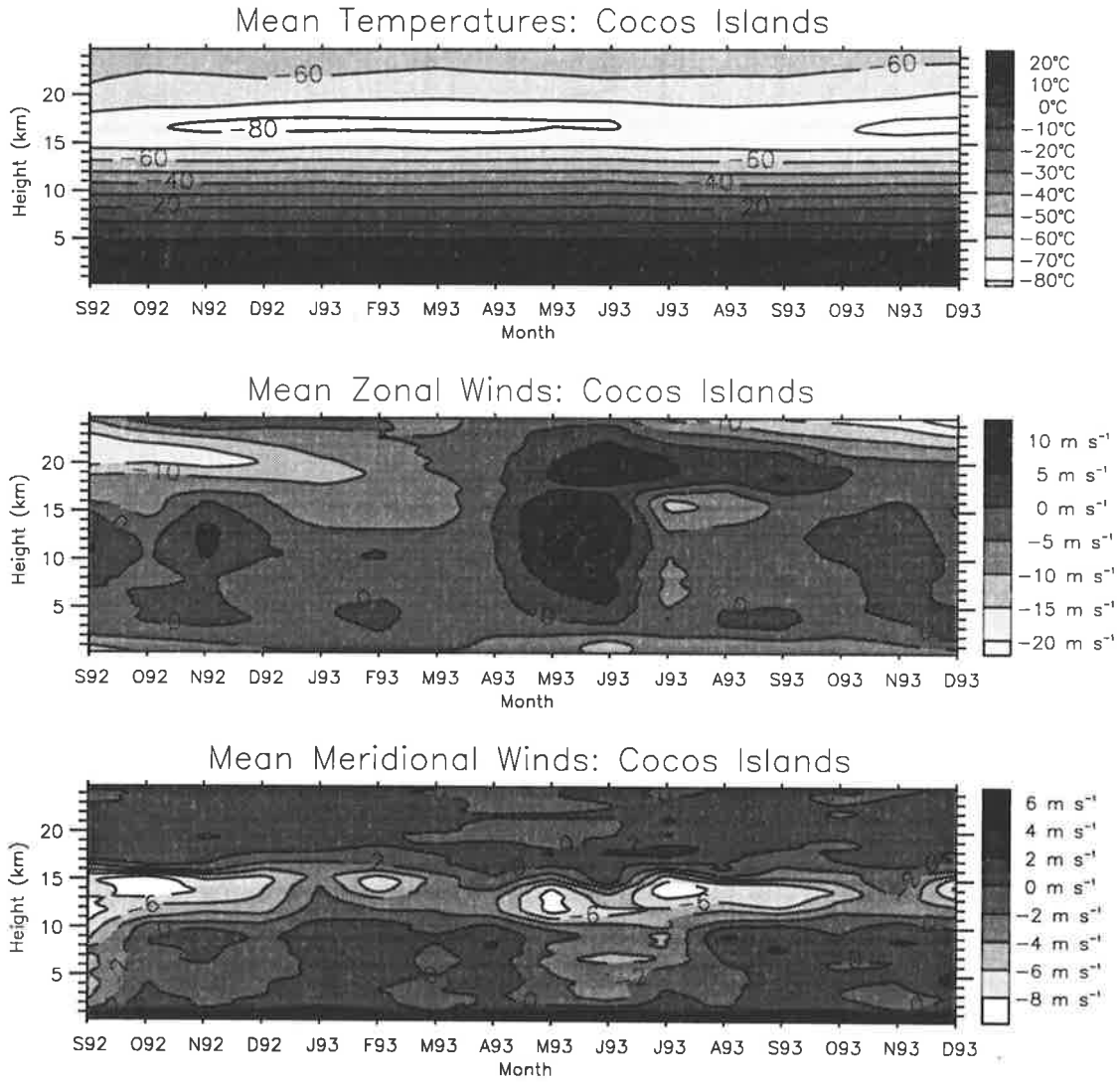

Figure 6.4: Time-height contours of monthly-mean temperature, zonal wind velocity and meridional wind velocity between September 1992 and December 1993 over the Cocos Islands. Positive zonal and meridional winds are eastward and northward, respectively.

QBO winds should also be eastward during approximately the same observation period at 12°S[6]. It seems likely, therefore, that a weak time-mean westward wind exists in the lower stratosphere over the Cocos Islands. Also, the midlatitude annual oscillation may be present to some extent [e.g., *Wallace*, 1973].

Figure 6.4 describes the basic state wind and temperature structures but gives no information about the seasonal variability of convective activity in the troposphere. Since convection is thought to generate gravity waves, especially in the tropics, some information about convective activity is clearly warranted. In particular, mesoscale convective systems are probably the most important source of small-scale gravity waves over the Cocos Islands. These may force waves by inducing lifting in the stratosphere on horizontal scales comparable to those of the mesoscale system itself [*Pfister et al.*, 1993a]. *Houze and Betts* [1981] report that 90% of rain observed during GATE[7] was contributed by mesoscale convective systems in which deep convective cells penetrated to the tropopause. Furthermore, *Houze and Betts* [1981] state that, on large horizontal and temporal scales, precipitation and vertical motion are closely coupled. Therefore, mean rainfall figures from the Cocos Islands should be indicative, at least qualitatively, of the seasonal variability of mesoscale convective activity over this site.

Figure 6.5 presents mean rainfall figures from both Darwin and the Cocos Islands. These were provided by the Australian Bureau of Meteorology. Mean rainfall figures from Darwin have been presented since these are notably different from those of the Cocos Islands. As was discussed by *May et al.* [1995], Darwin experiences a dry season between April and September and a wet season characterized by heavy rainfall between mid-December and either February or March[8]. In contrast, the Cocos Islands experience moderate rainfall between December and July, and have a very short dry season (if at all) during September and October. Such climatic differences may cause differences in the variance characteristics of gravity waves and these characteristics, over the Cocos Islands, are discussed in the following section.

6.3 Variance Characteristics

The characteristics of normalized temperature variance were described in detail in chapter 4. There it was established that gravity wave variances are largest at low latitudes, at least

[6]The QBO amplitude, at 22 km, is approximately twice as large at the equator than at 12°S (see Figure 6 of *Wallace* [1973]).

[7]Global Atmospheric Research Program's Atlantic Tropical Experiment.

[8]The two intervening periods are called transition seasons [*May et al.*, 1995]

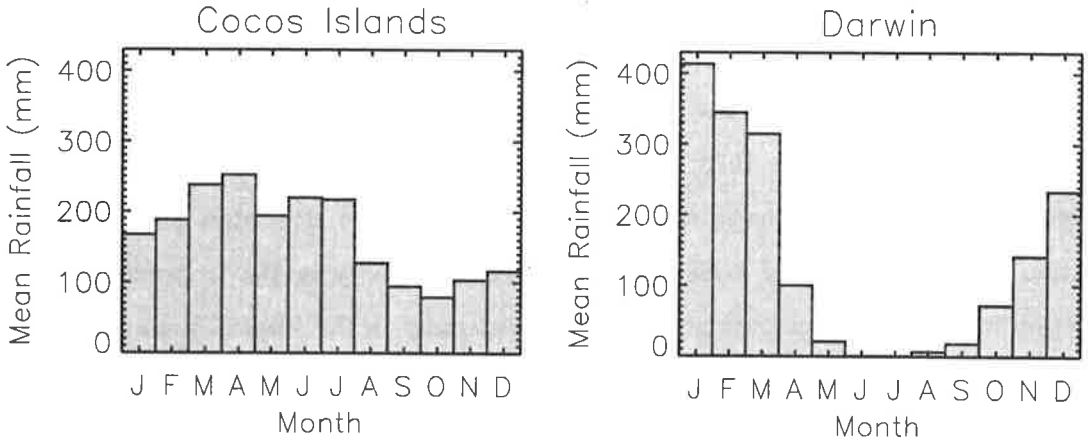

Figure 6.5: Mean rainfall at the Cocos Islands (12°S, 97°E) and Darwin (12°S, 131°E) during 88 and 50 years of record, respectively. Rainfall figures were provided by the Australian Bureau of Meteorology.

within the Australian sector of the southern hemisphere. However, no data from the Cocos Islands were considered. This section presents analyses of both normalized temperature and horizontal wind velocity variances which were observed by radiosonde over the Cocos Islands.

6.3.1 Temperature Variance

Figure 6.6 illustrates 3-month-mean vertical wavenumber power spectra and area preserving spectra of normalized temperature fluctuations. These were calculated in the troposphere (7.0–14.0 km) and lower stratosphere (18.0–25.0 km) by applying the same techniques as those used in previous chapters[9]. However, tropospheric power spectra were calculated between 7.0 and 14.0 km which is significantly different from the altitude ranges used in chapter 4. In that chapter it was suspected that temperature inversions may have biased variance estimates in the troposphere during some months. The altitude range used in this chapter was chosen so as to avoid temperature inversions which, by inspection of temperature profiles such as those illustrated in Figures 6.1 and 6.2, occur only rarely between 7.0 and 14.0 km. The mean Väisälä-Brunt frequency squared is at its smallest within this altitude range (see, for example, Figure 6.3) and is not strictly constant.

Stratospheric spectra of normalized temperature fluctuations from the Cocos Islands are similar to those found at Darwin and Gove which are also located at 12°S. Typical amplitudes

[9]Mean spectra were obtained by averaging normalized individual spectra as was described earlier. However, individual spectra were averaged in this manner over 3-month periods rather than 1-month periods as was the case in chapter 4. Recall that, in chapter 4, 3-month average spectra were in fact weighted arithmetic means of 1-month average spectra.

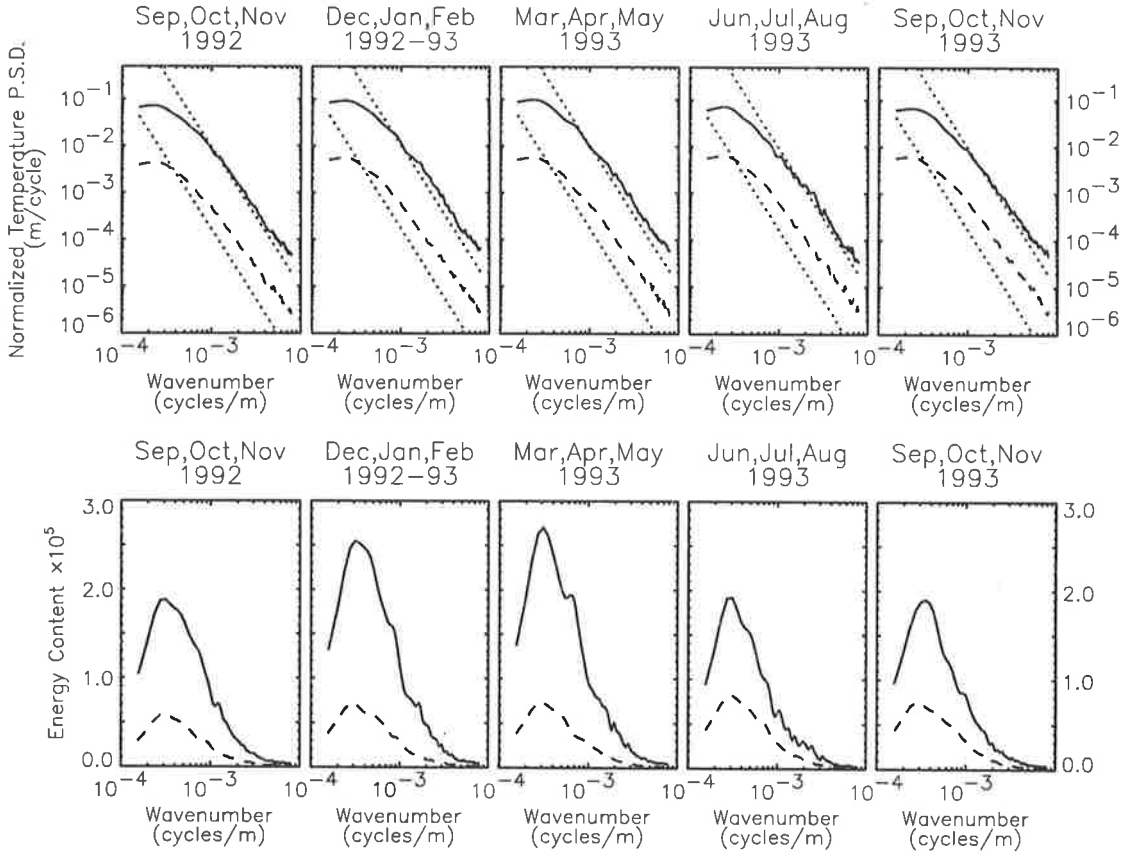

Figure 6.6: Vertical wavenumber power spectra and area preserving spectra of normalized temperature fluctuations observed at the Cocos Islands (12°S, 97°E). Solid lines indicate stratospheric spectra (18.0 to 25.0 km) while dashed lines indicate tropospheric spectra (7.0 to 14.0 km). Each spectrum is a 3-month average and the saturation limits due to *Smith et al.* [1987] are plotted for comparison purposes (dotted lines). The 95% confidence limits are approximately given by 0.85 and 1.15 multiplied by the spectral amplitude at each wavenumber. Tropospheric area preserving spectra have been multiplied by a factor of 5 so that they can appear on the same scale as stratospheric area preserving spectra.

within the high-wavenumber region of the spectra are consistent with, although slightly larger than, the theoretical saturation limits proposed by *Smith et al.* [1987]. These spectra display a noticeable seasonal variation with the largest amplitudes appearing during the 3-month period of March, April and May. In contrast, spectral amplitudes at Darwin and Gove are largest during December, January and February (see, for example, Figure 4.12).

Climatic differences in the occurrence of deep convective cells, which are anticipated to be an important source of gravity waves, probably account for the above discrepancy. As was discussed in the previous section, mean precipitation figures (see Figure 6.5) are suggestive of the occurrence frequency of mesoscale convective activity in the tropics. Mean precipitation is greatest between March and July at the Cocos Islands and between December and March

at Darwin. These periods correspond to the periods of greatest wave variance at both sites.

Tropospheric spectra of normalized temperature fluctuations from the Cocos Islands, which were calculated between 7.0 and 14.0 km, are similar to those from Darwin and Gove, which were calculated between 2.0 and 9.0 km. However, a direct comparison of spectral amplitudes and variance is difficult in this case since the height-mean Väisälä-Brunt frequency squared is almost a factor of two smaller between 7.0 and 14.0 km compared with its height-mean value between 2.0 and 9.0 km. Nevertheless, relative to the theoretical saturation limits of *Smith et al.* [1987], the observed spectra are approximately consistent with those from Darwin and Gove. The most notable difference is the high-wavenumber spectral slope, t, of the observed spectra. Spectral slopes are shallower in the upper troposphere over the Cocos Islands than in the lower troposphere over both Darwin and Gove. Also, there is less evidence of seasonal variations for spectra calculated between 7.0 and 14.0 km over the Cocos Islands.

To illustrate further the point regarding shallow spectral slopes, consider Figure 6.7. This diagram compares tropospheric spectra which were calculated between 2.0 and 9.0 km and between 7.0 and 14.0 km over the Cocos Islands. However, instead of a direct comparison of power spectra, each spectrum has been divided by the theoretical saturation limits proposed by *Smith et al.* [1987]. The purpose of this technique, following *Tsuda et al.* [1989, 1991], is to remove the anticipated N^4 dependence of spectral amplitudes at high vertical wavenumbers. The diagram indicates that, for vertical wavenumbers $m/2\pi \geq 2 \times 10^{-3}$ cpm, the spectral amplitudes calculated between 7.0 and 14.0 km are relatively larger than those calculated between 2.0 and 9.0 km during all seasons. A similar enhancement was found in the upper troposphere at Gove (see Figure 4.19).

Instrumental noise is one possible explanation for the variance enhancements described by Figures 6.8 and 4.19. The observed power spectra must include any variance that is caused by random measurement error although, from Figure 3.3, the geophysical signal is expected to dominate. Yet a gravity wave spectrum is height dependent, through its N dependence, whereas the simplest model for instrumental noise is a white noise type spectrum that is height independent. Consequently, a model noise spectrum will become most important, in relative terms, when gravity wave amplitudes are small. This occurs in regions of small Väisälä-Brunt frequency squared and most notably in the tropical upper troposphere (see, for example, Figure 4.1). Therefore, the enhanced spectral amplitudes depicted in Figure 6.8 and the enhanced, normalized variance depicted in Figure 4.19 (for

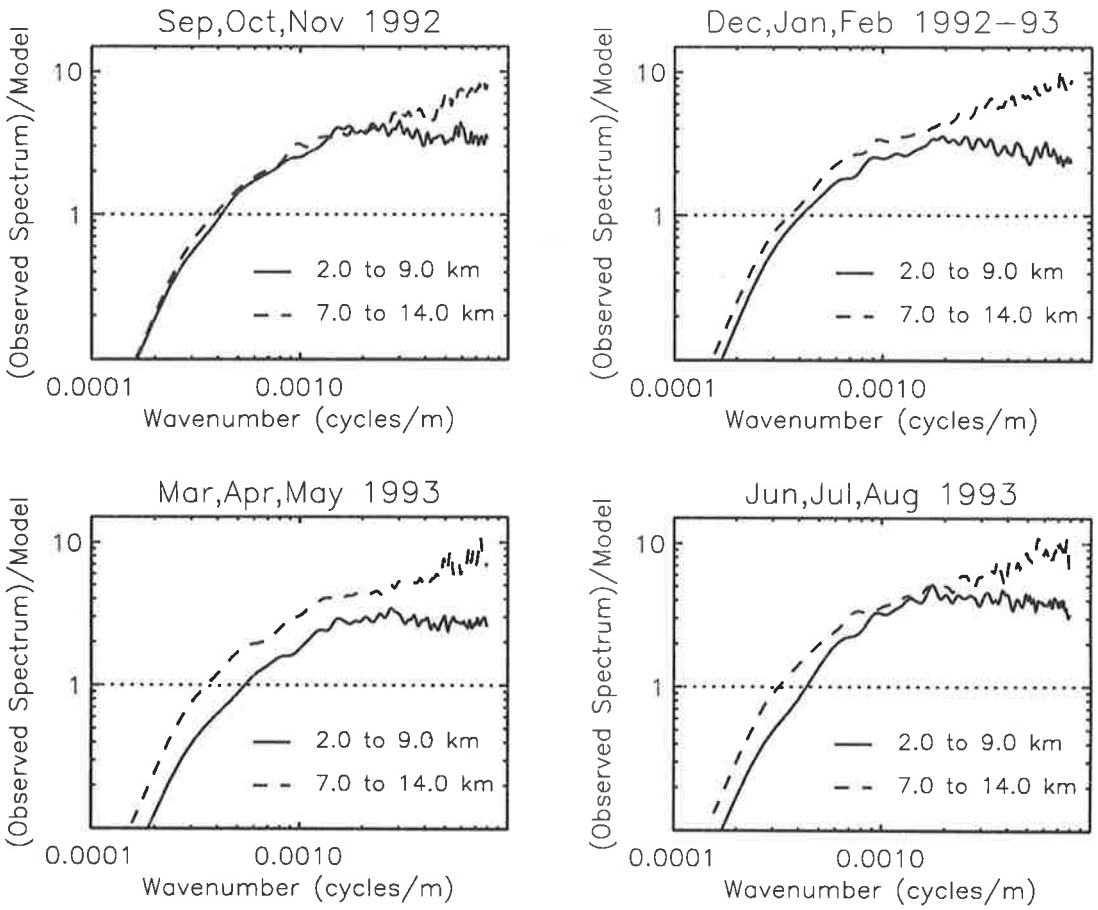

Figure 6.7: Vertical wavenumber power spectra of normalized temperature fluctuations within the lower troposphere (2.0 to 9.0 km) and upper troposphere (7.0 to 14.0 km) over the Cocos Islands. Each spectrum is a 3-month average and has been divided by the model saturation limits proposed by *Smith et al.* [1987] (dotted lines).

data obtained at Gove) may be the result of contamination due to instrumental noise. Noise contamination can be important in the tropical upper troposphere, and not elsewhere, since gravity wave amplitudes are smallest there. Note that both spectral amplitudes and variance are most affected at high vertical wavenumbers.

The characteristic vertical wavelength of temperature fluctuations observed in both the troposphere and lower stratosphere over the Cocos Islands is approximately 3 km and is consistent with observations at Gove. However, as was discussed in chapter 4, it is not clear that m_* is truly resolved since a reliable determination of $\overline{T}(z)$ is difficult using the data that were studied here. This point is important since recent modelling studies by *Alexander et al.* [1995] suggest that the dominant vertical scale of gravity waves generated by mesoscale

convection[10] is between approximately 6 and 10 km. A further attempt is made to estimate $2\pi/m_*$ in section 6.4.

6.3.2 Wind Speed Variance

Figure 6.8 illustrates 3-month-mean vertical wavenumber power spectra of total horizontal wind velocity fluctuations. These were calculated in the troposphere (7.0–14.0 km) and lower stratosphere (18.0–25.0 km) by using the same techniques as before. However, in this case there was no need to normalize wind velocity fluctuations before calculation of power spectral density. Each illustrated spectrum is the sum of zonal and meridional wind velocity component spectra and, as before, the theoretical saturation limits of *Smith et al.* [1987] are plotted for comparison purposes.

The wind velocity power spectra presented in Figure 6.8 suffer from the same errors as those presented in chapter 5 since the same sounding systems were used at both sites. Spectral amplitudes at vertical wavenumbers that are larger than approximately 10^{-3} cpm are probably attenuated and unreliable as a result of the cubic spline smoothing procedures that were discussed in section 3.2. Also, a noise floor is likely to be present (see Figure 3.4) although this too will be attenuated. Nevertheless, for $m/2\pi < 10^{-3}$ cpm, stratospheric spectral amplitudes do approach the theoretical saturation limits proposed by *Smith et al.* [1987] as expected. Similarly, tropospheric wind spectra have amplitudes that are larger than those of the theoretical saturation limits as was also found to be the case with tropospheric temperature spectra.

Area preserving spectra indicate that most of the observed variance occurs at vertical wavenumbers that are less than 10^{-3} cpm and that the dominant gravity waves are not affected by cubic spline smoothing procedures. Notice that spectral amplitudes in the troposphere and lower stratosphere are approximately the same for $m/2\pi > 1.1 \times 10^{-3}$ cpm. This is only evident in the area preserving plots since tropospheric power spectra are displaced by a factor of 10. A height-independent noise floor might explain such a result. However, the spectral characteristics of instrumental noise are not known from the available information concerning Digicora wind sounding systems.

Seasonal variations of horizontal wind velocity power spectra and normalized temperature power spectra are approximately consistent. This is expected of gravity wave fluctuations,

[10]Note, however, that their estimate of the dominant vertical scale was obtained from a power spectrum, rather than an area preserving spectrum. Thus $2\pi/m_*$ should be slightly less than the range of values that were quoted (see Figure 3.7).

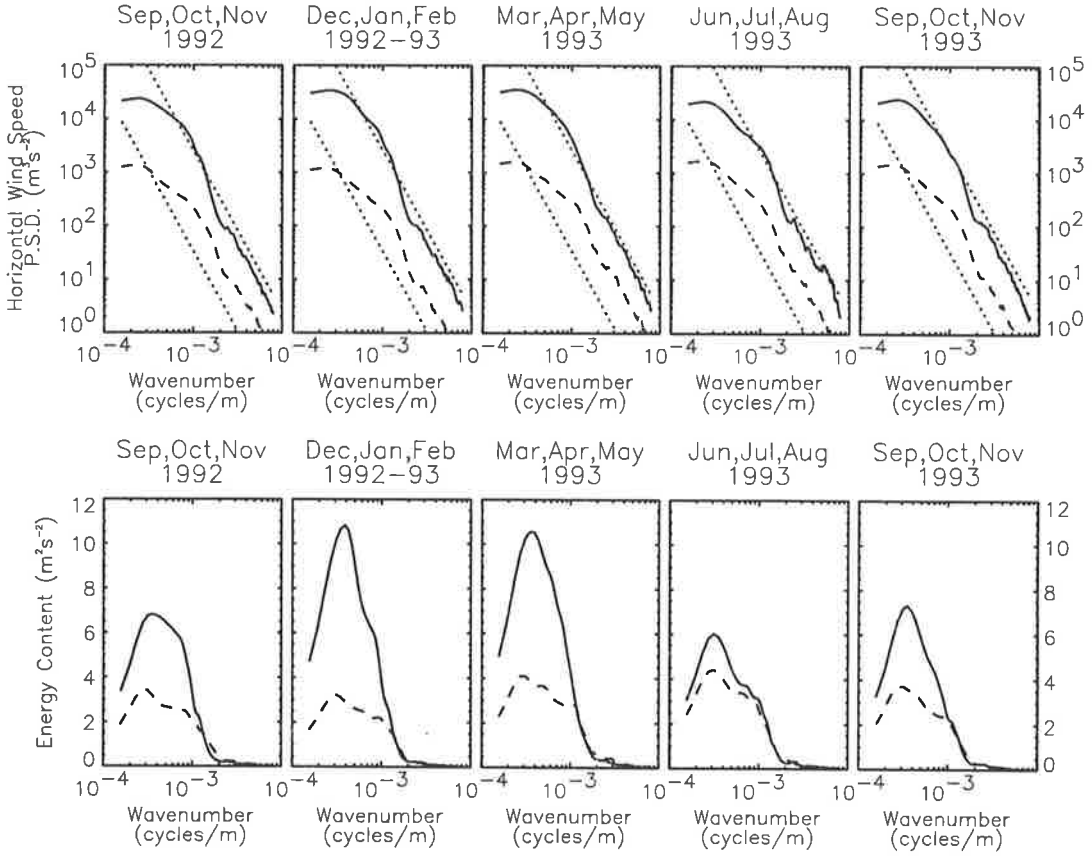

Figure 6.8: Vertical wavenumber power spectra and area preserving spectra of total horizontal wind velocity fluctuations observed at the Cocos Islands (12°S, 97°E). Solid lines indicate stratospheric spectra (18.0 to 25.0 km) while dashed lines indicate tropospheric spectra (7.0 to 14.0 km). Each spectrum is a 3-month average and the saturation limits due to *Smith et al.* [1987] are plotted for comparison purposes (dotted lines). The 95% confidence limits are approximately given by 0.85 and 1.15 multiplied by the spectral amplitude at each wavenumber. Tropospheric power spectra have been displaced downward by an order of magnitude so as to aid viewing.

within experimental error, and is found to be true in the lower stratosphere at least. Further details regarding the seasonal variations of both temperature and horizontal wind velocity variance are discussed in the following subsection.

6.3.3 Seasonal Variations

Figure 6.9 presents monthly-mean potential and horizontal kinetic energy (per unit mass) as a function of time within both the troposphere (7.0–14.0 km) and lower stratosphere (18.0–25.0 km). These quantities were calculated in the same manner as in the previous chapter. Notice that horizontal kinetic energy is consistently larger than potential energy. This is

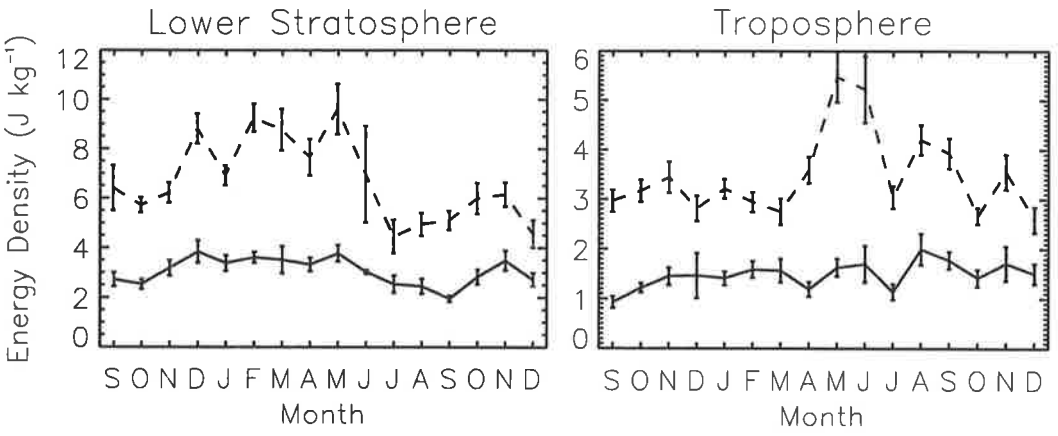

Figure 6.9: Time variations of monthly-mean potential energy per unit mass (solid lines) and horizontal kinetic energy per unit mass (dashed lines) within both the troposphere (7.0–14.0 km) and lower stratosphere (18.0–25.0 km) over the Cocos Islands. Error bars describe the standard errors of the means.

expected of a red-noise frequency spectrum of gravity waves ($p > 1$) due to the reduction of potential energy relative to kinetic energy for gravity waves with intrinsic frequencies near f, the inertial frequency [e.g., *Fritts et al.*, 1988].

It should be emphasized that, during some months, the number of soundings used for variance analysis was small, particularly within the lower stratosphere. Most notably, only 3 sondes reached 25 km during June 1993 and so the energy density estimates from this month are of poor reliability. Furthermore, the standard error of the mean is a poor estimate of measurement uncertainty in this instance. Figure 6.10 illustrates the number of soundings that were analyzed from each month within both the troposphere and lower stratosphere. The same data were used to determine the horizontal wind velocity power spectra that are presented in Figure 6.8.

The largest values of energy density in the lower stratosphere occur between the months of December 1992 and May 1993. This corresponds, approximately, to the times of maximum rainfall at the Cocos Islands as was noted earlier. The seasonal variation of lower stratospheric potential energy is consistent with that of kinetic energy as expected. However, the mean ratio of lower stratospheric kinetic to potential energy is $p = 2.2$ and monthly-mean values are consistently larger than 5/3. The standard error of the mean ratio is 0.1.

The largest values of energy density in the troposphere occur between the months of May 1993 and September 1993. However, the seasonal variation of tropospheric potential energy is not well correlated with the seasonal variation of horizontal kinetic energy. There

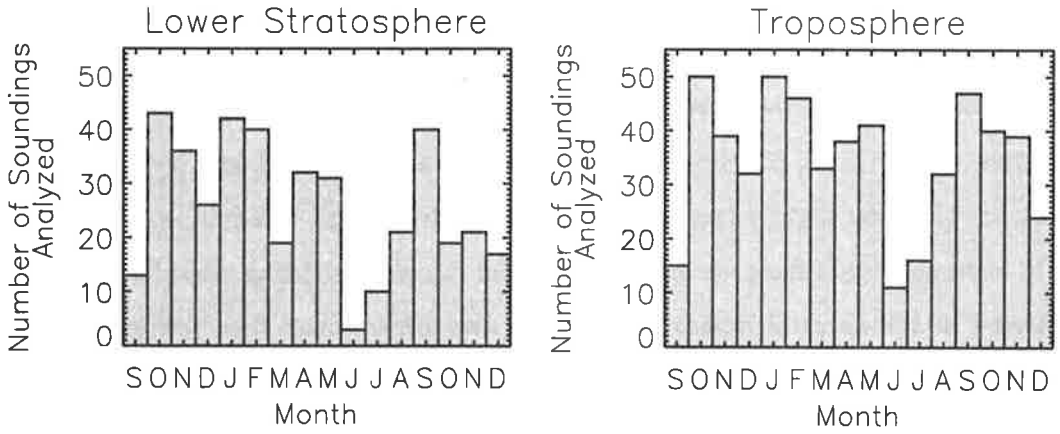

Figure 6.10: The number of soundings used to determine monthly-mean horizontal kinetic energy density (per unit mass) within the troposphere and lower stratosphere over the Cocos Islands.

is a large peak in kinetic energy during May 1993 and June 1993 which does not occur simultaneously in potential energy. The mean ratio of kinetic to potential energy is $p = 2.4$ while the standard error of the mean ratio is 0.1.

The estimates of gravity wave energy density that are presented in Figure 6.9 may be contaminated by equatorially trapped wave motions of large horizontal scale. It is appropriate to separate these motions from freely-propagating gravity waves since the former are resolved by satellite observations and computer models of the atmosphere whereas the latter, typically, are not. The following section delineates the relative contributions to the total variance by fluctuations with intrinsic frequencies that are both larger and smaller than f, the inertial frequency. This is possible at the Cocos Islands since the inertial period is 2.4 days and is resolved by sondes that are launched at 12-hour intervals.

6.4 Time Series Analysis

Kelvin and mixed Rossby-gravity waves are known to have comparable vertical scales to those of freely propagating gravity waves [e.g., *Wallace*, 1973] and their contribution to the observed variance at 12°S must be carefully examined. *Tsuda et al.* [1994b] extracted gravity wave components from near-equatorial radiosonde data by applying a high-pass filter to time variations of horizontal wind velocity and temperature at each altitude. However, such analysis is not possible over the entire data set in this instance since the time resolution is generally too poor and is also uneven. Nevertheless, data of sufficient quality and resolution

were available over two periods of 1-month duration each. These periods were between January 19, 1993, and February 18, 1993, and between October 7, 1992, and November 6, 1992. Time series analysis was attempted on both subsets of the data.

Following *Tsuda et al.* [1994b], each subset of data was filtered in time with a cutoff frequency, ω_c, that was slightly larger than the inertial frequency. In addition data were also filtered in altitude so that fixed vertical wavenumber ranges were being considered. Filtering was achieved in the spectral domain by using a two-dimensional Fast Fourier Transform (FFT) and band-pass filters with no tapering. The purpose of this analysis is to determine which frequency-wavenumber bands contain the majority of observed variance.

Figure 6.11 illustrates the two-dimensional filters that are utilized in this section. The cutoff period for untrapped gravity waves ($2\pi/\omega_c$) was chosen to be 3.5 days and is larger than the inertial period at 12°S ($2\pi/f = 2.4$ days). It was chosen to allow for both Doppler-shifting and aliasing effects which may cause gravity wave variance to appear at ground-based periods that are larger than the inertial period. The dominant ground-based periods of Kelvin and mixed Rossby-gravity waves, based on experimental reports in the literature, are 15 days and 4–5 days, respectively [*Wallace*, 1973]. These are both larger than the chosen cutoff period. More details regarding the purpose of each filter will be described where appropriate.

Aliasing effects, due to poor time resolution, are not expected to be important here since the intrinsic frequency spectrum is likely to be a red-noise spectrum based on the observed ratios of horizontal kinetic to potential energy density. Similarly, the ringing and edge effects that were described by *Forbes* [1988] (or more precisely their two-dimensional analogue) are not thought to be important since it is the total variance, considered over 6 km altitude intervals and averaged over the entire observation period, that is of interest. In contrast, the effects of Doppler shifting are unknown although the mean winds over the Cocos Islands are typically weaker than those found at higher latitudes.

6.4.1 Data Subset 1

Consider, firstly, the data subset between January 19, 1993, and February 18, 1993. During this period 62 sondes were released at approximately 12-hour intervals and reached typical altitudes of 24 km or more. Figure 6.12 illustrates the maximum altitudes of wind velocity measurements from each sounding. For those soundings where winds were not reported at some heights due to poor reception of VLF radio transmissions, the wind measurements were only retained up until the first batch of missing data. Maximum altitudes of temperature

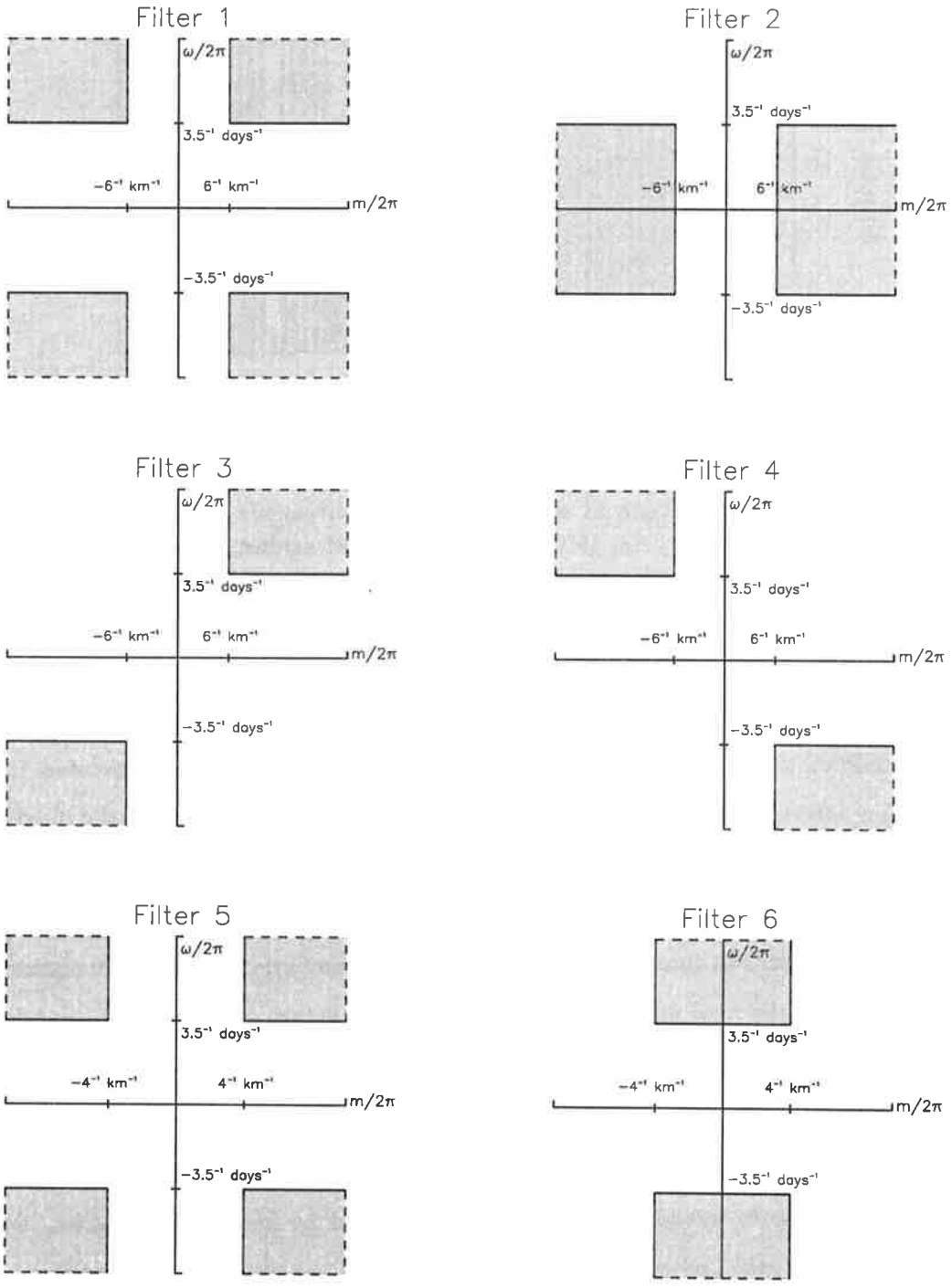

Figure 6.11: Schematic illustration of several band-pass filters in the frequency-wavenumber domain. Shaded areas describe the vertical and temporal scales that are passed by each filter.

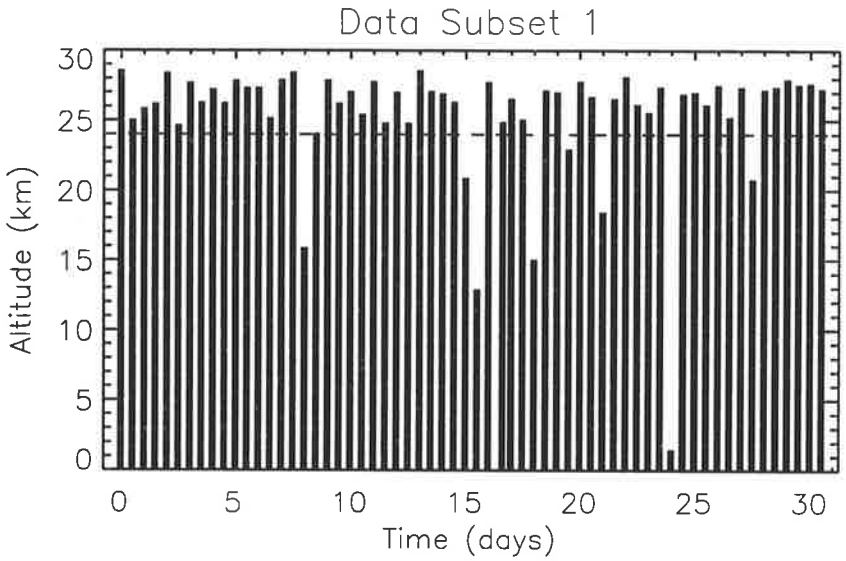

Figure 6.12: The highest altitude of wind velocity measurements for soundings between January 19, 1993, and February 18, 1993. These are plotted against launch times [following *Cadet and Teitelbaum*, 1979] relative to the first sounding which began at Gmt 10:00 on January 19, 1993. Launch times are only known to the nearest hour.

measurements may be higher than those of wind velocity measurements in some instances.

Each profile of zonal wind, meridional wind and temperature was interpolated (cubic spline) at 60-m intervals up to either 24 km (the dashed line in Figure 6.12) or the maximum altitude of measurement if this was smaller than 24 km. Missing winds and temperatures were then estimated by linear interpolation in time, at each height. Finally, a mean was subtracted from the various time series at all altitudes and temperature data were normalized by the mean. Thus the final data subset comprised three arrays of zonal wind, meridional wind and temperature data which had dimensions of 400 by 62 elements. Successive data points were separated by 60 m in altitude and 12 hours in time.

Possible errors in the analysis may arise since the data arrays are not necessarily equi-spaced in time and since missing data had to be estimated by linear interpolation. Sonde launch times[11] were only known to the nearest hour from the available information. Furthermore, each sounding is assumed to be an instantaneous, vertical "snapshot" of the atmosphere whereas, in reality, typical sondes take over an hour to reach 24 km and drift horizontally with the background winds. However, as was discussed in chapter 3, spectral

[11] All soundings between January 19, 1993, and February 18, 1993, started at Gmt 10:00 and Gmt 22:00 (to the nearest hour) with one exception. This sonde was released at Gmt 01:00 on February 5, 1993.

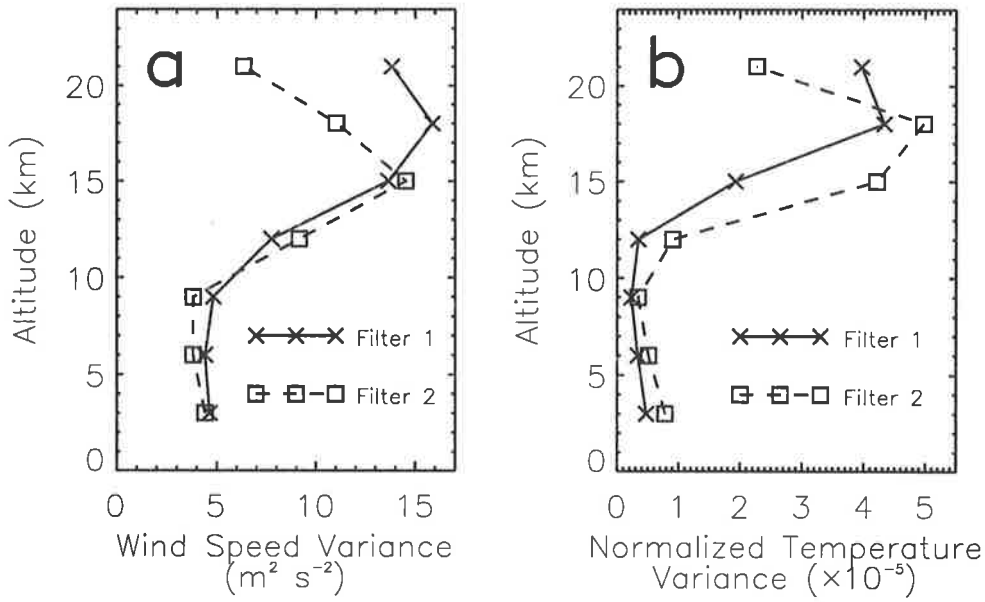

Figure 6.13: Variance profiles of (a) total horizontal wind velocity fluctuations and (b) normalized temperature fluctuations. These were calculated from observations between January 19, 1993, and February 18, 1993, after the application of Filter 1 (solid lines) and Filter 2 (dashed lines). See text for further details.

distortion due to finite sonde ascent velocity and horizontal drift is expected to be insignificant. This is especially the case when background winds are weak, as they are in the troposphere and lower stratosphere over the Cocos Islands.

It should be emphasized that total variances within broad frequency-wavenumber bands are of interest here. The problems described above may result in some distortion of the two-dimensional fluctuation power spectra. However, broad band variances are more reliable, in a statistical sense, and the relative distribution of broad band variance is less likely to be biased by spectral leakage.

Figure 6.13 compares variance profiles of horizontal wind velocity and temperature fluctuations after the application of Filters 1 and 2 (see Figure 6.11) to the raw data arrays. Variances were calculated within a 6-km running window and then averaged over time. Each variance profile is presented with a vertical resolution of 3 km and is oversampled by a factor of two. It is the relative distribution of variance within the frequency-wavenumber bands defined by Filters 1 and 2 that are of interest here.

Filter 1 passes fluctuations with ground-based periods that are smaller than 3.5 days

which corresponds, approximately, to freely-propagating gravity wave periods at 12°S. Filter 2 passes fluctuations with ground-based periods that are greater than 3.5 days and includes the dominant periods of Kelvin and mixed Rossby-gravity waves. Both filters exclude fluctuations with vertical scales that are larger than 6 km in order to be consistent with earlier analyses. There is no decisive cutoff for the gravity wave frequency spectrum due to the various problems described above but most notably due to aliasing and Doppler shifting. Therefore, it is only possible to make qualitative inferences about freely propagating gravity wave variance.

It is clear from Figure 6.13 that the majority of observed wind and temperature variance in the lower stratosphere occurs at periods that are consistent with those of gravity waves. In the troposphere, however, a significant portion of observed variance occurs at periods that are greater than the inertial period. This is most apparent for normalized temperature variance near the typical tropopause height.

Figure 6.14 compares variance profiles of wind velocity and temperature fluctuations after the application of Filters 3 and 4 to the raw data arrays. Variance profiles were calculated in the same manner as in Figure 6.13. Filters 3 and 4 divide the gravity wave portion of the frequency-wavenumber spectrum, which is defined by Filter 1, into upward propagating (Filter 3) and downward propagating (Filter 4) components. Upward propagating gravity waves have negative vertical phase speeds while downward propagating gravity waves have positive vertical phase speeds.

It is clear from Figure 6.14 that the majority of observed gravity wave variance appears in the upward propagating component in the lower stratosphere. However, in the troposphere this is not the case and approximately equal portions of variance appear in both upward propagating and downward propagating components. This pre-empts the rotary spectrum analysis that is attempted in the following section. Rotary spectrum analysis provides estimates of the proportion of upward propagating gravity wave variance during all months. Figure 6.14 allows independent confirmation of such estimates for a small subset of the data.

Figure 6.15 compares variance profiles of wind velocity and temperature fluctuations after the application of Filters 5 and 6 to the raw data arrays. Filter 5 passes gravity waves with vertical scales that are smaller than 4 km (including the harmonic at $\lambda_z = 4$ km) while Filter 6 passes gravity waves with vertical scales that are larger than 4 km (excluding the mean). The purpose of this analysis is to estimate the dominant vertical scales of gravity wave fluctuations.

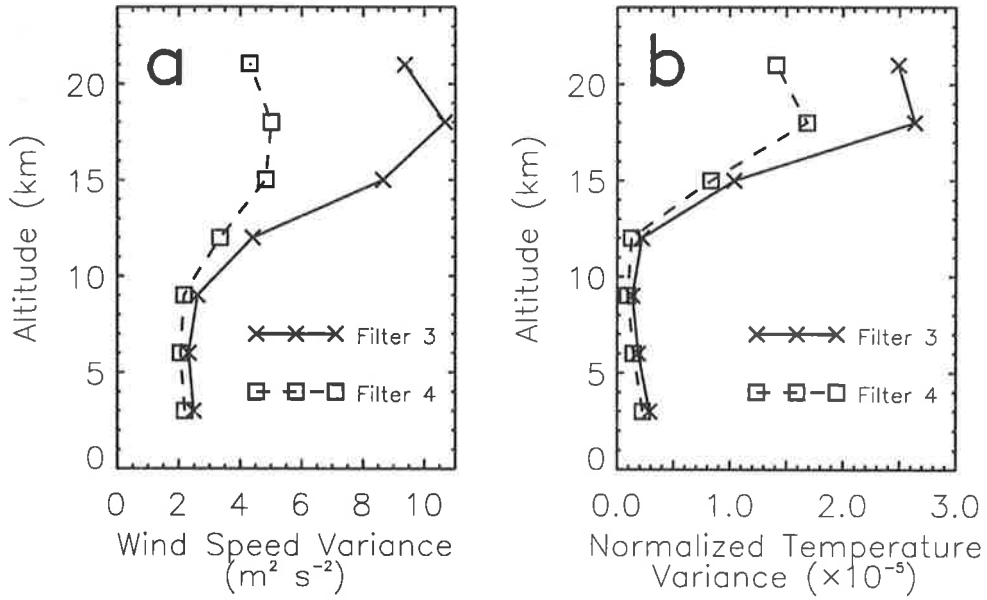

Figure 6.14: As in Figure 6.13, but for (a) total horizontal wind velocity fluctuations and (b) normalized temperature fluctuations that have passed through Filters 3 and 4.

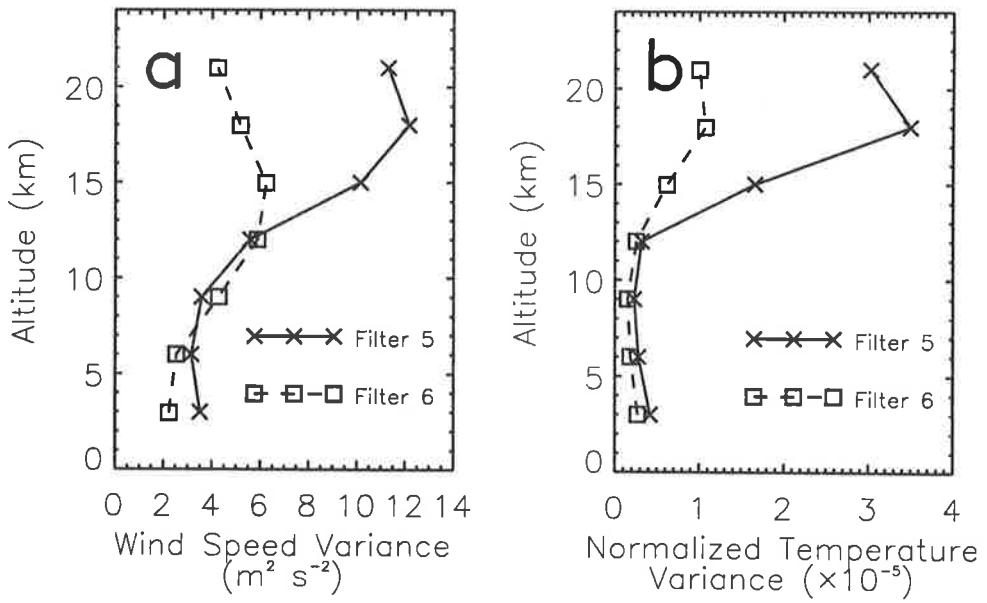

Figure 6.15: As in Figure 6.13, but for (a) total horizontal wind velocity fluctuations and (b) normalized temperature fluctuations that have passed through Filters 5 and 6.

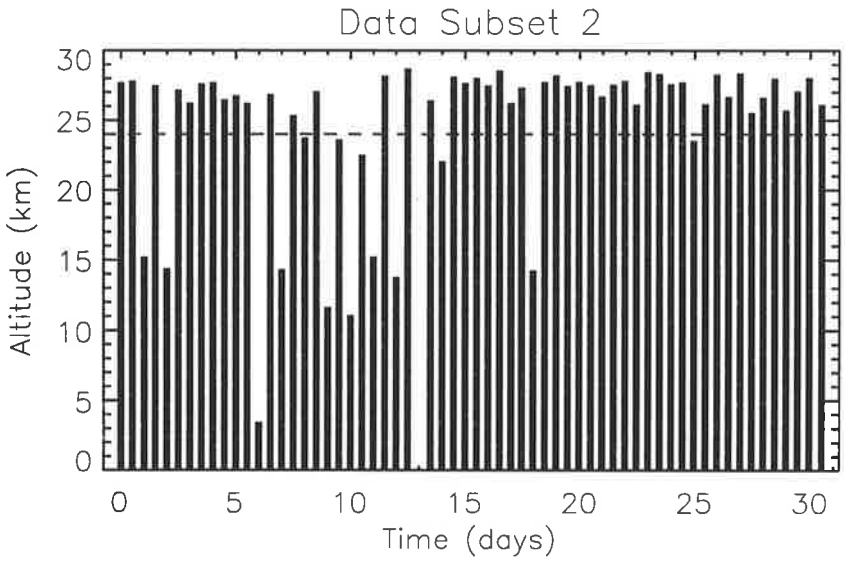

Figure 6.16: As in Figure 6.12, but for radiosonde soundings between October 7, 1992, and November 6, 1992. Launch times are relative to the first sounding which began at Gmt 11:00 on October 7, 1992.

It is clear from Figure 6.15 that the majority of observed gravity wave variance appears at vertical scales that are smaller than 4 km in the lower stratosphere. Since the majority of wave variance also appears within a small wavenumber band about the characteristic vertical wavenumber (see Figure 3.7), the estimate of m_* from the previous section ($2\pi/m_* \approx 3$ km) is likely to be valid. In the troposphere, however, approximately 50% of the observed variance appears at vertical scales that are larger than 4 km. Therefore, the characteristic vertical wavenumber is smaller here and is likely to be overestimated by the earlier spectral analyses.

6.4.2 Data Subset 2

Now consider the data subset between October 7, 1992, and November 6, 1992. During this period 61 sondes[12] were launched at approximately 12-hour intervals and the maximum altitudes of wind velocity measurements from these soundings are displayed in Figure 6.16. Sonde launch times were only known to the nearest hour. Notice that there are more missing measurements in this subset of the data than was the case in Figure 6.12.

The subset of data defined by Figure 6.16 was subjected to the same analysis as before. The results are displayed in Figures 6.17, 6.18 and 6.19. These are variance profiles of total horizontal wind velocity and temperature fluctuations which have been calculated after the

[12]Only one sonde was released on October 20, 1992.

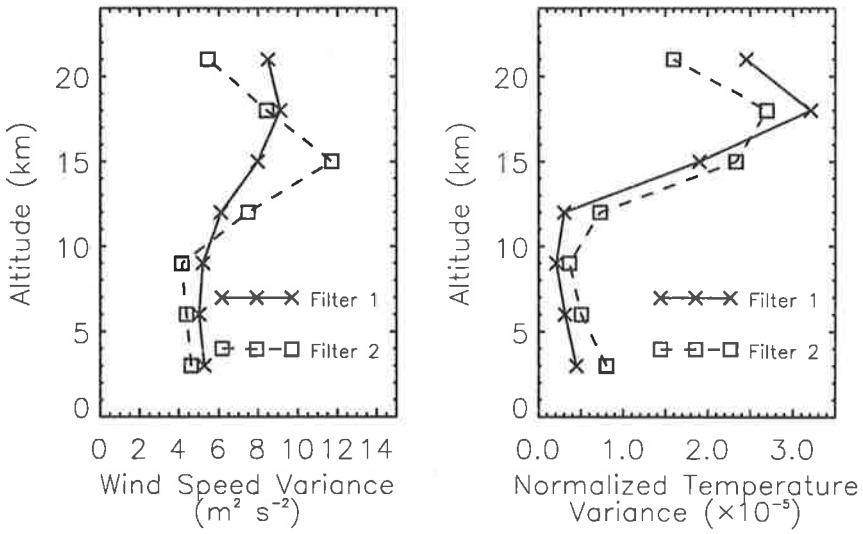

Figure 6.17: As in Figure 6.13, but for radiosonde data observed between October 7, 1992, and November 6, 1992.

application of various filters (Figure 6.11) to the raw data subset. Linear interpolation (in time) was used to estimate missing data and to ensure that the various time series, at each altitude, were equally spaced.

In the lower stratosphere, the majority of observed variance appears at temporal and vertical scales that are consistent with those expected of gravity waves. Furthermore, the majority of gravity wave variance appears in the upward propagating component. In the troposphere, however, a significant portion of variance appears at temporal scales that are greater than the inertial period. Also, gravity wave variance is divided equally into upward propagating and downward propagating components. The results displayed in Figure 6.17, 6.18 and 6.19 are comparable to those displayed in Figures 6.13, 6.14 and 6.15.

6.4.3 Concluding Comments

Time series analysis supports the notion that observed fluctuations of horizontal wind velocity and temperature in the lower stratosphere over the Cocos Islands are caused by inertio-gravity waves, at least during the periods of observation that were under investigation. These waves have ground-based time scales that are approximately equal to or smaller than the inertial period and vertical scales that are equal to or smaller than 6 km ($2\pi/m_* \approx 3$ km). In the troposphere, however, a gravity wave interpretation of observed fluctuations is less clear. It is difficult to ascribe a pure gravity wave interpretation in this case, even when

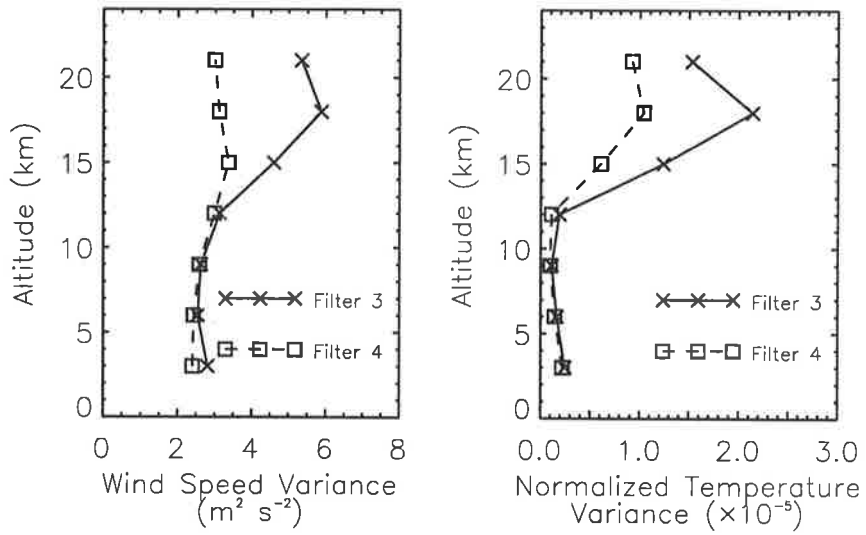

Figure 6.18: As in Figure 6.14, but for radiosonde data observed between October 7, 1992, and November 6, 1992.

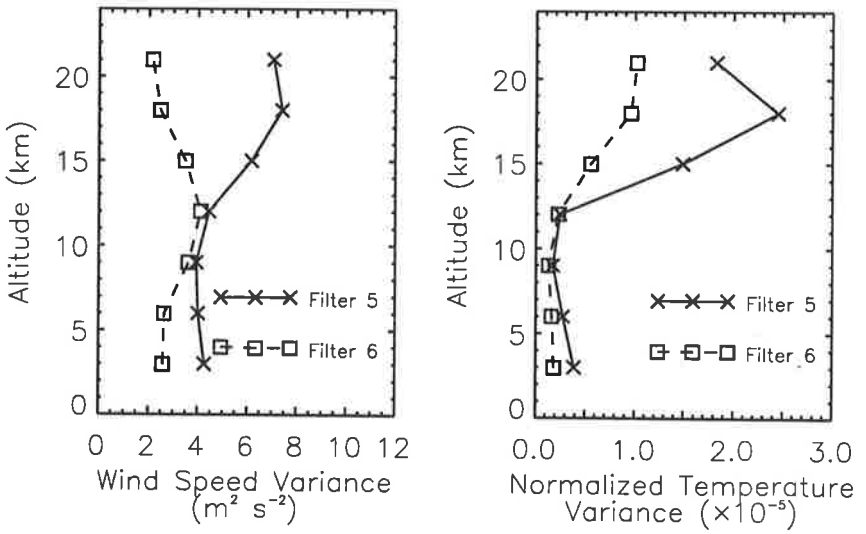

Figure 6.19: As in Figure 6.15, but for radiosonde data observed between October 7, 1992, and November 6, 1992.

Doppler shifting and aliasing effects are taken into consideration, since a significant portion of the observed variance appears at temporal scales that are larger than the inertial period.

Analyses of horizontal wind velocity and temperature measurements by *Tsuda et al.* [1994a], *Sato et al.* [1994] and *May et al.* [1995] support the findings of this section. *Sato et al.* [1994] analyzed routine radiosonde measurements, at significant levels and standard pressure levels, from 10 years of observation over Singapore (1°N, 104°E). These authors determined 10-year average frequency power spectra (in an energy content form) from 3-month data segments at various altitudes up to approximately 30 km. They found that, in the lower stratosphere, "short-period fluctuations [of the order of 2 days] have large energy comparable to long-period Kelvin waves" [*Sato et al.,* 1994, p. 871]. They also suggest that inertio-gravity plane waves crossing the equator are a likely cause of such fluctuations. Wave motions with periods of several days or more were found to have their largest amplitudes near the tropopause. Given that equatorial wave amplitudes are greatest at the equator, it is expected that short-period, inertio-gravity wave fluctuations should dominate in the lower stratosphere at 12°S.

Tsuda et al. [1994a] analyzed 25 days of high vertical resolution radiosonde measurements over Watukosek, Indonesia (8°S, 113°E). They found that gravity wave fluctuations became dominant above 25 km but that a 20-day Kelvin wave was "conspicuously enhanced" in a narrow region about the tropopause [*Tsuda et al.,* 1994a, p. 10504]. Inspection of the time-height zonal wind sections studied here, after low pass filtering in time (these are not shown), does not reveal the conspicuous enhancement of long period fluctuations that is clearly present in the time-height section studied by *Tsuda et al.* [1994a]. It is likely that equatorial wave amplitudes are considerably smaller at 12°S.

May et al. [1995] analyzed 50 MHz wind-profiler measurements of hourly-averaged, horizontal winds in the troposphere over Darwin (12°S, 131°E). They considered more than one year of horizontal wind velocity measurements between 1.5 and 8.5 km at a site that is approximately the same distance from the equator as the Cocos Islands. Frequency power spectra were found to have no obvious break in spectral form near the inertial period and showed little systematic difference from season to season [*May et al.,* 1995]. Furthermore, area preserving spectra revealed that a large portion of both zonal and meridional energy had periods of between 3 and 10 days [*May et al.,* 1995]. This agrees well with the tropospheric results reported here.

The analyses presented in the following sections will concentrate upon lower stratospheric

observations from the Cocos Islands since a gravity wave interpretation of observed fluctuations is most certain there. Ideally, all data under investigation should be subjected to time series analysis in order to determine the relative importance of inertio-gravity waves over near-equatorial locations. However, since this is not possible for the data considered here, it will be assumed that results from two small subsets of the data are also applicable during other times. This would seem reasonable given the results of similar studies in the literature.

6.5 Gravity Wave Propagation Directions

Following the analyses presented in chapter 5, the propagation directions of dominant gravity waves over the Cocos Islands are now investigated. This investigation focuses on lower stratospheric observations although tropospheric observations are also considered in some instances. Raw data are not filtered in time, as they were by *Tsuda et al.* [1994a,b], and so long-period equatorial waves may affect the results. However, based on the analyses from the previous section, gravity wave motions are assumed to be dominant in the lower stratosphere at all times and the influence of long-period waves is therefore thought to be marginal.

6.5.1 Hodograph Analysis

Figure 6.20 presents some examples of wind fluctuation hodographs[13] within the lower stratosphere. These typically display an anticlockwise sense of rotation with increasing altitude which is suggestive of upward propagation of gravity wave energy. There were no examples found where a monochromatic wave signal persisted for more than one cycle and so a broad superposition of upward propagating waves is typical[14]. This contrasts to some extent with results from Macquarie Island where, on occasion, monochromatic signals were found to persist for more than two wave cycles. Similarly, *Tsuda et al.* [1994b] report one example in which a wind hodograph in the lower stratosphere exhibited an ellipse over two wave cycles. Nevertheless, in both of these cases, the wind hodographs most frequently exhibited a superposition of several waves.

Despite the polychromatic nature of the wind hodographs displayed in Figure 6.20, there is nevertheless a preferred sense of horizontal alignment in each case which, by inspection,

[13]The observed winds were filtered in a similar manner to those in chapter 5 such that fluctuations with vertical scales larger than 5 km and smaller than 500 m were excluded.

[14]Note that only a small fraction of the available stratospheric wind profiles were viewed in hodograph form.

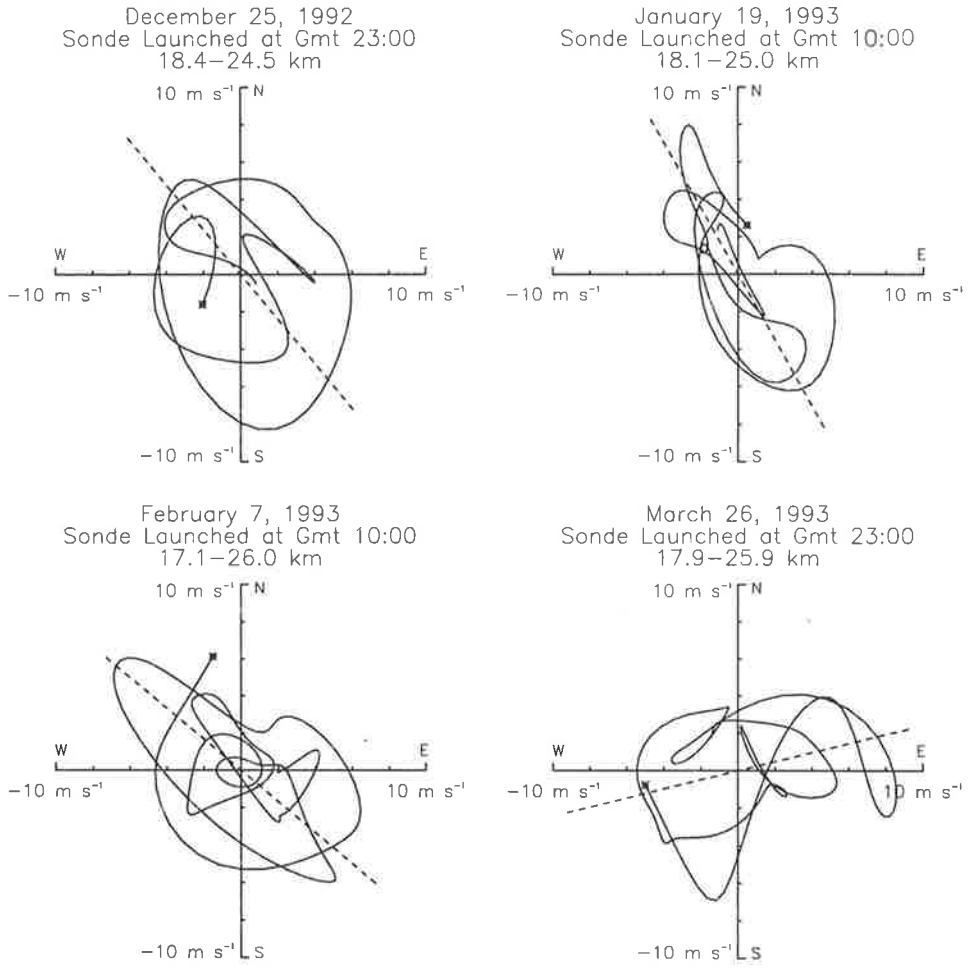

Figure 6.20: Some examples of wind fluctuation hodographs in the lower stratosphere over the Cocos Islands. The tip of the wind velocity vector at the lowest altitude is indicated by an asterisk in each plot. Dashed lines indicate the preferred sense of alignment of the polarized component which has been determined by Stokes parameter analysis.

is well represented by the dashed lines. These dashed lines were determined from the Stokes parameters and in particular from equation (3.28). However, the examples provided in Figure 6.20 are best case examples and this must be emphasized. They were chosen as examples for which a dominant sense of alignment was clearly present. Some hodographs displayed no preferred orientation of the observed wind fluctuations and may have been indicative of a horizontally isotropic wave field.

The degree of polarization parameter, d (see chapter 3), provides one method for determining whether or not a preferred sense of alignment, as defined by (3.28), is meaningful. This point was discussed in detail in chapter 5. The values of d for the examples displayed in Figure 6.20 were all greater than 0.65 which suggests a strongly polarized wave field. In

contrast, other examples were found where d was less than 0.4 and where inspection of wind hodographs revealed no clear sense of horizontal alignment. It is therefore important that some measure of the degree of wave field polarization or anisotropy is considered.

Following *Hamilton* [1991], it seems reasonable to assign a dominant horizontal direction of phase propagation for each example of Figure 6.20. However, as was discussed in chapter 3, it is first necessary to determine the dominant vertical directions of phase propagation. These can be obtained by rotary spectrum analysis.

6.5.2 Vertical Propagation

Figure 6.21 presents 3-month mean rotary power spectra of horizontal wind velocity fluctuations within the troposphere (7.0–14.0 km) and lower stratosphere (18.0–24.0 km) over the Cocos Islands. The wind velocity data considered were the same as those used to determine horizontal wind velocity power spectra and so Figure 6.10, which illustrates the number of soundings analyzed per month, is applicable here. Rotary power spectra were calculated using a Fast Fourier Transform (FFT) algorithm as described in chapter 3 and were normalized such that the sum of areas under the clockwise and anticlockwise component spectra was equivalent to the total horizontal wind velocity variance. Wind velocity fluctuations were determined by fitting and subtracting second-order polynomials from the zonal and meridional wind component profiles within the altitude ranges of interest.

In the lower stratosphere, approximately 70% of observed variance appears in the anticlockwise rotating component during all seasons. Furthermore, individual rotary component spectra, which are not shown, always had greater variance in the anticlockwise rotating component. Therefore, assuming an inertio-gravity wave interpretation of observed fluctuations, the majority of gravity wave energy in the lower stratosphere is upward propagating. Since elliptically polarized waves have both circular-clockwise and circular-anticlockwise components in general (see Figure 3.8), it is highly likely that the true proportion of upward propagating gravity wave energy is greater than 70%.

In the troposphere, approximately equal proportions of variance appear in both clockwise and anticlockwise rotating components. This suggests that there is no preferred direction of vertical energy propagation between 7.0 and 14.0 km. Notice the excellent agreement between conclusions drawn from rotary spectrum analysis and those drawn from two-dimensional filtering analysis (Figures 6.14 and 6.18) which is an independent analysis technique.

In order to investigate further the altitude dependence of rotary component spectra

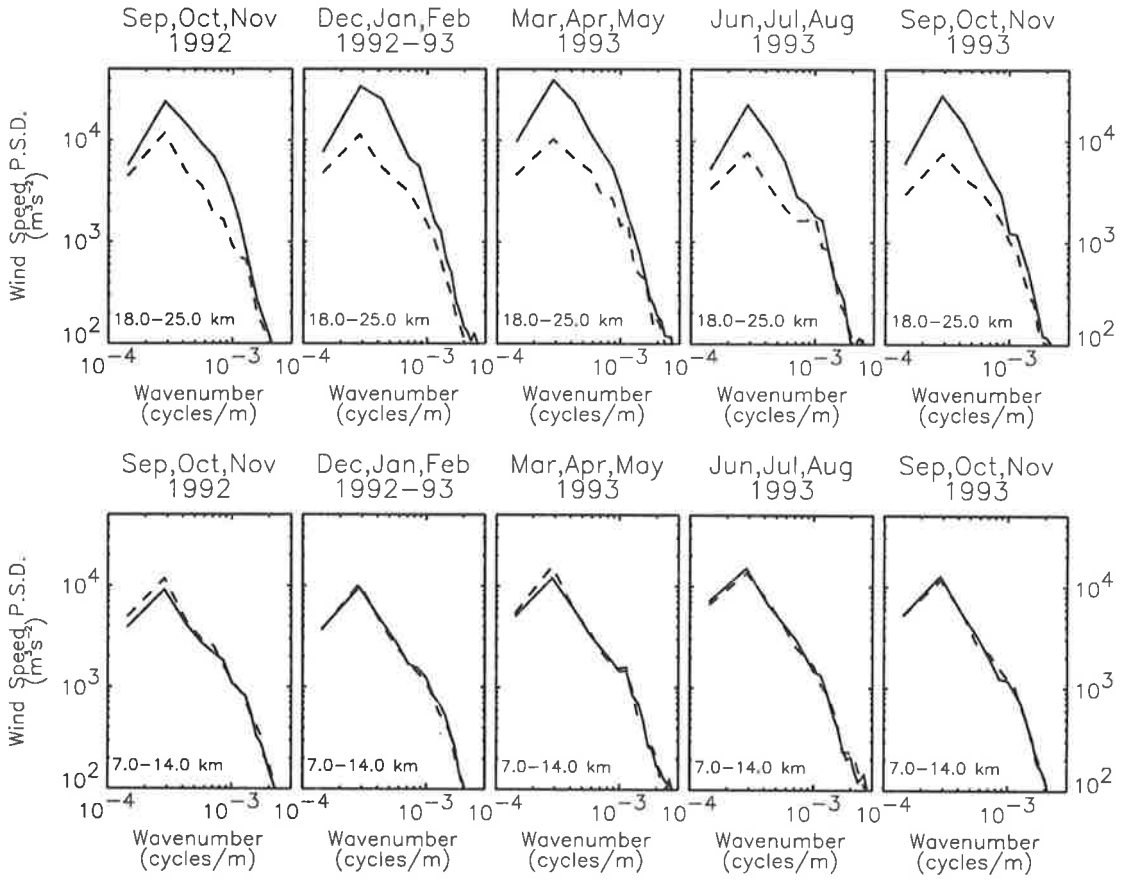

Figure 6.21: Rotary power spectra of horizontal velocity vector fluctuations within the troposphere (7.0 to 14.0 km) and lower stratosphere (18.0 to 25.0 km) over the Cocos Islands. Both clockwise (dashed lines) and anticlockwise (solid lines) component spectra are plotted.

consider Figure 6.22. This diagram displays the percentage of variance in the anticlockwise rotating component as a function of altitude and was constructed in the same manner as Figure 5.15 of chapter 5. Rotary component spectra were first calculated within a 5-km observation window which was centred upon a given height. The percentage of variance in the anticlockwise rotating component was then determined (from the areas under rotary component spectra) and was assigned to that height. An altitude profile was obtained by shifting the observation window in steps of 2 km and repeating the above procedure. Finally, individual profiles were averaged within 3-month time intervals so as to produce the illustrated results. Each profile of Figure 6.22 is oversampled in altitude by a factor of 2.5.

The results displayed in Figure 6.22 illustrate clear differences between tropospheric and stratospheric regimes. Above approximately 17 km there is a large majority of variance in the anticlockwise rotating component during all seasons. Below approximately 12 km there

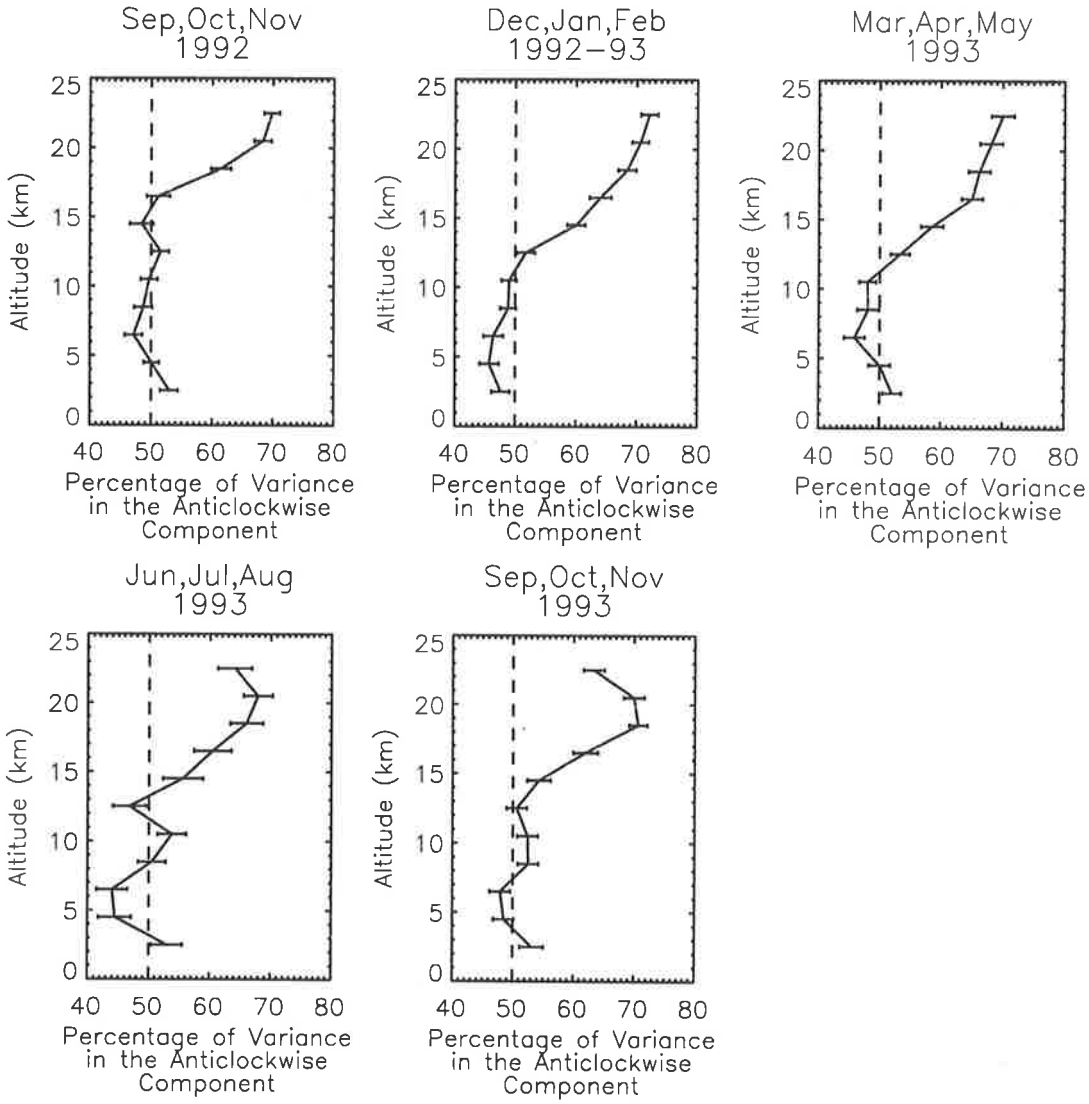

Figure 6.22: The percentage of variance in the anticlockwise rotating component as a function of altitude and averaged within 3-month time intervals. Error bars describe the standard errors of the means.

are equal amounts of variance, on average, in both the clockwise and anticlockwise rotating components. The transition between these two regimes varies from season to season. It is as high as approximately 17 km between September and November, 1992, and as low as approximately 12 km between March and May, 1993. The highest transition occurs during the dry season which is also the time of smallest wave variance in the lower stratosphere.

The calculated profile for the 3-month period of December, January and February (1992-93) is of particular interest. Below 11 km there is consistently more variance (approximately

53%) in the clockwise rotating component while above 15 km there is consistently more variance in the anticlockwise rotating component. One possible explanation is that an important source of gravity wave variance occurs within the middle or upper troposphere.

Tsuda et al. [1994b] found similar results in their study of radiosonde winds over Watukosek, Indonesia, between February 27 and March 22, 1990. They report that below 13 km both upward and downward energy propagating gravity waves were evenly detected but that above this height the majority of gravity waves were associated with upward energy propagation [*Tsuda et al.,* 1994b]. Therefore they suggest that the middle troposphere is the dominant source region of gravity waves. However, in the lowest 5 km of the troposphere, the number of waves with upward energy propagation was found to be slightly larger than those with downward energy propagation [*Tsuda et al.,* 1994b]. This suggests, argue *Tsuda et al.* [1994b], that some waves are either generated near to the ground or are reflected off the ground.

Both rotary spectrum and two-dimensional filtering analyses clearly demonstrate that the dominant gravity waves in the lower stratosphere over the Cocos Islands are upward propagating during all seasons. Therefore, the dominant directions of horizontal phase propagation, if such dominant directions exist, can now be determined following *Kitamura and Hirota* [1989] and *Hamilton* [1991]. The available data are divided into two subsets and will be loosely referred to as wet season and dry season data. Wet season data include observations from December 1992 to May 1993 which corresponds to the times of largest wave variance in the lower stratosphere. Dry season data include observations from June 1993 to November 1993 and also from September 1992 to November 1992. These times correspond to the times of smallest wave variance in the lower stratosphere.

6.5.3 Horizontal Propagation

Consider, firstly, the angular distributions of dominant horizontal alignments which are defined by (3.28). Horizontal alignments determined from individual soundings of the lower stratosphere (18.0–25.0 km) are illustrated in Figure 6.23. This figure displays wet season alignments in the same plot and dry season alignments in the same plot. Each alignment is described by a straight line whose length is proportional to the degree of polarization parameter, d. Also plotted are wet and dry season angular distributions of horizontal alignment in polar histogram form. Polar histograms treat each alignment equally and do not take into account the degree to which the wave field was polarized. The axis labels in this case

describe the number of profiles with a preferred sense of alignment, as defined by (3.28), within a given 30° interval.

Figure 6.23 demonstrates that, for dry season months, the wave field is preferentially aligned either near to or along the north-south axis in more cases than for any other alignment. During the wet season, however, the distribution of horizontal alignments is more even. Nevertheless, there is still a scarcity of cases where the wave field is preferentially aligned along the east-west axis. During both seasons, the degree of polarization parameter is often larger than 0.6 and can be large for any alignment. The importance of the north-south alignment suggests that the observed waves are freely-propagating since equatorially-trapped waves must have large or dominant east-west components at 12°S.

As was discussed earlier, it is important to consider some measure of the degree of wave field polarization during the time periods under investigation. Figure 6.24 illustrates histograms of the degree of polarization parameter, d, determined from individual soundings during wet season and dry season months. The mean values are illustrated by the dashed lines in each plot. These are $d = 0.61$ for both the wet and dry seasons.

Generally the wave field in the lower stratosphere is strongly polarized with 59% of soundings during the wet season and 56% of soundings during the dry season having $d > 0.6$. However, approximately 10% of soundings during both wet and dry seasons had $d < 0.4$. In these cases the angle of alignment defined by (3.28) is not strictly a "dominant" alignment. Rather, small values of d are suggestive of horizontal isotropy.

The angular distribution of alignments determined from those soundings that happen to have $d < 0.4$ in the lower stratosphere (not shown) do not indicate clear bias. If anything, they display a small bias toward east-west alignment during wet season months. Therefore, when the wave field is strongly polarized (large d) there is a preference toward north-south alignment of horizontal wind vector fluctuations, especially during the dry season. This is also evident from close inspection of Figure 6.23. When horizontal alignments determined from individual soundings are overlaid such that the length of each line is proportional to d, the eye tends to focus on those alignments that have large d.

The alignments described in Figure 6.23 are now assigned dominant directions of horizontal phase propagation. This was achieved by using temperature measurements in the manner discussed in chapter 5. Essentially, it is the sign of the covariance of $u'_{\|}$ and $\hat{T}'_{+90}$ which determines whether the horizontal phase propagation direction is parallel to or antiparallel to the $u'_{\|}$ axis. Here, $\hat{T}'_{+90}$ is determined using a negative Hilbert transform while

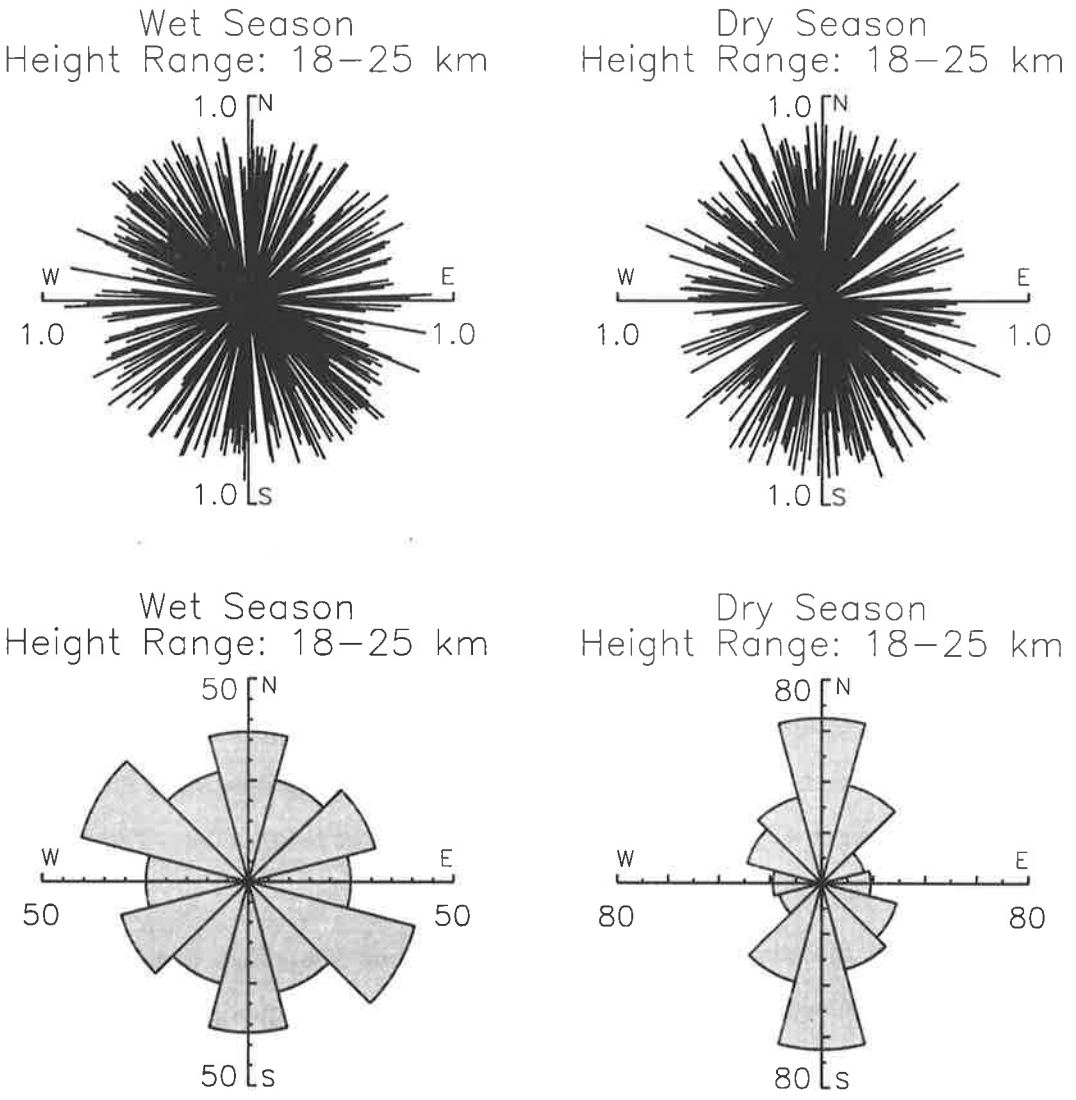

Figure 6.23: The angular distributions of dominant horizontal alignments in the lower stratosphere over the Cocos Islands. Data from wet season and dry season months are considered separately. The two plots of the top row illustrate dominant horizontal alignments inferred from individual soundings where the length of each line is normalized according to the degree of polarization. The two plots of the bottom row illustrate the same distributions in polar histogram form.

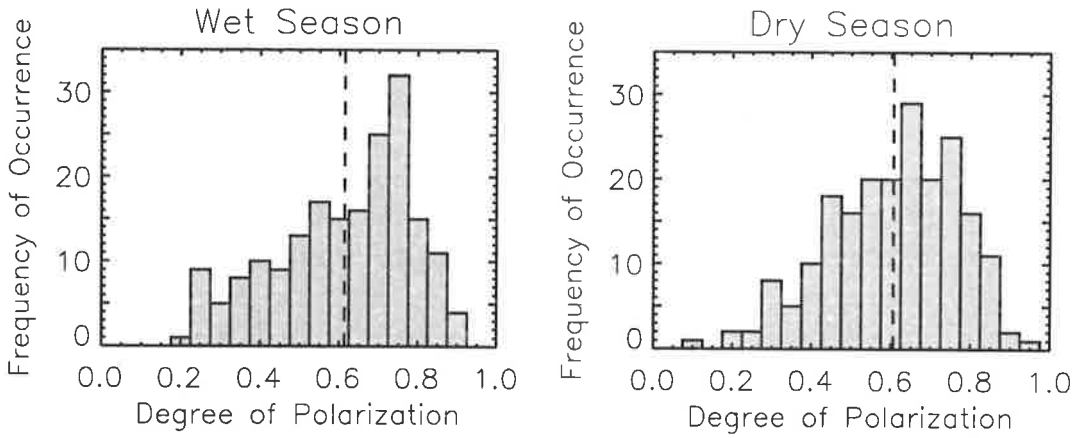

Figure 6.24: The distributions of d from the lower stratosphere (18.0–25.0 km) during both wet and dry seasons. Dashed lines indicate the mean values in each case.

the positive $u'_{\|}$ axis is assigned arbitrarily along one of the two alignment directions already defined from (3.28).

Figure 6.25 illustrates the angular distributions of dominant directions of horizontal phase propagation which have been determined from lower stratospheric observations as described above. This figure is the same as Figure 6.23 except that each horizontal alignment is now reduced to a single propagation direction based on the sign of $\overline{u'_{\|}\hat{T}'_{+90}}$. As before, wet season data and dry season data are considered separately. Individual propagation directions are overlaid where the length of each line is equal to the degree of polarization. The results are also plotted in polar histogram form.

The propagation directions determined from individual soundings during wet season months are most commonly found in the north-east and south-east quadrants. When plotted in histogram form, the wet-season angular distribution displays a clear eastward bias. Those soundings with dominant north-south alignments were reduced more often into the northward propagation direction. However, those soundings with dominant east-west alignments were reduced almost entirely into the eastward propagating direction. The most populous angular bin points in the east-north-east direction.

The propagation directions determined from individual soundings during dry season months are predominantly either northward or southward although, in this case, there is a small southward bias. Those few soundings with dominant east-west alignments were often reduced into the eastward propagating direction. However, the eastward bias is not nearly as prominent as that found during wet season months. The most populous angular

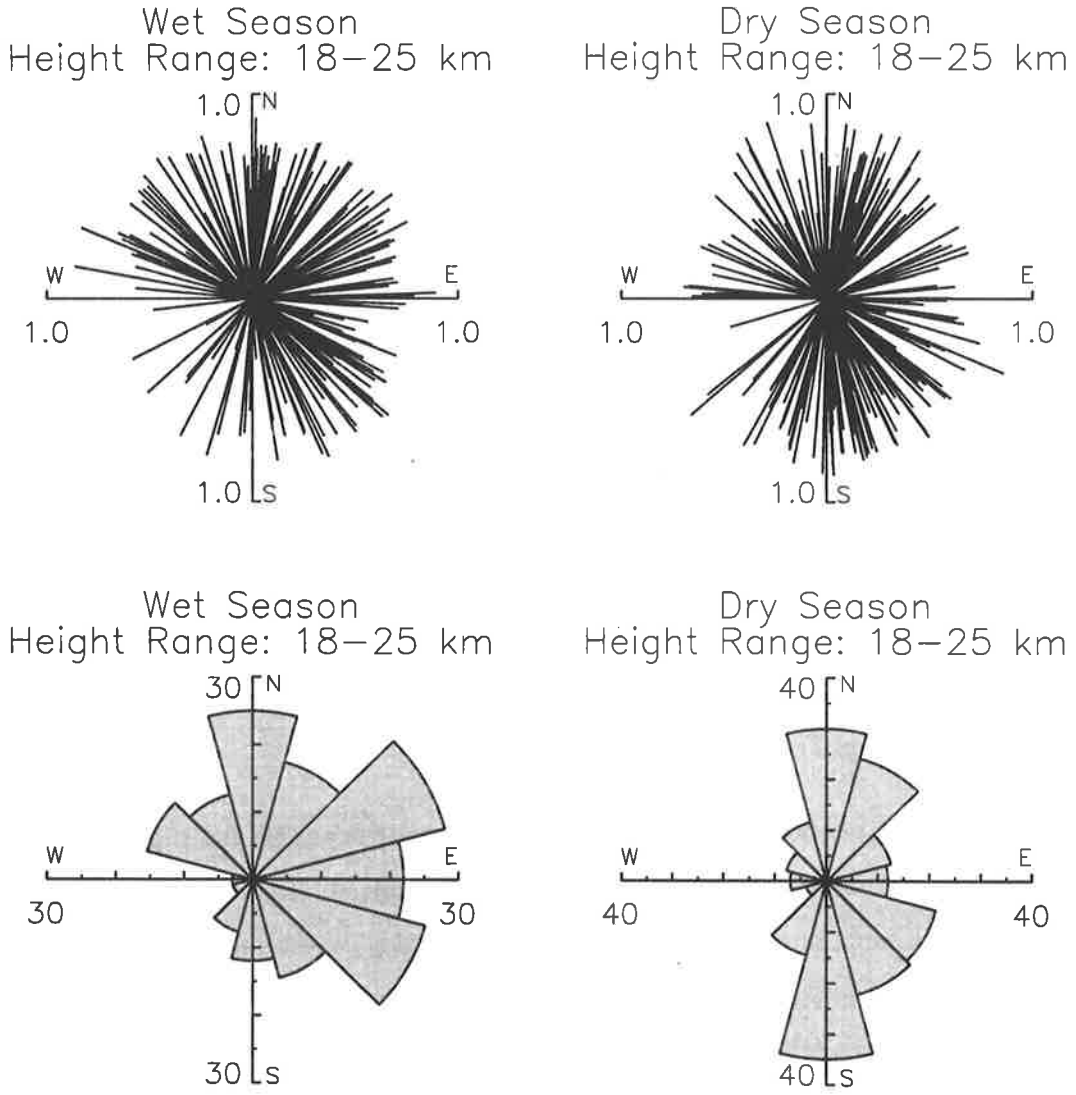

Figure 6.25: As in Figure 6.23, but for dominant directions of horizontal phase propagation. See text for further details.

bin points in the southward direction.

Results that are similar to those of Figure 6.25 are reported by *Tsuda et al.* [1994b] in their study of radiosonde winds and temperatures over Watukosek, Indonesia. They found that most waves detected between February 27 and March 22, 1990, were eastward propagating in the lower stratosphere. This is consistent with propagation directions determined over the Cocos Islands during wet season months.

Each horizontal direction displayed in Figure 6.25 is interpreted to be a dominant direction of horizontal phase propagation following *Hamilton* [1991]. This interpretation is supported by inspection of wind hodographs and by the degree of polarization parameter, d. Further evidence is provided by the correlation coefficient of $u'_{\|}$ and $\hat{T}'_{+90}$. If the wave field is horizontally isotropic then this coefficient will equal zero[15] whereas for a monochromatic wave propagating in an arbitrary direction this coefficient will equal unity.

Figure 6.26 illustrates the correlation coefficients of $u'_{\|}$ and $\hat{T}'_{+90}$ from individual soundings in histogram form[16]. As before, lower stratospheric data are studied and observations from the wet and dry seasons are considered separately. The mean values are 0.33 and 0.28 for the wet and dry seasons, respectively. Note that a correlation coefficient of 0.2, determined from a random sample of 141 observations, is significant to within approximately 95% confidence [see *Bevington*, 1969, p. 310].

Generally, the correlation coefficients of $u'_{\|}$ and $\hat{T}'_{+90}$ are reasonable and suggest that dominant directions of horizontal phase propagation can be assigned. However, 33% of soundings during wet season months and 44% of soundings during dry season months had correlation coefficients that were smaller than 0.2. Nevertheless, when these soundings were removed from Figure 6.25, the angular distributions were not found to be altered in a significant manner. Therefore, the broad results of Figure 6.25 are reasonable although in some instances the wave field might best be described as having no dominant direction of horizontal phase propagation.

[15]The contributions due to individual waves will be cancelled by other waves propagating in the opposite direction.

[16]In this case, the positive $u'_{\|}$ axis was not chosen arbitrarily. Rather, it was chosen such that the correlation coefficient of $u'_{\|}$ and $\hat{T}'_{+90}$ was always positive.

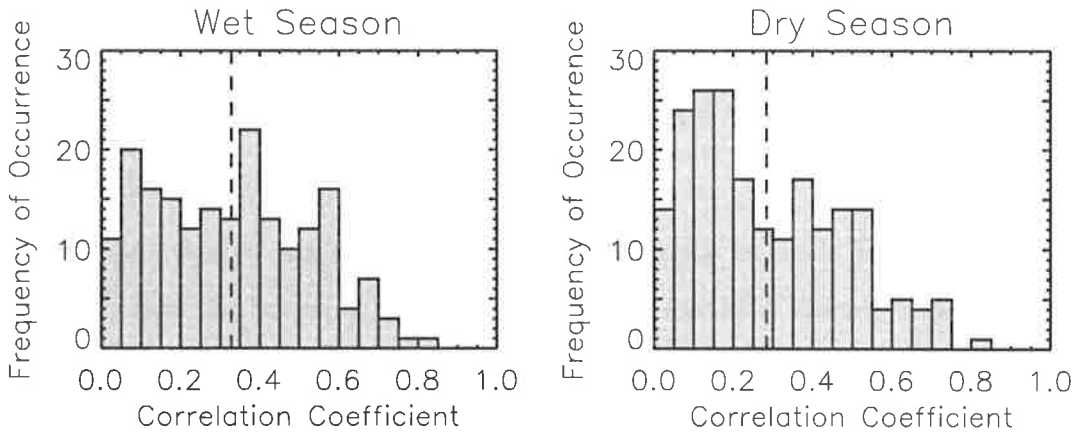

Figure 6.26: The correlation coefficients of $u'_{||}$ and $\hat{T}'_{+90}$ determined from radiosonde observations of the lower stratosphere (18.0–25.0 km). Wet season and dry season correlation coefficients are considered separately and mean values are indicated by dashed lines in each case.

6.6 Summary and Conclusions

In this chapter, the characteristics of gravity wave motions in the troposphere and lower stratosphere over the Cocos Islands have been investigated. These were delineated from radiosonde measurements of horizontal wind and temperature during a 16-month observation period between September 1992 and December 1993. The main results are listed below.

1. Vertical wavenumber power spectra of normalized temperature and horizontal wind velocity fluctuations within the lower stratosphere are consistent with theoretical expectations, at least to within approximate limits imposed by experimental uncertainty. They are also consistent with spectra from Gove and Darwin which are located at the same latitude as the Cocos Islands.

2. Spectral amplitudes within both the lower and upper troposphere are larger, at high vertical wavenumbers, than the theoretical saturation limits proposed by *Smith et al.* [1987]. However, they are consistent with tropospheric spectral amplitudes from Gove and Darwin.

3. There exists an annual oscillation of normalized temperature and horizontal wind velocity variance within the lower stratosphere. The largest variances are found between December and May and correspond with the times of largest mean rainfall.

4. Seasonal variations of horizontal wind velocity and normalized temperature variance within the lower stratosphere are consistent. However, the mean ratio of horizontal kinetic to potential energy is larger than 5/3 which is the preferred estimate from the literature.

5. The majority of observed variance, at vertical scales smaller than 6 km, appears at ground-based periods that are consistent with those expected of freely-propagating gravity waves, at least during two observation periods of 1-month duration each.

6. Gravity wave energy is predominantly upward propagating in the lower stratosphere. In the troposphere, however, there is often no preferred direction of vertical energy propagation.

7. A clear eastward bias is found in the dominant directions of horizontal phase propagation determined from individual soundings of the lower stratosphere during wet season months.

8. No clear bias is found in the dominant directions of horizontal phase propagation determined from individual soundings of the lower stratosphere during dry season months. However, there is a tendency toward north-south alignment of horizontal wind vector fluctuations during this time.

Mesoscale convective systems are likely to be the most important source of gravity waves over the Cocos Islands. While no evidence of gravity wave generation by convection is presented, the correlation between mean rainfall and observed variance in the lower stratosphere suggests that convection is important. Other studies [e.g., *Pfister et al.*, 1993a,b] provide circumstantial evidence of gravity wave generation by convection at tropical latitudes.

Rotary spectrum analysis of radiosonde winds during wet season months suggests that an important source of gravity waves occurs within the middle or upper troposphere. This is also supported by power spectrum analysis of normalized temperature fluctuations (Figure 6.7). Spectral amplitudes determined between 7.0 and 14.0 km are larger, relative to N^4, than those determined between 2.0 and 9.0 km during wet season months, especially March, April and May. However, during September, October and November 1992, spectral amplitudes determined between 2.0 and 9.0 km are the same as those determined between 7.0 and 14.0 km with the exception of some additional high spatial frequency noise in the latter case.

Thus the middle or upper troposphere is the most important source of gravity waves during the wet season.

The most energetic gravity waves detected in the lower stratosphere during the wet season were commonly found to either propagate eastward or to have an eastward component to the propagation direction. The removal of westward propagating waves by the background zonal winds is one possible explanation of this result. Mean zonal winds were westward in the lower stratosphere between December 1992 and March 1993, and near zero or marginally eastward during April and May 1993. However, the mean westward winds were weak during the wet season (of the order of 10 m s^{-1}) and were in fact larger between September and November 1992. Yet there was no clear preference for eastward propagating waves between September and November 1992.

Another possibility is that dominant eastward propagating waves are a signature of some dominant wave source during the wet season which is expected to be convection. *Pfister et al.* [1993a] modelled the impact of convective systems on the stratosphere as being that of time-dependent mountains. According to this picture, penetrative convection generates gravity waves at the tropopause in the same manner as do mountains in the lower troposphere, except that convective "mountains" are time dependent. The majority of momentum flux that is generated this way opposes the mean winds at the tropopause, even when these winds are small and of the order of 5 m s^{-1}. Thus the dominant directions of horizontal phase propagation displayed in Figure 6.25 are consistent with the wave generation model due to *Pfister et al.* [1993a] since the mean wind vectors at 16 km typically point towards the west-south-west during the wet season.

During the dry season, the most energetic waves displayed a tendency toward north-south alignment of horizontal wind vector fluctuations in the lower stratosphere. This may suggest that a significant portion of gravity wave energy was generated at either higher or lower latitudes. Alternatively, the narrow-band biasing effect described by *Eckermann et al.* [1995] may also explain this result, especially between September and November 1992 when the mean zonal winds are strong.

The speculated relationship between convective activity and gravity wave anisotropy in the lower stratosphere might be better understood by using data available over at least one full cycle of the QBO. Furthermore, a network of equatorial radiosonde stations, which measure lower stratospheric horizontal winds and temperatures, might provide additional information about this relationship. Since more countries are now archiving radiosonde data

at high vertical resolution [*Hamilton and Vincent*, 1995] a gravity wave investigation using a network of equatorial radiosonde stations may soon be possible.

The successful studies of *Tsuda et al.* [1994a,b] have demonstrated that important information about both equatorially trapped and freely propagating gravity waves can be obtained by using conventional radiosondes. However, these studies have demonstrated that small time intervals between successive soundings are necessary if large-scale equatorially trapped wave fluctuations are to be distinguished from those of inertio-gravity waves. *Tsuda et al.* [1994a,b] considered radiosondes that were launched at 6-hour time intervals. The results presented in this chapter might be further improved by using data with better time resolution over the entire observation period. Furthermore, they might also be improved by considering data available over a larger altitude range and horizontal wind velocity measurements that are known with greater accuracy and vertical resolution.

As in chapter 5, the Stokes parameter analyses have enabled a qualitative picture of climatological-mean wave field anisotropy to be obtained. Thus if the gravity wave spectral formulation due to *Fritts and VanZandt* [1993] is assumed to be valid then an estimate of climatological-mean momentum flux may be realised given that E_0 is known (see their equation 16). The following chapter explores this possibility by making use of an analysis technique proposed by *Eckermann et al.* [1996].

Chapter 7

Gravity Wave Momentum Flux

7.1 Introduction

The determination of climatological-mean vertical fluxes of zonal and meridional momentum is an important experimental goal, as clearly stated in various review papers [e.g., *Fritts et al.*, 1984; *Andrews*, 1987]. This chapter investigates the momentum fluxes of gravity waves in the troposphere and lower stratosphere using conventional radiosonde soundings. The data considered are simultaneous temperature and horizontal wind velocity measurements from Macquarie Island and the Cocos Islands which are available over 10-month and 16-month observation periods, respectively.

Momentum transfer due to gravity waves is thought to be most important near the mesopause and gravity wave momentum fluxes were first measured in this region by *Vincent and Reid* [1983]. They proposed a technique by which the vertical flux of horizontal momentum can be measured using ground-based Doppler radars. Their technique involves the measurement of radial Doppler velocities along pairs of narrow radar beams which lie in a vertical plane and are offset symmetrically from the vertical. If the statistics of the wave field are independent of horizontal position, then the vertical flux of horizontal momentum is proportional to the difference in radial velocity variances [*Vincent and Reid*, 1983]. Using measurements obtained from an MF radar at Adelaide (35°S, 138°E), *Vincent and Reid* [1983] calculated mean momentum fluxes that were in reasonable agreement with those required to explain the reversal of the meridional temperature gradients near the mesopause[1]. However, the calculated momentum fluxes were found to display considerable variability on

[1]Subsequent studies by *Reid and Vincent* [1987] and *Murphy and Vincent* [1993] have provided additional information about gravity wave momentum fluxes near the mesopause over Adelaide.

short time scales.

The measurement technique proposed by *Vincent and Reid* [1983] has since been applied at other locations using ground-based radars which can measure radial velocities near the mesopause. These include radars at Poker Flat, Alaska [*Fritts and Yuan*, 1989], Shigaraki, Japan [*Tsuda et al.*, 1990], Andoya, Norway [*Reid et al.*, 1988] and Jicamarca, Peru [*Fritts et al.*, 1992; *Hitchman et al.*, 1992] Often, the mean flow accelerations inferred from momentum flux calculations (see equation 1.21) are as large as, or larger than, 50 m s^{-1} day^{-1} at these sites. Therefore, breaking gravity waves are likely to have important effects upon the mean flow in the upper mesosphere and lower thermosphere, as has been anticipated theoretically [e.g., *Lindzen*, 1981].

Recently, the successful introduction of gravity wave drag parameterization schemes into general circulation models of the troposphere and lower stratosphere has emphasized the importance of gravity waves in these regions of the atmosphere [e.g., *Palmer et al.*, 1986; *McFarlane*, 1987]. Indeed, the parameterization schemes proposed by *Fritts and Lu* [1993] and *Hines* [1996a,b] suggest that gravity waves affect all regions of the lower and middle atmospheres through which they propagate. Therefore, the experimental determination of gravity wave momentum flux in the troposphere and lower stratosphere is clearly of importance. This was recognized in an early study by *Lilly* [1972].

Fritts et al. [1990] used the MU radar at Shigaraki, Japan, and the measurement technique proposed by *Vincent and Reid* [1983], to estimate gravity wave momentum fluxes in the lower atmosphere during a 6-day experimental campaign in March 1986. They found that the mean vertical flux of horizontal momentum (per unit mass) between 10.1 km and 19.1 km was 0.197 m^2 s^{-2} and was directed toward 267° azimuth[2]. They also inferred zonal mean-flow accelerations that were eastward below the jet stream, which was found to be present during the campaign period and peaked between 12 and 15 km, and westward above it. The inferred drag above the jet, which was of the order of -1.5 m s^{-1} day^{-1} [*Fritts et al.*, 1990], was in broad agreement with the drags required by *Palmer et al.* [1986] and *McFarlane* [1987] to improve their general circulation models. Consequently, *Fritts et al.* [1990] conclude that their study supports the notion that mountain wave drag has significant effect upon the midlatitude lower stratosphere.

Other experimental techniques have also been used to estimate gravity wave momentum fluxes in the troposphere and lower stratosphere. For example, *Lilly and Kennedy* [1973]

[2]This was measured clockwise from north [*VanZandt et al.*, 1990].

and *Brown* [1983] used aircraft observations to estimate the vertical flux of horizontal momentum associated with mountain waves as have *Nastrom and Fritts* [1992] who analyzed observations obtained from many commercial airline flights over mountainous regions of the western United States. In the latter case, the mean vertical flux of zonal momentum (per unit mass) was estimated to be -0.26 m^2 s^{-2} at typical airline cruise altitudes[3]. Similarly, radiosondes have been used to estimate the momentum flux of mountain waves [e.g., *Mobbs and Rees*, 1989]. Indeed, *Shutts et al.* [1994] demonstrated that the successive release of between 3 and 5 radiosondes with different ascent speeds can be used to determine mountain wave momentum flux. They used fluctuations of the rate of radiosonde ascent to infer the vertical velocity fluctuations of gravity waves.

According to *Shutts et al.* [1994], the rate of radiosonde ascent is the least ambiguous measure of gravity wave activity. This can be obtained by differentiating radiosonde altitude with respect to time. The altitude of radiosondes is estimated from pressure measurements using the hydrostatic equation,

$$z - z_0 = -H_p \ln(\mathrm{p}/\mathrm{p}_0) \tag{7.1}$$

where H_p is pressure scale height and p_0 is the measured pressure at some reference altitude, z_0. Thus the random measurement error of ascent velocity estimates is related to the random measurement error of pressure measurements [e.g., *Mobbs and Rees*, 1989; *Shutts et al.*, 1994] which, from *Ivanov et al.* [1989], is 10 Pa for the data considered in this thesis.

If σ_z and σ_p are the root-mean-square random measurement errors of radiosonde altitude and pressure, respectively, then

$$\sigma_z \approx \left|\frac{dz}{d\mathrm{p}}\right| \sigma_p \tag{7.2}$$

$$= \frac{H_p}{\mathrm{p}}\, \sigma_p \tag{7.3}$$

where $\sigma_p \approx 10$ Pa. Therefore, the random measurement error of radiosonde altitude is inversely proportional to pressure[4]. In the troposphere, p is large and σ_z is of the order of 1 m, as was noted by *Mobbs and Rees* [1989]. However, at heights near 25 km, p is considerably smaller and σ_z is of the order of 20 m. Assuming time is known with good accuracy, then these correspond to ascent speed measurement errors of 0.14 m s^{-1} and 2.8 m s^{-1}, respectively. In the latter case, the measurement error is of the same order as the

[3]Most measurements were obtained between about 9 and 14 km [*Nastrom and Gage*, 1985].
[4]Equation (7.3) is also presented by *Sidi et al.* [1988].

ascent speed fluctuation amplitudes near 25 km. However, *Shutts et al.* [1994] considered radiosonde measurements at lower altitudes while *Mobbs and Rees* [1989] were interested in wave motions in the lower troposphere.

If the pressure measurements are assumed to be contaminated by white noise, then the ascent speed estimates are contaminated by violet noise which has variance that grows with altitude [*Sidi et al.,* 1988]. This follows from the Fourier transform derivative theorem since ascent speed is obtained by differentiating radiosonde altitude with respect to time. Given that the gravity wave vertical velocity spectrum is red noise for $m > m_*$, where $2\pi/m_* \approx 2.5$ km in the lower stratosphere, then it may be possible to separate the noise and dominant gravity wave components by judicious smoothing of ascent speed data, even at heights near 25 km. However, it is necessary to assume that the vertical velocity fluctuations of the atmosphere are equivalent to the fluctuations of radiosonde ascent speed. Strictly, this should be verified experimentally.

If w is the vertical velocity of the atmosphere then, from *Sidi et al.* [1988],

$$w = w_a + w_b \tag{7.4}$$

where w_a is the vertical velocity of the atmosphere relative to the radiosonde and w_b is the vertical velocity of the radiosonde relative to the ground or the ascent speed. Thus w' can only be inferred from conventional radiosonde soundings if w_a is either constant or slowly varying with altitude. Experimental evidence that suggests this is the case is presented by *Reid* [1972] who estimated w_a using crude anemometers mounted on the outside of radiosondes. One profile was presented which showed w_a to be slowly varying with altitude and to possess irregularities of considerably smaller amplitude than the fluctuations of w_b. More recently, *Sidi et al.* [1988] measured w_a using a two-axis ionic anemometer although they did not present profiles of such measurements. Both *Reid* [1972] and *Sidi et al.* [1988] analyzed estimates of w, rather than of w_b.

Although *Shutts et al.* [1988, 1994] analyzed measurements of w_b in their successful case studies of exceptional mountain wave events, it is not clear from the literature that w_b can be used to extract climatological information about the gravity wave field, especially in the lower stratosphere[5]. It seems likely that only large-amplitude, and probably atypical, mountain waves can be measured in this way. Consequently, no attempt will be made to estimate momentum flux directly using ascent speed fluctuations in this chapter. Instead, the

[5]Indeed, *Low* [1996] has suggested that the observed ascent speed variations might be accounted for by plausible variations of the drag force acting upon the sonde.

possibility that vertical fluxes of zonal and meridional momentum might be estimated from simultaneous radiosonde measurements of temperature and horizontal wind velocity will be explored. These measurements have been demonstrated to provide valuable climatological information about gravity waves in earlier chapters, especially in the lower stratosphere.

The gravity wave spectral formulation proposed by *Fritts and VanZandt* [1993] suggests that the vertical fluxes of zonal and meridional momentum are functions of total wave energy density, E_0, and some measure of wave field anisotropy. In chapter 4, the total energy density of gravity waves was estimated, while in chapters 5 and 6, qualitative pictures of the degree of wave field anisotropy in the lower stratosphere over Macquarie Island and the Cocos Islands were presented. Consequently, it is plausible that gravity wave momentum fluxes may be estimated at these sites. A technique is discussed in the following section which allows momentum fluxes to be estimated from radiosonde data.

7.2 Theoretical Development

The theory presented in this section is also described by *Eckermann et al.* [1996]. A technique is discussed whereby the vertical fluxes of zonal and meridional momentum may be estimated using simultaneous measurements of temperature and horizontal wind velocity. This technique makes use of the gravity wave spectral formulation due to *Fritts and VanZandt* [1993].

Under conventional Liouville-Green approximations, the vertical fluxes of zonal and meridional momentum (per unit mass) due to a monochromatic gravity wave are defined by $\overline{u'w'}\delta_-$ and $\overline{v'w'}\delta_-$, respectively, where $\delta_- = (1 - f^2/\omega^2)$ [e.g., *Fritts and Vincent*, 1987]. This follows from the more general Eliassen-Palm flux which is derived elsewhere [e.g., *Andrews and McIntyre*, 1976]. The zonal and meridional mean flow accelerations ($\overline{u}_t$ and $\overline{v}_t$, respectively) caused by the vertical fluxes of zonal and meridional momentum due to a monochromatic gravity wave are given by

$$\overline{u}_t = -\frac{1}{\rho_0}\frac{d}{dz}\left(\rho_0\overline{u'w'}\delta_-\right) \tag{7.5}$$

$$\overline{v}_t = -\frac{1}{\rho_0}\frac{d}{dz}\left(\rho_0\overline{v'w'}\delta_-\right) \tag{7.6}$$

where the subscript t is a time derivative and ρ_0 is basic state density[6] [e.g., *Fritts and Vincent*, 1987]. Note that the vertical flux of zonal momentum (momentum transfer per

[6]This may be determined from radiosonde pressure and temperature measurements using the ideal gas equation.

unit area per unit time) is typically defined as $\rho_0 \overline{u'w'}\delta_-$. However, in this chapter, the terms $\overline{u'w'}\delta_-$ and $\overline{v'w'}\delta_-$ will be referred to, for convenience, as momentum fluxes per unit mass, following *Fritts and VanZandt* [1993].

Since measurements of w' are not considered here, for the reasons outlined in section 7.1, it is not possible to estimate $\overline{u'w'}\delta_-$ and $\overline{v'w'}\delta_-$ directly from observed wind velocity fluctuation profiles. However, gravity wave fluctuations of vertical velocity are related to those of normalized temperature according to (1.10). Therefore, for a monochromatic wave,

$$\overline{u'w'}\delta_- = \frac{g\omega}{N^2}\,\overline{u'\hat{T}'_{+90}}\,\delta_- \tag{7.7}$$

where $\hat{T}'_{+90} = i\hat{T}'$ and may be estimated from observations of normalized temperature fluctuations by the application of a negative Hilbert transform [*Eckermann et al.,* 1996]. Similarly, $\overline{v'w'}\delta_-$ is given by (7.7) but with v' substituted for u'. The discussions presented hereinafter will concentrate upon the vertical flux of zonal momentum since analogous arguments are equally valid for the vertical flux of meridional momentum.

Equation (7.7) indicates that, for a monochromatic gravity wave, $\overline{u'w'}\delta_-$ is a function of intrinsic frequency and the amplitudes of u' and $\hat{T}'$. However, the intrinsic frequency of gravity waves cannot be estimated directly from radiosonde measurements since successive soundings are typically too widely spaced in time[7]. Furthermore, monochromatic gravity wave signals are very rarely observed in radiosonde profiles of temperature and horizontal wind velocity and a superposition of many waves exists in general. Consequently, (7.7) must be extended to accommodate a spectrum of gravity waves while some knowledge of the intrinsic frequency distribution of this spectrum must be assumed.

In this chapter, the semi-empirical gravity wave spectral formulation proposed by *Fritts and VanZandt* [1993] is assumed to be valid. Thus the three-dimensional spectrum of gravity wave energy is assumed to be upward propagating and separable in vertical wavenumber, m, intrinsic frequency, ω, and azimuthal direction of propagation, ϕ, as described by *Fritts and VanZandt* [1993] and as reported in chapter 2. Some important polarization equations, which follow from these assumptions and the Boussinesq approximation, are given below

$$E_{u'}(\mu,\omega,\phi) = E_0 A(\mu)B(\omega)\Phi(\phi)\left[\cos^2\phi + \frac{f^2}{\omega^2}\sin^2\phi\right]\gamma(\omega) \tag{7.8}$$

$$E_{w'}(\mu,\omega,\phi) = \frac{\omega^2}{N^2}\,E_0 A(\mu)B(\omega)\Phi(\phi)\delta_-(\omega) \tag{7.9}$$

$$E_{\hat{T}'}(\mu,\omega,\phi) = \frac{N^2}{g^2}\,E_0 A(\mu)B(\omega)\Phi(\phi)\delta_-(\omega) \tag{7.10}$$

[7] Even if this was not the case, the wave frequency would be measured in the ground-based reference frame.

where $\mu = m/m_*$ and the other terms are defined in chapter 2. Note that (7.8) and (7.9) are equivalent to equations (4) and (7) of *Fritts and VanZandt* [1993] while (7.10) follows from their equation (8), as was discussed earlier. Note also that $B(\omega) \propto \omega^{-p}$, where p is anticipated to be of the order of 5/3, and so a continuous red-noise-like frequency distribution of gravity waves is assumed.

Following *Fritts and VanZandt* [1993] and *Eckermann et al.* [1996], the spectral dependence of $\overline{u'\hat{T}'_{+90}}$ is now determined from (7.8) and (7.10). For a given Fourier component, this covariance depends upon the fluctuation amplitudes $(E_{u'})^{1/2}$ and $(E_{\hat{T}'})^{1/2}$ and their phase relationship which is not defined by the spectral formulation. However, $u'_{||}$ and $\hat{T}'_{+90}$ are in phase for monochromatic gravity waves where $u'_{||}$ is the horizontal wind velocity fluctuation in the direction ϕ. Hence, the covariance of u' and $\hat{T}'_{+90}$, for a given Fourier component, is equal to the covariance of $u'_{||}$ and $\hat{T}'_{+90}$ multiplied by $\cos\phi$. It therefore follows that the covariance spectrum is given by,

$$E_{u'\hat{T}'_{+90}}(\mu,\omega,\phi) = \frac{N}{g}\, E_0 A(\mu) B(\omega) \Phi(\phi) \cos\phi \left(\delta_-(\omega)\gamma(\omega)\right)^{1/2} \tag{7.11}$$

where $E_{u'\hat{T}'}$ is power spectral density. The total covariance is obtained by integration such that,

$$\begin{aligned}
\overline{u'\hat{T}'_{+90}} &= \int_0^\infty \int_f^N \int_0^{2\pi} \frac{N}{g} E_0 A(\mu) B(\omega) \Phi(\phi) \cos\phi \left(\delta_-(\omega)\gamma(\omega)\right)^{1/2} d\phi\, d\omega\, d\mu \\
&= \frac{E_0 b_x N}{g} \int_f^N B_0 \omega^{-p} \left(\delta_-(\omega)\gamma(\omega)\right)^{1/2} d\omega \\
&= \frac{E_0 b_x N}{g}\, D_{u'\hat{T}'_{+90}}(p,f,N)
\end{aligned} \tag{7.12}$$

where $b_x = \int_0^{2\pi} \Phi(\phi)\cos\phi\, d\phi$ and is one of the anisotropy parameters defined by *Fritts and VanZandt* [1993]. This covariance is now related to the net vertical flux of zonal momentum per unit mass.

The spectral dependence of $\overline{u'w'\delta_-}$ is given by

$$E_{u'w'\delta_-}(\mu,\omega,\phi) = \frac{\omega}{N}\, E_0 A(\mu) B(\omega) \Phi(\phi) \cos\phi \delta_-^{3/2}(\omega)\gamma^{1/2}(\omega) \tag{7.13}$$

where $E_{u'w'\delta_-}$ is power spectral density[8]. Thus the net vertical flux of zonal momentum (per unit mass), which is obtained by integrating over all waves in the spectrum, is

$$\overline{u'w'\delta_-} = \int_0^\infty \int_f^N \int_0^{2\pi} \frac{\omega}{N} E_0 A(\mu) B(\omega) \Phi(\phi) \cos\phi \delta_-^{3/2}(\omega)\gamma^{1/2}(\omega)\, d\phi\, d\omega\, d\mu$$

[8] Note that (7.13) differs from equation (10) of *Fritts and VanZandt* [1993] due to the fact that an additional $\delta_-(\omega)$ term is included here while their $\delta_+(\omega)$ term is removed since $\overline{u'_\perp w'}$ is taken to be zero [*Eckermann et al.*, 1996].

$$= \frac{E_0 b_x}{N} \int_f^N B_0 \omega^{1-p} \delta_-^{3/2}(\omega) \gamma^{1/2}(\omega)\, d\omega$$
$$= \frac{E_0 b_x}{N} D_{u'w'\delta_-}(p, f, N) \tag{7.14}$$

where $D_{u'w'\delta_-}$ differs from $D_{u'\hat{T}'_{+90}}$ [*Eckermann et al.*, 1996]. Combining (7.12) and (7.14) yields

$$\overline{u'w'\delta_-} = \frac{g}{N^2} \left[\frac{D_{u'w'\delta_-}(p, f, N)}{D_{u'\hat{T}'_{+90}}(p, f, N)} \right] \overline{u'\hat{T}'_{+90}} \tag{7.15}$$

which relates $\overline{u'w'\delta_-}$ to $\overline{u'\hat{T}'_{+90}}$ without any need to determine the anisotropy parameter b_x. Hence $\overline{u'w'\delta_-}$ can be calculated from radiosonde measurements of horizontal wind velocity and temperature, provided that certain assumptions regarding the wave field are invoked. Note that (7.15) is the spectral analogue of (7.7) and so the ratio of $D_{u'w'\delta_-}$ to $D_{u'\hat{T}'_{+90}}$ is reasonably interpreted as a characteristic intrinsic frequency, $\overline{\omega}$, of the gravity wave field [*Eckermann et al.*, 1996].

The key term which is to be determined experimentally is the covariance of zonal wind velocity fluctuations and Hilbert-transformed normalized temperature fluctuations. This is proportional to the vertical flux of zonal momentum (per unit mass) where the constant of proportionality depends upon the intrinsic frequency distribution of gravity waves. By analogy, the vertical flux of meridional momentum is proportional to the covariance of meridional wind velocity fluctuations and Hilbert-transformed normalized temperature fluctuations where the constant of proportionality is the same as that given in (7.15). Thus $\overline{v'\hat{T}'_{+90}}$ should also be determined experimentally.

The characteristic intrinsic frequency, $\overline{\omega}$, is a function of p, f and N and can be calculated numerically. At any given site, f is known while N can be determined from conventional radiosonde measurements. The value of p most often cited in the literature is 5/3, although this might just as easily be 2. Indeed, the ratios of horizontal kinetic and potential energy in the lower stratosphere over Macquarie Island suggest that p may be even larger. Given the uncertainty regarding the correct estimate of p, the dependence of $\overline{\omega}$ on p must be carefully examined.

Figure 7.1 illustrates $\overline{\omega}$ as a function of p for $1.5 < p < 3.0$ with f and N fixed. The values of f and N were chosen to be appropriate to the troposphere and lower stratosphere over Macquarie Island and the Cocos Islands. At Macquarie Island, $f = 1.2 \times 10^{-4}$ rad s^{-1} while representative values of $N = 0.012$ rad s^{-1} and $N = 0.021$ rad s^{-1} were chosen for the troposphere and lower stratosphere, respectively. Similarly, at the Cocos Islands,

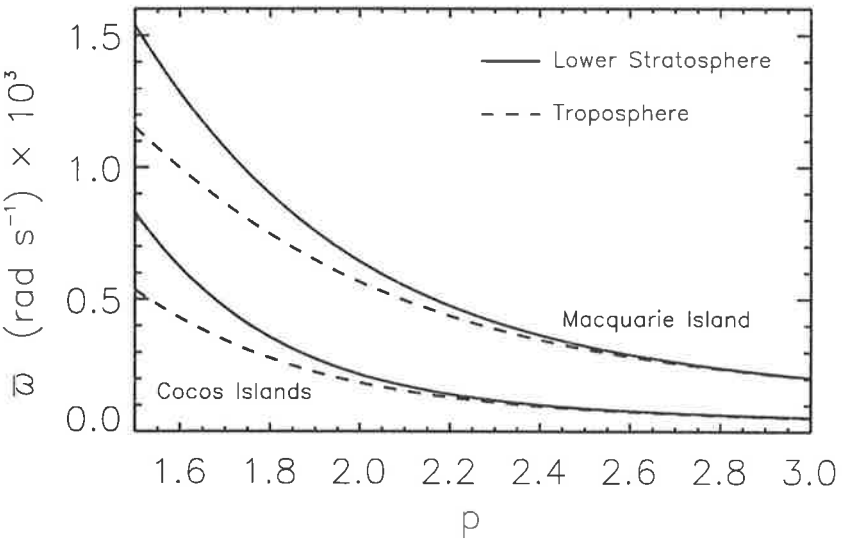

Figure 7.1: The characteristic intrinsic frequency, $\overline{\omega}$, as a function of spectral index, p, for fixed f and N which are appropriate to Macquarie Island and the Cocos Islands [after *Eckermann et al.*, 1996]. See text for further details.

$f = 3.0 \times 10^{-5}$ rad s^{-1} while representative values of $N = 0.01$ rad s^{-1} and $N = 0.024$ rad s^{-1} were chosen. Notice that $\overline{\omega}$ is always larger when typical values of f and N from Macquarie Island are assumed since f is considerably larger here than at the Cocos Islands.

It is evident from Figure 7.1 that $\overline{\omega}$ is strongly dependent on p in both the troposphere and lower stratosphere. Therefore, some uncertainty is introduced into momentum flux estimates from (7.15) due to the fact that the intrinsic frequency distribution of gravity waves is unknown. Here p is assumed to be 5/3 despite the fact that the ratio of horizontal kinetic to potential energy can be significantly different from 5/3. This is reasonable as a first approximation based on evidence from the literature[9].

7.3 Momentum Flux Estimates

The technique for estimating gravity wave momentum fluxes using (7.15) is now tested on radiosonde data from Macquarie Island and the Cocos Islands. The aim is to investigate whether or not meaningful estimates of the vertical fluxes of zonal and meridional momentum can be obtained. The results presented must be regarded as a first approximation since additional information concerning the intrinsic frequency distribution of gravity waves over

[9] *Nastrom et al.* [1996] have proposed that there exists a sharp peak in the intrinsic frequency spectrum of gravity waves at $\omega = f$. This may explain why the observed frequency spectra have shallower slopes than those deduced from the observed ratios of horizontal kinetic and potential energy.

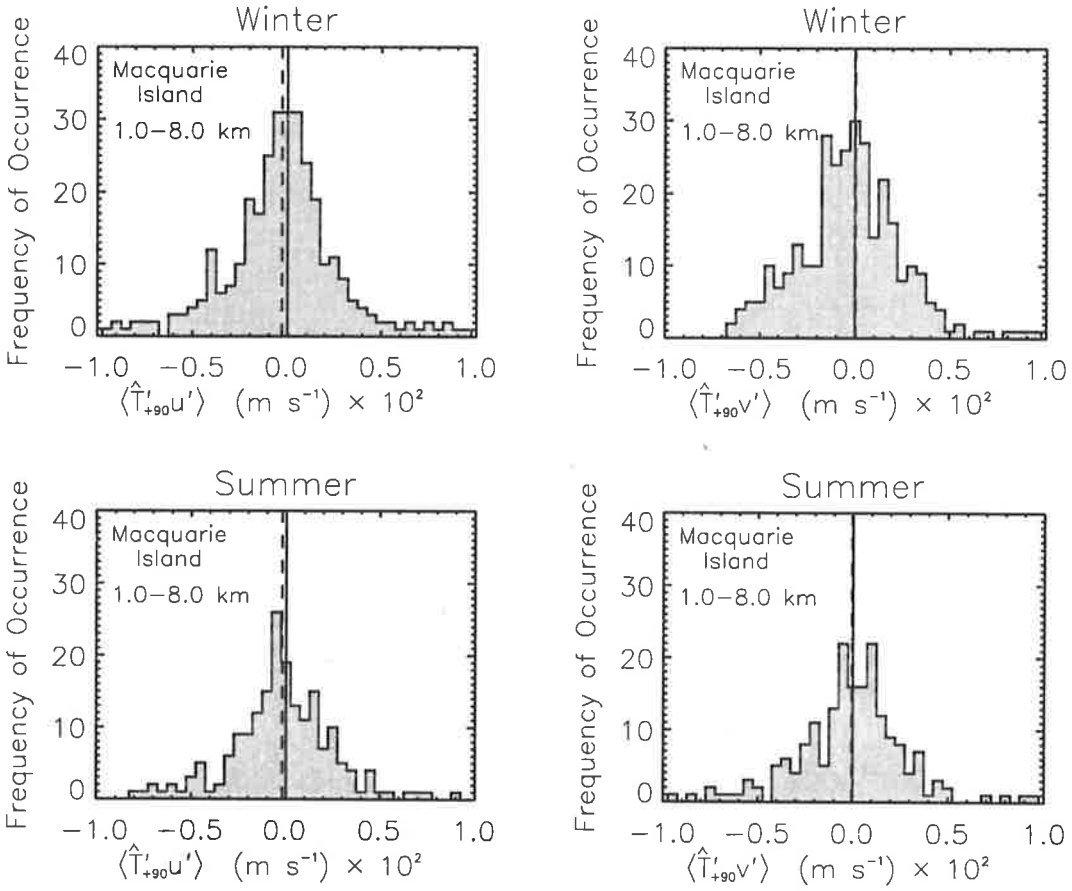

Figure 7.2: Distributions of the covariances of component horizontal wind velocity and Hilbert-transformed normalized temperature fluctuations (denoted by $\langle u'\hat{T}'_{+90} \rangle$ and $\langle v'\hat{T}'_{+90} \rangle$) determined in the troposphere (1.0–8.0 km) over Macquarie Island. The results from summer and winter months are considered separately and dashed lines describe the mean covariances. See text for further details.

Macquarie Island and the Cocos Islands is clearly needed.

7.3.1 Macquarie Island

Figures 7.2 and 7.3 illustrate the covariances of component horizontal wind velocity and Hilbert-transformed normalized temperature fluctuations determined from radiosonde measurements of the troposphere (1.0–8.0 km) and lower stratosphere (16.0–23.0 km), respectively, over Macquarie Island. These results were divided into winter and summer months as described in section 5.5 and the covariances determined from individual soundings are plotted in histogram form. Dashed lines indicate the mean values in each case.

First consider the tropospheric results presented in Figure 7.2. The seasonal-mean covariances determined during summer and winter are approximately zero in each case. This

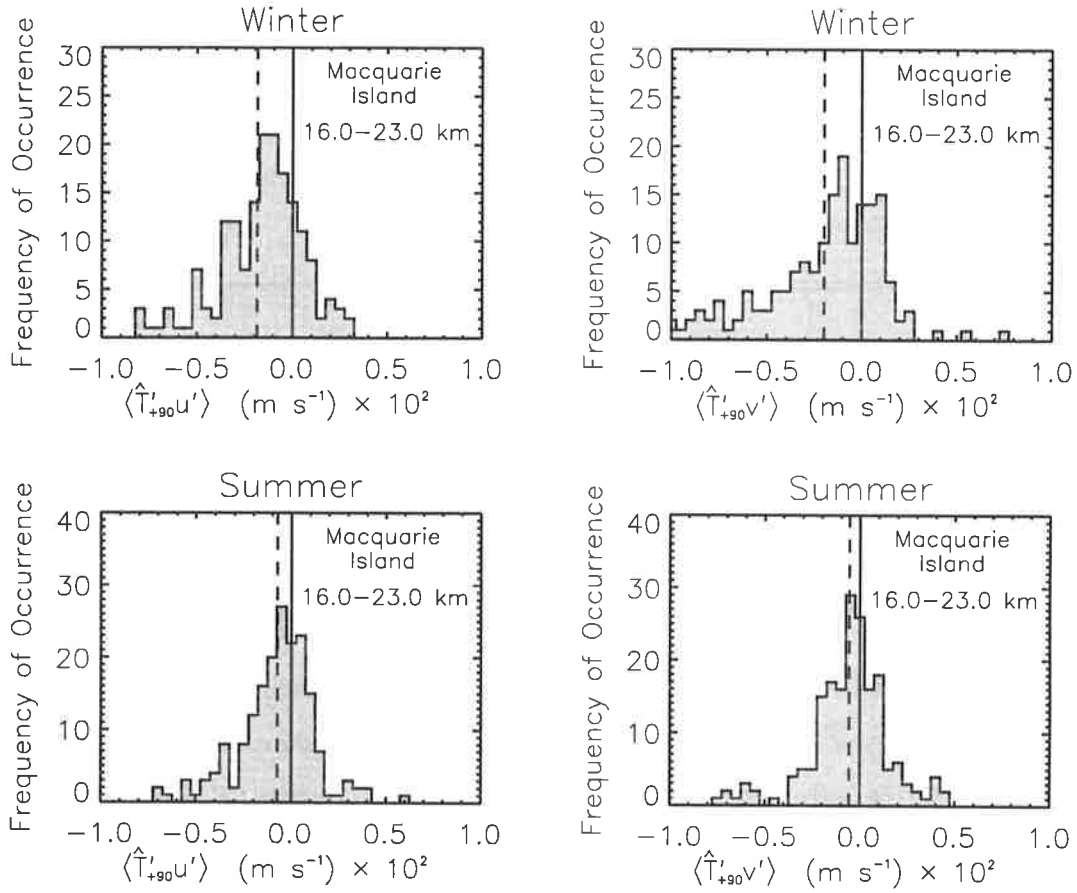

Figure 7.3: As in Figure 7.2, but for distributions of the covariances of component horizontal wind velocity and Hilbert-transformed normalized temperature fluctuations determined in the lower stratosphere (16.0–23.0 km) over Macquarie Island.

suggests, from (7.15), that the climatological-mean vertical fluxes of zonal and meridional momentum are zero in the troposphere over Macquarie Island. One possible explanation is that the wave field is horizontally isotropic. Although some observed variance may not be caused by gravity waves, the gravity wave component should nevertheless display correlation between u' and $\hat{T}'_{+90}$ or v' and $\hat{T}'_{+90}$ if the wave field is directional. However, it is also true that (7.15) cannot discriminate between, for example, the upward flux of eastward momentum and the downward flux of westward momentum without additional information. Consequently, the results displayed in Figure 7.2 are not inconsistent with a wave field in the troposphere that is dominated by trapped mountain waves generated by the prevailing eastward air flow over Macquarie Island[10].

Now consider the results determined in the lower stratosphere which are illustrated in

[10]Recall that lee-wave clouds are commonly found in satellite images of cloud structures over Macquarie Island [*Mitchell et al.*, 1990].

Altitude Range (km)	Season	$\overline{u'\hat{T}'_{+90}}$ (m s^{-1})	$\overline{v'\hat{T}'_{+90}}$ (m s^{-1})	$\overline{\omega}$ (rad s^{-1})	$\overline{u'w'\delta_-}$ (m^2 s^{-2})	$\overline{v'w'\delta_-}$ (m^2 s^{-2})
1.0–8.0	Winter	−0.00029	3.2×10^{-5}	9.1×10^{-4}	−0.018	0.002
	Summer	−0.00020	-4.6×10^{-5}	9.1×10^{-4}	−0.012	−0.003
16.0–23.0	Winter	−0.0019	−0.0020	1.1×10^{-3}	−0.046	−0.049
	Summer	−0.00072	−0.00055	1.1×10^{-3}	−0.018	−0.013

Table 7.1: Climatological-mean vertical fluxes of zonal and meridional momentum (per unit mass) determined in the troposphere (1.0–8.0 km) and lower stratosphere (16.0–23.0 km) over Macquarie Island. See text for further details.

Figure 7.3. These indicate non-zero and negative mean covariances during both summer and winter, but especially during winter. Thus the climatological-mean vertical fluxes of horizontal momentum, assuming upward energy propagation, are directed toward the south-west and, as expected, are consistent with the dominant propagation directions determined in chapter 5. Note that there exists considerable variability about the mean covariances in each case. Given the Gaussian nature of these distributions, it is likely that only climatological information regarding gravity wave momentum fluxes can be extracted[11].

Table 7.1 summarizes the mean covariance results presented in Figures 7.2 and 7.3. In addition, the net vertical fluxes of component horizontal momentum (per unit mass) are estimated from (7.15) where $\overline{\omega}$ was calculated using the mean Väisälä-Brunt frequency and $p = 5/3$. The standard deviations from the mean covariances are of the order of 3.5×10^{-3} m s^{-1} in the troposphere and 2.5×10^{-3} m s^{-1} in the lower stratosphere. These imply standard errors in the means of approximately 2×10^{-4} m s^{-1} in both cases given that more soundings were analyzed in the troposphere. Thus the mean covariances determined in the lower stratosphere are reasonably interpreted to be non-zero and negative during both summer and winter, but especially during winter. In contrast, the mean covariances determined in the troposphere cannot be resolved from zero with reasonable confidence.

The vertical fluxes of zonal and meridional momentum (per unit mass) are largest in the lower stratosphere during winter where they are each of the order of -0.05 m^2 s^{-2}. Thus

[11] A detailed error analysis is needed but is not attempted in this preliminary study.

the net vertical flux of horizontal momentum during winter is of the order of 0.07 m^2 s^{-2} and is directed toward the south-west assuming upward energy propagation. Note that this value is smaller than the momentum fluxes reported by *Fritts et al.* [1990] and *Nastrom and Fritts* [1992] which were determined at comparable altitudes. However, Macquarie Island is essentially an oceanic site since mountain waves generated by the island are likely to be trapped within the troposphere. In contrast, *Fritts et al.* [1990] and *Nastrom and Fritts* [1992] determined gravity wave momentum fluxes over mountainous regions of Japan and the United States, respectively. Therefore, the wave fields they observed may have been considerably different[12].

As was noted in the previous section, it is the altitude dependence of the vertical fluxes of component horizontal momentum that ultimately determines the influence of gravity waves upon the mean flow. The altitude dependence of gravity wave momentum fluxes determined from radiosonde measurements over Macquarie Island is now explored. This is achieved in the same manner as in Table 7.1 except that each momentum flux estimate is averaged over a 2-km altitude interval[13], rather than a 7-km altitude interval, and the results are combined to form momentum flux profiles. Furthermore, the previous long term averages are now relaxed to either 2 or 3-month averages so as to achieve a better understanding of the temporal variations.

Figure 7.4 illustrates mean profiles of the vertical fluxes of zonal and meridional momentum (per unit mass) in the troposphere and lower stratosphere over Macquarie Island. These were constructed from u', v' and $\hat{T}'_{+90}$ estimates which were obtained by fitting and subtracting third-order polynomials from the observed profiles of u, v and T followed by the application of a Hilbert transform to the normalized temperature fluctuations. Notice that each profile lacks data near the typical tropopause height of 10 km. These were not considered because it is difficult to remove the temperature discontinuity at the tropopause as part of the background temperature profile. When momentum flux estimates were determined from individual profiles near 10 km, they were found to have significantly larger standard deviations from the mean than those found at other heights. No doubt this was caused by the spurious temperature fluctuation that results when a fitted polynomial is subtracted from a step-like discontinuity in background temperature. Consequently, the momentum flux estimates that are presented have been divided into tropospheric (0.5–9.5 km) and lower

[12]There appears to be a significant difference between gravity wave variances observed in the lower atmosphere over land and sea [*Jasperson et al.*, 1990].

[13]This is of the same order as the characteristic vertical wavelength.

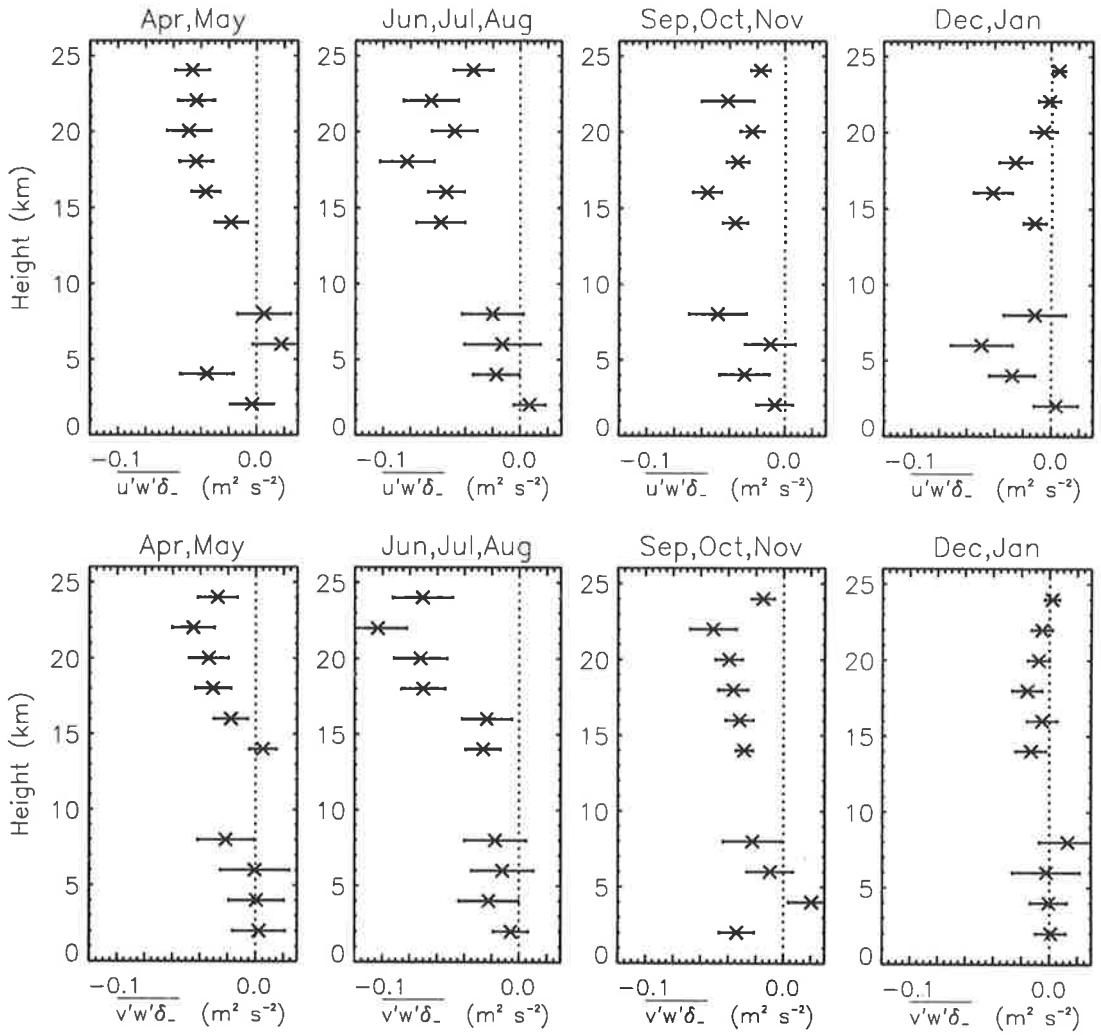

Figure 7.4: Mean profiles of the vertical fluxes of zonal and meridional momentum (per unit mass) determined over Macquarie Island. Error bars denote the standard errors of the means.

stratospheric (12.5–25.5 km) altitude segments. Third-order polynomials were fitted and then removed from the observed u, v and T profiles of each segment independently, before the momentum fluxes were estimated using (7.15).

The application of a Hilbert transform to normalized temperature data that are sampled at 50-m intervals over fixed altitude ranges must be carefully tested for unwanted side effects. For a continuous function, $f(z)$, the Hilbert transform is given by

$$F_{\mathrm{Hi}} = \frac{-1}{\pi z} * f(z) \tag{7.16}$$

where $*$ represents a convolution and where the divergence at $z = 0$ is allowed for by using the Cauchy principle value of the integral [*Bracewell,* 1986]. However, in practice, the Hilbert

transform is computed in the Fourier domain using an FFT algorithm and the discrete convolution theorem. This theorem is valid if the input signal, f_j, is periodic with period M such that it is completely defined by M values of f_j [*Press et al.*, 1988]. Thus the Hilbert transform of an observed data series is likely to include erroneous end points since f_j is not periodic in general.

Clearly, some end points of Hilbert-transformed normalized temperature data must be discarded if gravity wave momentum flux is to be determined accurately. Fortunately, the number of such points that are likely to be affected significantly is small since $1/\pi z$ quickly approaches zero. Thus each point in a Hilbert-transformed data series depends mostly upon its immediate neighbours in the raw data series. For the purposes of the analyses in this section, the first and last 500 m of data are discarded after the application of a Hilbert transform to a given normalized temperature data segment[14]. Consequently, the profiles of Figure 7.4 display momentum flux estimates between 1.0 and 9.0 km in the troposphere and between 13.0 and 25.0 km in the lower stratosphere[15].

It is evident from Figure 7.4 that the largest absolute values of the vertical fluxes of zonal and meridional momentum, for heights below 25 km over Macquarie Island, occur in the lower stratosphere during June, July and August. These fluxes are near zero in the troposphere but approach values of -0.1 m^2 s^{-2} between 15.0 and 25.0 km. In contrast, the vertical fluxes of zonal and meridional momentum determined during December and January are approximately zero at such heights while the momentum fluxes determined in the lower stratosphere during the equinoxes are intermediate to the June, July, August and December, January results. Tropospheric momentum fluxes, on the other hand, are mostly zero. However, there is possibly a small negative bias to the tropospheric vertical fluxes of zonal momentum as is also found in Figure 7.2. Nevertheless, this bias is typically on the limit of experimental uncertainty.

The error bars of Figure 7.4 are standard errors of the mean and so 95% confidence limits are given by approximately twice these error ranges. No errors were assumed to be associated with the determination of $\overline{\omega}$ which is a function of f, N and p. However, this quantity is clearly uncertain and the intrinsic frequency distribution of gravity waves is important in determining the absolute value of the net vertical flux of horizontal momentum. Nevertheless,

[14] A reasonable estimate of the number of data points that must be discarded may be obtained by comparing the Hilbert transform of a given raw data series with the Hilbert transform after zero padding [after *Press et al.*, 1988].

[15] Data that have been averaged within a 2-km altitude interval have been assigned to the midpoint of that interval.

Months	$\overline{u}_t$ (m s^{-1} day^{-1})	$\overline{v}_t$ (m s^{-1} day^{-1})
April,May	−0.64	−0.48
June,July,August	−0.81	−1.13
September,October,November	−0.42	−0.50
December,January	−0.10	−0.09

Table 7.2: Inferred accelerations of the mean flow in the lower stratosphere (17.0–25.0 km) over Macquarie Island.

if the covariances of (u, v) and $\hat{T}'_{+90}$ are found to be non-zero with good confidence then it is reasonable to conclude that the vertical flux of horizontal momentum is also non-zero, regardless of the intrinsic frequency distribution of gravity waves.

The zonal and meridional mean flow accelerations over Macquarie Island are estimated using (7.5) and (7.6) where ρ_0 is obtained from radiosonde measurements of pressure and temperature. As a first approximation, it is assumed that the vertical flux of horizontal momentum (per unit mass) is zero in the troposphere and approaches a constant value[16] between 17.0 and 25.0 km. Thus the inferred accelerations are also zero in the troposphere but approach values in the lower stratosphere that are given by

$$(\overline{u}_t,\, \overline{v}_t) = -\left(\overline{u'w'\delta_-},\, \overline{v'w'\delta_-}\right) \frac{1}{\rho_0}\frac{d\rho_0}{dz} \tag{7.17}$$

where $\overline{u'w'\delta_-}$ and $\overline{v'w'\delta_-}$ are height-averaged momentum fluxes. Table 7.2 presents the mean-flow accelerations that have been averaged between 17.0 and 25.0 km and inferred from (7.17). The largest occur during June, July and August and are of the order of -1 m s^{-1} day^{-1} for both the zonal and meridional components.

7.3.2 The Cocos Islands

Figures 7.5 and 7.6 illustrate the covariances of component wind velocity fluctuations and Hilbert-transformed normalized temperature fluctuations which have been determined from radiosonde measurements of the troposphere (7.0–14.0 km) and lower stratosphere (18.0–25.0 km), respectively, over the Cocos Islands. These results are divided into wet season and dry season months as described in section 6.5 and, as before, the covariances determined

[16] In other words, the derivatives of the vertical fluxes of zonal and meridional momentum (per unit mass), with respect to altitude, are assumed to be zero between 17.0 and 25.0 km.

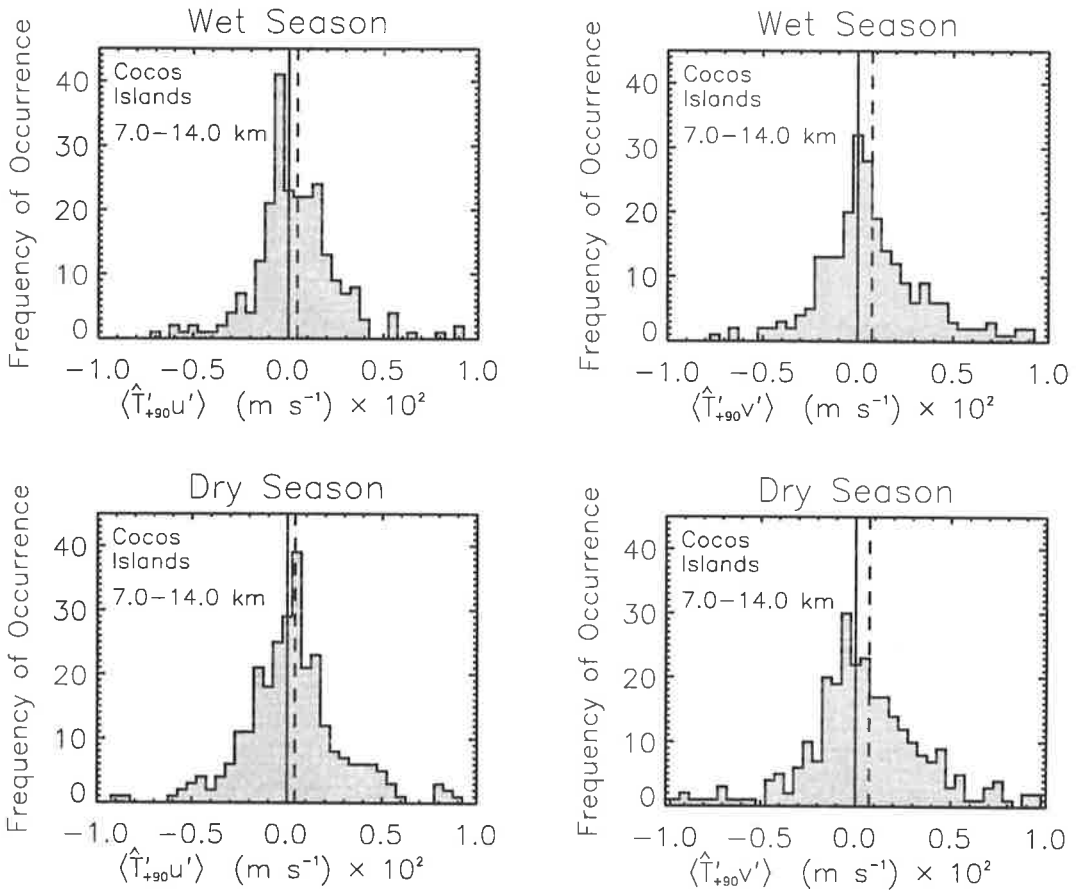

Figure 7.5: As in Figure 7.2, but for distributions of the covariances of component horizontal wind velocity and Hilbert-transformed normalized temperature fluctuations determined in the troposphere (7.0–14.0 km) over the Cocos Islands.

from individual soundings are plotted in histogram form. Dashed lines indicate the mean values in each case.

In the troposphere (Figure 7.5), the calculated covariances are almost evenly distributed about zero but have small positive biases which are independent of the season. This implies that the net vertical flux of horizontal momentum is small (if not zero) between 7.0 and 14.0 km over the Cocos Islands. However, the net direction is unclear since it is not known whether the majority of waves are upward or downward propagating. In fact, a significant portion of the observed variance in the troposphere may not be caused by untrapped gravity waves (see Figures 6.13 and 6.17) which further complicates the interpretation of Figure 7.5.

In the lower stratosphere (Figure 7.6), on the other hand, there is a significant and positive bias to the histogram of $\overline{u'\hat{T}'_{+90}}$ covariances during the wet season. There is also a smaller positive bias during the dry season while the $\overline{v'\hat{T}'_{+90}}$ covariances are evenly distributed

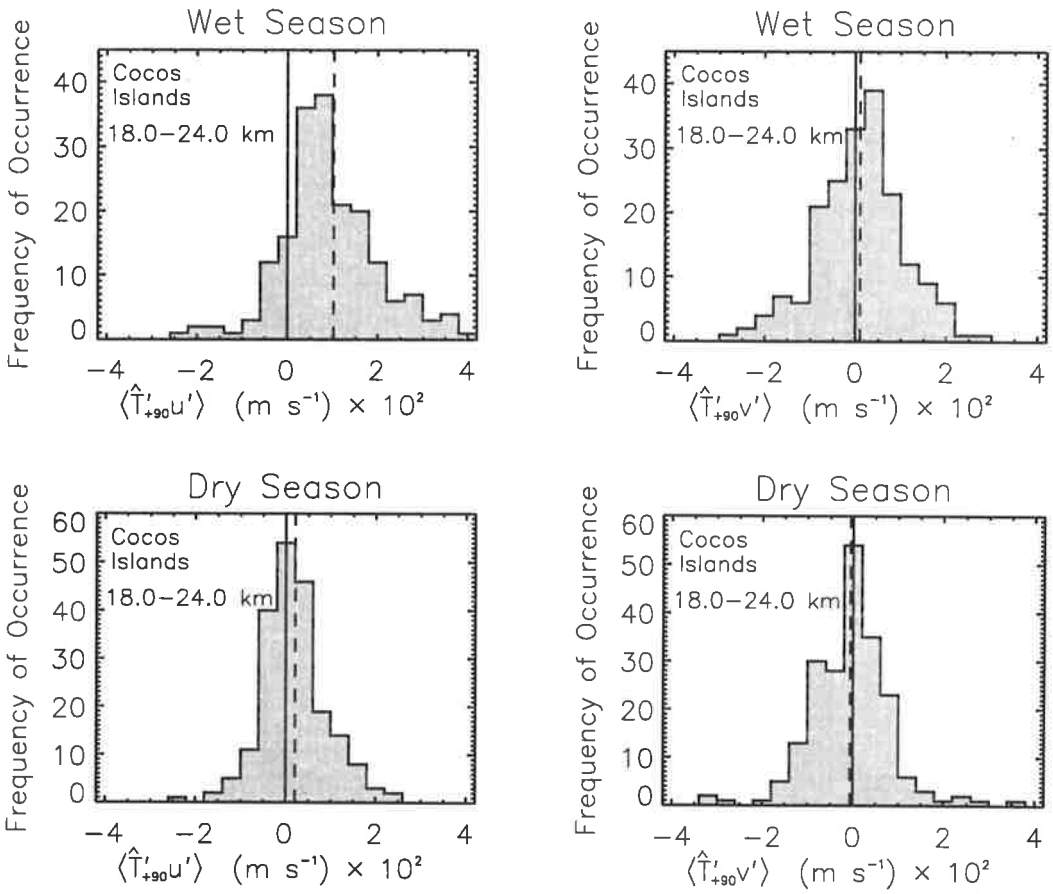

Figure 7.6: As in Figure 7.2, but for distributions of the covariances of component horizontal wind velocity and Hilbert-transformed normalized temperature fluctuations determined in the lower stratosphere (18.0–25.0 km) over the Cocos Islands.

about zero, to good approximation, during both seasons. Note that the range of values along the x-axis of Figure 7.6 is considerably larger than the range of values in Figure 7.5. This is because the horizontal wind and temperature variances are larger in the lower stratosphere and, as a consequence, so are their covariances. Figure 7.6 indicates that there is a net upward flux of eastward momentum during the wet season given that the majority of wave energy is upward propagating in the lower stratosphere. This result is in agreement with the dominant propagation directions displayed in Figure 6.25 as expected.

Table 7.3 summarizes the mean covariance results presented in Figures 7.5 and 7.6 and also presents the estimated vertical fluxes of horizontal momentum. The momentum fluxes were determined using (7.15) where $\overline{\omega}$ was calculated using the mean Väisälä-Brunt frequency and $p = 5/3$. The standard deviations from the mean covariances are of the order of 0.008 m s^{-1} in the troposphere and 0.01 m s^{-1} in the lower stratosphere. These imply

Altitude Range (km)	Season	$\overline{u'\hat{T}'_{+90}}$ (m s^{-1})	$\overline{v'\hat{T}'_{+90}}$ (m s^{-1})	$\overline{\omega}$ (rad s^{-1})	$\overline{u'w'\delta_-}$ (m^2 s^{-2})	$\overline{v'w'\delta_-}$ (m^2 s^{-2})
7.0–14.0	Wet	0.00047	0.00075	0.00036	0.02	0.03
	Dry	0.00040	0.00073	0.00035	0.02	0.03
18.0–25.0	Wet	0.010	0.0011	0.00052	0.08	0.009
	Dry	0.0021	−0.00060	0.00052	0.02	−0.005

Table 7.3: Climatological-mean vertical fluxes of zonal and meridional momentum (per unit mass) determined in the troposphere (7.0–14.0 km) and lower stratosphere (18.0–25.0 km) over the Cocos Islands. See text for further details.

Months	$\overline{u}_t$ (m s^{-1} day^{-1})	$\overline{v}_t$ (m s^{-1} day^{-1})
Sep,Oct,Nov (1992)	0.21	−0.09
Dec,Jan,Feb	1.10	0.14
Mar,Apr,May	0.61	0.05
Jun,Jul,Aug	0.01	−0.29
Sep,Oct,Nov (1993)	0.38	0.06

Table 7.4: Inferred accelerations of the mean flow in the lower stratosphere (18.0–24.0 km) over the Cocos Islands.

standard errors of the mean of approximately 2×10^{-4} m s^{-1} and 10^{-3} m s^{-1}, respectively. Hence the mean covariances in the troposphere are non-zero to reasonable confidence as are the mean covariances of u' and $\hat{T}'_{+90}$ within the lower stratosphere. In contrast, the mean covariances of v' and $\hat{T}'_{+90}$ within the lower stratosphere cannot be resolved from zero with reasonable confidence.

Vertical profiles of the vertical fluxes of zonal and meridional momentum over the Cocos Islands are illustrated in Figure 7.7. These were constructed in the same manner as in Figure 7.4 by considering data segments from the troposphere (3.0–13.0 km) and lower stratosphere (18.0–24.0 km) and by averaging momentum flux estimates within 2-km altitude intervals and over 3-month time intervals. The technique that was used does differ slightly from the one used to construct Figure 7.4 in that a second-order polynomial was subtracted

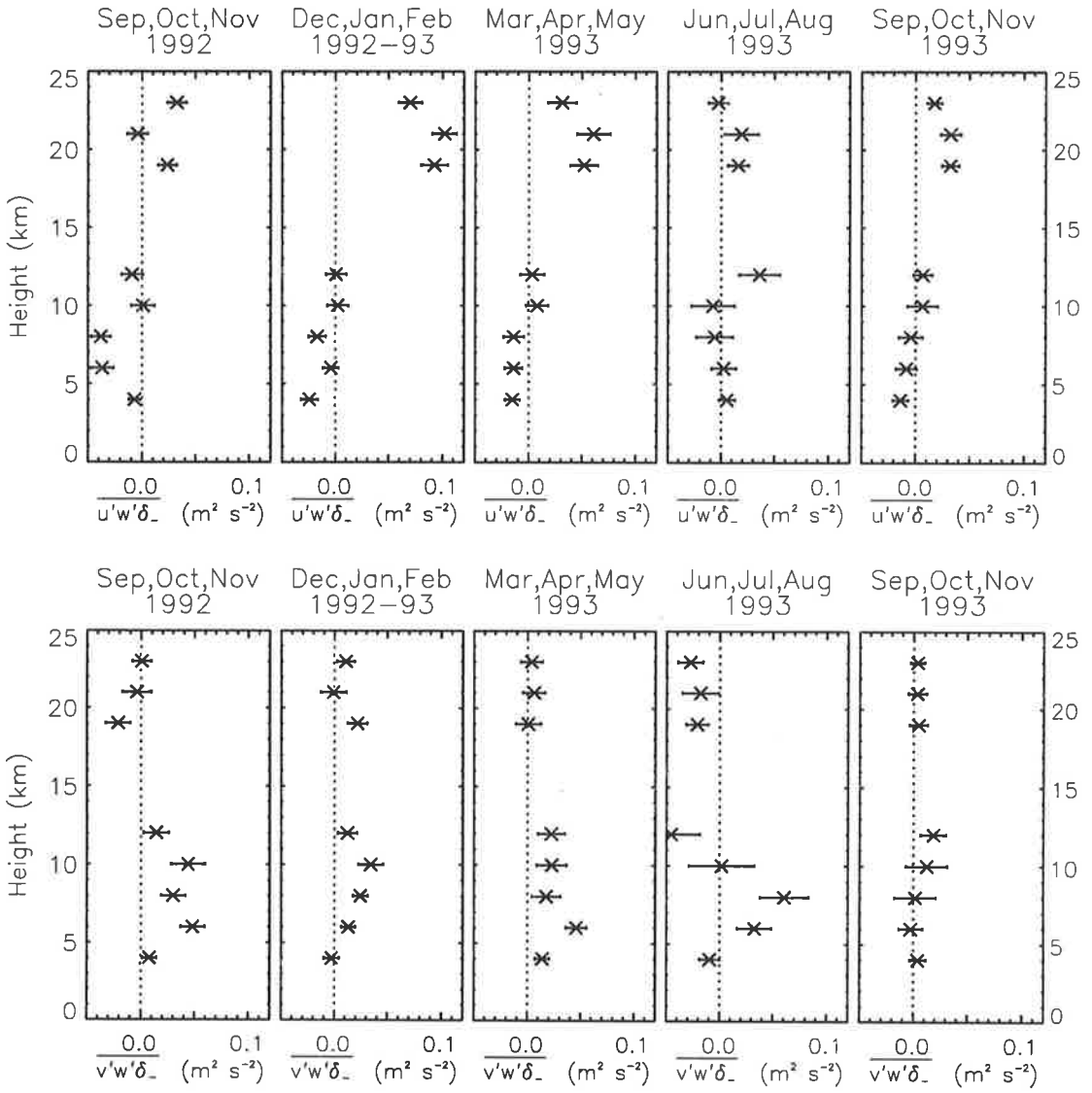

Figure 7.7: Mean profiles of the vertical fluxes of zonal and meridional momentum (per unit mass) determined over the Cocos Islands. Error bars denote the standard errors of the means.

from the lower-stratospheric data segments in order to obtain u', v' and $\hat{T}'_{+90}$ vertical profiles. This was judged to be appropriate because of the smaller altitude range of measurements in the lower stratosphere over the Cocos Islands.

The results presented in Figure 7.7 demonstrate that the vertical fluxes of zonal momentum are near zero within the troposphere. Similarly, the vertical fluxes of meridional momentum are also near zero although they do display a small positive bias in some instances. In the lower stratosphere, it is the vertical flux of zonal momentum that becomes significant during the wet season. This is as large as 0.1 m^2 s^{-2} during the 3-month period

of December, January and February but is near zero during June, July and August.

Table 7.4 presents the inferred mean flow accelerations within the lower stratosphere where the majority of wave energy is known to be upward propagating. These were determined using (7.17) and thus it is assumed, as a first approximation, that the observed momentum fluxes (per unit mass) are constant between 18.0 and 24.0 km. The largest inferred zonal acceleration is 1.1 m s^{-1} day^{-1} and occurs during the 3-month period of December, January and February. This is of the same order as the largest inferred zonal acceleration over Macquarie Island although of opposite sign.

7.4 Discussion

The results presented here indicate that plausible estimates of the net vertical fluxes of zonal and meridional momentum can be obtained from simultaneous radiosonde measurements of horizontal wind and temperature. At the very least, it is possible to determine whether or not the net vertical fluxes of component horizontal momentum are non-zero and, if they are non-zero, it is possible to determine their signs. This is true regardless of the intrinsic frequency distribution of gravity waves and, in all probability, regardless of the extent to which the wave field can be considered to be separable. Notable seasonal and geographic variations of net gravity wave momentum fluxes were found using radiosonde measurements from Macquarie Island and the Cocos Islands.

The magnitudes of the estimated momentum fluxes are dependent upon the intrinsic frequency distribution of gravity waves assuming that the spectrum of wave energy is separable. Thus there is some uncertainty in the magnitudes since the intrinsic frequency distribution is not known from the available data. Here it is assumed, as a first approximation following *Fritts and VanZandt* [1993], that the energy spectrum is separable and that the intrinsic frequency distribution is given by $B(\omega) \propto \omega^{-p}$ where $p = 5/3$. However, both assumptions have no firm theoretical basis, as was noted by *Fritts and VanZandt* [1993]. Yet an intrinsic frequency spectrum given by $B(\omega) \propto \omega^{-5/3}$ is commonly assumed in the literature based on experimental evidence. In contrast, the experimental evidence regarding intrinsic frequency and vertical wavenumber separability remains equivocal [*Fritts and Chou*, 1987; *Senft and Gardner*, 1991; *Fritts and Wang*, 1991; *Gardner et al.*, 1993b].

If the wave energy spectrum is separable and $B(\omega)$ is proportional to ω^{-p} then the ratio of horizontal kinetic to potential energy is approximately equal to p, assuming that p is

greater than about 1.1. The mean ratios of horizontal kinetic to potential energy in the lower stratosphere over Macquarie Island and the Cocos Islands are 3.1 and 2.2, respectively, and the monthly-mean ratios are consistently larger than 5/3. When these values are used to determine ϖ from Figure 7.1, the estimated momentum fluxes (and consequently the inferred accelerations) are reduced by factors of approximately 6 and 4, respectively. Note, however, that the horizontal kinetic to potential energy ratio determined in the lower stratosphere over Macquarie Island does vary with season, probably in response to the annual oscillation of the mean winds. During June, July and August, which are the months of largest (u, v) and $\hat{T}'_{+90}$ covariances, the mean ratio is approximately 2.5. This suggests that the momentum flux estimates could be a factor of 3 smaller than those determined by assuming $p = 5/3$.

An alternative approach might be to estimate ϖ from individual wind hodographs using (3.30). However, this approach has been avoided here because of the issues raised by *Eckermann and Hocking* [1989] and *Hines* [1989]. Nevertheless, *Cho* [1995] has demonstrated that reliable estimates of intrinsic frequency can be obtained from the autospectra and cross spectra of the component horizontal winds. Yet *Cho* [1995] analyzed radar data, obtained over a short campaign period, which had sufficient time and altitude resolution to resolve both the dominant vertical and temporal scales of gravity waves. It is uncertain if this technique is applicable to a large data set of radiosonde measurements for which successive soundings are too widely spaced in time to establish the time coherence of observed fluctuations. However, the technique may provide valuable information when applied to conventional radiosonde data and should be investigated further in any future studies. Note that *Eckermann* [1996] has demonstrated that the cross spectral technique due to *Cho* [1995] is related to the Stokes parameter technique for determining gravity wave characteristics. Note also that this cross spectral technique takes into account the transverse wind shear effect described by *Hines* [1989].

The determination of ϖ is clearly the weakest element of the momentum flux analyses that have been presented in this chapter. More information about the intrinsic frequency distribution of gravity waves is obviously needed. In particular, the use of $p = 5/3$ is inconsistent with the observed ratios of horizontal wind velocity and normalized temperature variances. This value was chosen as a first approximation and does result in estimates of the vertical fluxes of horizontal momentum that are of the same order as those found elsewhere at similar altitudes [e.g., *Fritts et al.*, 1990]. However, if the wave fields over Macquarie Island and the Cocos Islands are truly dominated by inertio-gravity waves, as the observed variance

ratios would suggest, then the momentum fluxes that are presented may well overestimate the true values.

Given the uncertainty of the momentum flux results, the inferred accelerations must be considered, at best, as order of magnitude estimates. Furthermore, an additional source of uncertainty arises for these estimates when the background wind shear is large, which is especially the case over Macquarie Island during winter. The windshifting effects described by *Eckermann* [1995] can result in amplitude variations of gravity waves with altitude that are not associated with wave dissipation. Also, the background wind dependence of vertical wavenumber may cause some wave energy to be removed from the band of wavenumbers that can be resolved by conventional radiosondes [*Eckermann et al.,* 1995]. These problems are discussed further by *Eckermann et al.* [1996].

Despite the obvious uncertainties, the analysis technique that has been investigated in this chapter is nevertheless profitable because it can be applied to a large and existing data set of radiosonde measurements. Even if order of magnitude estimates are the best that can be expected, the information obtained is of importance since it can be utilized by modellers who seek to parameterize the effects of gravity waves on the mean flow of the middle atmosphere. The anisotropy parameters used in the parameterization scheme due to *Fritts and VanZandt* [1993] may be estimated from (7.12) while momentum flux estimates in the lower stratosphere may provide useful initial conditions for other schemes. As more meteorological services begin archiving their radiosonde measurements at high vertical resolution [*Hamilton and Vincent,* 1995], and as measurement technology continues to improve, it may soon become possible to obtain useful information about gravity wave momentum flux, similar to the results presented here, on a global scale.

Chapter 8

Concluding Comments and Future Research

The results presented in this thesis demonstrate that high-vertical-resolution operational radiosonde soundings can provide valuable knowledge about atmospheric gravity waves. In the past, these waves have often been studied using either isolated radiosonde soundings or several soundings from an experimental campaign. The clear advantage of operational radiosondes is their ability to provide climatological information about the dynamics of the troposphere and lower stratosphere. However, until recently, operational radiosonde data were archived at poor vertical resolution and so were unsuitable for gravity wave analysis. This study is the first to have attempted gravity wave analyses of high-vertical-resolution radiosonde measurements from a network of stations in the southern hemisphere. The main results and conclusions are summarized at the ends of chapters 4, 5, 6 and 7.

The outlook for future research using operational radiosonde measurements, which are archived by various national meteorological services, is detailed by *Hamilton and Vincent* [1995]. Not only is our knowledge of gravity waves likely to benefit, but also our understanding of equatorially-trapped waves and the quasi-biennial oscillation. Indeed, the equatorial middle atmosphere is especially interesting because of the coexistence of trapped and untrapped waves and because of the complicated basic state dynamics. A recent study of ship-based radiosonde data by *Ogino et al.* [1995] has concluded, in accordance with the results presented here, that gravity wave energy in the lower stratosphere is largest near the equator. Their study also concluded that cumulonimbus convection is probably the most important source of gravity waves in the lower stratosphere at low latitudes. A similar understanding

is deduced from the results presented here, based on the correlation between gravity wave variance and mean rainfall at near-equatorial locations, although more conclusive evidence is strictly needed.

A new technique for estimating gravity wave momentum fluxes was tested in chapter 7. This technique yielded reasonable results using simultaneous radiosonde measurements of horizontal wind velocity and temperature. However, the technique did have weaknesses and may need to be refined if used in later studies. Gravity wave momentum fluxes were also estimated from simultaneous radiosonde measurements of horizontal wind velocity and temperature in a concurrent study by *Sato and Dunkerton* [1996]. Although they considered time series data and were interested mainly in equatorially-trapped waves, their (direct estimate) technique was essentially the same as that used here. This emphasizes the importance of considering simultaneous horizontal wind velocities and temperatures in the absence of direct and reliable estimates of the vertical velocity fluctuation.

The main source of error for the momentum flux analysis of chapter 7 results from the lack of detailed knowledge about the intrinsic frequency distribution of gravity waves which is of crucial importance. Indeed, it is difficult to reconcile the observed ratios of horizontal kinetic and potential energy in the lower stratosphere with the observed frequency spectra of past studies, even when Doppler shifting is taken into account. However, similar results from the lower stratosphere over Illinois, in the United States, are reported by *Nastrom et al.* [1996]. They argue that the observed ratios can be brought into agreement with theory if there exists an enhancement of gravity wave energy near the inertial frequency [*Nastrom et al.*, 1996]. Furthermore, they conclude that the proposed enhancement needs to be investigated experimentally in future studies. If correct, then this may justify the use of $p = 5/3$ in the momentum flux calculations, as a first approximation, since near-inertial waves would not contribute significantly to the observed covariances of horizontal wind velocity and Hilbert-transformed normalized temperature fluctuations. Thus further investigation of the intrinsic frequency distribution would also be of value in the context of the present study. *Nastrom et al.* [1996] note that such an investigation might involve the analysis of archived VHF radar measurements.

In addition to the above proposal and results, *Nastrom et al.* [1996] also presented evidence that suggests that the slopes and amplitudes of individual vertical wavenumber power spectra of horizontal wind velocity and normalized temperature, in both the troposphere and lower stratosphere, are correlated. They found that those spectra which happened to

have large amplitudes tended to have shallow slopes at high vertical wavenumbers. This is an interesting result since, as noted by *Nastrom et al.* [1996], it is inconsistent with the current theories of wave saturation. However, the relationship between wave amplitudes and the high-wavenumber slopes of individual spectra was not investigated in the present study. It seems likely that the same correlation would be found in the data considered here and clearly this possibility should be investigated further in any subsequent study.

The results presented throughout this thesis have addressed the problem of the lack of detailed climatological information about atmospheric gravity wave activity in the troposphere and lower stratosphere. Experimental estimates of the total wave energy density[1], the degree of wave field anisotropy and the vertical fluxes of horizontal momentum have been reported from the Australian sector of the southern hemisphere. These results, together with results from other recent studies of radiosonde data [e.g., *Whiteway and Duck*, 1996; *Nastrom et al.*, 1996], have contributed to a growing body of experimental knowledge. Following some important theoretical advances [e.g., *Fritts and VanZandt*, 1993; *Fritts and Lu*, 1993; *Hines*, 1996a,b], it is hoped that the broad research program, to which this thesis has contributed, may ultimately lead to the successful understanding and modelling of the effects of gravity waves upon the mean flow of the lower and middle atmospheres.

[1]The estimates of E_0 were obtained by assuming that $B(\omega) \propto \omega^{-5/3}$ which may not be correct at all (or even some) stations.

Appendix A

Vaisala RS80 Temperature Sensor Response Time

The temperature sensor response times that have been used in this thesis to obtain the corrected stratospheric power spectra of normalized temperature fluctuations have themselves been estimated from the results presented in two Vaisala test reports [*Turtiainen*, 1991a,b]. According to *Turtiainen* [1991b], the response time τ of a temperature sensor in flowing air is theoretically given by

$$\tau = C_1 + C_2/h \tag{A.1}$$

where h is the surface heat transfer coefficient and where C_1 and C_2 are constants that depend upon the sensor dimensions and materials. The surface heat transfer coefficient is a complicated function of sensor ventilation speed, air density, and air temperature which, for a cylindrical sensor, is given by

$$h = \frac{\mathrm{k}Nu}{D} \tag{A.2}$$

where

$$Nu = 0.184 + 0.324Re^{0.5} + 0.291Re^{x} \tag{A.3}$$

$$x = 0.247 + 0.0407Re^{0.168} \tag{A.4}$$

$$Re = \frac{V_0 D\rho}{\mu} \tag{A.5}$$

and where k is the thermal conductivity of air, Nu is the Nusselt number, D is the radius of the sensor[1], Re is the Reynolds number, V_0 is the ventilation speed, ρ is air density and μ

[1] *Turtiainen* [1991b] uses $D = 0.0006$ m but notes that the choice of this parameter is not critical.

is the dynamic viscosity of air [*Turtiainen*, 1991b]. The thermal conductivity and dynamic viscosity may be determined by using

$$\mathrm{k} = \frac{2.64638 \times 10^{-3}\, T^{3/2}}{T + 245.4 \times 10^{-12/T}} \tag{A.6}$$

and

$$\mu = \frac{1.458 \times 10^{-6}\, T^{3/2}}{T + 110.4} \tag{A.7}$$

where T is air temperature[2] [*Turtiainen*, 1991b]. Thus if C_1 and C_2 are known for a given type of sensor then τ can be computed theoretically at any height provided that T, ρ, and the sensor's ventilation speed are known.

The constants C_1 and C_2 were estimated for the Vaisala RS80–15 temperature sensor by *Turtiainen* [1991b]. This was achieved by experimentally determining the response time at ground level conditions for three different ventilation speeds. Thus τ was known for three values of h allowing C_1 and C_2 to be estimated by least squares curve fitting. The values were found to be $C_1 \approx 0$ and $C_2 = 782$. Note that the response time was experimentally determined by measuring the time taken for the sensor to reach 63.2% of a sudden step function increase of environmental temperature. Figure A.1 displays the height dependence of τ where (A.1) has been used and where h was determined using the mean temperature and pressure profiles observed at Adelaide during December 1991. Atmospheric density was calculated from the temperature and pressure measurements using the ideal gas equation and the sensor ventilation rate was taken to be equivalent to the mean balloon ascent velocity.

In the work by *Turtiainen* [1991a], temperature sensor response times were measured using a radiosonde in flight where the step function increase in environmental temperature was generated using a heating element attached to the sonde. The results, however, were consistently smaller than the corresponding theoretical values which were calculated using C_1 and C_2 given above. This leads to the conclusion of the report [*Turtiainen*, 1991a, p. 5] which states that "the response time of [the] RS80 temperature sensor in flight was found to be equal [to] or less than the theoretically computed values presented in the earlier reports." Thus it appears that (A.1) with $C_1 = 0$ and $C_2 = 782$ is overestimating the temperature sensor response time within the lower stratosphere given that all measurements by *Turtiainen* [1991a] were made at pressures that were less than or equal to 44 hPa.

As a result of the above conclusion, it seems more appropriate to find C_1 and C_2 for the lower stratosphere by fitting (A.1) to the 12 measurements of τ that were reported by

[2]Equations (A.1) to (A.5) were obtained from *Kerlin et al.* [1982] while (A.6) and (A.7) where reported from the *U.S. Standard Atmosphere* [1976].

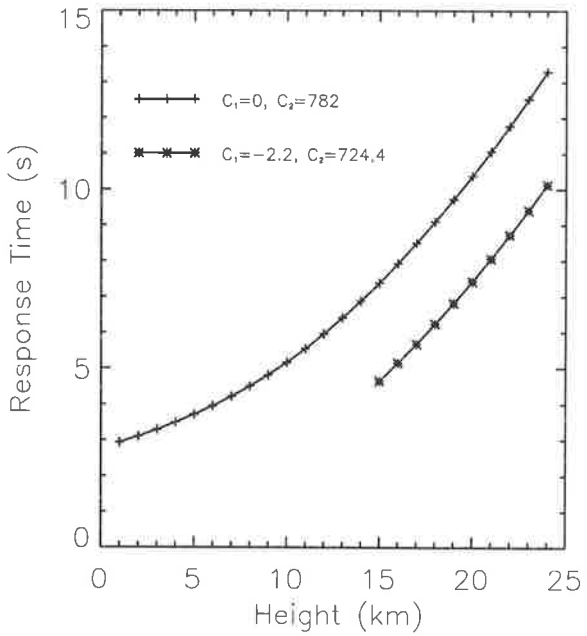

Figure A.1: The height dependence of the Vaisala RS80 temperature sensor's response time for different values of C_1 and C_2 (see text for more details). The response time was calculated using (A.1) where the surface heat transfer coefficient, a function of temperature and density, was determined using the mean temperature and pressure profiles observed at Adelaide during December 1991.

Turtiainen [1991a]. This was the approach taken here. The best fit parameters were found to be $C_1 = -2.2$ and $C_2 = 724.4$ and the height dependence of τ using these parameters has been plotted in Figure A.1 where h was determined, as before, from the mean pressure and temperature profiles observed at Adelaide during December 1991. Clearly, this new curve is not strictly valid near ground level since it underestimates the ground level measurements of τ. Nevertheless, it does provide a superior fit to those measurements of τ that have been made within the lower stratosphere.

The corrections to the observed power spectra of normalized temperature fluctuations in this thesis have been calculated using (3.6) where τ was found from (A.1) with $C_1 = -2.2$ and $C_2 = 724.4$. This leads to height-averaged response times that are of the order of 7 to 8 s within the 17 to 24 km altitude range and 1 to 2 s within the 2 to 9 km altitude range. The value of τ between 2 and 9 km is no doubt an underestimate of the true value within this height interval. However, this is not important since even when the parameters $C_1 = 0$ and $C_2 = 782$ are used, the response time is still sufficiently small that the correction for tropospheric power spectra is negligible at all but the very highest

wavenumbers. Consequently, all observed tropospheric vertical wavenumber power spectra have not been altered in any way.

The method that has been chosen in order to obtain values for the parameters C_1 and C_2 is not the only plausible procedure. Given the available information, however, it is believed to provide the best estimates of τ within the lower stratosphere. Nevertheless, the approach may result in nonnegligible errors for the response time estimates. These are difficult to quantify and will affect the high-wavenumber spectral slope, t, of corrected power spectra which, as a consequence, may be biased in some way. It is important to note, however, that the spectral parameters m_*, c_*, and E_0 will not be significantly affected by this problem. As a result, only estimates of t from stratospheric power spectra need to be treated with some caution.

Another possible source of error for corrected vertical wavenumber power spectra arises due to the assumption that τ is constant in obtaining (3.6). Figure A.1 indicates that τ is not constant within the height intervals of interest to this study. However, (3.6) is still valid to good approximation if height-averaged response times are used. To demonstrate this a normalized temperature fluctuation profile has been numerically simulated for altitudes between 17 and 24 km. This was obtained by summing a series of sinusoids with amplitudes that were determined from a standard gravity wave model and by applying the constraints imposed due to the slow response of the radiosonde's temperature sensor.

The fluctuation profile was simulated by first generating a model gravity wave power spectrum using (4.2) with $2\pi F_0 = 0.05$ m/cycle, $m_*/2\pi = 5.0 \times 10^{-4}$ cycles/m and $t = 3$. A series of 100 sinusoids was then calculated at wavenumbers $m_i = 2\pi \times 10^{-4} i$ where i is an integer between 1 and 100 and where each sinusoid was assigned a random phase φ. The amplitudes, $A_i(m_i)$, were determined from the model spectrum since these are given by the square root of twice the variance within the relevant wavenumber band about wavenumber m_i. The summation of individual sinusoids, sampled at 7-m altitude intervals between 16 and 24 km, gives the simulated environmental fluctuation profile. This technique follows the work of *Eckermann* [1990b].

The fluctuation profile measured by a radiosonde with temperature sensor response time τ is related to the environmental fluctuation profile according to (3.4) where T and T_s may be replaced by $\hat{T}'$ and $\hat{T}_s'$, respectively, assuming $\overline{T_s}(z)$ does not differ significantly from $\overline{T}(z)$ and assuming $\overline{T}(z)$ is approximately constant over the altitude range of interest. However, if τ is variable in height then (3.4) cannot be solved analytically. The simulated fluctuation

profile was thus obtained using the Runge-Kutta method where $\tau(z)$ was given by the curve of Figure A.1 defined by $C_1 = -2.2$ and $C_2 = 724.4$. The first kilometre of data was discarded in order to allow sufficient altitude for any transient effects to become negligible. Thus the final simulated profile comprised data that was sampled at 7-m intervals between 17 and 24 km.

The simulated fluctuation profile was spectrally analyzed using the Blackman-Tukey algorithm and was further modified using (3.6) where τ was given by the height-averaged response time between 17 and 24 km. Although not shown here, the resultant power spectrum was found to be in good agreement with the original model spectrum. This indicates that (3.6) is valid to good approximation over 7-km altitude intervals if τ is given by its height-averaged value.

Appendix B

Normalized Temperature Power Spectra

The mean vertical wavenumber power spectra of normalized temperature fluctuations that were not presented earlier are illustrated in this appendix. As before, solid lines represent stratospheric power spectra, dashed lines represent tropospheric power spectra and the dotted lines represent the theoretical saturation limits proposed by *Smith et al.* [1987]. The various spectra are plotted in both conventional logarithmic and area preserving forms while the 95% confidence limits are given by approximately 0.85 and 1.15 multiplied by the spectral amplitude at each vertical wavenumber. Stratospheric power spectra have been corrected for response time distortion as defined by (3.6) where the response time was estimated in the manner described in appendix A.

The height intervals used for power spectrum analysis are described in Table 4.2 where the height intervals used for Casey and Mawson were the same as those used for Davis. Data segments for which continuous measurements were unavailable throughout the entire height interval of interest or for which a tropopause was found within this interval were not considered for analysis. Spectra were calculated using 12 months of data from each station excluding Willis Island (10 months), Casey (23 months) and Mawson (23 months). For more details about the analysis techniques used[1], see the relevant discussions in chapters 3 and 4.

[1]The mean spectra from all stations, with the exceptions of Casey and Mawson, were obtained by averaging normalized individual spectra over 1-month time intervals. The 3-month average spectra were then obtained using a weighted arithmetic mean of the 1-month average spectra. However, the mean spectra from Casey and Mawson were obtained by averaging normalized individual spectra over the full 2 or 3-month time intervals (as was the case for the mean spectra from Macquarie Island and the Cocos Islands that were illustrated in chapters 5 and 6). Although this situation is not ideal, it is hardly likely to cause significant problems when comparing different spectra.

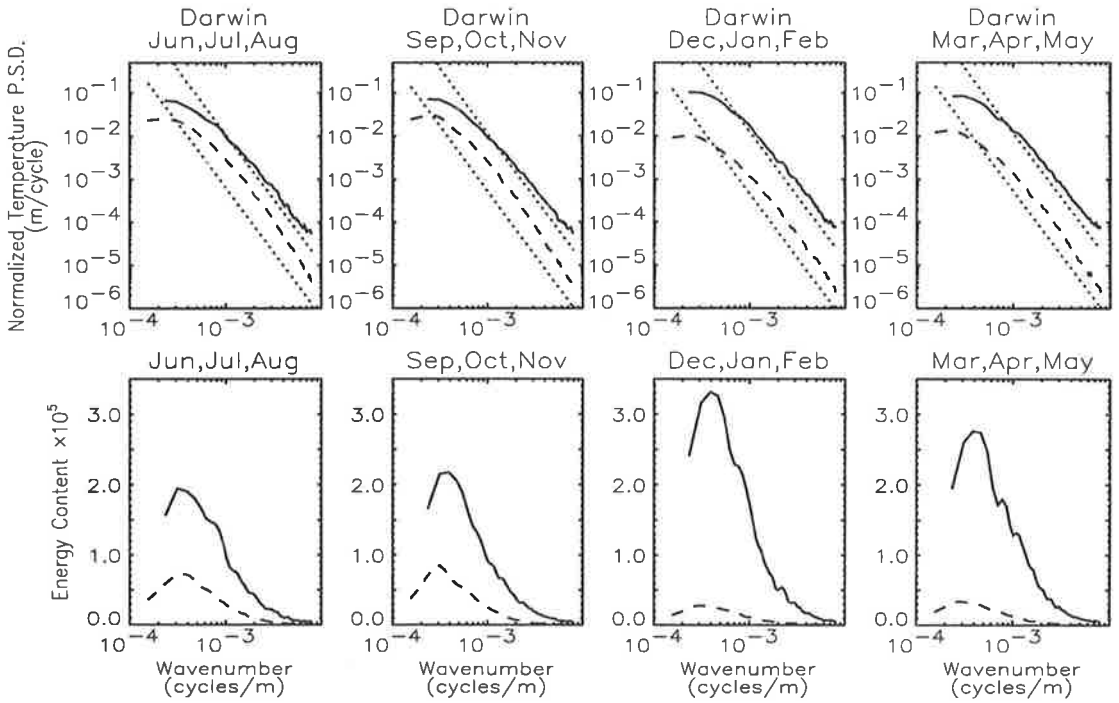

Figure B.1: Mean vertical wavenumber power spectra and area preserving spectra of normalized temperature fluctuations observed over Darwin (12°S, 131°E) between June 1991 and May 1992.

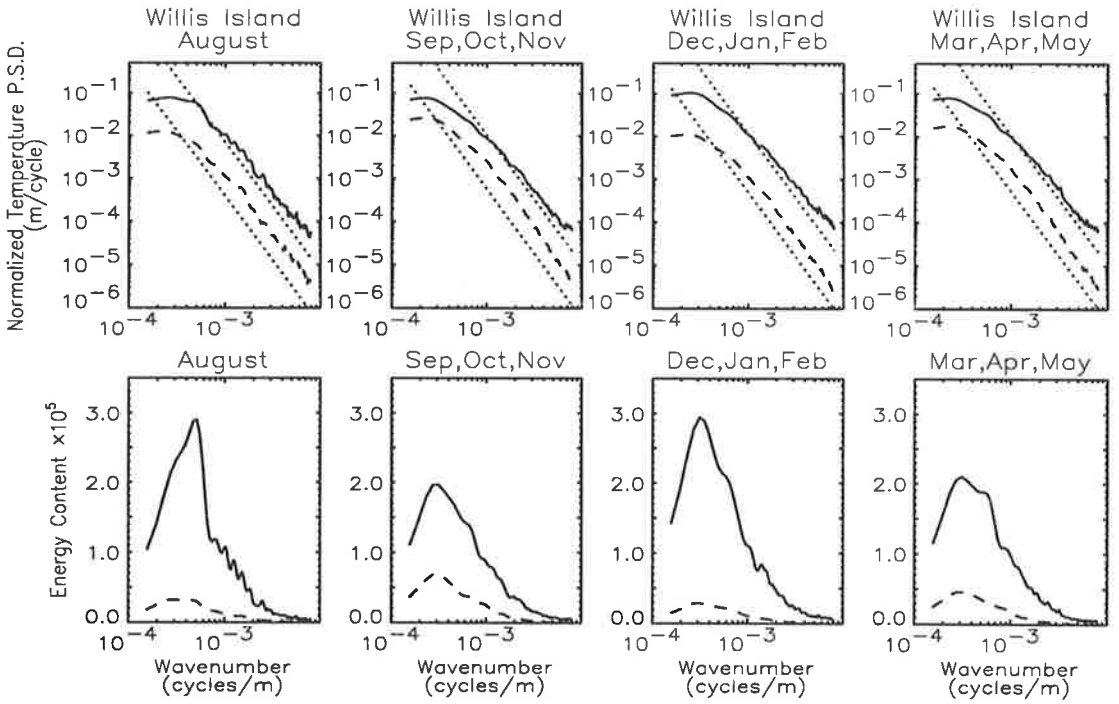

Figure B.2: Mean vertical wavenumber power spectra and area preserving spectra of normalized temperature fluctuations observed over Willis Island (16°S, 150°E) between August 1991 and May 1992.

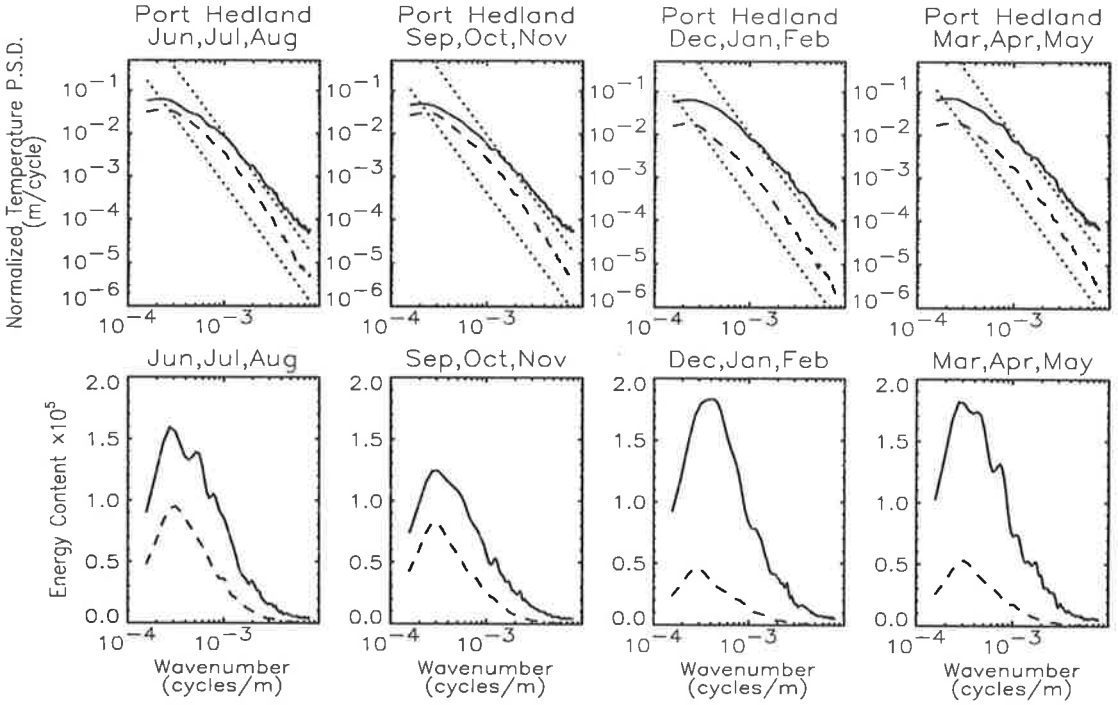

Figure B.3: Mean vertical wavenumber power spectra and area preserving spectra of normalized temperature fluctuations observed over Port Hedland (20°S, 118°E) between June 1991 and May 1992.

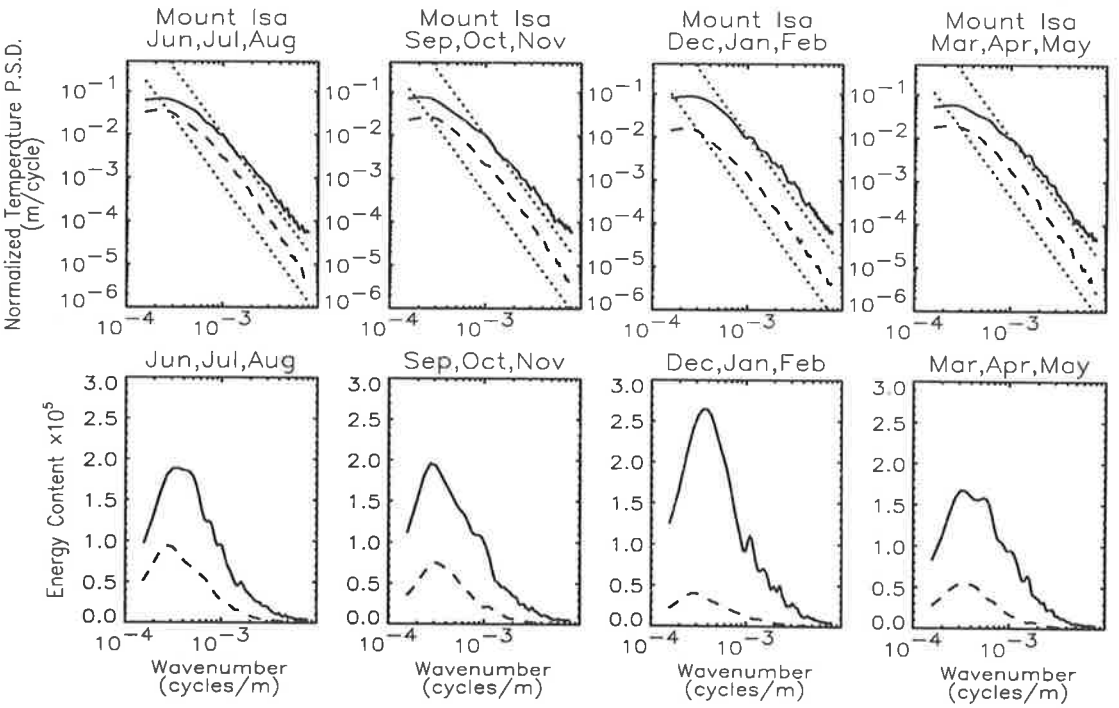

Figure B.4: Mean vertical wavenumber power spectra and area preserving spectra of normalized temperature fluctuations observed over Mount Isa (20°S, 139°E) between June 1991 and May 1992.

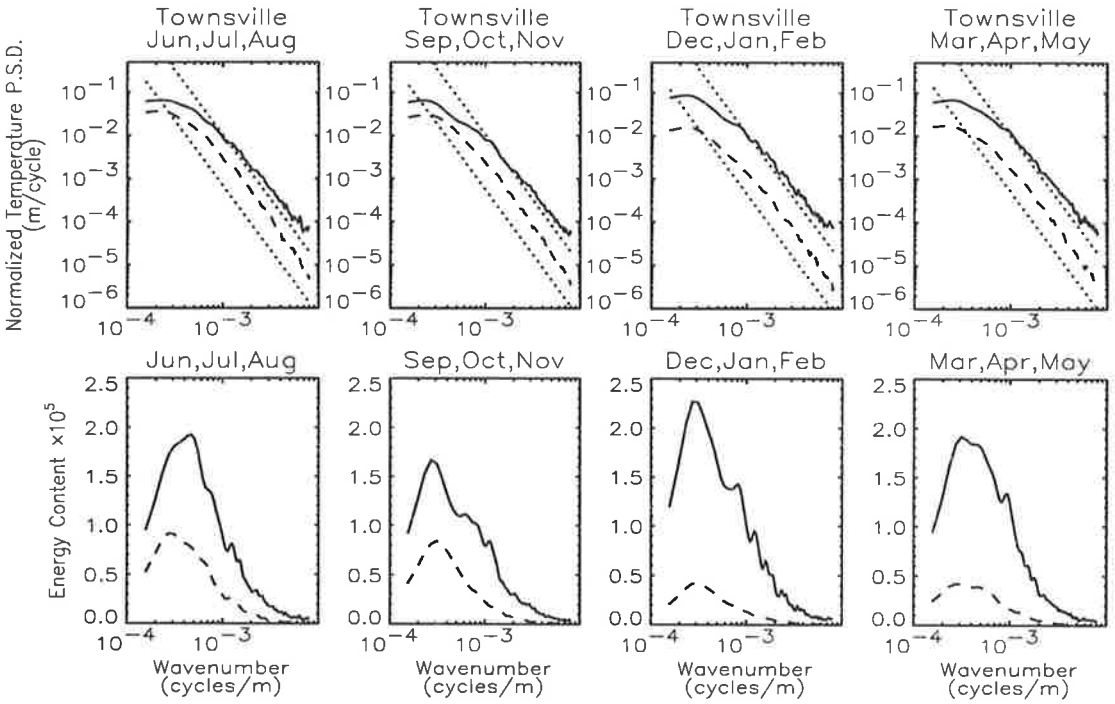

Figure B.5: Mean vertical wavenumber power spectra and area preserving spectra of normalized temperature fluctuations observed over Townsville (19°S, 147°E) between June 1991 and May 1992.

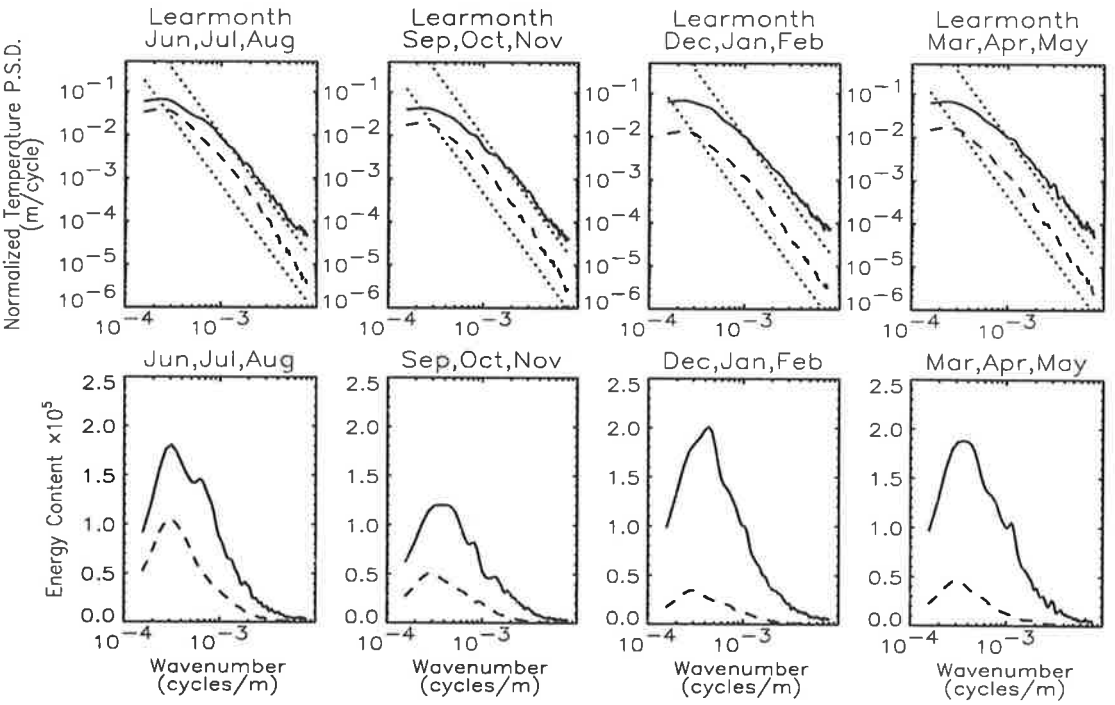

Figure B.6: Mean vertical wavenumber power spectra and area preserving spectra of normalized temperature fluctuations observed over Learmonth (22°S, 114°E) between June 1991 and May 1992.

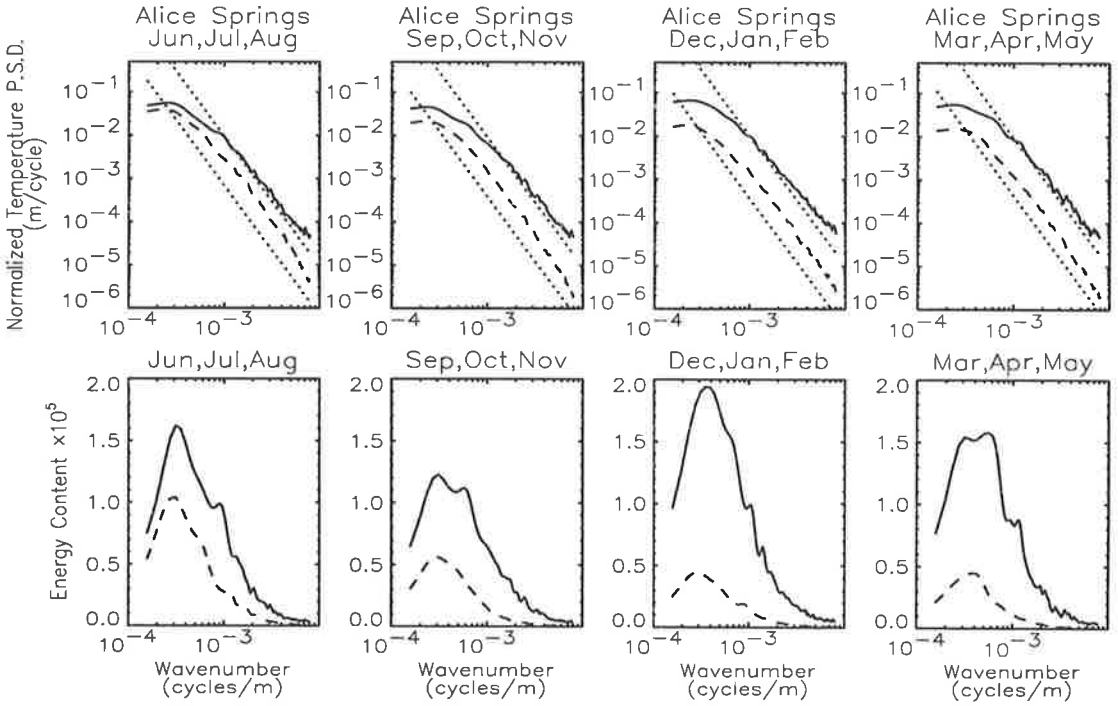

Figure B.7: Mean vertical wavenumber power spectra and area preserving spectra of normalized temperature fluctuations observed over Alice Springs (23°S, 134°E) between June 1991 and May 1992.

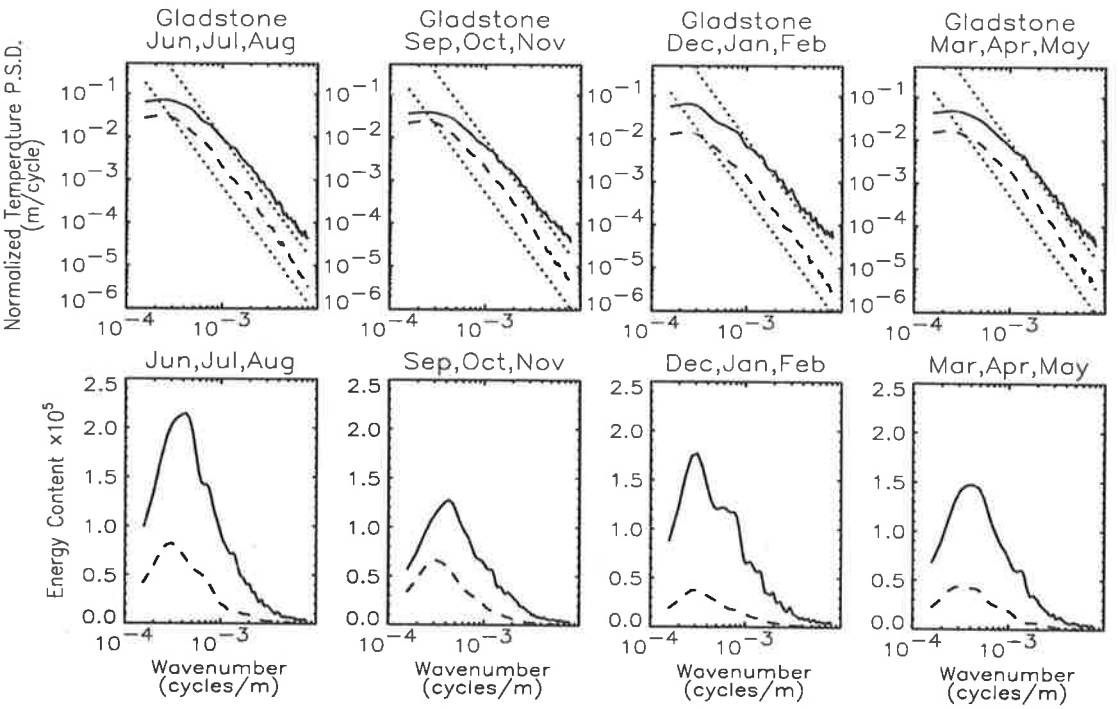

Figure B.8: Mean vertical wavenumber power spectra and area preserving spectra of normalized temperature fluctuations observed over Gladstone (24°S, 151°E) between June 1991 and May 1992.

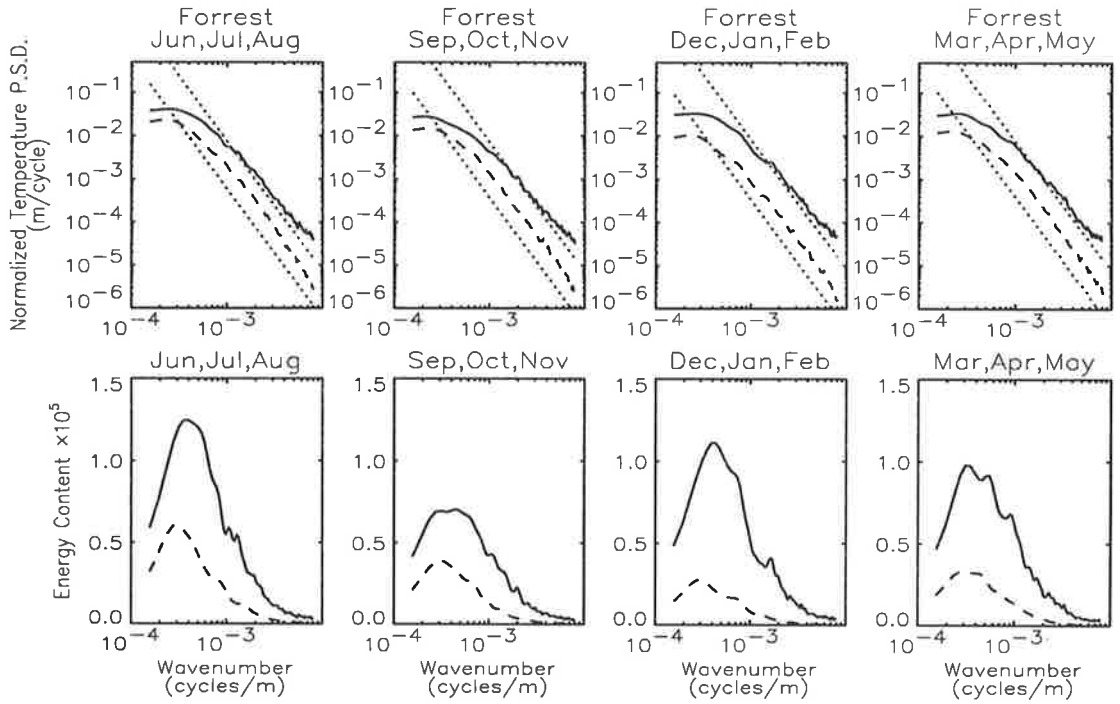

Figure B.9: Mean vertical wavenumber power spectra and area preserving spectra of normalized temperature fluctuations observed over Forrest (31°S, 129°E) between June 1991 and May 1992.

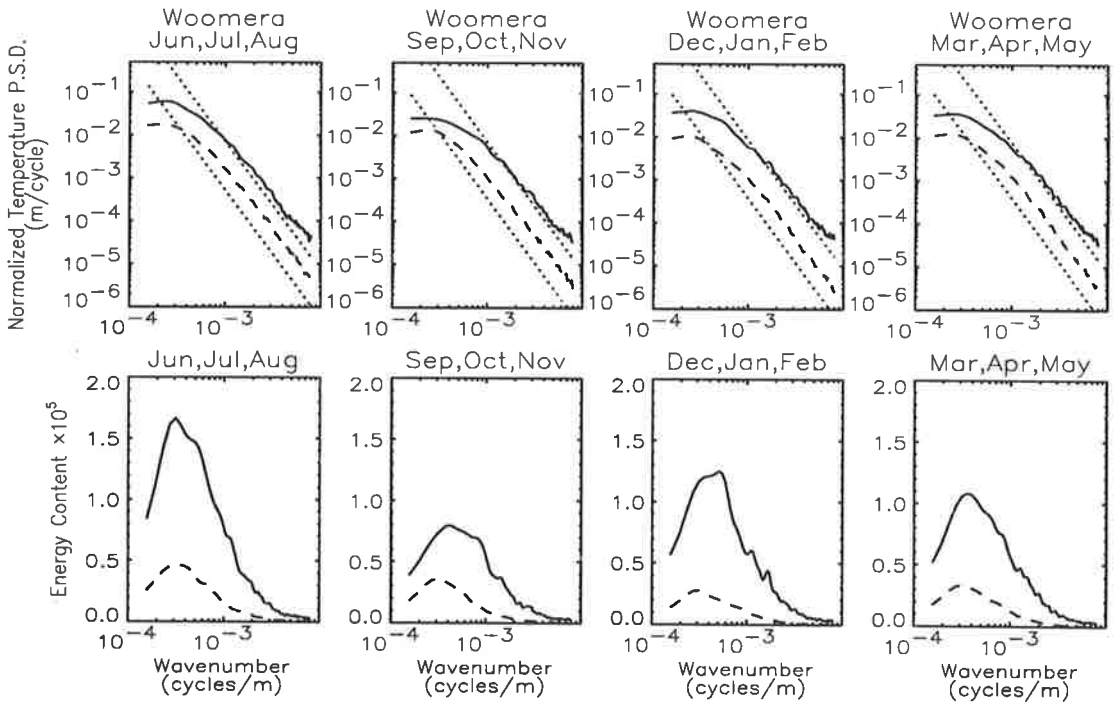

Figure B.10: Mean vertical wavenumber power spectra and area preserving spectra of normalized temperature fluctuations observed over Woomera (31°S, 137°E) between June 1991 and May 1992.

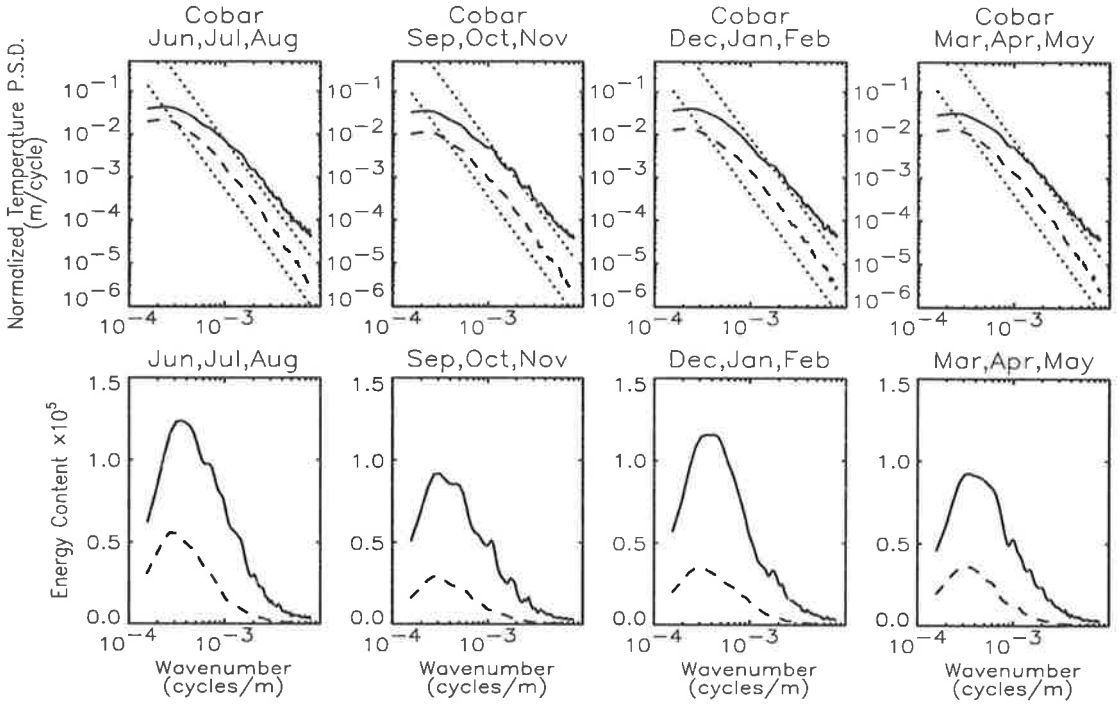

Figure B.11: Mean vertical wavenumber power spectra and area preserving spectra of normalized temperature fluctuations observed over Cobar (31°S, 146°E) between June 1991 and May 1992.

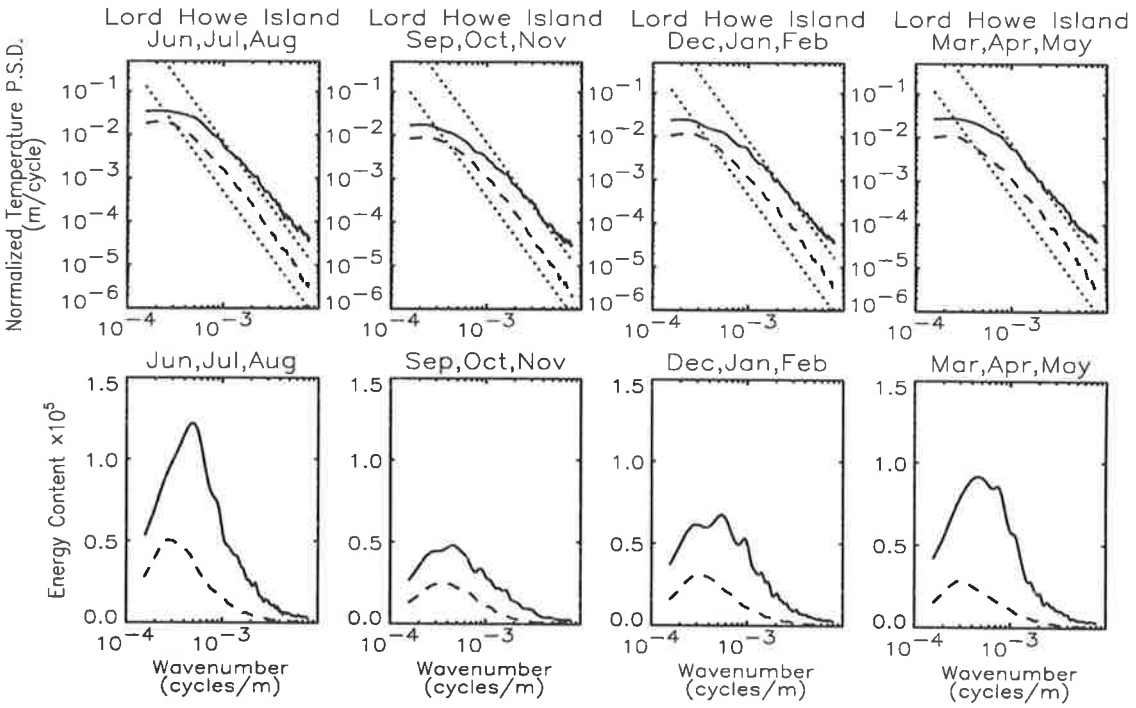

Figure B.12: Mean vertical wavenumber power spectra and area preserving spectra of normalized temperature fluctuations observed over Lord Howe Island (32°S, 159°E) between June 1991 and May 1992.

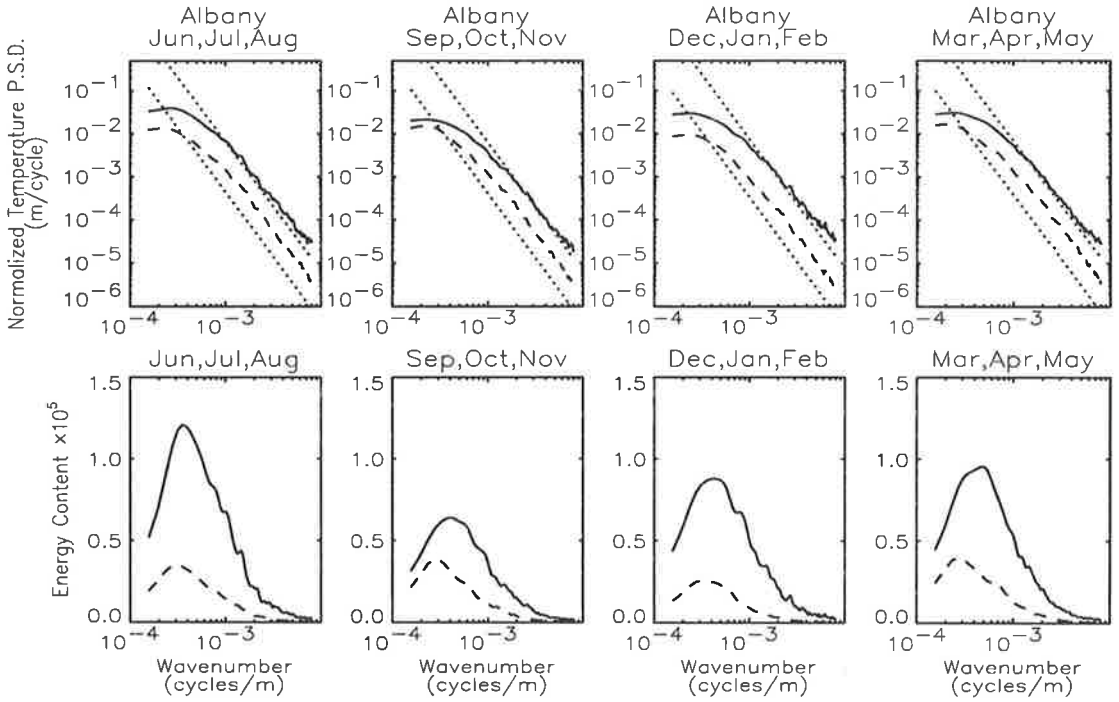

Figure B.13: Mean vertical wavenumber power spectra and area preserving spectra of normalized temperature fluctuations observed over Albany (35°S, 118°E) between June 1991 and May 1992.

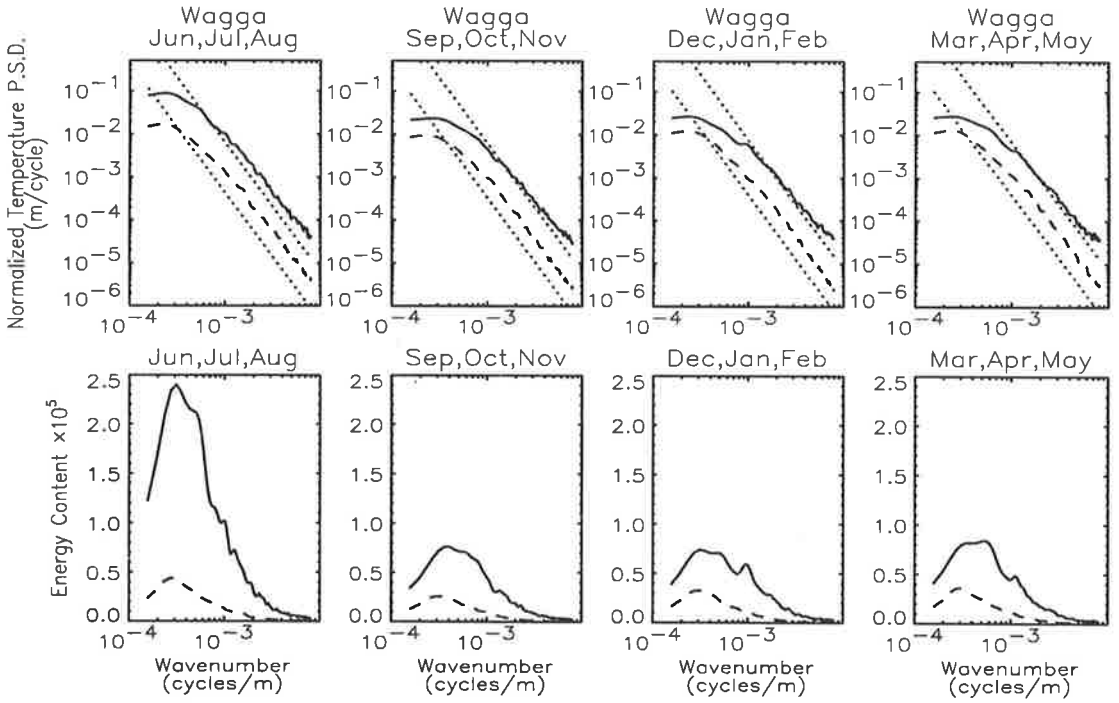

Figure B.14: Mean vertical wavenumber power spectra and area preserving spectra of normalized temperature fluctuations observed over Wagga (35°S, 147°E) between June 1991 and May 1992.

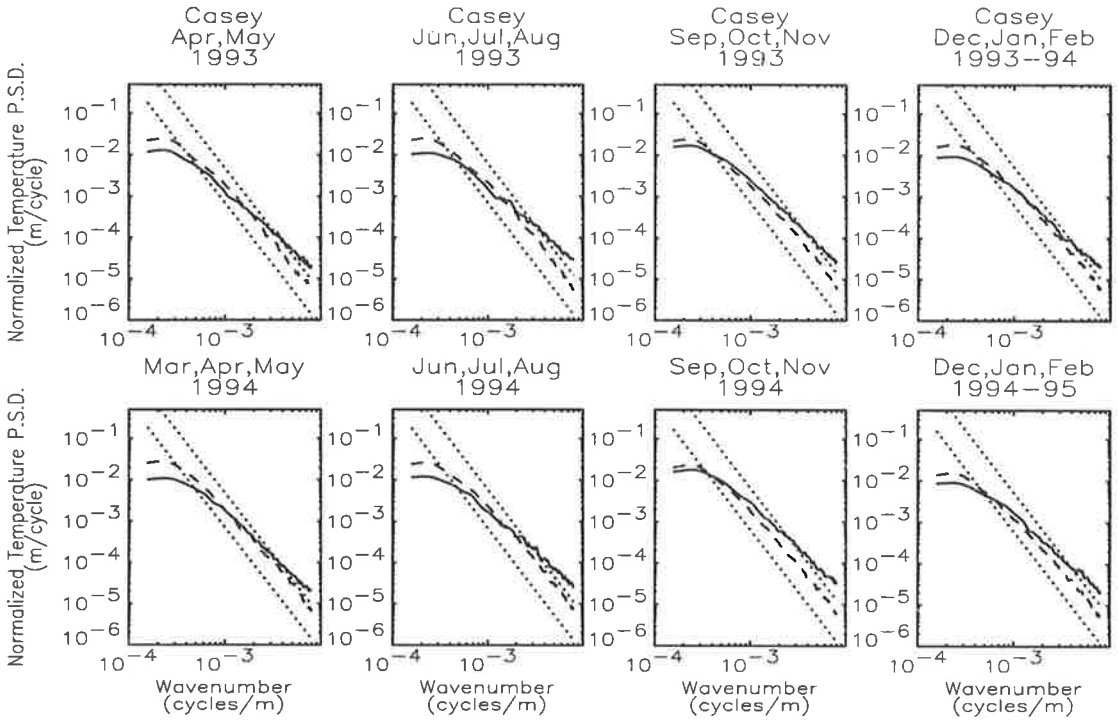

Figure B.15: Mean vertical wavenumber power spectra of normalized temperature fluctuations observed over Casey (66°S, 111°E) between April 1993 and February 1995.

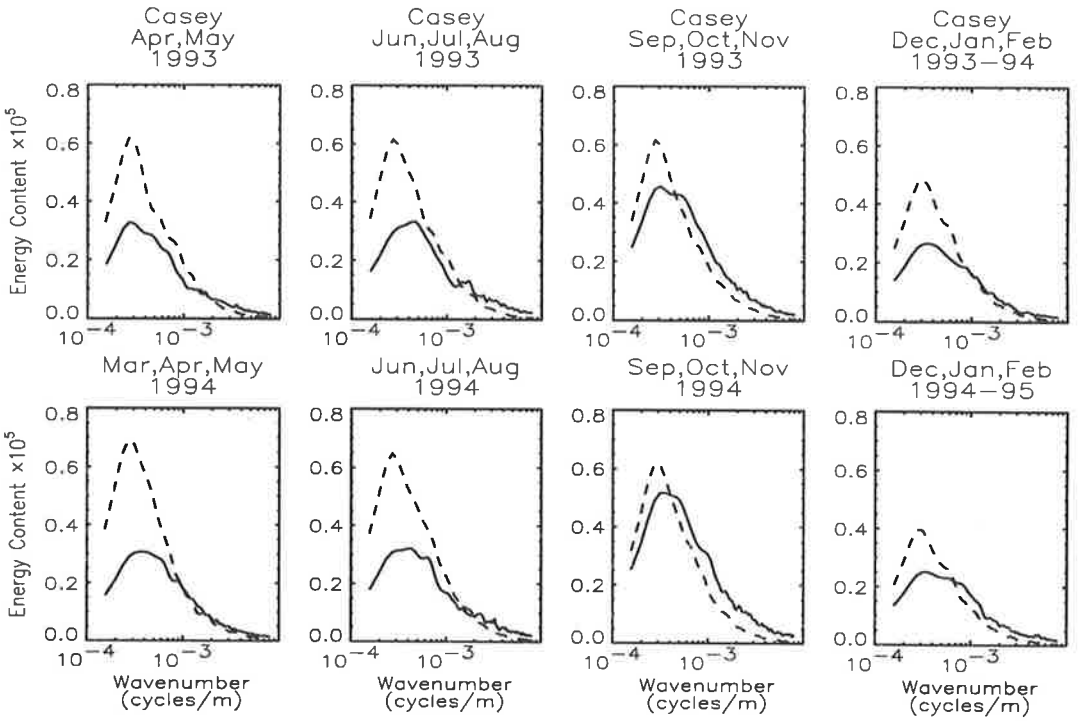

Figure B.16: Mean vertical wavenumber area preserving spectra of normalized temperature fluctuations observed over Casey (66°S, 111°E) between April 1993 and February 1995.

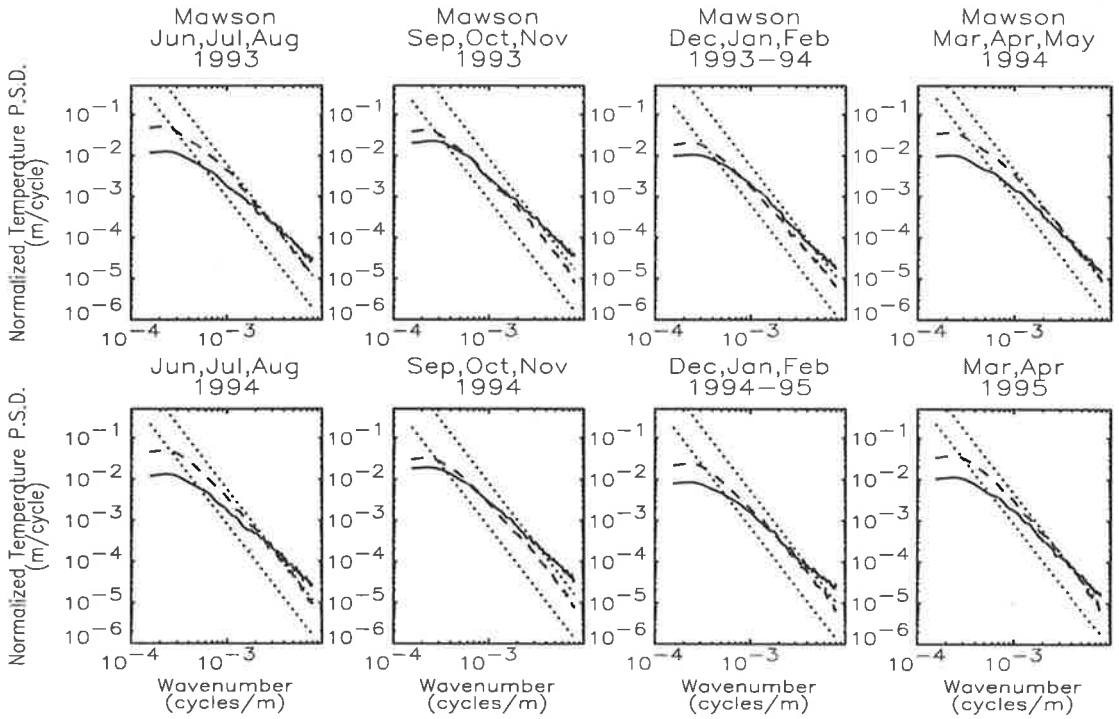

Figure B.17: Mean vertical wavenumber power spectra of normalized temperature fluctuations observed over Mawson (68°S, 63°E) between June 1993 and April 1995.

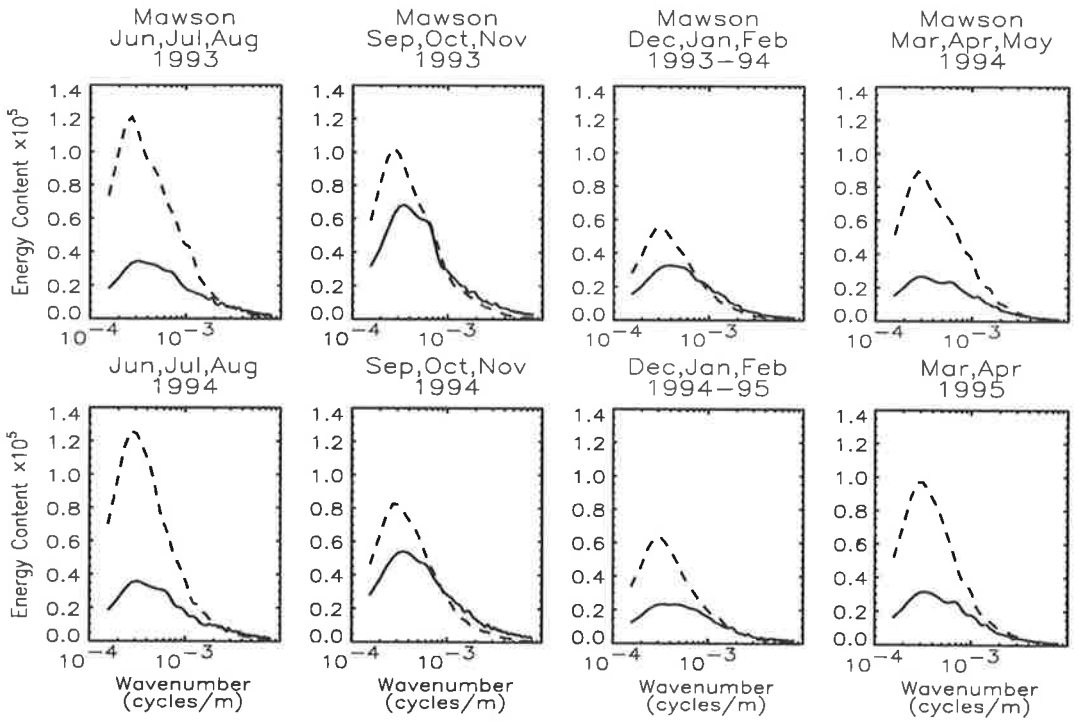

Figure B.18: Mean vertical wavenumber area preserving spectra of normalized temperature fluctuations observed over Mawson (68°S, 63°E) between June 1993 and April 1995.

Appendix C

Radiosonde Data from the South Pole

In this appendix, vertical wavenumber power spectra of normalized temperature fluctuations, which were observed by radiosonde over the South Pole, are presented. The data considered were obtained during February 1995 and were kindly supplied by Matt Pfenninger[1]. The purpose of this appendix is to compare observed spectra from the South Pole with those determined at lower latitudes in an attempt to ascertain if the trend illustrated in Figure 4.23 is continued, that is the trend towards smaller gravity wave variances at higher latitudes. These results were not presented in the main body of this thesis because, at the time of writing, useful information about the radiosondes' temperature sensor response times, measurement accuracy and measurement precision were unknown[2]. The emphasis here is on the total normalized temperature variance rather than on the fine details of the spectral form.

Figure C.1 illustrates the mean temperature, Väisälä-Brunt frequency squared and component horizontal wind velocity profiles determined from 40 radiosonde soundings which happened to reach 30 km or higher during February 1995. The South Pole is approximately 2.8 km above sea level, the mean tropopause height is near 8 km and there exists a notable temperature inversion between ground level and approximately 4 km. Consequently, gravity wave spectral analysis of the tropospheric data is not practicable since the dominant gravity waves are unlikely to be adequately resolved from the background. Note that the mean horizontal winds at the South Pole are unique since there are no zonal winds but rather

[1] University of Illinois

[2] The radiosondes launched at the South Pole were manufactured by Atmospheric Instrumentation Research [*M. Pfenninger*, private communication, 1996].

two orthogonal meridional wind directions. However, it is not known along which lines of longitude the plotted winds lie since the conventions used for the determination of wind direction were not known from the available information. It is sufficient, for the purposes of this appendix, to know that the wind velocity components are orthogonal and that their magnitudes are weak (since they are both meridional).

The vertical wavenumber power spectra of normalized temperature fluctuations are illustrated in Figure C.2. These were determined using an FFT algorithm where spectral leakage was minimized by the application of a Welch window [*Press et al.,* 1988]. The raw data, which were smoothed into 50-m altitude bins, were spectrally analyzed over 6-km altitude segments between 12 and 30 km and also over this full 18-km altitude range. No correction was made for any possible response time distortion since no information was available about the response times of the temperature sensors that were used. The temperature fluctuation profiles were estimated by subtracting second-order polynomials from the 6-km altitude segments and third-order polynomials from the 18-km altitude segments. Mean spectra were obtained by arithmetic averaging.

It is evident, from Figure C.2, that the observed spectra from each 6-km altitude range, and also from the full 18-km altitude range, are attenuated in comparison to the theoretical saturation limits proposed by *Smith et al.* [1987] at all but the very highest vertical vertical wavenumbers. Furthermore, they are attenuated in comparison to the stratospheric spectra observed at lower latitudes, especially at low vertical wavenumbers. The mean normalized temperature variance between 12 and 30 km during February 1995 was found to be 5.2×10^{-6} at the South Pole. Thus the trend towards smaller normalized temperature variances at higher latitudes, as illustrated in Figure 4.23, appears to be continued to the South Pole on the basis of the evidence presented in this appendix.

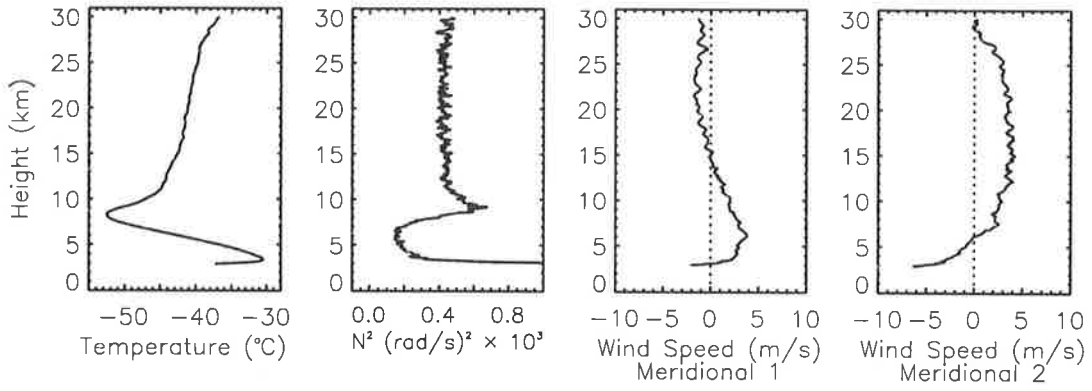

Figure C.1: Mean temperature, Väisälä-Brunt frequency squared and component horizontal wind velocity profiles observed by radiosondes over the South Pole during February 1995.

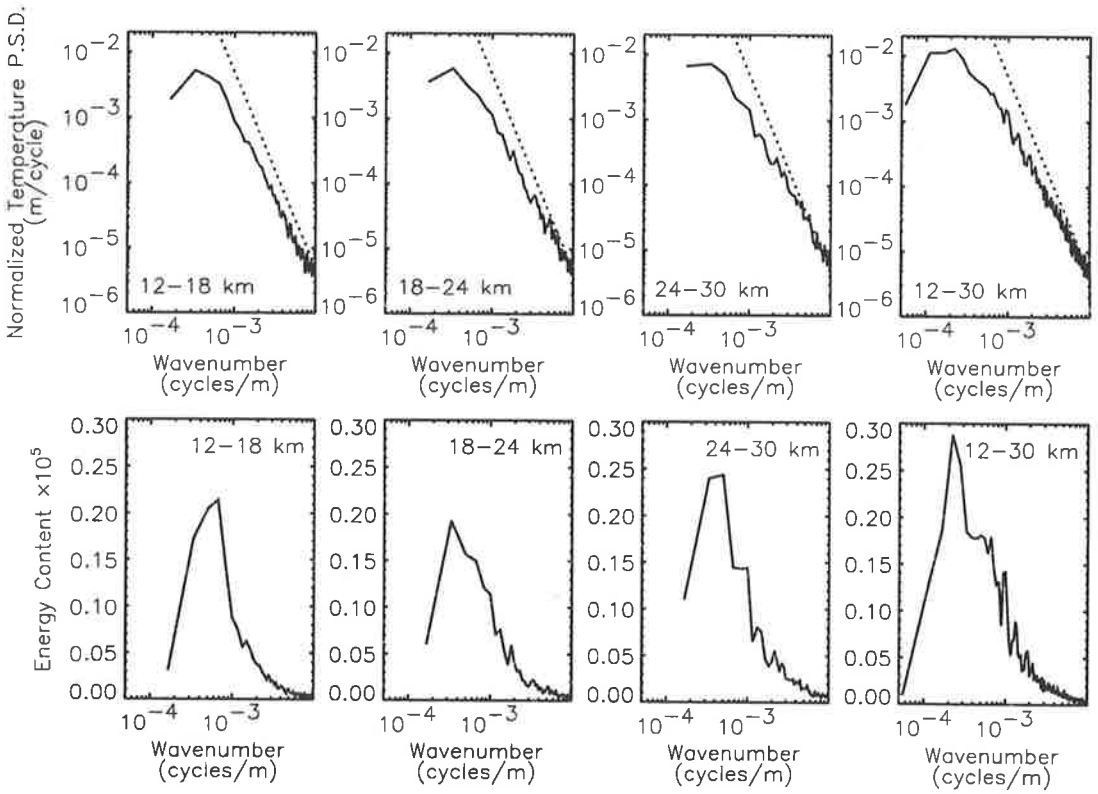

Figure C.2: Mean vertical wavenumber power spectra and area preserving spectra of normalized temperature fluctuations determined within different altitude ranges over the South Pole from observations obtained during February 1995. The dotted lines are the theoretical saturation limits proposed by *Smith et al.* [1987].

Appendix D

Gravity Wave Activity in the Lower Atmosphere: Seasonal and Latitudinal Variations

This is a preprint of a paper by S. J. Allen and R. A. Vincent, published in *J. Geophys. Res.*, *100,* 1327–1350, 1995.

DEPT. OF PHYSICS AND MATHEMATICAL PHYSICS
UNIVERSITY OF ADELAIDE
Adelaide, South Australia, 5005

Gravity wave activity in the lower atmosphere: Seasonal and latitudinal variations

SIMON J. ALLEN AND ROBERT A. VINCENT

Department of Physics and Mathematical Physics, University of Adelaide, Adelaide, South Australia

Abstract

A climatology of gravity wave activity in the lower atmosphere based on high-resolution radiosonde measurements provided by the Australian Bureau of Meteorology is presented. These data are ideal for investigating gravity wave activity and its variation with position and time. Observations from 18 meteorological stations within Australia and Antarctica, covering a latitude range of 12°S – 68°S and a longitude range of 78°E – 159°E, are discussed. Vertical wavenumber power spectra of normalized temperature fluctuations are calculated within both the troposphere and the lower stratosphere and are compared with the predictions of current gravity wave saturation theories. Estimates of important model parameters such as the total gravity wave energy per unit mass are also presented. The vertical wavenumber power spectra are found to remain approximately invariant with time and geographic location with only one significant exception. Spectral amplitudes observed within the lower stratosphere are found to be consistent with theoretical expectations but the amplitudes observed within the troposphere are consistently larger than expected, often by as much as a factor of about 3. Seasonal variations of stratospheric wave energy per unit mass are identified with maxima occurring during the low-latitude wet season and during the midlatitude winter. These variations do not exceed a factor of about 2. Similar variations are not found in the troposphere where temperature fluctuations are likely to be contaminated by convection and inversions. The largest values of wave energy density are typically found near the tropopause.

1. Introduction

It is now well appreciated that gravity waves play a crucial role in determining the circulation and mean state of the atmosphere. If wave effects are to be fully understood and modeled then more information on the geographic and seasonal variations of wave activity and on wave sources is needed.

A wide variety of observational techniques have been used to study mesoscale fluctuations in the lower and middle atmospheres and their variations in time and space. These include balloon soundings [e.g., *Fritts et al.*, 1988; *Sidi et al.*, 1988; *Kitamura and Hirota*, 1989; *Cot and Barat*, 1990; *Tsuda et al.*, 1991], radar observations [e.g., *Tsuda et al.*, 1989; *Fritts et al.*, 1990], rocketsonde measurements [e.g., *Dewan et al.*, 1984; *Hamilton*, 1991; *Eckermann et al.*, 1994], and lidar studies [e.g., *Wilson et al.*, 1991; *Senft et al.*, 1993].

To date, much of our detailed knowledge of wave sources and effects in the lower atmosphere has come from ground-based wind-profiling radar studies [e.g., *Eckermann and Vincent*, 1993]. Instrumented commercial aircraft observations made in the troposphere and lower stratosphere during the Global Atmospheric Sampling Program also provided important information about wave fluxes over varying terrain and source regions [*Nastrom and Fritts*, 1992; *Fritts and Nastrom*, 1992]. While aircraft measurements provide coverage over both continental and oceanic regions, radar and lidar observations are primarily confined to land-based sites, except for a few ship-borne lidar measurements. Despite the excellent temporal resolution of the ground-based instruments it is unlikely that there will be sufficient numbers of such instruments deployed to enable wave climatologies to be established on a global scale, especially in the southern hemisphere.

Despite the large number of observational studies, certain theoretical questions remain unresolved. Initially, the debate was centered upon the relative importance of gravity waves as compared with two-dimensional turbulence in forming the fluctuations observed in the atmosphere. *Dewan* [1979] and *VanZandt* [1982] argued for a gravity wave interpretation, suggesting that mesoscale fluctuations are the direct result of a superposition of many gravity waves. However, *Gage* [1979], *Lilly* [1983], and *Gage and Nastrom* [1985] argued that two-dimensional turbulence is the main cause of mesoscale fluctuations. It is likely that both waves and stratified turbulence are present in the atmosphere, although it is now widely accepted that gravity wave motions are dominant [e.g., *Vincent and Eckermann*, 1990].

Recently, debate has focused upon the physical process apparently acting to limit wave amplitude growth with height. A common feature of many experimental studies is approximately invariant vertical wavenumber and frequency power spectra, despite the exponential decrease of density with height, and regardless of season and geographic location. This feature, first recognized by *VanZandt* [1982] and based on similar studies of oceanic gravity wave power spectra, led to the concept of a "universal" spectrum of atmospheric gravity waves with amplitudes constrained to remain below some fixed value. Several saturation theories have since emerged [*Dewan and Good*, 1986; *Smith et al.*, 1987; *Weinstock*, 1990; *Hines*, 1991].

Each theory proposes a physical mechanism thought to be responsible for limiting wave amplitude growth and each predicts, approximately, the saturated vertical wavenumber power spectrum amplitudes that should be observed. However, due to theoretical uncertainties in the various proposed mechanisms, it has proven difficult to distinguish between them on the basis of spectral amplitude calculations alone. The question of which physical mechanism is acting at high vertical wavenumbers is still, very much, an open one. It seems likely that the successful theory will best account for some of the more unusual experimental findings such as recent lidar measurements within the stratosphere [*Hines*, 1993].

Very recently, *Fritts and VanZandt* [1993] and *Fritts and Lu* [1993] developed a gravity wave parameterization scheme which describes the influence of a broad spectrum of waves on the mean state of the atmosphere. The scheme is based on the concept of a "universal" spectrum which is separable in frequency and vertical wavenumber. Only a few parameters are required to constrain this model and the scheme links the work of theorists, who model large-scale motions in the atmosphere, and experimentalists who use convenient analytical tools such as power spectrum analysis. However, the extent to which wave activity and influence varies with height, season, and geographic location is poorly understood at present. Despite the constraining influence of the proposed saturation theories there still exists the possibility for significant variations in the wave field, both at low vertical wavenumbers and, in some instances, at high vertical wavenumbers also. Quantifying these variations is an important experimental problem.

Balloon-borne radiosonde soundings provide one potentially important source of information on gravity waves and their effects in the troposphere and lower stratosphere. Early work by, for example, *Sawyer* [1961] and *Thompson* [1978] provided evidence for large-scale inertial waves in the lower stratosphere and more recently, *Kitamura and Hirota* [1989] emphasized the importance of radiosonde observations in their study of inertial-scale disturbances over Japan. Radiosonde soundings are carried out daily on a world-wide basis, providing a wealth of information on winds, temperatures, and humidity. One reason why radiosonde measurements have been little used in wave studies is that measurements are reported and archived at relatively infrequent height intervals, leading to poor height resolution. Recently, however, the Australian Bureau of Meteorology began routinely recording and archiving high-resolution data from radiosondes, with pressure, temperature and relative humidity measurements made every 10 s, or about 50 m in altitude. These data are ideal for investigations of wave energies and power spectra in the troposphere and lower stratosphere.

The Australian soundings are taken once or twice per day from stations whose locations vary from the tropics to the Antarctic. The observations also cover a significant spread of longitudes in the Australian sector. By suitably combining measurements made at a range of longitudes in relatively narrow latitude bands it is possible to build up a climatology of wave activity which is not biased by localized source effects, such as topography. Here we explore the extent to which this extensive data set of high-resolution radiosonde measurements can contribute to solving some of the problems described above.

Section 2 of this paper details some background theory as well as discussing the state of current saturation models of temperature fluctuation spectra. In section 3 the radiosonde data set that was used, the analysis procedures that were employed, and the possible sources of measurement errors are described. Vertical wavenumber power spectra of normalized temperature fluctuations are presented in section 4 as are estimates of the total gravity wave energy density, E_0, which is an important component of the *Fritts and VanZandt* [1993] parameterization scheme. A discussion of the results is given in section 5 followed by the conclusions in section 6. The consequences of radiosonde temperature-sensor response time with regards to measurement accuracy are described in an appendix.

2. Gravity Wave Power Spectra Theory

Fritts and VanZandt [1993] (hereinafter referred to as FV93) presented a model three-dimensional gravity wave power spectrum which makes use of functional forms of the one-dimensional vertical wavenumber and frequency power spectra that are in good agreement with experimental findings. They assumed a total energy spectrum that is separable in vertical wavenumber, m, intrinsic frequency, ω, and azimuthal direction of propagation, ϕ, and is given by

$$E(\mu,\omega,\phi) = E_0 A(\mu) B(\omega) \Phi(\phi) \tag{1}$$

where

$$A(\mu) = A_0 \mu^s / \left(1 + \mu^{s+t}\right) \tag{2}$$

$$B(\omega) = B_0 \omega^{-p} \tag{3}$$

and where $\mu = m/m_*$, $m = 2\pi/\lambda_z$, λ_z is the vertical wavelength, m_* is the characteristic wavenumber (in units of radians per meter), E_0 is the total gravity wave energy per unit mass (energy density), A_0 and B_0 are defined by the normalization constraints of $A(\mu)$ and $B(\omega)$, the function $\Phi(\phi)$ contains the dependence on wave field anisotropy and the parameters s, t, and p are to be determined by comparison with the slopes of observed power spectra.

The quantity E_0, an important parameter of the FV93 formulation, is chosen in this paper as the measure for gravity wave activity. It is defined by

$$E_0 = \frac{1}{2}\left[\overline{u'^2} + \overline{v'^2} + \overline{w'^2} + \frac{g^2 \overline{\hat{T}'^2}}{N^2}\right] \tag{4}$$

where u', v', and w' are the zonal, meridional, and vertical components of first-order wind velocity perturbations, respectively, g is the acceleration due to gravity, N is the Vaisala-Brunt frequency, $\hat{T}' = T'/\overline{T}$ is the normalized temperature fluctuation, and $\overline{T}$ and T' are the background and first-order perturbation of atmosphere temperature, respectively. Strictly, measurements of three component wind velocity and temperature are required to completely define E_0. However, it is possible to estimate this parameter from temperature measurements alone by making use of the appropriate gravity wave polarization equation and the three-dimensional model spectrum of FV93. This arises since u', v', w', and $\hat{T}'$ are all coupled to each other through gravity wave polarization equations.

Consider the equation relating the three-dimensional power spectrum of normalized temperature fluctuations to that of total energy,

$$E_{\hat{T}'}(\mu,\omega,\phi) = \frac{N^2}{g^2}\,\frac{(1-f^2/\omega^2)}{(1-f^2/N^2)}\,E(\mu,\omega,\phi) \tag{5}$$

where f is the inertial frequency. This follows from the equations presented by FV93 which in turn can be derived from standard textbook formulations of the polarization equations, at least those involving the Boussinesq approximation [e.g., *Gossard and Hooke*, 1975]. By integrating both sides of (5) with respect to μ, ω, and ϕ using (1), (2), (3), and the normalization condition for $\Phi(\phi)$, namely, $\int_0^{2\pi}\Phi(\phi)d\phi = 1$, the following equation is derived relating the energy density E_0 to the total normalized temperature variance,

$$E_0 = \frac{g^2}{N^2}\,\frac{1}{B_0 C_{In}}\,\overline{\hat{T}'^2} \tag{6}$$

where

$$C_{In} = \frac{f^{1-p}}{1-\tilde{f}^2}\left[\frac{1-\tilde{f}^{p-1}}{p-1} - \frac{1-\tilde{f}^{p+1}}{p+1}\right] \tag{7}$$

and where $\tilde{f} = f/N$, p is the slope of the one-dimensional frequency spectrum, and B_0 is given by FV93. The best estimate of p from the literature is 5/3 and this value will be assumed hereinafter. In obtaining (6), three assumptions have been made: first, the three-dimensional energy spectrum is assumed to be separable in m, ω, and ϕ; second, the one-dimensional frequency spectrum is assumed to be of the form $B(\omega) \propto \omega^{-p}$ where p is 5/3; third, the Boussinesq approximation is assumed valid since this is used in obtaining (5). The normalized temperature variance from a given height interval is easily measured, and (6) will be used in a later section to calculate the gravity wave energy density.

A more typical analysis of radiosonde temperature measurements involves calculating vertical wavenumber power spectra of normalized temperature fluctuations. These, together with results derived from other experimental techniques, provide a good picture as to the nature and shape of vertical wavenumber gravity wave fluctuation spectra. Generally, a high-wavenumber "tail" region, displaying a -3 power law form and having approximately invariant spectral amplitudes, is observed and this is separated from the low-wavenumber source-dependent region by the so-called characteristic wavenumber m_*. Spectral amplitudes in the low-wavenumber region can increase with height but must do so in accordance with wave action conservation. The typical observed shape is well represented by the modified-Desaubies form, $A(\mu)$, first introduced by *VanZandt and Fritts* [1989].

The spectral amplitudes of the high wavenumber "tail" region have been predicted by several authors on the basis of the physical mechanism thought most important in causing gravity waves to saturate. When theoretical uncertainties are taken into consideration, however, these predictions are difficult to differentiate, and for the purposes of this paper the saturation limit of *Smith et al.* [1987] will be used as a convenient reference. This limit is given below for the power spectral density of normalized temperature fluctuations as a function of inverse vertical wavelength,

$$E_{\hat{T}'}(1/\lambda_z) \approx \frac{N^4}{6g^2}\,\frac{1}{p}\,\frac{1}{(2\pi)^2}\,\frac{1}{(1/\lambda_z)^3} \tag{8}$$

where λ_z is the vertical wavelength and, as before, p is the slope of the one-dimensional frequency spectrum. In their original paper, *Smith et al.* [1987] derived the saturation limit for the specific case

of a one-dimensional vertical wavenumber power spectrum of total horizontal wind velocity, which was assumed to take the form defined by (2) with $s = 0$ and $t = 3$. Equation (8) follows from this using a suitable polarization equation and assuming that the one-dimensional frequency spectrum is given by $B(\omega) \propto \omega^{-p}$ [see *Fritts et al.*, 1988].

The purpose of spectral analysis in this paper is not so much to confirm the agreement between theory and experiment, something that appears to have been accepted already, but rather to study how the shape and amplitudes of vertical wavenumber power spectra can vary with geographic position and time. The extent of these variations is not well known at present and the available data set of high-resolution radiosonde measurements is ideal for addressing the problem. Details of the experimental data that were used are provided in the following section.

3. Experimental Data and Analysis Procedures

3.1. Radiosonde Measurements

The Australian Bureau of Meteorology launches one or two radiosondes per day from 36 meteorological stations and has recently begun archiving these measurements. Observations from 18 stations have been chosen for use in this study and these are shown, with the exception of Davis (69°S, 78°E), in Figure 1. Pressure, temperature, and relative humidity measurements are recorded at 10-s intervals which correspond, approximately, to 50-m altitude intervals. Data were available for at least a 1-year period (June 1991 to May 1992) from all but two of the stations, Davis and Willis Island. Only 10 months of data were available from these sites.

Each meteorological station in Figure 1 makes use of radiosondes manufactured by Vaisala Oy and the data obtained were subjected to quality control procedures developed by that company. These procedures include removing suspect measurements and replacing them by linear interpolation. A measurement is deemed to be suspect if it does not satisfy certain rejection criteria based on known physical constraints. In addition, the raw measurements, made at approximately 2-s intervals, are smoothed in order to obtain the 10-s "filtered" data that are used here.

Temperature measurements are of particular interest in this study. Figure 2 displays examples of temperature profiles observed by radiosondes launched from Darwin (12°S, 131°E) and Davis (69°S, 78°E) during the months of January and July. These examples are chosen because of their extreme natures. The tropopause over Darwin is typically found near 16 km, whereas the same level over Davis occurs, on average, at about 9 km. Typical tropopause levels from other locations tend to fall between these heights. Notice that successive profiles, corresponding to a 12-hour delay between soundings, have been displaced by 10°C. The data obtained from other stations were not always at 12-hour intervals, as indicated by these examples. From many stations, measurements from only one sounding per day were available.

3.2. Vertical Wavenumber Power Spectrum Analysis

Radiosonde profiles of normalized temperature fluctuations, $\hat{T}'$, were spectrally analyzed in two altitude intervals, usually between 2.0 and 9.0 km in the troposphere and 17.0 and 24.0 km in the stratosphere. However, at some stations slightly different height ranges were used and these are listed in Table 1. Notice also the shaded regions of Figure 2 which correspond to the particular intervals used for the analysis of observations made at Davis and Darwin. The principal reason for choosing these ranges was to ensure a stationary power spectrum since, according to theory, the vertical wavenumber power spectrum of normalized temperature fluctuations is dependent upon N^4. Therefore height regions in which the Vaisala-Brunt frequency is approximately constant should be used.

Data segments for which continuous measurements were unavailable throughout the entire height interval of interest or for which a tropopause was found within this interval were not included in the power spectrum analysis. The former condition often arose when the sonde did not reach the maximum height required for a given station as defined in Table 1. The latter condition also arose from time to time and the relevant profiles were excluded to ensure a constant background Vaisala-Brunt frequency profile. Approximately 30% of all available stratospheric data segments were rejected in this manner. This figure, however, was much smaller for tropospheric data. The particular height ranges that were employed at each station were chosen in order to minimize the number of profiles rejected.

Normalized temperature fluctuation profiles were calculated by estimating $\overline{T}$ with a fitted second-order polynomial over the particular height interval being investigated. These were then spectrally analyzed using the Blackman-Tukey algorithm with a 90% lag Bartlett window where the data points were first prewhitened by differencing. The technique follows *Dewan et al.* [1984] who used the same algorithm to analyze horizontal wind velocity fluctuations derived from rocket-laid vertical smoke trails.

The vertical wavenumber power spectra calculated from individual temperature profiles were then averaged in order to improve the confidence limits of spectral amplitude estimates. Following the suggestion of T. E. VanZandt (private communication, 1992), normalized individual power spectra were averaged, that is, each spectrum was divided by its total variance before averaging. The purpose of this technique was to ensure that all spectra contribute equally to the shape of the mean spectrum. Once calculated, the mean spectrum was renormalized by multiplying by the averaged total variance.

A possible source of error in the analysis procedure arises due to the fact that radiosonde observations are unequally spaced in altitude. Although successive measurements were recorded at 10-s intervals, the corresponding altitudes traversed by the sonde tended to vary; typical height intervals were found to be between 40 and 60 m. Strictly speaking, the Blackman-Tukey algorithm cannot be applied to unequally spaced data such as this.

The approach used here was to interpolate the measurements at 50-m intervals using cubic spline

interpolation and to assume that the calculated power spectrum was not significantly different from the spectrum that would be found were the original data points equally spaced. In order to be confident of this, however, a comparison was made between vertical wavenumber power spectra of radiosonde normalized temperature fluctuations calculated with both the Blackman-Tukey algorithm and with a particular discrete Fourier transform. This latter technique was proposed by *Ferraz-Mello* [1981] and was devised specifically for the purposes of making accurate estimates of power spectral density from unequally spaced data. The comparison was found to be very favorable and so the Blackman-Tukey algorithm appears to have valid application in this case.

A further source of error for vertical wavenumber power spectral density calculations from radiosonde temperature data arises from the nature of balloon observations. Instrumented balloons rise slowly in the vertical at speeds of approximately 5 m s^{-1} and also drift horizontally with the background winds. As a consequence, any observed power spectra are not strictly vertical wavenumber power spectra since the observations are not made simultaneously in time, nor are they obtained along a vertical line from the point of the balloon's release. *Sidi et al.* [1988] and *Gardner and Gardner* [1993] have considered this problem for radiosonde measurements of a broad spectrum of predominantly saturated gravity waves. Both studies suggest that any errors introduced to the vertical wavenumber power spectrum estimates are usually negligible. *Gardner and Gardner* [1993] did, however, conclude that nonnegligible distortion may be possible when horizontal wind speeds reach approximately 60 m s^{-1} or larger. Nevertheless, for the data used here, it is argued that even this distortion is small when compared with the much greater distortion caused by the relatively slow response of the radiosonde's temperature sensor at stratospheric heights. The response time is peculiar to the type of sensor used and, if large enough, will prevent the radiosonde from accurately measuring rapid changes in temperature as the balloon moves vertically. The measured power spectra can, however, be corrected and this correction procedure will now be discussed.

3.3. Radiosonde Instrumental Response

It is well known that a temperature sensor will behave in such a way that the rate of change of the sensor's temperature is proportional to the difference between the temperature of the sensor and that of its surrounding environment [*Fritschen and Gay*, 1979]. Mathematically, this may be expressed as

$$\frac{dT_s}{dt} = -\frac{1}{\tau}\,[T_s - T] \tag{9}$$

where T_s is the sensor temperature, T is the environment temperature, and τ is defined as the response time constant. The value of τ is peculiar to the type of sensor used and to the environment in which it is placed.

The response of a given temperature sensor to any time-varying environment temperature $T(t)$ is completely defined by (9). The steady state response to a sinusoidally varying environment is of particular importance, however, since this describes a filter function, $I(\omega)$, which relates the environment or input spectrum $X(\omega)$ to the measured spectrum $X_s(\omega)$ according to $X_s(\omega) = I(\omega)X(\omega)$ at each angular frequency ω [e.g., *Bath*, 1974]. Here $X(\omega)$ and $X_s(\omega)$ refer to the Fourier transforms

of $T_s(t)$ and $T(t)$, respectively, rather than their power spectral densities. If $I(\omega)$ is known then the environment spectrum can be recovered from the observed spectrum since $X(\omega) = X_s(\omega)/I(\omega)$.

Consider the case of a balloon which rises at constant vertical velocity V_0 and carries a temperature sensor with known response time τ. Suppose also that the sensor is measuring a background or environment temperature profile that is sinusoidally dependent upon height z but is independent of time, that is, $T(z) = A\exp[i(mz + \phi)]$ where $m = 2\pi/\lambda_z$ and where the complex notation has its usual meaning. Equation (9) is therefore given by

$$\frac{dT_s}{dz} + \frac{1}{\beta}T_s = \frac{1}{\beta}T \tag{10}$$

where $\beta = V_0\tau$. The "steady state" solution of this new equation for constant β is readily calculated,

$$T_s(z) = \frac{A}{1 + im\beta}\exp[i(mz + \phi)] \tag{11}$$

and thus defines a filter function $I(m) = 1/[1+im\beta]$, analogous to the function $I(\omega)$ discussed earlier, which relates the Fourier transform of $T_s(z)$ to that of $T(z)$ at each spatial frequency or wavenumber m. Since power spectral density is simply the absolute value squared of a Fourier transform it follows that the observed vertical wavenumber power spectrum is related to the true or environment power spectrum according to the following equation

$$E_{T_s}(m) = \frac{1}{1 + (m\beta)^2}E_T(m) \tag{12}$$

where $E_{T_s}(m)$ and $E_T(m)$ are vertical wavenumber power spectra of $T_s(z)$ and $T(z)$ fluctuations respectively. Equation (12) can therefore be used to correct observed vertical wavenumber power spectra of temperature fluctuations and to recover their true forms provided that V_0 and τ are known and are constants. Furthermore, the relation is also valid for vertical wavenumber power spectra of normalized temperature fluctuations provided that $\overline{T_s}(z)$ does not differ significantly from $\overline{T}(z)$. We believe that this is a reasonable assumption.

Figure 3 displays the measurement distortion of a modified-Desaubies vertical wavenumber power spectrum with $m_*/2\pi = 5 \times 10^{-4}$ cycles per meter and with spectral amplitudes chosen to represent typical observations of normalized temperature fluctuations. The parameter β was assigned the value of 40 m. This corresponds to the typical balloon ascent velocity ($V_0 = 5$ m s^{-1}) and to estimates of response times ($\tau = 8$ s) within the altitude range 17–24 km. Notice that the spectral distortion is only significant at high vertical wavenumbers. Notice also that the total observed variance is not significantly reduced since the shaded area of Figure 3 comprises just 4% of the total area under the modified-Desaubies spectrum.

Estimating the radiosonde's temperature sensor response time poses a difficult problem since τ depends upon air temperature and air density. A broad discussion of how these estimates can be obtained and to what extent they are reliable is given in the appendix. The discussion is based on experimental results presented in two Vaisala Oy test reports. However, it should be noted here that there is some uncertainty as to the correct value for the response time τ. This may result in a bias for the spectral parameter, t, of corrected power spectra, although estimates of both the characteristic

wavenumber and the total wave variance will not be significantly affected. More details are provided in the appendix.

The height-averaged response times were found to lie between 7 and 8 s within the 17 to 24-km altitude range and between 1 and 2 s within the 2 to 9-km altitude range. The response times were not constant within these ranges but may be considered as constants to good approximation. This point is discussed further in the appendix and is not believed to result in serious errors, despite the fact that τ was assumed to be constant in the derivation of (12). Since the response time is small within the troposphere, the correction to the observed power spectrum, for the wavenumber range that is being investigated here, is marginal. As a result the correction technique will only be applied to stratosphere power spectra.

In Figure 4 the mean vertical wavenumber power spectra of normalized temperature fluctuations observed at Adelaide (35°S, 139°E) for both summer and winter months within the altitude range 17–24 km are presented. Also plotted are the corrected power spectra, as defined by (12), where τ was obtained using the technique described in the appendix and where an average V_0 was used since the balloon ascent velocity is known for each individual temperature profile. We believe that the corrected spectrum provides the best estimate of the true normalized temperature power spectral density. All of the stratosphere power spectra that are presented and discussed in the following sections will have undergone this correction procedure.

4. Power Spectra and Energy Density Variations

Vertical wavenumber power spectra of normalized temperature fluctuations within the troposphere and lower stratosphere are presented in this section. Figure 5 displays seasonally averaged spectra from three different stations (Gove, Adelaide, and Hobart) which were chosen to represent low-latitude and midlatitude sites. The seasonally averaged spectra from other locations, with the exception of Davis, were found to be similar to these. Figure 6 displays time and zonally averaged vertical wavenumber power spectra. These were obtained by averaging spectra from each station into seven latitude bands as described in Table 2. The purpose of presenting the spectra in this manner is to look for seasonal and latitudinal variations of the gravity wave spectral form.

Each power spectrum of Figures 5 and 6 has been presented with a maximum wavenumber of 8.0×10^{-3} cycles per meter. However, the Nyquist spatial frequency for data interpolated at 50-m altitude intervals is 0.01 cycles per meter. The cutoff wavenumber was chosen since the mean separation of adjacent points for a given temperature profile was found to vary about 50 m. As a consequence, spectral amplitudes at the very highest wavenumbers may be biased due to aliasing.

Seasonal variations of the gravity wave spectral form are difficult to observe in the spectra of Figure 5, confirming the "universal" nature of the gravity wave field. Small variations can be seen but are most noticeable within the low-wavenumber, source-dependent, region of the spectrum, as might be expected. For example, the winter months at Adelaide and Hobart are characterized by an increase

in frontal activity at ground level. Since cold fronts are known gravity wave sources [*Eckermann and Vincent*, 1993], it is plausible to suppose that the source-dependent region of the spectrum will display larger amplitudes during winter than during summer. Also *Kitamura and Hirota* [1989] have suggested a relationship between wave disturbances and the subtropical jet at the tropopause level which peaks during winter months. We do observe larger spectral amplitudes during winter and within the low-wavenumber region of the spectrum at stratospheric heights but this is much less obvious within the troposphere. The opposite should be true at low-latitude sites, such as Gove, where increased source spectrum activity is expected during the monsoon season (December to February). The observed spectra within the stratosphere do show slightly larger amplitudes during this period and within the source-dependent region, but surprisingly this is not the case at tropospheric heights where larger spectral amplitudes are found during the dry season.

Latitudinal variations of the gravity wave spectral form (Figure 6) are generally not significant, although the stratosphere power spectrum observed at Davis (latitude band 7) is an exception. This shows smaller spectral amplitudes and a shallower slope than is expected theoretically and in comparison with the spectra observed at other latitudes. Curiously, the troposphere and stratosphere power spectra are very similar in this case, despite the significant increase of atmosphere stability near the tropopause.

The power spectra of Figures 5 and 6 confirm the approximate invariance of the gravity wave field with time and geographic location. However, the stratosphere power spectrum observed at Davis is an exception. Nevertheless, all other stations, which are located near a range of different geographic features, show remarkably similar spectra within both the troposphere and the lower stratosphere. Most are not shown here for the purpose of brevity, although each station, with the exception of Willis Island, has contributed to the spectra that are presented in Figure 6. The invariance of the spectral form occurs despite, what are assumed to be, large differences in the source spectrum of waves at each different location.

Table 3 presents estimates of the spectral parameters E_0, t, $m_*/2\pi$, and $c_* = N/m_*$, which are all defined within the FV93 model formulation. These are determined from the shape and spectral amplitudes of the observed spectra at each station. The estimates of E_0 were obtained using (6) and (7) where $\overline{\hat{T}'^2}$ is simply the area under the relevant power spectrum and where an averaged Vaisala-Brunt frequency, N, was used. Estimates of t and $m_*/2\pi$, and hence c_* also, were found using the Levenberg-Marquardt least squares curve-fitting algorithm with a fitting function given below.

$$F(m) = F_0 \frac{m/m_*}{1 + (m/m_*)^{t+1}} \tag{13}$$

The three unknown parameters, F_0, m_*, and t, were obtained by fitting to monthly mean spectra and then averaging these estimates over all time. Table 3 provides a description, at least to a certain extent, of the mean behavior of the gravity wave field at each station. However, other important parameters, such as the wave field anisotropy, cannot be estimated from radiosonde temperature measurements alone.

The spectral parameter, t, for stratosphere power spectra was found to be consistently smaller

than 3, the expected value from linear saturation theory. However, this parameter for troposphere power spectra was found to be very close to 3 at most stations. Recall that each stratospheric power spectrum has been corrected for spectral distortion that is believed to be associated with the radiosonde's temperature sensor response time. The troposphere power spectra have not undergone this correction procedure, however, since the response time is small at tropospheric heights. It is possible that estimates of t within the stratosphere are biased since there is some uncertainty as to the correct value for τ. As a consequence, all values within the relevant column of Table 3 should be treated with some caution. More details about this problem are provided in the appendix, but it should be noted that estimates of other spectral parameters will not be affected.

The characteristic wavelength, $2\pi/m_*$, was found to be close to 2.5 km within both the troposphere and the lower stratosphere. Therefore the difference between characteristic phase speeds, c_*, within the two regions is determined mainly by differences in N. The gravity wave energy density is generally larger within the troposphere than the lower stratosphere, although observations from Gove, Darwin, and Willis Island provide exceptions.

The total gravity wave energy density, as estimated using (6), is chosen here as the measure for gravity wave activity. Time and latitude variations of the wave field are best studied using this parameter. Figure 7 displays contours of E_0 as a function of time and latitude for both the troposphere and the lower stratosphere. These were obtained by averaging the data into 1-month bins for six of the seven latitude bands that were described in Table 2. Data from Davis were not included since these were not available over the full 12-month period.

The energy densities of Figure 7 were calculated from the areas under monthly mean vertical wavenumber power spectra. Thus they refer to the total energy density of waves within the 1.43×10^{-4} to 8.00×10^{-3} cycles per meter wavenumber range. Also, the raw 6 by 12 data array was rebinned using bilinear interpolation in order to obtain a smoother contour pattern. Therefore the resolution is greater than is justified from the original measurements.

Seasonal variations of stratosphere wave activity are easily recognized in Figure 7. These clearly confirm the seasonal trends described earlier which were inferred from the variations of power spectrum form. At low latitudes (10°S to 20°S) a clear annual variation is observed with wave energy peaking during the monsoon months of December to February. However, at middle latitudes (30°S to 40°S) a maximum is seen during the winter months when cold fronts sweep across southern Australia. A transition between these two regimes occurs at intermediate latitudes (20°S to 30°S) where a semiannual variation is observed.

The seasonal variations of troposphere wave activity are, surprisingly, not well correlated with those in the stratosphere. At middle latitudes (30°S to 40°S) a small peak in wave activity is seen during winter months but the variation is much smaller than that observed in the stratosphere. However, at lower latitudes (10°S to 30°S) a strong peak in energy density is observed between July and November which is in contrast with the stratosphere case where the maximum is found between December and February. This sudden increase in tropospheric wave energy does not coincide with

particular meteorological events, nor can it be associated with any one geographic feature since the maximum is seen at a number of different stations including Port Hedland, Alice Springs, Townsville, and Willis Island.

Latitudinal variations of gravity wave activity are evident in the contour plots of Figure 7. Generally, the yearly averaged energy density (Table 3) is found to decrease with latitude so that the highest values are observed at the low-latitude sites. This is particularly noticeable within the stratosphere, although it is less obvious at tropospheric heights. The trend can also be seen in the power spectra of Figure 6.

The variation of gravity wave energy density with height and time can be examined using the radiosonde data from each station. Figures 8, 9, and 10 present time-height contours of normalized temperature variance and total gravity wave energy density observed at Gove, Adelaide, and Davis which were chosen to represent low-, middle, and high-latitude sites, respectively. These were obtained by calculating the normalized temperature variance within 4-km intervals for each observed temperature profile which had continuous measurements up to at least 24 km. The measurements were then averaged into 1-month bins giving a 6 by 12 array of variance data. Finally, the energy densities were obtained using (6) and (7) and the contours were calculated after bilinear interpolation. Also plotted (Figures 11, 12, and 13) are the time-height contours of temperature and Vaisala-Brunt frequency squared from each station. These were included to provide details concerning the background atmosphere and have also been obtained by averaging the data into 4 km by 1 month bins.

The normalized temperature variances of Figures 8, 9, and 10 have been calculated by estimating $\overline{T}(z)$ with a fitted second-order polynomial. These are given by $\sum_{i=1}^{M}(\hat{T'}_i - \overline{\hat{T'}})^2/(M-1)$ for all i such that z_i is in the appropriate height range where $\hat{T'}_i = (T_i - \overline{T}(z_i))/\overline{T}(z_i)$ and where M is the number of data points that lie within this height range. Since the data are partitioned into 4 km height bins the energy densities refer to energy densities of gravity waves within the wavenumber range 2.5×10^{-4} cycles per meter to approximately 0.01 cycles per meter. Therefore they are not strictly comparable to the energy densities of Figure 7 since these refer to waves within a slightly larger wavenumber range.

The time-height contours of temperature observed at Gove (Figure 11) behave as expected showing a steady decrease in temperature from ground level until the tropopause is reached at approximately 17 km where the temperature begins to increase with height. There are no seasonal variations in the position of the tropopause or in the observed temperature gradients. The contours of Vaisala-Brunt frequency squared show a steplike increase at the tropopause with values in the stratosphere exceeding those of the troposphere by a factor of approximately 6. Here also there are no significant seasonal variations. The contours of gravity wave energy density tend to follow those of normalized temperature variance (Figure 8). In the troposphere, energy densities are of the order of 3 J kg^{-1}, although are generally larger between July and October, particularly at the lowest heights. This is in agreement with the seasonal variations described earlier. Once the tropopause is reached, however, the energy density is found to increase significantly taking values of the order of 10–16 J kg^{-1}

at approximately 18 km. This rapid increase is followed by an equally rapid decrease near 20 km. However, the height range of measurements is not sufficient to determine the lowest value to which the energy density falls within the lower stratosphere.

Similar results are seen for the time-height contours of energy density observed at Adelaide and Davis. At Adelaide (Figure 9) a noticeable peak in wave energy density is found between 8 and 15 km, depending on the season. This follows the position of the tropopause as indicated by the contours of Vaisala-Brunt frequency squared (Figure 12). However, the peak in E_0 is not as large as the one found at Gove, nor is it as sharp. Notice also the large energy density values found within the lowest 4-km height bin. A discussion of these is left until the following section.

The contours of energy density observed at Davis (Figure 10) are particularly interesting in that a large peak is found at approximately 10 km between December 1992 and April 1993 but is not evident at this same height between July 1992 and December 1992. Referring to the contours of Vaisala-Brunt frequency squared (Figure 13), the period of December 1992 to April 1993 is characterized by a strong N^2 vertical gradient at 10 km. However, between July 1992 and December 1992 this gradient is much weaker. Thus there is correlation between gravity wave energy density and the gradient of Vaisala-Brunt frequency squared within the vicinity of the tropopause. Also the energy density values within the lowest 4-km height bin are quite large, as was found to be the case at Adelaide.

5. Discussion

High-resolution radiosonde measurements made in the Australian sector of the southern hemisphere enable the variance of temperature to be investigated as a function of height, latitude, and season. The main results are given.

1. The vertical wavenumber power spectra have slopes that are close to -3 at most stations, especially within the troposphere.

2. There are clear seasonal variations of wave activity in the lower stratosphere (heights near 20 km) with the time of maximum activity changing from low-latitudes to midlatitudes. Seasonal variations of wave activity in the troposphere are, on the other hand, less clear.

3. Strong increases of normalized temperature variance are observed near the tropopause at times when there are large vertical gradients in atmosphere stability.

The observed power spectra within the stratosphere have high-wavenumber slopes that are slightly shallower than the theoretical expectation. This may result from a bias in estimates of temperature sensor response time as discussed in the appendix or from aliasing due to high spatial frequency noise. Furthermore, the sonde's horizontal drift will result in some distortion of the vertical wavenumber power spectra which are expected to have shallower slopes as a consequence [*Gardner and Gardner*, 1993]. All of these factors may be contributing to the spectral shape that is observed and so estimates of the spectral parameter t should not be regarded as inconsistent with the predicted

−3 value within the stratosphere. The slopes of troposphere spectra, however, are in good agreement with theoretical expectations. These have not undergone the response time correction procedure as have those in the stratosphere and are less susceptible to problems associated with the sonde's drift since horizontal wind speeds tend to be weaker within the troposphere. Note, however, that the troposphere spectral amplitudes are larger than the gravity wave saturation limits of *Smith et al.* [1987].

It is often assumed that the small-scale temperature variations of the type discussed here are caused by gravity waves, an interpretation we have followed. While the vertical wavenumber spectral slopes are in the general range predicted by recent theories, the assumption that all temperature fluctuations are due to waves needs to be carefully examined, especially within the troposphere. Processes such as convection and inversions cause fluctuations on single profiles that are either difficult to distinguish from wave activity or difficult to remove from the background temperature profile. Both of these factors are likely to explain the large values of E_0 that are found within the lowest 4-km height bins of the time-height contour plots (Figures 8, 9, and 10). If some of the observed variance within these bins is not due to gravity waves then the values of E_0 will be overestimated. This may also explain the observed spectral amplitudes which are consistently larger in the troposphere than the theoretical gravity wave saturation limits of *Smith et al.* [1987]. A similar result was reported by *Tsuda et al.* [1991] after analysis of temperature profiles observed from Kyoto within a comparable height range.

The large increase of gravity wave energy density observed within the low-latitude troposphere (Figure 7) between July and November may also be explained in a similar manner. Low-altitude temperature inversions are more common at low latitudes during these months. As an example, Figure 2 shows the temperature profiles observed at Darwin between July 20 and July 29 and between January 20 and January 29. The profiles observed during July show strong temperature inversions between 1 and 3 km. Such strong inversions are less evident in the corresponding profiles from January. These inversions must contribute to the observed normalized temperature variance between 2.0 and 9.0 km during July and similar inversions are found at all other low-latitude stations. As a consequence, the total gravity wave energy density within the 2.0 to 9.0 km altitude range will be overestimated at these stations. Whether this is sufficient to explain the large increase described in Figure 7 is not known. Although they are not shown here, the power spectra calculated for both months are of similar shape but larger spectral amplitudes are found during July, particularly at the smallest vertical wavenumbers.

In the stratosphere it is more certain that small-scale temperature fluctuations are due to gravity waves. *Kitamura and Hirota* [1989], for example, show that the temperature and wind fluctuations in the lower stratosphere are consistent with the polarization relations of inertia-gravity waves. We find that, except for the Antarctic station of Davis, the stratospheric spectral amplitudes and slopes are generally consistent with theoretical expectations, and seasonal changes occur predominantly within the source-dependent region of the spectrum.

The spectral amplitudes in the stratosphere at Davis are interesting since they are smaller, particularly at the lowest vertical wavenumbers, than those observed at other stations. The spectral slopes are also more shallow than at other stations. In contrast, the spectral amplitudes within the troposphere are consistent with those found elsewhere which would appear to eliminate weak wave source activity as a cause. An alternative possibility is that the wave spectrum in the lower stratosphere is influenced in some way by the strong background zonal winds that are found over Davis (e.g., as proposed by *Fritts and Lu* [1993]). Generally, these are larger than at any other station studied in this paper. However, the zonal winds over Davis do show a strong seasonal variation with a maximum occurring during winter months. Therefore it would be reasonable to expect seasonal variations of the observed spectral amplitudes since the summer winds are comparable with those observed at other stations. Although they are not shown here, the observed spectra from the stratosphere over Davis show very little seasonal variation and the mean spectrum of Figure 6 is representative of the wave spectrum during all seasons. This appears to suggest that the interaction between the wave spectrum and the background zonal wind field is not responsible for the small spectral amplitudes and energy densities that are observed in the stratosphere over Davis. Our findings will be investigated further as information from other Antarctic stations becomes available.

Figure 14 summarizes the seasonal and latitudinal variations of normalized temperature variance and E_0 at heights near 20 km. The error bars indicate the 95% confidence limits of estimates from each latitude band. This diagram, together with Figure 7, emphasizes the annual cycle in wave activity at low latitudes which is out-of-phase with wave activity at midlatitudes. In all seasons, but especially in summer, there is a strong equatorward gradient in energy density, with E_0 increasing by a factor of about 5 from polar to equatorial latitudes. These results agree well with other studies in the northern hemisphere. *Kitamura and Hirota* [1989] found that wave activity in the midlatitude lower stratosphere over Japan maximized in winter, and that wave activity increased toward the equator. Lidar studies at altitudes of 35 km over western Europe also show an annual cycle of temperature variability with a winter maximum and an equatorward gradient in the temperature fluctuations [*Souprayen*, 1993].

It is possible that Kelvin waves or other equatorially trapped waves have made sizeable contributions to the normalized temperature variances that were observed at low-latitude sites. Without wind velocity measurements, however, it is impossible to study the polarization of waves, and we are therefore unable to determine the significance of this contribution.

It should be noted that E_0 is the measure of wave activity used in the *Fritts and VanZandt* [1993] parameterization scheme. However, other schemes may use different indicators of wave activity. In some cases these parameters can still be estimated from our figures and tables. For example, C. O. Hines (private communication, 1994) has developed a scheme which uses the root-mean-square of the horizontal wind perturbation as the input parameter. This may be estimated from normalized temperature variance measurements using the following equation,

$$\overline{V_H'^2} = \overline{u'^2} + \overline{v'^2} \approx \frac{pg^2}{N^2}\overline{\hat{T}'^2} \tag{14}$$

where V_H' is the first-order perturbation of total horizontal wind velocity. Equation (14) is derived from standard polarization equations by assuming that the spectrum of waves is separable in all variables and that the one-dimensional frequency spectrum is given by $B(\omega) \propto \omega^{-p}$. From Figure 14 and using $p = 5/3$ it can be seen that the root-mean-square of V_H' varies from approximately 1.5 m s^{-1} at Davis to approximately 4.0 m s^{-1} at 10°S.

The local increases in temperature variance and E_0 at the tropopause are interesting features which must also be treated with caution. They may be artifacts due to the high-pass filtering of the temperature profiles in the presence of the sharp gradients at the tropopause. However, we believe that this contribution is not great. To demonstrate this a simulated background temperature profile, $\overline{T}(z)$, was sampled at 50-m intervals over a 4 km height range. For the first 2 km of this range the profile was given by a straight line with a gradient of −6°C per kilometer and for the last 2 km by a straight line with a gradient of 2°C per kilometer. Thus the tropopause was simulated as an abrupt kink in the profile at a position of exactly halfway along the given 4 km height range. This represents an extreme example since the transition is rarely observed to be this sharp. By fitting a second-order polynomial, also sampled at 50-m intervals, to the simulated background profile, it is possible to calculate a normalized temperature variance in the usual manner. This simulates the contribution to the variance from the tropopause in an extreme case. We calculated the normalized temperature variance to be 7.4×10^{-6}. This may then be compared with the observed peak variances at Davis ($\approx 3.5 \times 10^{-5}$), Adelaide ($\approx 2.0 \times 10^{-5}$), and Gove ($\approx 8.0 \times 10^{-5}$) which suggests that the method of analysis is not significantly influencing these results.

The enhancements of wave energy density near the tropopause may be indicative of gravity wave "supersaturation" in this region. *VanZandt and Fritts* [1989] proposed that vertically propagating waves, upon encountering a sudden increase in atmosphere stability, will have larger than saturation amplitudes over a distance of approximately one vertical wavelength. This arises due to the N dependence of vertical wavenumber as defined by the gravity wave dispersion relation. Furthermore, the energy that is dissipated as waves return to their saturation amplitudes can result in enhanced wave drag provided that the spectrum of waves is azimuthally anisotropic [*VanZandt and Fritts*, 1989]. The "supersaturation" hypothesis as well as other possible explanations for these results will be discussed elsewhere.

6. Conclusions

A climatological study of gravity wave activity based on a data set of high-resolution radiosonde measurements has been presented. The utility of radiosonde data in gravity wave studies has also been investigated in some detail. It was found that the radiosonde temperature sensor's slow response at stratospheric heights can cause significant spectral distortion at high vertical wavenumbers. A correction technique was developed to address this concern.

The advantage of using radiosonde measurements for gravity wave research is their extensive geographic and temporal coverage. This allows estimates of important spectral parameters to be made

which are not biased by localized source effects. It also allows seasonal and latitudinal variations of gravity wave activity to be identified. Inspection and comparison of stratosphere power spectra indicate that most of the variations occur at low vertical wavenumbers. The stratosphere spectral amplitudes at high wavenumbers, with the exception of those observed at Davis, are generally consistent with the theoretical saturation limits proposed by *Smith et al.* [1987]. Variations of the gravity wave spectral form within the troposphere are more difficult to interpret. These results are likely to be contaminated by convection and temperature inversions.

Climatological studies of gravity waves are important in defining the extent of wave activity throughout the atmosphere. If theorists and modelers believe that more work of this nature is needed within the lower atmosphere then a global-scale study of radiosonde data will provide an important contribution. All that is needed is for certain stations throughout the world, which are already launching radiosondes on a daily basis, to archive their data at high resolution. However, it should be noted that temperature measurements alone are not sufficient to fully describe the gravity wave field. In particular, the degree of wave field anisotropy is an important parameter which requires wind velocity measurements in order to be estimated.

A. Appendix: Temperature Sensor Response Time

The temperature sensor response times that have been used in obtaining the corrected stratosphere power spectra have themselves been estimated from the results presented in two Vaisala Oy test reports [*Turtiainen*, 1991a,b]. According to *Turtiainen* [1991b], the response time τ of a temperature sensor in a flowing gas is theoretically given by

$$\tau = C_1 + C_2/h \tag{15}$$

where h is the surface heat transfer coefficient and where C_1 and C_2 are constants that depend upon the sensor dimensions and materials. This result has been obtained from *Kerlin et al.* [1982]. The surface heat transfer coefficient is a complicated function of sensor ventilation speed, air density, and air temperature [*Turtiainen*, 1991b], and the height dependence of τ follows from this term. Thus if C_1 and C_2 are known for a given type of sensor then τ can be computed theoretically at any height providing that T, ρ, and the sensor's ventilation speed are known.

The constants C_1 and C_2 were estimated by *Turtiainen* [1991b] for the Vaisala RS80–15 temperature sensor. This was achieved by experimentally determining the response time at ground level conditions for three different ventilation speeds. Thus τ was known for three values of h allowing C_1 and C_2 to be estimated by least squares curve fitting. The values were found to be $C_1 \approx 0$ and $C_2 = 782$. Note that the response time was experimentally determined by measuring the time taken for the sensor to reach 63.2% of a sudden step function increase of environment temperature. Figure 15 displays the height dependence of τ where (A1) has been used and where h was determined using the mean temperature and pressure profiles observed at Adelaide during December 1991. Atmosphere density was calculated from the temperature and pressure measurements using the ideal

gas equation and the sensor ventilation rate was taken to be equivalent to the mean balloon ascent velocity.

In the work by *Turtiainen* [1991a, p. 5] temperature sensor response times were measured using a radiosonde in flight where the step function increase in environment temperature was generated using a heating element attached to the sonde. The results, however, were consistently smaller than the corresponding theoretical values which were calculated using C_1 and C_2 given above. This leads to the conclusion of the report which states that "the response time of RS80 temperature sensor in flight was found to be equal or less than the theoretically computed values presented in the earlier reports." Thus it appears that (A1) with $C_1 = 0$ and $C_2 = 782$ is overestimating the temperature sensor response time within the lower stratosphere given that all measurements by *Turtiainen* [1991a] were made at pressures that were less than or equal to 44 hPa.

As a result of the above problem we believe that it is more appropriate to find C_1 and C_2 for the stratosphere by fitting (A1) to the results presented by *Turtiainen* [1991a]. We have done this for the 12 measurements of response time τ that are given in this report and have been made at various different pressures, temperatures, and ventilation speeds. The parameters were found to be $C_1 = -2.2$ and $C_2 = 724.4$ and the height dependence of τ using these parameters has been plotted in Figure 15 where h was determined, as before, from the mean pressure and temperature profiles observed at Adelaide during December 1991. Clearly, this new curve is not strictly valid near ground level since it underestimates the ground level measurements of τ. Nevertheless, it does provide a superior fit to those measurements of τ that have been made within the stratosphere.

The corrections to the observed power spectra of this study have been calculated using (12) where τ was found from (A1) with $C_1 = -2.2$ and $C_2 = 724.4$. This leads to height-averaged response times that are of the order of 7 to 8 s within the 17 to 24 km altitude range and 1 to 2 s within the 2 to 9 km altitude range. The value of τ between 2 and 9 km is no doubt an underestimate of the true value within this height interval. However, this is not important since even when the parameters $C_1 = 0$ and $C_2 = 782$ are used, the response time is still sufficiently small that the correction for tropospheric power spectra is negligible at all but the very highest wavenumbers. Consequently, all observed tropospheric vertical wavenumber power spectra have not been altered in any way.

The method that has been chosen in order to obtain values for the parameters C_1 and C_2 is not the only plausible procedure. Given the available information, however, we believe that it provides the best estimates of τ within the lower stratosphere. Nevertheless, our approach may result in nonnegligible errors for the response time estimates. These are difficult to quantify and will affect the high-wavenumber spectral slope, t, of corrected power spectra which, as a consequence, may be biased in some way. It is important to note, however, that the spectral parameters m_*, c_*, and E_0 will not be significantly affected by this problem. As a result, only estimates of t from stratosphere power spectra need be treated with some caution.

Another possible source of error for corrected vertical wavenumber power spectra arises due to the assumption that τ is constant in obtaining (12). Figure 15 indicates that τ is not constant within the

height intervals of interest to this study. However, (12) is still valid to good approximation if height-averaged response times are used. To demonstrate this a normalized temperature fluctuation profile has been numerically simulated for altitudes between 17 and 24 km. This was obtained by summing a series of sinusoids with amplitudes that were determined from a standard gravity wave model and by applying the constraints imposed due to the slow response of the radiosonde's temperature sensor.

The fluctuation profile was simulated by first generating a model gravity wave power spectrum using (13) with $2\pi F_0 = 0.05$ m/cycle, $m_*/2\pi = 5.0 \times 10^{-4}$ cycles/m and $t = 3$. A series of 100 sinusoids was then calculated at wavenumbers $m_i = 2\pi \times 10^{-4} i$ where i is an integer between 1 and 100 and where each sinusoid has been assigned a random phase ϕ. The amplitudes, $A_i(m_i)$, were determined from the model spectrum since these are given by the square root of twice the variance within the relevant wavenumber band about wavenumber m_i. The summation of individual sinusoids, sampled at 7-m altitude intervals between 16 and 24 km, gives the simulated environment fluctuation profile. This technique follows the work of *Eckermann* [1990].

The fluctuation profile measured by a radiosonde with temperature sensor response time τ is related to the environment fluctuation profile according to (10) where T and T_s may be replaced by $\hat{T}'$ and $\hat{T}'_s$, respectively, assuming $\overline{T_s}(z)$ does not differ significantly from $\overline{T}(z)$ and assuming $\overline{T}(z)$ is approximately constant over the altitude range of interest. However, if τ is variable in height then (10) cannot be solved analytically. The simulated fluctuation profile was thus obtained using the Runge-Kutta method where $\tau(z)$ was given by the curve of Figure 15 defined by $C_1 = -2.2$ and $C_2 = 724.4$. The first kilometer of data was discarded in order to allow sufficient altitude for any transient effects to become negligible. Thus the final simulated profile comprised data that was sampled at 7-m intervals between 17 and 24 km.

The simulated fluctuation profile was spectrally analyzed using the Blackman-Tukey algorithm and was further modified using (12) where τ was given by the height-averaged response time between 17 and 24 km. Although not shown here, the resultant power spectrum was found to be in good agreement with the original model spectrum. This indicates that (12) is valid to good approximation over 7-km altitude intervals if τ is given by its height-averaged value.

Acknowledgements: The provision of data by the National Climate Centre, Australian Bureau of Meteorology is gratefully acknowledged. We also thank S. K. Avery, S. D. Eckermann, W. K. Hocking, T. Tsuda, and T. E. VanZandt for their helpful suggestions and/or careful reading of earlier versions of the manuscript. This work is supported by the Australian Research Council and S.J.A. acknowledges the support of an Australian Postgraduate Research Award.

References

Bath, M., *Spectral Analysis in Geophysics*, vol. 7, *Developments in Solid Earth Geophysics*, Elsevier Science, New York, 1974.

Cot, C., and J. Barat, A "universal" wave spectrum for atmospheric temperature and velocity fluctuations in the stratosphere?, *Geophys. Res. Lett., 17*, 1577–1580, 1990.

Dewan, E. M., Stratospheric wave spectra resembling turbulence, *Science, 204*, 832–835, 1979.

Dewan, E. M., and R. E. Good, Saturation and the "universal" spectrum for vertical profiles of horizontal scalar winds in the atmosphere, *J. Geophys. Res., 91*, 2742–2748, 1986.

Dewan, E. M., N. Grossbard, A. F. Quesada, and R. E. Good, Spectral analysis of 10 m resolution scalar velocity profiles in the stratosphere, *Geophys. Res. Lett., 11*, 80–83, 1984. (Correction, *Geophys. Res. Lett., 11*, 624, 1984.)

Eckermann, S. D., Effects of nonstationarity on spectral analysis of mesoscale motions in the atmosphere, *J. Geophys. Res., 95*, 16685–16703, 1990.

Eckermann, S. D., and R. A. Vincent, VHF radar observations of gravity-wave production by cold fronts over southern Australia, *J. Atmos. Sci., 50*, 785–806, 1993.

Eckermann, S. D., I. Hirota, and W. K. Hocking, Gravity wave and equatorial wave morphology of the stratosphere derived from long-term rocket soundings, *Q. J. R. Meteorol. Soc.*, in press, 1994.

Ferraz-Mello, S., Estimation of periods from unequally spaced observations, *Astron. J., 86*, 619–624, 1981.

Fritschen, L. J., and L. W. Gay, *Environmental Instrumentation*, Springer-Verlag, New York, 1979.

Fritts, D. C., and W. Lu, Spectral estimates of gravity wave energy and momentum fluxes, II, Parameterization of wave forcing and variability, *J. Atmos. Sci., 50*, 3695–3713, 1993.

Fritts, D. C., and G. D. Nastrom, Sources of mesoscale variability of gravity waves, II, Frontal, convective, and jet stream excitation, *J. Atmos. Sci., 49*, 111-127, 1992.

Fritts, D. C., and T. E. VanZandt, Spectral estimates of gravity wave energy and momentum fluxes, I, Energy dissipation, acceleration, and constraints, *J. Atmos. Sci., 50*, 3685–3694, 1993.

Fritts, D. C., T. Tsuda, T. Sato, S. Fukao, and S. Kato, Observational evidence of a saturated gravity wave spectrum in the troposphere and lower stratosphere, *J. Atmos. Sci., 45*, 1741–1759, 1988.

Fritts, D. C., T. Tsuda, T. E. VanZandt, S. A. Smith, T. Sato, S. Fukao, and S. Kato, Studies of velocity fluctuations in the lower atmosphere using the MU radar, II, Momentum fluxes and energy densities, *J. Atmos. Sci., 47*, 51–66, 1990.

Gage, K. S., Evidence for a $k^{5/3}$ power law inertial range in mesoscale two-dimensional turbulence, *J. Atmos. Sci., 36*, 1950–1954, 1979.

Gage, K. S., and G. D. Nastrom, On the spectrum of atmospheric velocity fluctuations seen by MST/ST radar and their interpretation, *Radio Sci., 20*, 1339–1347, 1985.

Gardner, C. S., and N. F. Gardner, Measurement distortion in aircraft, space shuttle, and balloon observations of atmospheric density and temperature perturbation spectra, *J. Geophys. Res., 98*, 1023–1033, 1993.

Gossard, E. E., and W. H. Hooke, *Waves in the Atmosphere*, Elsevier Science, New York, 1975.

Hamilton, K., Climatological statistics of stratospheric inertia-gravity waves deduced from historical rocketsonde wind and temperature data, *J. Geophys. Res., 96*, 20831–20839, 1991.

Hines, C. O., The saturation of gravity waves in the middle atmosphere, II, Development of Doppler-spread theory, *J. Atmos. Sci., 48*, 1360–1379, 1991.

Hines, C. O., Pseudosaturation of gravity waves in the middle atmosphere: An interpretation of certain lidar observations, *J. Atmos. Terr. Phys., 55*, 441–445, 1993.

Kerlin, T. W., R. L. Shepard, H. M. Hashemian, and K. M. Petersen, *Response of Installed Temperature Sensors. Temperature, Its Measurement and Control in Science and Industry*, vol. 5, American Institute of Physics, New York, 1982.

Kitamura, Y., and I. Hirota, Small-scale disturbances in the lower stratosphere revealed by daily rawin sonde observations, *J. Meteorol. Soc. Jpn., 67*, 817–830, 1989.

Lilly, D. K., Stratified turbulence and the mesoscale variability of the atmosphere, *J. Atmos. Sci., 40*, 749–761, 1983.

Nastrom, G. D., and D. C. Fritts, Sources of mesoscale variability of gravity waves, I, Topographic excitation, *J. Atmos. Sci., 49*, 101–110, 1992.

Sawyer, J. S., Quasi-periodic wind variations with height in the lower stratosphere, *Q. J. R. Meteorol. Soc., 87*, 24–33, 1961.

Senft, D. C., C. A. Hostetler, and C. S. Gardner, Characteristics of gravity wave activity and spectra in the upper stratosphere and upper mesosphere at Arecibo during early April 1989, *J. Atmos. Terr. Phys., 55*, 425–439, 1993.

Sidi, C., J. Lefrere, F. Dalaudier, and J. Barat, An improved atmospheric buoyancy wave spectrum model, *J. Geophys. Res., 93*, 774–790, 1988.

Smith, S. A., D. C. Fritts, and T. E. VanZandt, Evidence for a saturated spectrum of atmospheric gravity waves, *J. Atmos. Sci., 44*, 1404–1410, 1987.

Souprayen, C., Climatologie des ondes de gravite dans l'atmosphere moyenne: Contribution a leur parametrisation dans les modeles numiriques, Ph.D. thesis, l'Univ. Pierre et Marie Curie Paris, 1993.

Thompson, R. O. R. Y., Observation of inertial waves in the stratosphere, *Q. J. R. Meteorol. Soc., 104*, 691–698, 1978.

Tsuda, T., T. Inoue, D. C. Fritts, T. E. VanZandt, S. Kato, T. Sato, and S. Fukao, MST radar observations of a saturated gravity wave spectrum, *J. Atmos. Sci., 46*, 2440–2447, 1989.

Tsuda, T., T. E. VanZandt, M. Mizumoto, S. Kato, and S. Fukao, Spectral analysis of temperature and Brunt-Vaisala frequency fluctuations observed by radiosondes, *J. Geophys. Res., 96*, 17265–17278, 1991.

Turtiainen, H., Response time of RS80 temperature sensor in flight, technical report, Vaisala Oy, Finland, 1991a.

Turtiainen, H., Response time test of Vaisala RS80 temperature sensor, technical report, Vaisala Oy, Finland, 1991b.

VanZandt, T. E., A universal spectrum of buoyancy waves in the atmosphere, *Geophys. Res. Lett., 9*, 575–578, 1982.

VanZandt, T. E., and D. C. Fritts, A theory of enhanced saturation of the gravity wave spectrum due to increases in atmospheric stability, *Pure Appl. Geophys., 130*, 399–420, 1989.

Vincent, R. A., and S. D. Eckermann, VHF radar observations of mesoscale motions in the troposphere: Evidence for gravity wave Doppler shifting, *Radio Sci., 25*, 1019–1037, 1990.

Weinstock, J., Saturated and unsaturated spectra of gravity waves and scale dependent diffusion, *J. Atmos. Sci., 47*, 2211–2225, 1990.

Wilson, R., M. L. Chanin, and A. Hauchecorne, Gravity waves in the middle atmosphere observed by Rayleigh lidar, 2, Climatology, *J. Geophys. Res., 96*, 5169–5183, 1991.

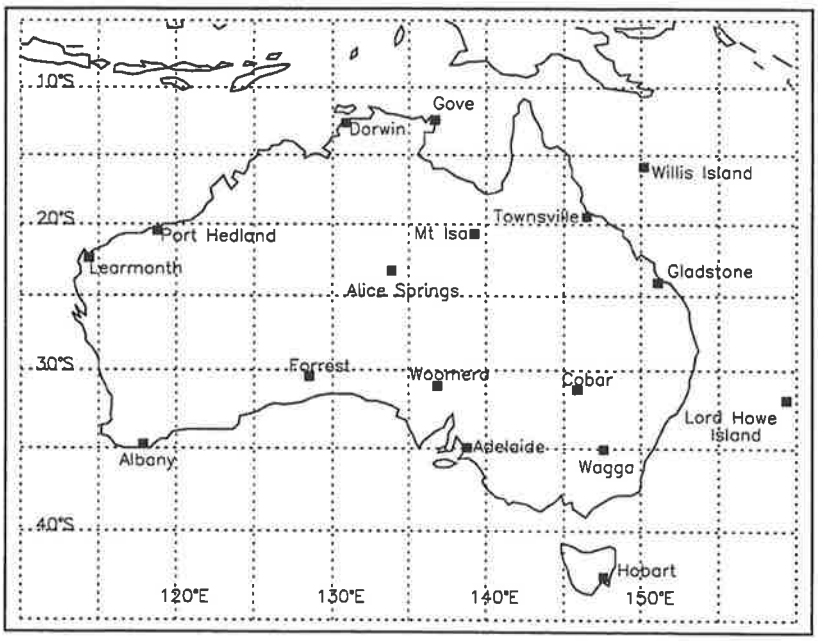

Figure 1: The geographic distribution of radiosonde stations used in the study. Davis (69°S, 78°E), in Antarctica, is not shown.

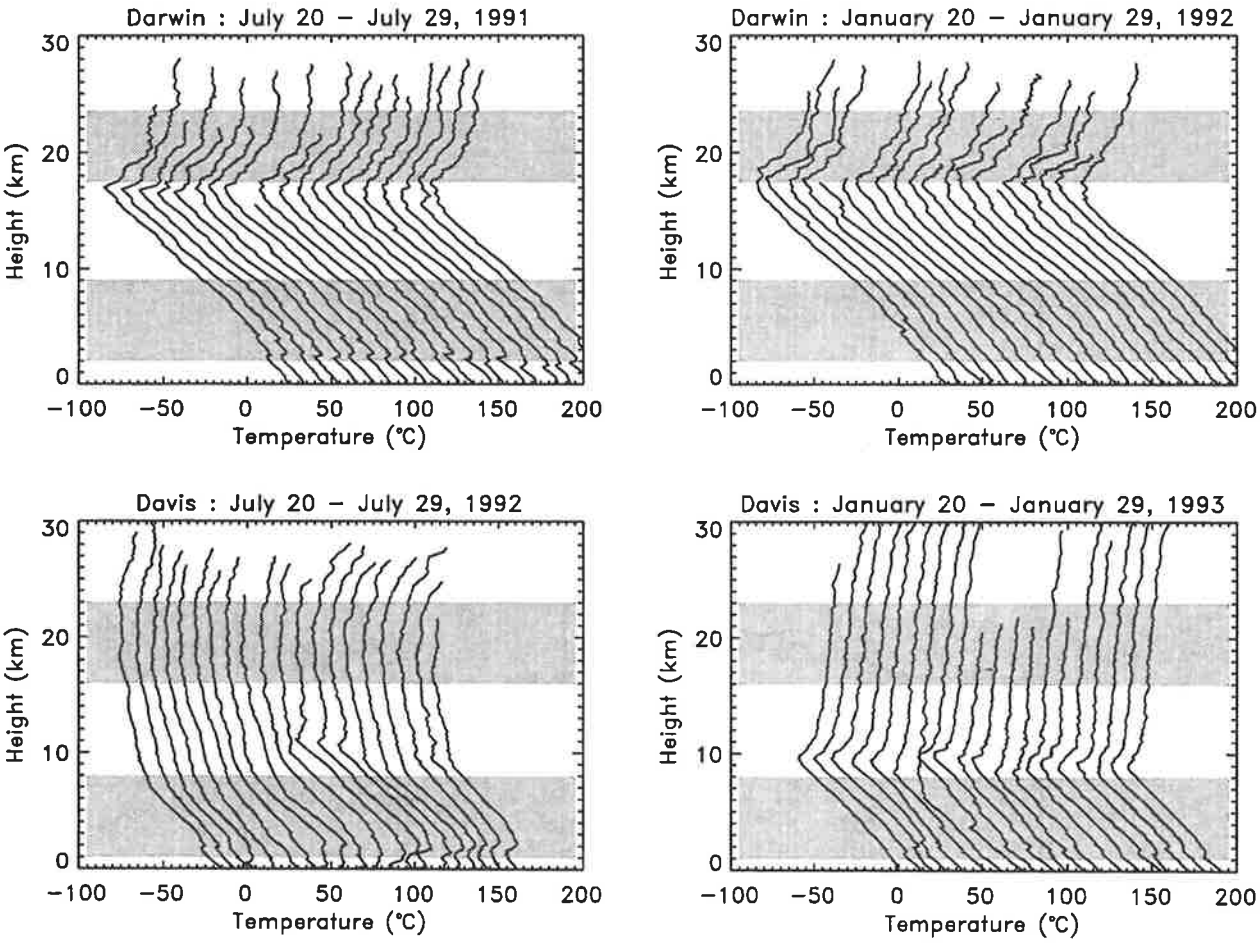

Figure 2: Examples of temperature profiles observed at Darwin (12°S, 131°E) and Davis (69°S, 78°E) during the months of January and July. Radiosondes were launched at 12-hour intervals during these periods. Successive profiles are displaced by 10°C, and the shaded areas correspond to the height ranges for which temperature profiles were spectrally analyzed.

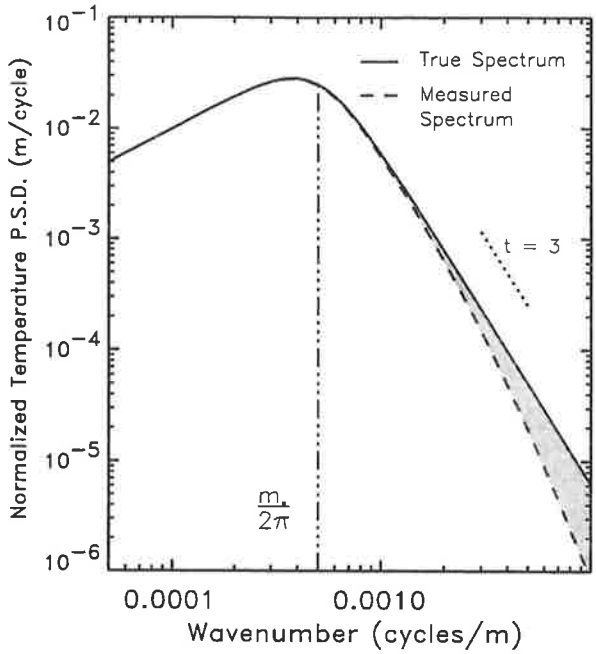

Figure 3: The theoretical distortion of a modified-Desaubies vertical wavenumber power spectrum measured by a radiosonde with temperature sensor response time $\tau = 8$ s and with vertical ascent velocity $V_0 = 5\ \mathrm{m\,s^{-1}}$. The shaded region comprises 4% of the total area under the modified-Desaubies spectrum.

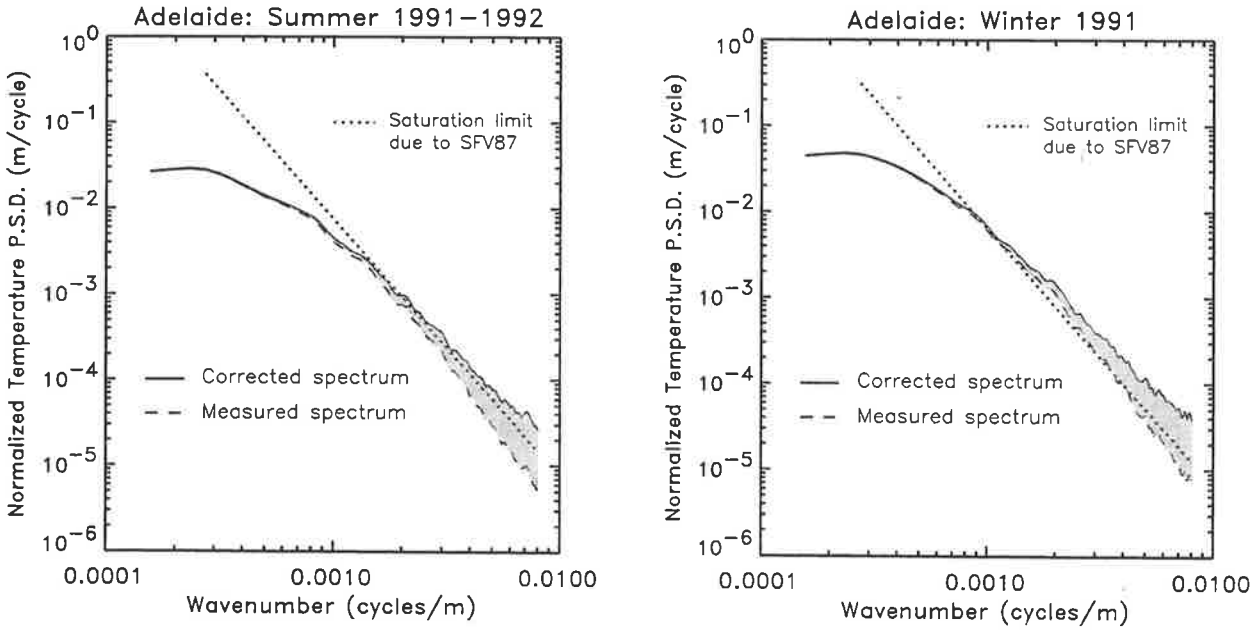

Figure 4: The mean vertical wavenumber power spectra of normalized temperature fluctuations (dashed lines) observed at Adelaide (35°S, 139°E) for both summer and winter months. All spectra were calculated within the 17–24 km altitude range. Also plotted are the corrected spectra (solid lines), where the correction technique is described in the text, and the theoretical saturation limits of *Smith et al.* [1987] (denoted by SFV87). The shaded regions comprise approximately 5% of the total area under each corrected spectrum.

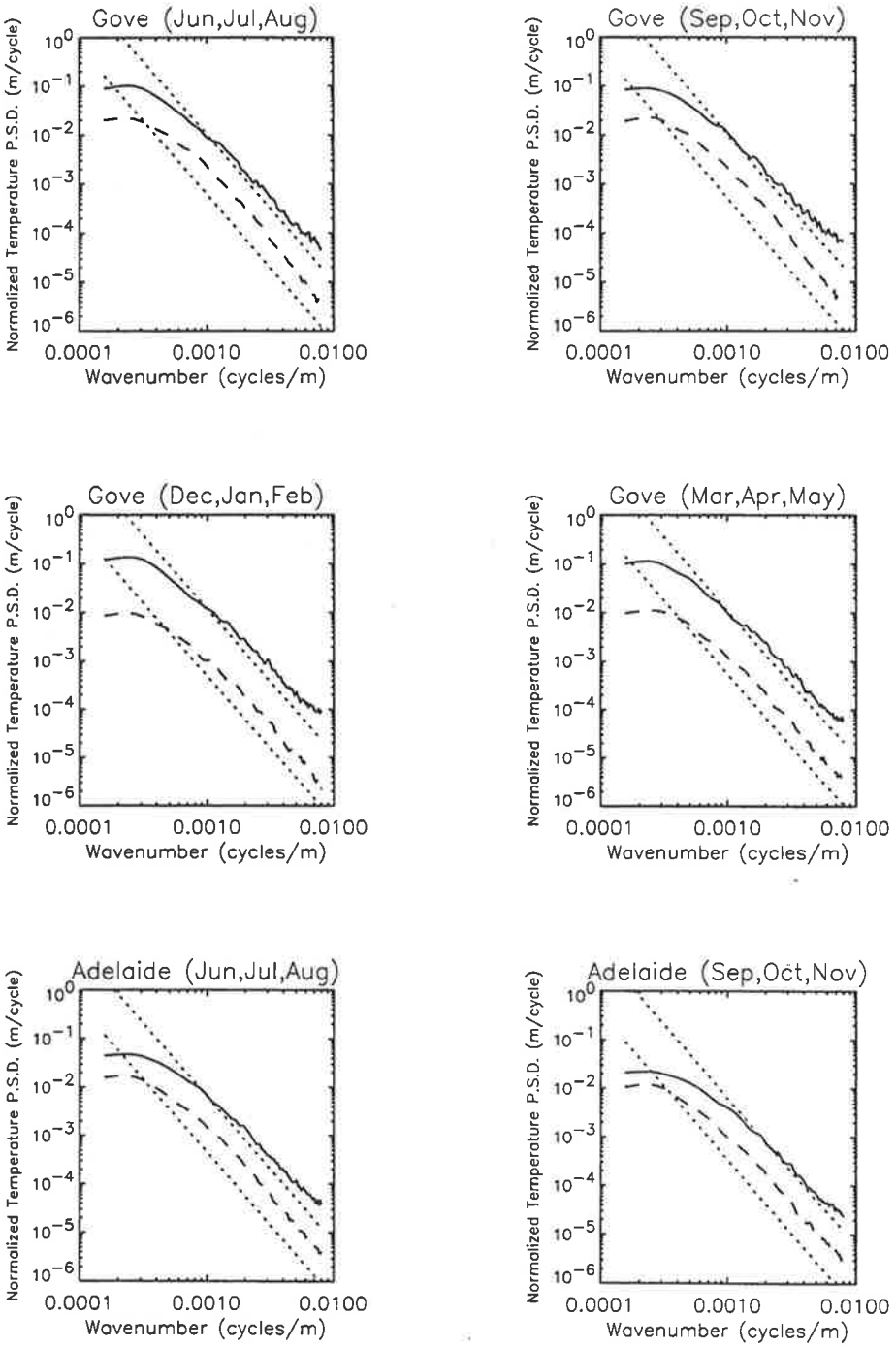

Figure 5: Vertical wavenumber power spectra of normalized temperature fluctuations for the troposphere (dashed lines) and lower stratosphere (solid lines). The theoretical saturation limits of *Smith et al.* [1987] are also plotted for comparison purposes (dotted lines). Each spectrum is a 3-month average, and results from Gove, Adelaide, and Hobart are presented. The 95% confidence limits are approximately given by 0.85 and 1.15 multiplied by the spectral amplitude at each wavenumber.

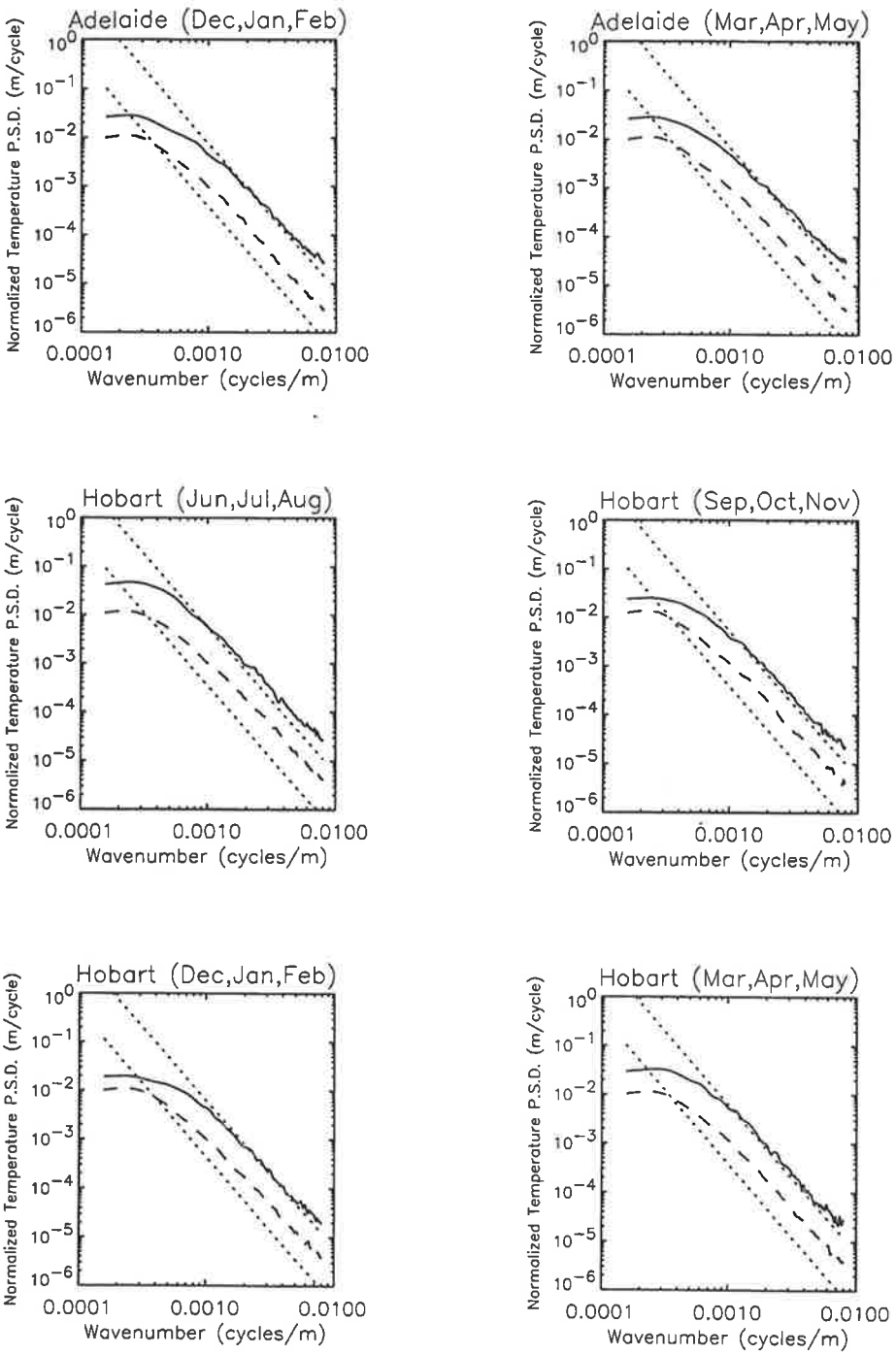

Figure 5: (Continued)

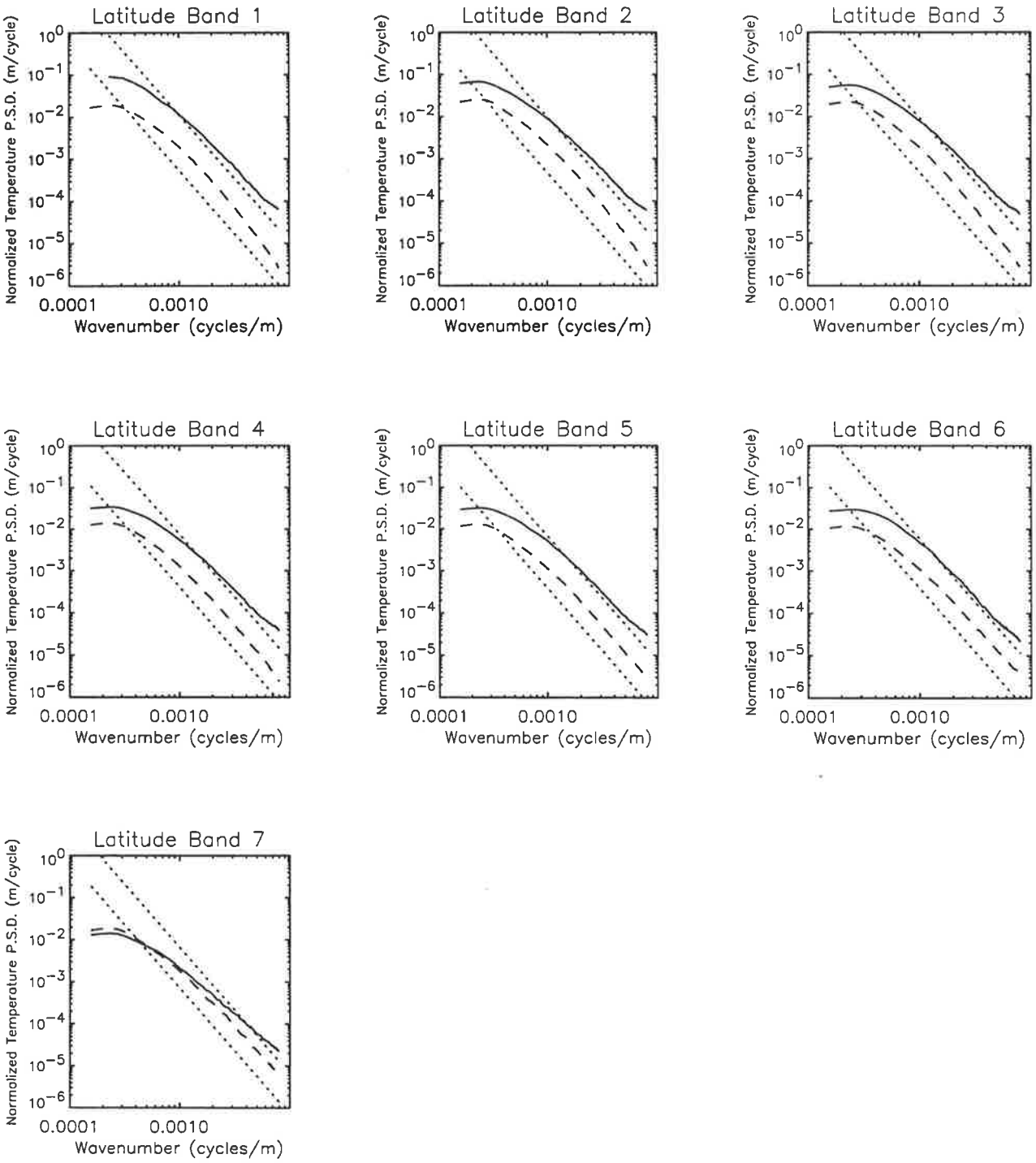

Figure 6: Vertical wavenumber power spectra of normalized temperature fluctuations for the troposphere (dashed lines) and lower stratosphere (solid lines). The theoretical saturation limits of *Smith et al.* [1987] are also plotted for comparison purposes (dotted lines). Each spectrum is the result of averaging all individual power spectra into seven latitude bands as described in Table 2. The 95% confidence limits are approximately given by 0.95 and 1.05 multiplied by the spectral amplitude at each wavenumber.

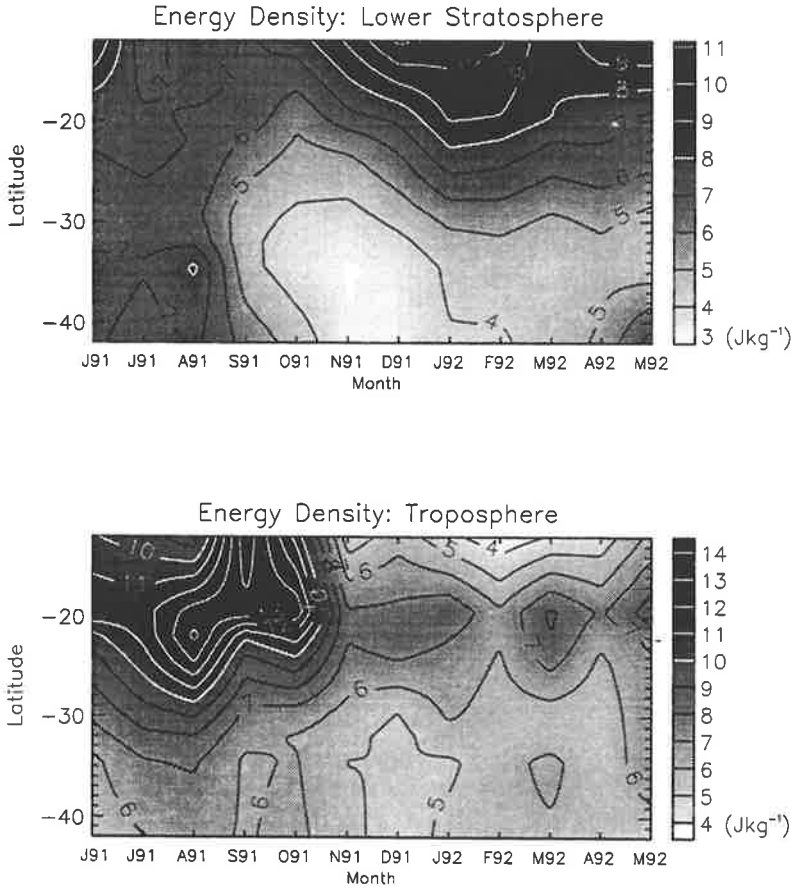

Figure 7: Time-latitude contours of total gravity wave energy density, E_0, for the troposphere and lower stratosphere. The energy density is calculated using (6) where $\overline{\tilde{T}'^2}$ is the normalized temperature variance within the height intervals described in Table 1.

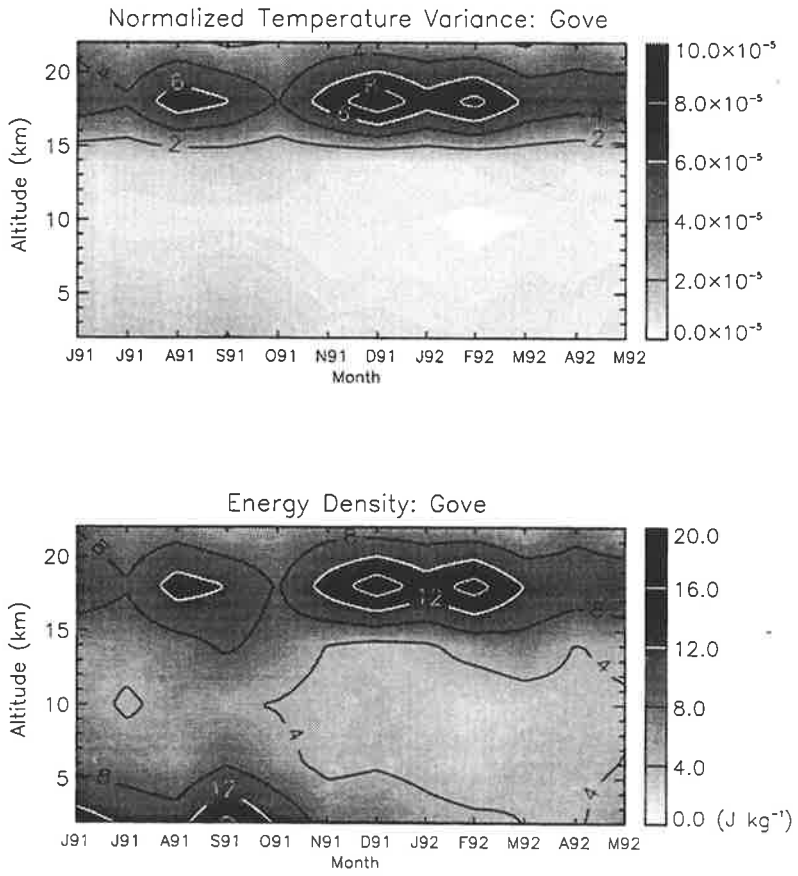

Figure 8: Time-height contours of normalized temperature variance and total gravity wave energy density observed at Gove between June 1991 and May 1992. The raw data have been interpolated to produce a smoother contour pattern.

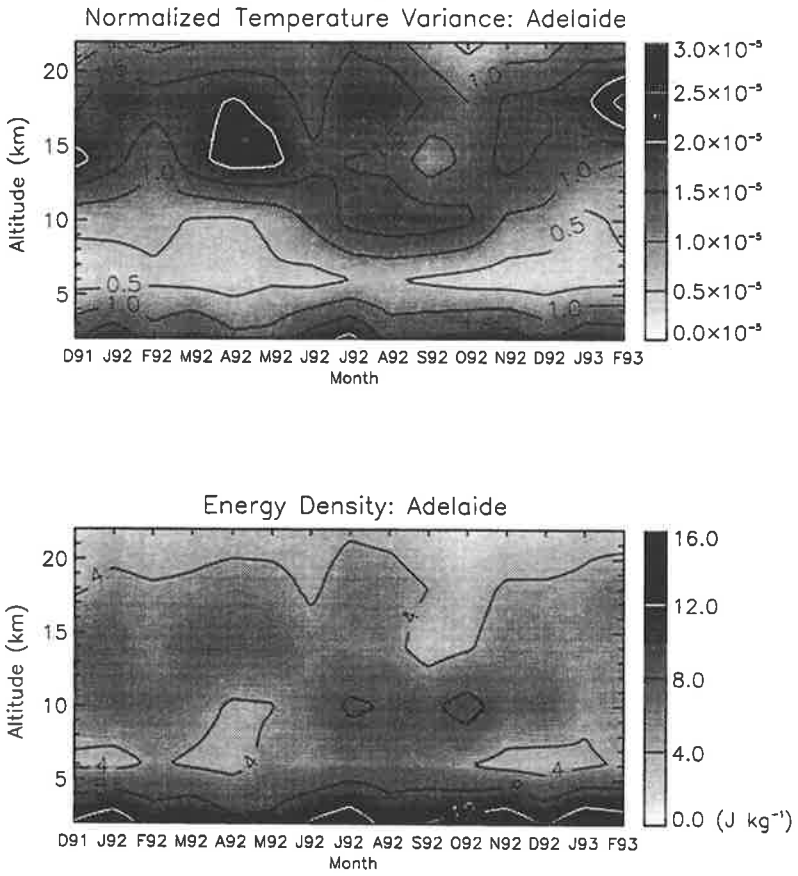

Figure 9: Time-height contours of normalized temperature variance and total gravity wave energy density observed at Adelaide between December 1991 and February 1993. The raw data have been interpolated to produce a smoother contour pattern.

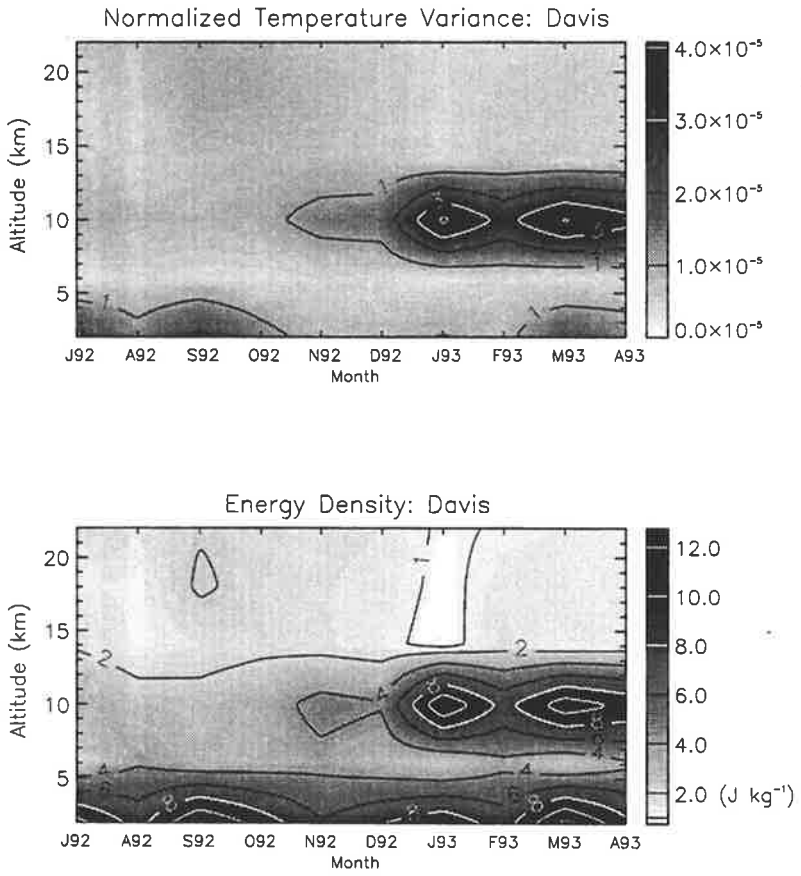

Figure 10: Time-height contours of normalized temperature variance and total gravity wave energy density observed at Davis between July 1992 and April 1993. The raw data have been interpolated to produce a smoother contour pattern.

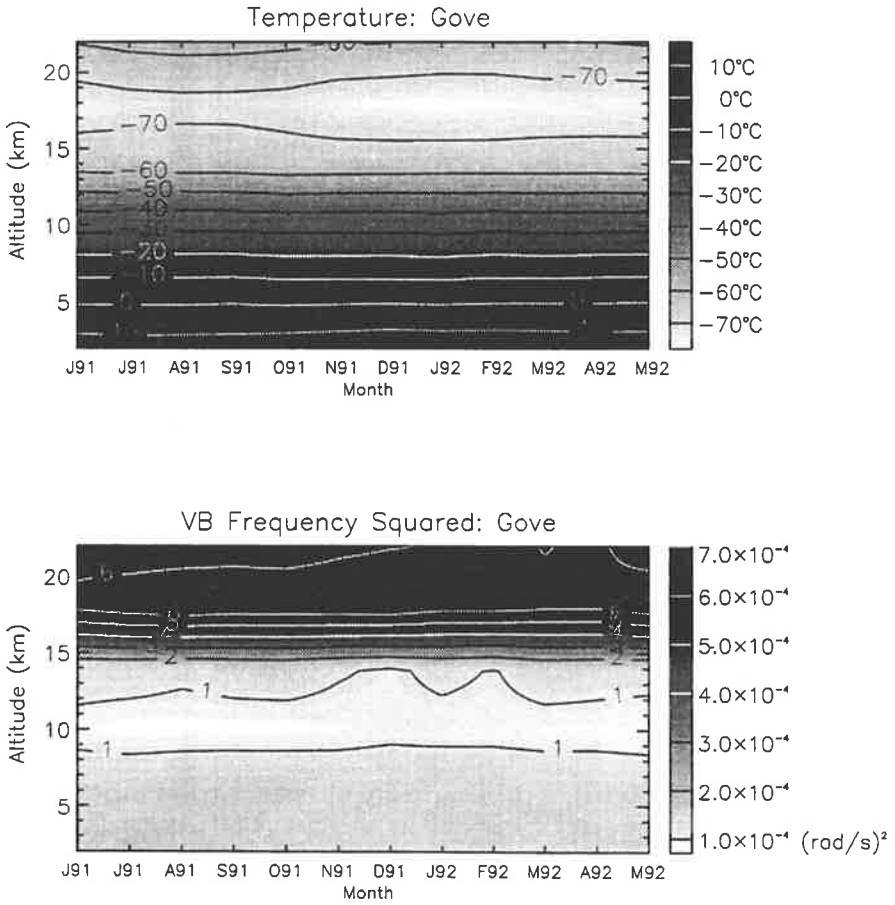

Figure 11: Time-height contours of temperature and Vaisala-Brunt frequency squared observed at Gove between June 1991 and May 1992. The raw data have been interpolated to produce a smoother contour pattern.

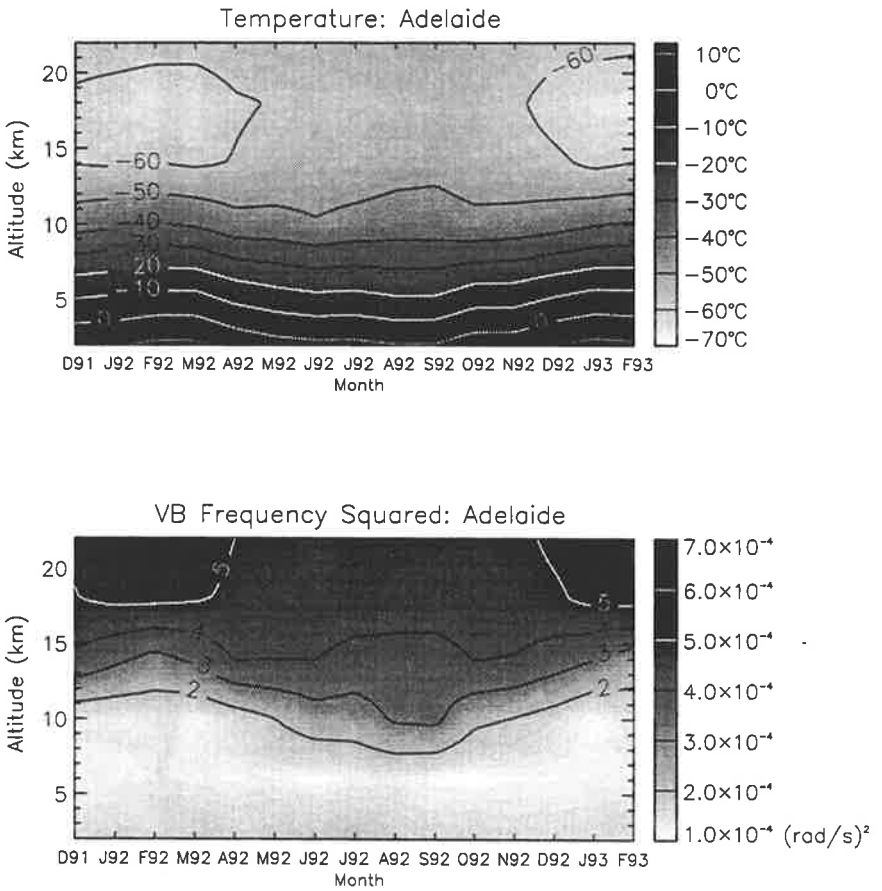

Figure 12: Time-height contours of temperature and Vaisala-Brunt frequency squared observed at Adelaide between December 1991 and February 1993. The raw data have been interpolated to produce a smoother contour pattern.

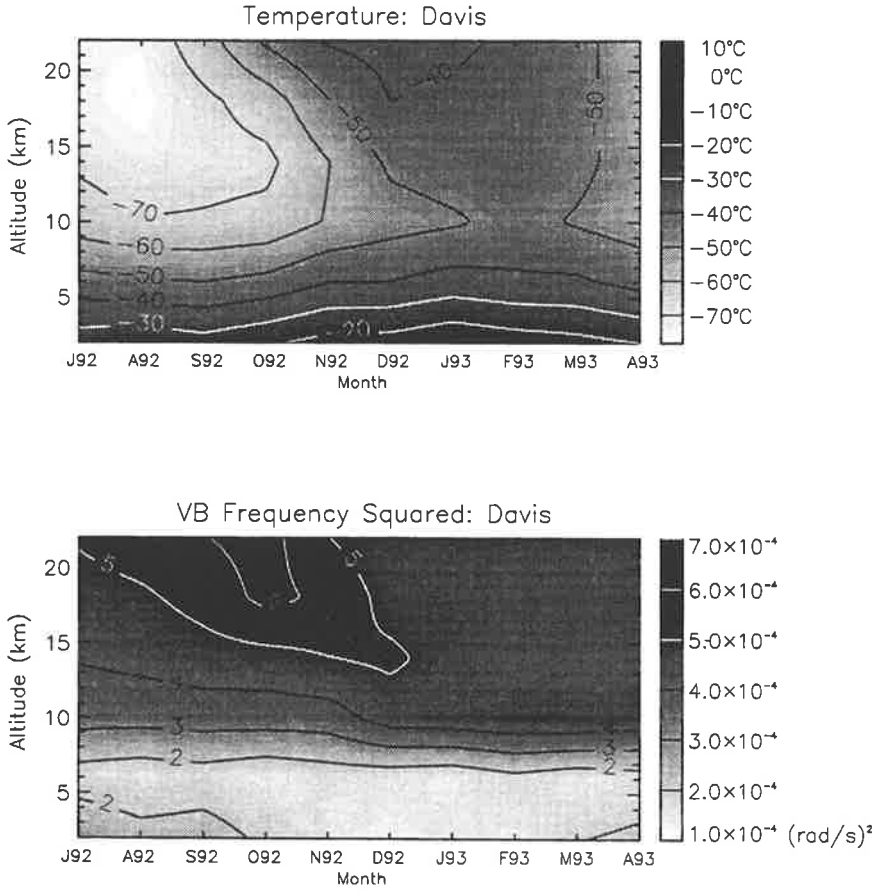

Figure 13: Time-height contours of temperature and Vaisala-Brunt frequency squared observed at Davis between July 1992 and April 1993. The raw data have been interpolated to produce a smoother contour pattern.

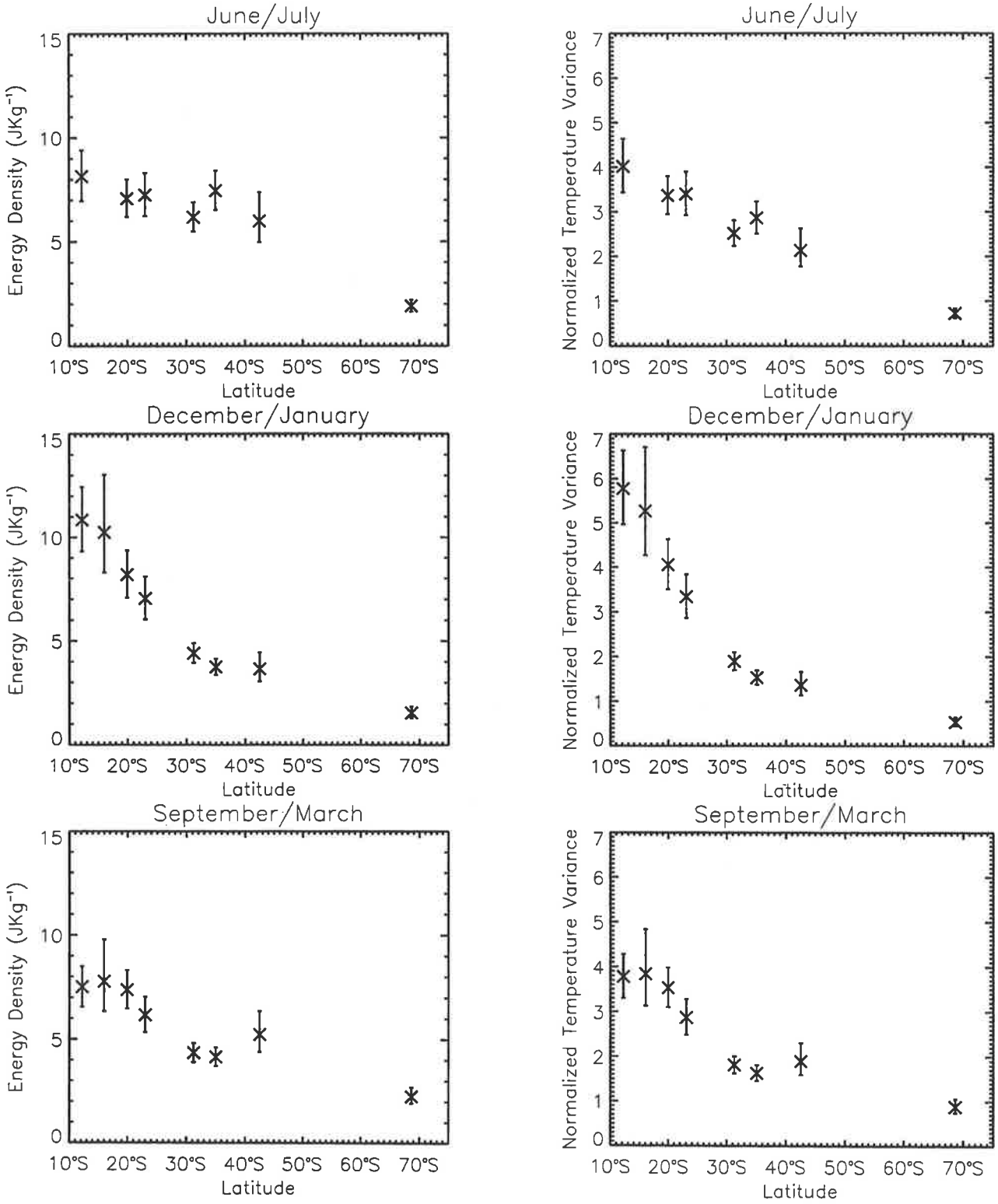

Figure 14: The variation of normalized temperature variance and gravity wave energy density as a function of latitude within the lower stratosphere (17.0 to 24.0 km in most cases). Data from the various stations have been averaged into latitude bands as described in Table 2 and over 2-month periods in each case. Furthermore, the results from Willis Island are included for the months of December/January and September/March. Normalized temperature variance estimates have been multiplied by a factor of 10^5 and error bars indicate the 95% confidence limits of each estimate.

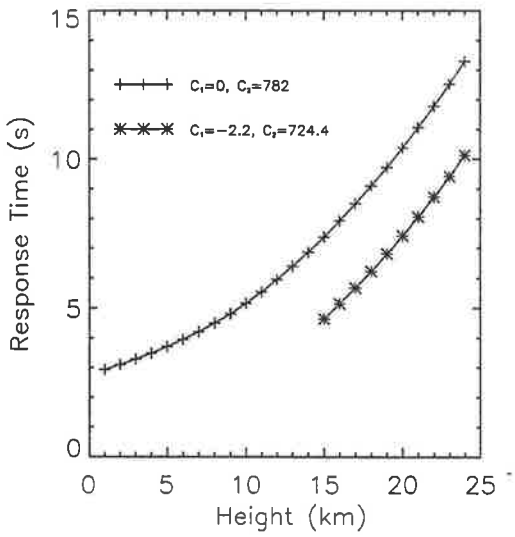

Figure 15: The height dependence of temperature sensor response time for different values of C_1 and C_2 (see text for more details). The response time was calculated using (A1) where the surface heat transfer coefficient, a function of temperature and density, was determined using the mean temperature and pressure profiles observed at Adelaide during December 1991.

Table 1. Information Concerning the Radiosonde Data Used in the Study

Station Name	WMO Station Number	Location deg South, deg East	Height Intervals for Data Analysis, km		Time Intervals	Total Number of Available Soundings	Number of Soundings Analyzed	
			Troposphere	Stratosphere			Troposphere	Stratosphere
Adelaide	94672	35.0, 138.5	2.0–9.0	17.0–24.0	May 1991 – Feb. 1993	1344	1224	909
Albany	94802	35.0, 117.5	2.0–9.0	17.0–24.0	March 1991 – May 1992	519	481	364
Alice Springs	94326	23.4, 133.5	2.0–9.0	17.0–24.0	May 1991 – May 1992	366	336	244
Cobar	94711	31.3, 145.5	2.0–9.0	17.0–24.0	April 1991 – May 1992	528	498	373
Darwin	94120	12.2, 130.5	2.0–9.0	17.5–23.5	June 1991 – May 1992	730	655	453
Davis	89571	68.6, 78.0	1.0–8.0	16.0–23.0	July 1992 – April 1993	556	481	435
Forrest	94646	30.5, 128.1	2.0–9.0	17.0–24.0	April 1991 – May 1992	421	402	343
Gladstone	94380	23.5, 151.2	2.0–9.0	17.0–24.0	June 1991 – May 1992	435	408	263
Gove	94150	12.2, 136.5	2.0–9.0	17.5–24.5	June 1991 – May 1992	457	431	313
Hobart	94975	42.5, 147.2	2.0–9.0	16.0–23.0	April 1991 – May 1992	852	799	452
Learmonth	94302	22.1, 114.0	2.0–9.0	17.0–24.0	June 1991 – May 1992	348	339	239
Lord Howe Island	94995	32, 159	2.0–9.0	17.0–24.0	June 1991 – May 1992	444	401	287
Mount Isa	94332	20.4, 139.3	2.0–9.0	17.0–24.0	April 1991 – May 1992	575	520	350
Port Hedland	94312	20.2, 118.4	2.0–9.0	18.0–25.0	Nov. 1990 – May 1992	531	519	474
Townsville	94292	19.2, 146.5	2.0–9.0	17.0–24.0	June 1991 – May 1992	341	334	234
Wagga	94910	35.1, 147.2	2.0–9.0	17.0–24.0	May 1991 – May 1992	485	447	331
Willis Island	94299	16, 150	2.0–9.0	17.5–24.5	Aug. 1991 – May 1992	304	286	249
Woomera	94659	31.1, 136.5	2.0–9.0	17.0–24.0	April 1991 – May 1992	544	505	393

Table 2. The Division of Stations Into Seven Latitude Bands

Latitude Band	Radiosonde Stations	Number of Profiles Analyzed	
		Stratosphere	Troposphere
1	Gove, Darwin	766	1086
2	Mt. Isa, Townsville, Port Hedland	1058	1373
3	Gladstone, Learmonth, Alice Springs	746	1083
4	Forrest, Woomera, Cobar, Lord Howe Island	1396	1806
5	Wagga, Albany, Adelaide	1252	1660
6	Hobart	452	799
7	Davis	435	481

Table 3. Spectral Parameter Estimates

Station	t		$m_*/2\pi$, Cycles per Meter		c_*, m s^{-1}		E_0, J kg^{-1}	
	Tr	St	Tr	St	Tr	St	Tr	St
Adelaide	2.8	2.5	3.8×10^{-4}	4.0×10^{-4}	4.7	9.0	5.7	4.5
Albany	2.8	2.6	3.8×10^{-4}	4.0×10^{-4}	4.7	9.0	6.0	4.5
Alice Springs	3.1	2.5	4.2×10^{-4}	3.7×10^{-4}	4.5	10.5	9.1	6.4
Cobar	3.0	2.5	4.1×10^{-4}	3.7×10^{-4}	4.4	9.9	6.5	4.9
Darwin	3.1	2.6	4.8×10^{-4}	4.2×10^{-4}	4.0	9.9	7.7	8.1
Davis	2.7	2.2	3.6×10^{-4}	3.3×10^{-4}	5.8	10.8	6.3	2.0
Forrest	3.0	2.4	4.3×10^{-4}	3.8×10^{-4}	4.2	9.7	6.5	4.6
Gladstone	3.0	2.5	4.0×10^{-4}	3.6×10^{-4}	4.8	10.9	8.0	6.4
Gove	3.0	2.5	4.5×10^{-4}	3.3×10^{-4}	4.3	12.5	6.6	9.8
Hobart	2.7	2.6	3.5×10^{-4}	4.1×10^{-4}	5.0	8.7	5.5	5.1
Learmonth	3.1	2.5	4.4×10^{-4}	3.9×10^{-4}	4.2	10.3	8.6	6.9
Lord Howe Island	2.9	2.4	4.2×10^{-4}	3.9×10^{-4}	4.3	9.5	5.6	3.9
Mount Isa	3.0	2.5	4.3×10^{-4}	3.7×10^{-4}	4.4	11.8	9.5	7.5
Port Hedland	3.1	2.5	4.6×10^{-4}	3.5×10^{-4}	3.9	11.4	10.5	7.1
Townsville	3.0	2.5	4.2×10^{-4}	4.0×10^{-4}	4.6	10.5	9.3	7.5
Wagga	2.8	2.5	3.7×10^{-4}	3.9×10^{-4}	4.7	9.3	5.8	5.0
Willis Island	3.0	2.5	4.5×10^{-4}	3.3×10^{-4}	4.3	12.3	7.2	8.4
Woomera	2.8	2.5	3.7×10^{-4}	3.9×10^{-4}	4.8	9.5	6.1	5.3

Tr = Troposphere, St = Stratosphere

References

Alexander, M. J., J. R. Holton, and D. R. Durran, The gravity wave response above deep convection in a squall line simulation, *J. Atmos. Sci., 52*, 2212–2226, 1995.

Allen, K. R., and R. I. Joseph, A canonical statistical theory of oceanic internal waves, *J. Fluid Mech., 204*, 185–228, 1989.

Allen, S. J., and R. A. Vincent, Gravity wave activity in the lower atmosphere: Seasonal and latitudinal variations, *J. Geophys. Res., 100*, 1327–1350, 1995.

Andrews, D. G., The influence of atmospheric waves on the general circulation of the middle atmosphere, *Phil. Trans. R. Soc. London Ser. A, 323*, 693–705, 1987.

Andrews, D. G., and M. E. McIntyre, Planetary waves in horizontal and vertical shear: The generalized Eliassen-Palm relation and the mean zonal acceleration, *J. Atmos. Sci., 33*, 2031–2048, 1976.

Andrews, D. G., and M. E. McIntyre, Generalized Eliassen-Palm and Charney-Drazin theorems for waves on axisymmetric mean flows in compressible atmospheres, *J. Atmos. Sci., 35*, 175–185, 1978a.

Andrews, D. G., and M. E. McIntyre, On the wave-action and its relatives, *J. Fluid Mech., 89*, 647–664, 1978b.

Andrews, D. G., J. R. Holton, and C. B. Leovy, *Middle Atmosphere Dynamics*, Academic Press, Orlando, 1987.

Bacmeister, J. T., M. R. Schoeberl, L. R. Lait, P. A. Newman, and B. Gary, ER-2 mountain wave encounter over Antarctica: Evidence for blocking, *Geophys. Res. Lett., 17*, 81–84, 1990.

Balsley, B. B., and D. A. Carter, The spectrum of atmospheric velocity fluctuations at 8 km and 86 km, *Geophys. Res. Lett., 9*, 465–468, 1982.

Balsley, B. B., and D. A. Carter, Mountain waves in the tropical Pacific atmosphere: A comparison of vertical wind fluctuations over Pohnpei and Christmas Island using VHF wind profilers, *J. Atmos. Sci., 46*, 2698–2715, 1989.

Balsley, B. B., and R. Garello, The kinetic energy density in the troposphere, stratosphere and mesosphere: A preliminary study using the Poker Flat MST radar in Alaska, *Radio Sci., 20*, 1355–1361, 1985.

Banks, P. M., and G. Kockarts, *Aeronomy*, Academic Press, New York, 1973.

Barat, J., and C. Cot, Wind shear rotary spectra in the atmosphere, *Geophys. Res. Lett., 19*, 103–106, 1992.

Bath, M., *Spectral Analysis in Geophysics*, vol. 7, *Developments in Solid Earth Geophysics*, Elsevier Science, New York, 1974.

Bauer, S. J., *Physics of Planetary Ionospheres*, Springer-Verlag, Berlin, 1973.

Beatty, T. J., C. A. Hostetler, and C. S. Gardner, Lidar observations of gravity waves and their spectra near the mesopause and stratopause at Arecibo, *J. Atmos. Sci., 49*, 477–496, 1992.

Bevington, P. R., *Data Reduction and Error Analysis for the Physical Sciences*, McGraw-Hill, New York, 1969.

Blackman, R. B., and J. W. Tukey, *The Measurement of Power Spectra From the Point of View of Communications Engineering*, Dover Publications, New York, 1958.

Blumen, W., Geostrophic Adjustment, *Rev. Geophys. Space Phys., 10*, 485–528, 1972.

Booker, J. R., and F. P. Bretherton, The critical layer for internal gravity waves in a shear flow, *J. Fluid Mech., 27*, 513–539, 1967.

Born, M., and E. Wolf, *Principles of Optics*, Pergamon Press, Sydney, 1970.

Bracewell, R. N., *The Fourier Transform and its Applications*, McGraw-Hill, Singapore, 1986.

Brasseur, G., and S. Solomon, *Aeronomy of the Middle Atmosphere*, D. Reidel Publishing Company, Dordrecht-Holland, 1984.

Bretherton, F. P., The propagation of groups of internal gravity waves in a shear flow, *Q. J. R. Meteorol. Soc., 92*, 466–480, 1966.

Bretherton, F. P., On the mean motion induced by internal gravity waves, *J. Fluid Mech., 36*, 785–803, 1969.

Bretherton, F. P., and C. J. R. Garrett, Wave trains in inhomogeneous moving media, *Proc. R. Soc. London Ser. A, 302*, 529–554, 1968.

Brillinger, D. R., The spectral analysis of stationary interval functions, in *Proceedings of the 6th Berkely Symposium on Mathematical Statistics and Probability*, edited by L. Lecam, J. Neyman, and E. L. Scott, 483–513, University of California Press, Berkely, 1972.

Brillinger, D. R., Statistical inference for irregularly observed processes, in *Time Series Analysis of Irregularly Observed Data, Lect. Notes in Statis. 25*, edited by E. M. Parzen, 38–57, Springer-Verlag, New York, 1983.

Brown, P. R. A., Aircraft measurements of mountain waves and their associated momentum flux over the British Isles, *Q. J. R. Meteorol. Soc., 109*, 849–865, 1983.

Cadet, D., and H. Teitelbaum, Observational evidence of internal inertia-gravity waves in the tropical stratosphere, *J. Atmos. Sci., 36*, 892–907, 1979.

Cho, J. Y. N., Inertio-gravity wave parameter estimation from cross-spectral analysis, *J. Geophys. Res., 100*, 18727–18737, 1995.

CIRA 1972, *COSPAR International Reference Atmosphere*, Akademie-Verlag, Berlin, 1972.

CIRA 1986, *COSPAR International Reference Atmosphere: 1986*, Part II: Middle Atmosphere Models, Pergamon Press, 1990.

Clarke, R. H., The morning glory: An atmospheric hydraulic jump, *J. Appl. Meteor., 11*, 304–311, 1972.

Clarke, R. H., On the mortality of morning glories, *Aust. Met. Mag., 37*, 167–172, 1989.

Cocos (Keeling) Islands Annual Report 1986–87, Department of Territories, Australian Government Publishing Service, Canberra, 1988.

Cornish, C. R., and M. F. Larsen, Observations of low-frequency inertia-gravity waves in the lower stratosphere over Arecibo, *J. Atmos. Sci., 46*, 2428–2439, 1989.

Cot, C., and J. Barat, Spectral analysis of high resolution temperature profiles in the stratosphere, *Geophys. Res. Lett., 16*, 1165–1168, 1989.

Cot, C., and J. Barat, A "universal" wave spectrum for atmospheric temperature and velocity fluctuations in the stratosphere?, *Geophys. Res. Lett., 17*, 1577–1580, 1990.

Crohn, P. W., The geology and geomorphology of Macquarie Island with special emphasis on heavy metal trace element distribution, *ANARE Research Notes, 39*, 1986.

Crook, N. A., Trapping of low-level internal gravity waves, *J. Atmos. Sci., 45*, 1533–1541, 1988.

De la Torre, A., A. Giraldez, and P. Alexander, Saturated gravity wave spectra measured with balloons in Mendoza (Argentina), *Geophys. Res. Lett., 21*, 2039–2042, 1994.

Dewan, E. M., Stratospheric wave spectra resembling turbulence, *Science, 204*, 832–835, 1979.

Dewan, E. M., The saturated-cascade model for atmospheric gravity wave spectra, and the wavelength-period (W-P) relations, *Geophys. Res. Lett., 21*, 817–820, 1994.

Dewan, E. M., and R. E. Good, Saturation and the "universal" spectrum for vertical profiles of horizontal scalar winds in the atmosphere, *J. Geophys. Res., 91*, 2742–2748, 1986.

Dewan, E. M., N. Grossbard, R. E. Good, and J. Brown, Power spectral densities of zonal and meridional winds in the stratosphere, *Physica Scripta, 37*, 154–157, 1988.

Dewan, E. M., N. Grossbard, A. F. Quesada, and R. E. Good, Spectral analysis of 10 m resolution scalar velocity profiles in the stratosphere, *Geophys. Res. Lett., 11*, 80–83, 1984. (Correction, *Geophys. Res. Lett., 11*, 624, 1984.)

Dunkerton, T. J., Theory of the mesopause semiannual oscillation, *J. Atmos. Sci., 39*, 2681–2690, 1982.

Dunkerton, T. J., and D. P. Delisi, Climatology of the equatorial lower stratosphere, *J. Atmos. Sci., 42*, 376–396, 1985.

Eckermann, S. D., Atmospheric gravity waves: Observations and theory, Ph.D. thesis, University of Adelaide, 1990a.

Eckermann, S. D., Effects of nonstationarity on spectral analysis of mesoscale motions in the atmosphere, *J. Geophys. Res., 95,* 16685–16703, 1990b.

Eckermann, S. D., Effect of background winds on vertical wavenumber spectra of atmospheric gravity waves, *J. Geophys. Res., 100*, 14097–14112, 1995.

Eckermann, S. D., Hodographic analysis of gravity waves: Relationships among Stokes parameters, rotary spectra, and cross-spectral methods, *J. Geophys. Res.*, in press, 1996.

Eckermann, S. D., and W. K. Hocking, Effect of superposition on measurements of atmospheric gravity waves: A cautionary note and some reinterpretations, *J. Geophys. Res., 94*, 6333–6339, 1989.

Eckermann, S. D., and R. A. Vincent, Falling sphere observations of anisotropic gravity wave motions in the upper stratosphere over Australia, *Pure Appl. Geophys., 130*, 509–532, 1989.

Eckermann, S. D., and R. A. Vincent, VHF radar observations of gravity-wave production by cold fronts over southern Australia, *J. Atmos. Sci., 50*, 785–806, 1993.

Eckermann, S. D., S. J. Allen, and R. A. Vincent, Computation of gravity-wave Eliassen-Palm fluxes from contemporaneous horizontal-velocity and temperature data: A feasibility study, Manuscript in Preparation, 1996.

Eckermann, S. D., I. Hirota, and W. K. Hocking, Gravity wave and equatorial wave morphology of the stratosphere derived from long-term rocket soundings, *Q. J. R. Meteorol. Soc., 121*, 149–186, 1995.

Ecklund, W. L., B. B. Balsley, M. Crochet, D. A. Carter, A. C. Riddle, and R. Garello, Vertical wind speed power spectra from the troposphere and stratosphere obtained under light wind conditions, *Handbook for MAP, 9*, 269, 1983.

Eliassen, A., and E. Palm, On the transfer of energy in stationary mountain waves, *Geofys. Publik., 22*, 1–23, 1961.

Endlich, R. M., R. C. Singleton, and J. W. Kaufman, Spectral analysis of detailed vertical wind speed profiles, *J. Atmos. Sci., 26*, 1030–1041, 1969.

Ferraz-Mello, S., Estimation of periods from unequally spaced observations, *Astron. J., 86*, 619–624, 1981.

Forbes, A. M. G., Fourier transform filtering: A cautionary note, *J. Geophys. Res., 93*, 6958–6962, 1988.

Fritschen, L. J., and L. W. Gay, *Environmental Instrumentation*, Springer-Verlag, New York, 1979.

Fritts, D. C., Gravity wave saturation in the middle atmosphere: A review of theory and observations, *Rev. Geophys. Space Phys., 22*, 275–308, 1984.

Fritts, D. C., and H.-G. Chou, An investigation of the vertical wavenumber and frequency spectra of gravity wave motions in the lower stratosphere, *J. Atmos. Sci., 44*, 3610–3624, 1987.

Fritts, D. C., and W. Lu, Spectral estimates of gravity wave energy and momentum fluxes, II, Parameterization of wave forcing and variability, *J. Atmos. Sci., 50*, 3695–3713, 1993.

Fritts, D. C., and Z. Luo, Gravity wave excitation by geostrophic adjustment of the jet stream, part I: Two-dimensional forcing, *J. Atmos. Sci., 49*, 681–697, 1992.

Fritts, D. C., and T. E. VanZandt, Effects of Doppler shifting on the frequency spectra of atmospheric gravity waves, *J. Geophys. Res., 92*, 9723–9732, 1987.

Fritts, D. C., and T. E. VanZandt, Spectral estimates of gravity wave energy and momentum fluxes, I, Energy dissipation, acceleration, and constraints, *J. Atmos. Sci., 50*, 3685–3694, 1993.

Fritts, D. C., and R. A. Vincent, Mesospheric momentum flux studies at Adelaide, Australia: Observations and a gravity wave-tidal interaction model, *J. Atmos. Sci., 44*, 605–619, 1987.

Fritts, D. C., and D. Wang, Doppler-shifting effects on frequency spectra of gravity waves observed near the summer mesopause at high latitude, *J. Atmos. Sci., 48*, 1535–1544, 1991.

Fritts, D. C., and L. Yuan, Measurement of the momentum fluxes near the summer mesopause at Poker Flat, Alaska, *J. Atmos. Sci., 46*, 2569–2579, 1989.

Fritts, D. C., T. Tsuda, T. Sato, S. Fukao, and S. Kato, Observational evidence of a saturated gravity wave spectrum in the troposphere and lower stratosphere, *J. Atmos. Sci., 45*, 1741–1759, 1988.

Fritts, D. C., L. Yuan, M. H. Hitchman, L. Coy, E. Kudeki, and R. F. Woodman, Dynamics of the equatorial mesosphere observed using the Jicamarca MST radar during June and August 1987, *J. Atmos. Sci., 49*, 2353–2371, 1992.

Fritts, D. C., T. Tsuda, T. E. VanZandt, S. A. Smith, T. Sato, S. Fukao, and S. Kato, Studies of velocity fluctuations in the lower atmosphere using the MU radar, II, Momentum fluxes and energy densities, *J. Atmos. Sci., 47*, 51–66, 1990.

Fritts, D. C., M. A. Geller, B. B. Balsley, M. L. Chanin, I. Hirota, J. R. Holton, S. Kato, R. S. Lindzen, M. R. Schoeberl, R. A. Vincent, and R. F. Woodman, Research status and recommendations from the Alaska Workshop on gravity waves and turbulence in the middle atmosphere Fairbanks, Alaska, 18–22 July, 1983, *Bull. Am. Meteor. Soc., 65*, 149–159, 1984.

Gage, K. S., Evidence for a $k^{5/3}$ power law inertial range in mesoscale two-dimensional turbulence, *J. Atmos. Sci., 36*, 1950–1954, 1979.

Gage, K. S., and G. D. Nastrom, On the spectrum of atmospheric velocity fluctuations seen by MST/ST radar and their interpretation, *Radio Sci., 20*, 1339–1347, 1985.

Gardner, C. S., Introduction to ALOHA-90: The airborne lidar and observations of the Hawaiian airglow campaign, *Geophys. Res. Lett., 18*, 1313–1316, 1991.

Gardner, C. S., Diffusive filtering theory of gravity wave spectra in the atmosphere, *J. Geophys. Res., 99*, 20601–20622, 1994.

Gardner, C. S., Introduction to ALOHA/ANLC-93: The 1993 airborne lidar and observations of the Hawaiian airglow/airborne noctilucent cloud campaigns, *Geophys. Res. Lett., 22*, 2789–2792, 1995.

Gardner, C. S., and N. F. Gardner, Measurement distortion in aircraft, space shuttle, and balloon observations of atmospheric density and temperature perturbation spectra, *J. Geophys. Res., 98*, 1023–1033, 1993.

Gardner, C. S., C. A. Hostetler, and S. J. Franke, Gravity wave models for the horizontal wave number spectra of atmospheric velocity and density fluctuations, *J. Geophys. Res., 98*, 1035–1049, 1993a.

Gardner, C. S., C. A. Hostetler, and S. Lintelman, Influence of the mean wind field on the separability of atmospheric perturbation spectra, *J. Geophys. Res., 98*, 8859–8872, 1993b.

Garrett, C. J. R., and W. H. Munk, Space-time scales of internal waves, *Geophys. Fluid Dyn., 2*, 225–264, 1972.

Garrett, C. J. R., and W. H. Munk, Space-time scales of internal waves: A progress report, *J. Geophys. Res., 80*, 291–297, 1975.

Garrett, C. J. R., and W. H. Munk, Internal waves in the ocean, *Ann. Rev. Fluid Mech., 11*, 339–369, 1979.

Gary, B. L., Observational results using the microwave temperature profiler during the Airborne Antarctic Ozone Experiment, *J. Geophys. Res., 94*, 11223–11231, 1989.

Geller, M. A., Dynamics of the middle atmosphere, *Space Sci. Rev., 34*, 359–375, 1983.

Gill, A. E., *Atmosphere-Ocean Dynamics*, Academic Press, New York, 1982.

Gonella, J., A rotary-component method for analysing meteorological and oceanographic vector time series, *Deep-Sea Res., 19*, 833–846, 1972.

Gossard, E. E., and W. H. Hooke, *Waves in the Atmosphere*, Elsevier Science, New York, 1975.

Hamilton, K., Climatological statistics of stratospheric inertia-gravity waves deduced from historical rocketsonde wind and temperature data, *J. Geophys. Res., 96*, 20831–20839, 1991.

Hamilton, K., and R. A. Vincent, High-resolution radiosonde data offer new prospects for research, *Eos, 76*, 497 and 506–507, 1995.

Hecht, E., *Optics*, Addison-Wesley Publishing Company, Sydney, 1987.

Hines, C. O., Internal atmospheric gravity waves at ionospheric heights, *Can. J. Phys., 38*, 1441–1481, 1960.

Hines, C. O., The upper atmosphere in motion, *Q. J. R. Meteorol. Soc., 89*, 1–42, 1963.

Hines, C. O., Tropopausal mountain waves over Arecibo: A case study, *J. Atmos. Sci., 46*, 476–488, 1989.

Hines, C. O., The saturation of gravity waves in the middle atmosphere, I, Critique of linear-instability theory, *J. Atmos. Sci., 48*, 1348–1359, 1991a.

Hines, C. O., The saturation of gravity waves in the middle atmosphere, II, Development of Doppler-spread theory, *J. Atmos. Sci., 48*, 1360–1379, 1991b.

Hines, C. O., The saturation of gravity waves in the middle atmosphere, III, Formation of the turbopause and of turbulent layers beneath it, *J. Atmos. Sci., 48*, 1380–1385, 1991c.

Hines, C. O., Pseudosaturation of gravity waves in the middle atmosphere: An interpretation of certain lidar observations, *J. Atmos. Terr. Phys., 55*, 441–445, 1993a.

Hines, C. O., The saturation of gravity waves in the middle atmosphere, IV, Cutoff of the incident wave spectrum, *J. Atmos. Sci., 50*, 3045–3060, 1993b.

Hines, C. O., Comments on "observations of low-frequency inertia-gravity waves in the lower stratosphere over Arecibo", *J. Atmos. Sci., 52*, 607–610, 1995.

Hines, C. O., Doppler-spread parameterization of gravity-wave momentum deposition in the middle atmosphere, part I: Basic formulation, *J. Atmos. Terr. Phys.*, submitted, 1996a.

Hines, C. O., Doppler-spread parameterization of gravity-wave momentum deposition in the middle atmosphere, part II: Broad spectra and quasi monochromatic waves, including orowaves, *J. Atmos. Terr. Phys.*, submitted, 1996b.

Hirota, I., Observational evidence of the semiannual oscillation in the tropical middle atmosphere — A review, *Pure Appl. Geophys., 118*, 217–238, 1980.

Hirota, I., Climatology of gravity waves in the middle atmosphere, *J. Atmos. Terr. Phys., 46*, 767–773, 1984.

Hitchman, M. H., and C. B. Leovy, Estimation of the Kelvin wave contribution to the semiannual oscillation, *J. Atmos. Sci., 45*, 1462–1475, 1988.

Hitchman, M. H., K. W. Bywaters, D. C. Fritts, L. Coy, E. Kudeki, and F. Surucu, Mean winds and momentum fluxes over Jicamarca, Peru, during June and August 1987, *J. Atmos. Sci., 49*, 2372–2383, 1992.

Holloway, G., and P. Müller, Topographic stress in the oceans, *Eos, 71*, 343–344, 1990.

Holton, J. R., *An Introduction to Dynamic Meteorology*, Academic Press, New York, 1992.

Holton, J. R., and R. S. Lindzen, An updated theory for the quasi-biennial cycle of the tropical stratosphere, *J. Atmos. Sci., 29*, 1076–1080, 1972.

Holton, J. R., and W. M. Wehrbein, A numerical model of the zonal mean circulation of the middle atmosphere, *Pure Appl. Geophys., 118*, 284–306, 1980.

Houghton, J. T., The stratosphere and mesosphere, *Q. J. R. Meteorol. Soc., 104*, 1–29, 1978.

Houze, R. A., Jr., and A. K. Betts, Convection in GATE, *Rev. Geophys. Space Phys., 19*, 541–576, 1981.

Hughes, B. A., The effect of internal waves on surface wind waves, II, Theoretical analysis, *J. Geophys. Res., 83*, 455–465, 1978.

Ivanov, A., A. Kats, S. Kurnosenko, N. Nash, and N. Zaitseva, WMO international radiosonde comparison phase III, *World Meteorological Organization Instruments and Observing Methods, 40*, 1991.

Jasperson, W. H., G. D. Nastrom, and D. C. Fritts, Further study of terrain effects on the mesoscale spectrum of atmospheric motions, *J. Atmos. Sci., 47*, 979–987, 1990.

Jenkins, G. M., and D. G. Watts, *Spectral Analysis and its Applications*, Holden-Day, San Francisco, 1968.

Jones, W. L., Propagation of internal gravity waves in fluids with shear flow and rotation, *J. Fluid Mech., 30*, 439–448, 1967.

Karhunen, P., Extension of multifrequency composite NAVAID windfinding, *Vaisala News, 124*, 15–19, 1991.

Karoly, D. J., G. L. Roff, and M. J. Reeder, Gravity wave activity associated with tropical convection detected in TOGA COARE sounding data, *Geophys. Res. Lett., 23*, 261–264, 1996.

Kerlin, T. W., R. L. Shepard, H. M. Hashemian, and K. M. Petersen, *Response of Installed Temperature Sensors. Temperature, Its Measurement and Control in Science and Industry*, vol. 5, American Institute of Physics, New York, 1982.

Kitamura, Y., and I. Hirota, Small-scale disturbances in the lower stratosphere revealed by daily rawin sonde observations, *J. Meteorol. Soc. Jpn., 67*, 817–830, 1989.

Koop, C. G., A preliminary investigation of the interaction of internal gravity waves with a steady shearing motion, *J. Fluid Mech., 113*, 347–386, 1981.

Kraus, J. D., *Radio Astronomy*, McGraw-Hill, New York, 1966.

Kuo, F. S., and H. Y. Lue, Effect of the wave-shear interaction on gravity wave activity in the lower and middle atmosphere, *J. Atmos. Terr. Phys., 56*, 1147–1155, 1994.

Kuo, F. S., H. Y. Lue, C. M. Huang, C. L. Lo, C. H. Liu, S. Fukao, and Y. Muraoka, A study of velocity fluctuation spectra in the troposphere and lower stratosphere using MU radar, *J. Atmos. Terr. Phys., 54*, 31–48, 1992.

Lally, V. E., Upper air in situ observing systems, in *Handbook of Applied Meteorology*, edited by D. D. Houghton, 352–360, John Wiley & sons, Brisbane, 1985.

Lange, A. A., Meteorological observations using NAVAID methods, *World Meteorological Organization Technical Note, 185*, 1985.

Leaman, K. D., and T. B. Sanford, Vertical energy propagation of inertial waves: A vector spectral analysis of velocity profiles, *J. Geophys. Res., 80*, 1975–1979, 1975.

Leovy, C. B., Simple models of thermally driven mesospheric circulations, *J. Atmos. Sci., 21*, 327–341, 1964.

Lighthill, J., *Waves in Fluids*, Cambridge University Press, Melbourne, 1978.

Lilly, D. K., Wave momentum flux—A GARP problem, *Bull. Am. Meteor. Soc., 20*, 17–23, 1972.

Lilly, D. K., Stratified turbulence and the mesoscale variability of the atmosphere, *J. Atmos. Sci., 40*, 749–761, 1983.

Lilly, D. K., and P. J. Kennedy, Observations of a stationary mountain wave and its associated momentum flux and energy dissipation, *J. Atmos. Sci., 30*, 1135–1152, 1973.

Lindzen, R. S., Tides and gravity waves in the upper atmosphere, in *Mesospheric Models and Related Experiments*, edited by G. Fiocco, 122–130, D. Reidel Publishing Company, Dordrecht-Holland, 1971.

Lindzen, R. S., Turbulence and stress owing to gravity wave and tidal breakdown, *J. Geophys. Res., 86*, 9707–9714, 1981.

Lindzen, R. S., *Dynamics in Atmospheric Physics*, Cambridge University Press, Melbourne, 1990.

Lindzen, R. S., and J. R. Holton, A theory of the quasi-biennial oscillation, *J. Atmos. Sci., 25*, 1095–1107, 1968.

Low, D. J., Studies of the lower atmosphere with a VHF wind profiler, Ph.D. thesis, University of Adelaide, 1996.

Lu, W., and D. C. Fritts, Spectral estimates of gravity wave energy and momentum fluxes, III, Gravity wave-tidal interactions, *J. Atmos. Sci., 50*, 3714–3727, 1993.

Luo, Z., and D. C. Fritts, Gravity-wave excitation by geostrophic adjustment of the jet stream, part II: Three-dimensional forcing, *J. Atmos. Sci., 50*, 104–115, 1993.

Madden, R. A., and E. J. Zipser, Multi-layered structure of the wind over the equatorial Pacific during the Line Islands Experiment, *J. Atmos. Sci., 27*, 336–342, 1970.

Maekawa, Y., S. Fukao, T. Sato, S. Kato, and R. F. Woodman, Internal inertia-gravity waves in the tropical lower stratosphere observed by the Arecibo radar, *J. Atmos. Sci., 41*, 2359–2367, 1984.

Marks, C. J., Some features of the climatology of the middle atmosphere revealed by Nimbus 5 and 6, *J. Atmos. Sci., 46*, 2485–2508, 1989.

Matsuno, T., A dynamical model of the stratospheric sudden warming, *J. Atmos. Sci., 28*, 1479–1494, 1971.

May, P. T., W. L. Ecklund, and G. D. Hess, Spectral and bispectral characteristics of wind variability at Darwin, Australia observed by a VHF radar wind profiler, *Q. J. R. Meteorol. Soc., 121*, 527–544, 1995.

McFarlane, N. A., The effect of orographically excited gravity wave drag on the general circulation of the lower stratosphere and troposphere, *J. Atmos. Sci., 44*, 1775–1800, 1987.

McIntyre, M. E., On the "wave momentum" myth, *J. Fluid Mech., 106*, 331–347, 1981.

McIntyre, M. E., and T. N. Palmer, Breaking planetary waves in the stratosphere, *Nature, 305*, 593–600, 1983.

McIntyre, M. E., and T. N. Palmer, The "surf zone" in the stratosphere, *J. Atmos. Terr. Phys., 46*, 825–849, 1984.

McIntyre, M. E., and T. N. Palmer, A note on the general concept of wave breaking for Rossby and gravity waves, *Pure Appl. Geophys., 123*, 964–975, 1985.

Medvedev, A. S., and G. P. Klaassen, Vertical evolution of gravity wave spectra and the parameterization of associated wave drag, *J. Geophys. Res., 100*, 25841–25853, 1995.

Meek, C. E., I. M. Reid, and A. H. Manson, Observations of mesospheric wind velocities, II, Cross sections of power spectral density for 48–8 hours, 8–1 hours, and 1 hour to 10 min over 60–110 km for 1981, *Radio Sci., 20*, 1383–1402, 1985.

Mengel, J. G., H. G. Mayr, K. L. Chan, C. O. Hines, C. A. Reddy, N. F. Arnold, and H. S. Porter, Equatorial oscillations in the middle atmosphere generated by small scale gravity waves, *Geophys. Res. Lett., 22*, 3027–3030, 1995.

MET Program Manual: Application Programs, Technical Manual, Vaisala Oy, Finland, 1989.

Mitchell, R. M., R. P. Cechet, P. J. Turner, and C. C. Elsum, Observation and interpretation of wave clouds over Macquarie Island, *Q. J. R. Meteorol. Soc., 116*, 741–752, 1990.

Mobbs, S. D., and J. M. Rees, Studies of atmospheric internal gravity waves at Halley station, Antarctica, using radiosondes, *Antarctic Sci., 1*, 65–75, 1989.

Moore, M. I., P. J. Thomson, and T. G. L. Shirtcliffe, Spectral analysis of ocean profiles from unequally spaced data, *J. Geophys. Res., 93*, 655–664, 1988.

Mowbray, D. E., and B. S. H. Rarity, A theoretical and experimental investigation of the phase configuration of internal waves of small amplitude in a density stratified liquid, *J. Fluid Mech., 28*, 1–16, 1967.

Müller, P., G. Holloway, F. Henyey, and N. Pomphrey, Nonlinear interactions among internal gravity waves, *Rev. Geophys., 24*, 493–536, 1986.

Munk, W., Internal waves and small-scale processes, in *Evolution of Physical Oceanography*, edited by B. A. Warren and C. Wunsch, 264–291, MIT Press, Cambridge-USA, 1981.

Murphy, D. J., Measurements of energy and momentum in the mesosphere, Ph.D. thesis, University of Adelaide, 1990.

Murphy, D. J., and R. A. Vincent, Estimates of momentum flux in the mesosphere and lower thermosphere over Adelaide, Australia, from March 1985 to February 1986, *J. Geophys. Res., 98*, 18617–18638, 1993.

Nash, J., and F. J. Schmidlin, WMO international radiosonde comparison, *World Meteorological Organization Instruments and Observing Methods, 30*, 1987.

Nastrom, G. D., and D. C. Fritts, Sources of mesoscale variability of gravity waves, I, Topographic excitation, *J. Atmos. Sci., 49*, 101–110, 1992.

Nastrom, G. D., and K. S. Gage, A climatology of atmospheric wavenumber spectra of wind and temperature observed by commercial aircraft, *J. Atmos. Sci., 42*, 950–960, 1985.

Nastrom, G. D., D. C. Fritts, and K. S. Gage, An investigation of terrain effects on the mesoscale spectrum of atmospheric motions, *J. Atmos. Sci., 44*, 3087–3096, 1987.

Nastrom, G. D., T. E. VanZandt, and J. M. Warnock, Vertical wavenumber spectra of wind and temperature from high-resolution balloon soundings in the lower atmosphere over Illinois, *J. Geophys. Res.*, submitted, 1996.

Naujokat, B., K. Labitzke, R. Lenschow, B. Rajewski, M. Wiesner, and R.-C. Wohlfart, The stratospheric winter 1993/1994: A winter with some minor warmings and an early final warming, *Beilage zur Berliner Wetterkarte*, SO 24/94, 1994.

O'Brien, J. J., and R. D. Pillsbury, Rotary wind spectra in a sea breeze regime, *J. Appl. Meteor., 13*, 820–825, 1974.

Ogino, S., M. D. Yamanaka, and S. Fukao, Meridional variation of lower stratospheric gravity wave activity: A quick look at Hakuho-Maru J-COARE cruise rawinsonde data, *J. Meteorol. Soc. Jpn., 73*, 407–413, 1995.

Palmer, T. N., G. J. Shutts, and R. Swinbank, Alleviation of a systematic westerly bias in general circulation and numerical weather prediction models through an orographic gravity wave drag parametrization, *Q. J. R. Meteorol. Soc., 112*, 1001–1039, 1986.

Pfister, L., S. Scott, M. Loewenstein, S. Bowen, and M. Legg, Mesoscale disturbances in the tropical stratosphere excited by convection: Observations and effects on the stratospheric momentum budget, *J. Atmos. Sci., 50*, 1058–1075, 1993a.

Pfister, L., K. R. Chan, T. P. Bui, S. Bowen, M. Legg, B. Gary, K. Kelly, M. Proffitt, and W. Starr, Gravity waves generated by a tropical cyclone during the STEP tropical field program: A case study, *J. Geophys. Res., 98*, 8611–8638, 1993b.

Phillips, O. M., *The Dynamics of the Upper Ocean*, Cambridge University Press, Melbourne, 1977.

Plumb, R. A., The interaction of two internal waves with the mean flow: Implications for the theory of the quasi-biennial oscillation, *J. Atmos. Sci., 34*, 1847–1858, 1977.

Plumb, R. A., and A. D. McEwan, The instability of a forced standing wave in a viscous stratified fluid: A laboratory analogue of the quasi-biennial oscillation, *J. Atmos. Sci., 35*, 1827–1839, 1978.

Press, W. H., S. A. Teukolsky, W. T. Vetterling, and B. P. Flannery, *Numerical Recipes in C*, Cambridge University Press, Melbourne, 1988.

Rees, M. H., *Physics and Chemistry of the Upper Atmosphere*, Cambridge University Press, Melbourne, 1989.

Reid, I. M., and R. A. Vincent, Measurements of mesospheric gravity wave momentum fluxes and mean flow accelerations at Adelaide, Australia, *J. Atmos. Terr. Phys., 49*, 443–460, 1987.

Reid, I. M., R. Rüster, P. Czechowsky, and G. Schmidt, VHF radar measurements of momentum fluxes in the summer polar mesosphere over Andenes (69°N, 16°E), Norway, *Geophys. Res. Lett., 15*, 1263–1266, 1988.

Reid, S. J., An observational study of lee waves using radiosonde data, *Tellus, 24*, 593–596, 1972.

Sato, K., and T. J. Dunkerton, Estimates of momentum flux associated with equatorial Kelvin and gravity waves, *J. Geophys. Res.*, submitted, 1996.

Sato, K., F. Hasegawa, and I. Hirota, Short-period disturbances in the equatorial lower stratosphere, *J. Meteorol. Soc. Jpn., 72*, 859–872, 1994.

Sato, K., H. Hashiguchi, and S. Fukao, Gravity waves and turbulence associated with cumulus convection observed with the UHF/VHF clear-air Doppler radars, *J. Geophys. Res., 100*, 7111–7119, 1995.

Sawyer, J. S., Quasi-periodic wind variations with height in the lower stratosphere, *Q. J. R. Meteorol. Soc., 87*, 24–33, 1961.

Schmidlin, F. J., WMO international radiosonde intercomparison phase II, 1985, *World Meteorological Organization Instruments and Observing Methods, 29*, 1988.

Schoeberl, M. R., The penetration of mountain waves into the middle atmosphere, *J. Atmos. Sci., 42*, 2856–2864, 1985.

Schoeberl, M. R., and D. F. Strobel, The zonally averaged circulation of the middle atmosphere, *J. Atmos. Sci., 35*, 577–591, 1978.

Senft, D. C., and C. S. Gardner, Seasonal variability of gravity wave activity and spectra in the mesopause region at Urbana, *J. Geophys. Res., 96*, 17229–17264, 1991.

Senft, D. C., C. A. Hostetler, and C. S. Gardner, Characteristics of gravity wave activity and spectra in the upper stratosphere and upper mesosphere at Arecibo during early April 1989, *J. Atmos. Terr. Phys., 55*, 425–439, 1993.

Shutts, G. J., P. Healey, and S. D. Mobbs, A multiple sounding technique for the study of gravity waves, *Q. J. R. Meteorol. Soc., 120*, 59–77, 1994.

Shutts, G. J., M. Kitchen, and P. H. Hoare, A large amplitude gravity wave in the lower stratosphere detected by radiosonde, *Q. J. R. Meteorol. Soc., 114*, 579–594, 1988.

Sidi, C., J. Lefrere, F. Dalaudier, and J. Barat, An improved atmospheric buoyancy wave spectrum model, *J. Geophys. Res., 93*, 774–790, 1988.

Smith, R. B., The influence of mountains on the atmosphere, in *Advances in Geophysics, 21*, edited by B. Saltzman, Academic Press, New York, 87–230, 1979.

Smith, S. A., D. C. Fritts, and T. E. VanZandt, Comparison of mesospheric wind spectra with a gravity wave model, *Radio Sci., 20*, 1331–1338, 1985.

Smith, S. A., D. C. Fritts, and T. E. VanZandt, Evidence for a saturated spectrum of atmospheric gravity waves, *J. Atmos. Sci., 44*, 1404–1410, 1987.

Souprayen, C., Climatologie des ondes de gravite dans l'atmosphere moyenne: Contribution a leur parametrisation dans les modeles numeriques, Ph.D. thesis, l'Univ. Pierre et Marie Curie Paris, 1993.

Streten, N. A., The climate of Macquarie Island and its role in atmospheric monitoring, *Pap. Proc. R. Soc. Tasm., 122*, 91–106, 1988.

Thompson, R. O. R. Y., Observation of inertial waves in the stratosphere, *Q. J. R. Meteorol. Soc., 104*, 691–698, 1978.

Thorpe, S. A., The excitation, dissipation, and interaction of internal waves in the deep ocean, *J. Geophys. Res., 80*, 328–338, 1975.

Thorpe, S. A., An experimental study of critical layers, *J. Fluid Mech., 103*, 321–344, 1981.

Tsuda, T., Y. Murayama, H. Wiryosumarto, S. W. B. Harijono, and S. Kato, Radiosonde observations of equatorial atmosphere dynamics over Indonesia, 1, Equatorial waves and diurnal tides, *J. Geophys. Res., 99*, 10491–10505, 1994a.

Tsuda, T., Y. Murayama, H. Wiryosumarto, S. W. B. Harijono, and S. Kato, Radiosonde observations of equatorial atmosphere dynamics over Indonesia, 2, Characteristics of gravity waves, *J. Geophys. Res., 99*, 10507–10516, 1994b.

Tsuda, T., Y. Murayama, M. Yamamoto, S. Kato, and S. Fukao, Seasonal variation of the momentum flux in the mesosphere observed with the MU radar, *Geophys. Res. Lett., 17*, 725–728, 1990.

Tsuda, T., T. E. VanZandt, M. Mizumoto, S. Kato, and S. Fukao, Spectral analysis of temperature and Brunt-Vaisala frequency fluctuations observed by radiosondes, *J. Geophys. Res., 96*, 17265–17278, 1991.

Tsuda, T., T. Inoue, D. C. Fritts, T. E. VanZandt, S. Kato, T. Sato, and S. Fukao, MST radar observations of a saturated gravity wave spectrum, *J. Atmos. Sci., 46*, 2440–2447, 1989.

Tsuda, T., Y. Murayama, H. Wiryosumarto, S. Kato, S. W. B. Harijono, S. Fukao, M. Karmini, C. M. Mangan, S. Saraspriya, and A. Suripto, A preliminary report on radiosonde observations of the equatorial atmosphere dynamics over Indonesia, *J. Geomagn. Geoelectr., 44*, 1041–1055, 1992.

Turtiainen, H., Response time of RS80 temperature sensor in flight, technical report, Vaisala Oy, Finland, 1991a.

Turtiainen, H., Response time test of Vaisala RS80 temperature sensor, technical report, Vaisala Oy, Finland, 1991b.

Uccellini, L. W., A case study of apparent gravity wave initiation of severe convective storms, *Mon. Weather Rev., 103*, 497–513, 1975.

Uccellini, L. W., and S. E. Koch, The synoptic setting and possible energy sources for mesoscale wave disturbances, *Mon. Weather Rev., 115*, 721–729, 1987.

U.S. Standard Atmosphere Supplements, U.S. Government Printing Office, Washington, D.C., 1966.

U.S. Standard Atmosphere, U.S. Government Printing Office, Washington, D.C., 1976.

VanZandt, T. E., A universal spectrum of buoyancy waves in the atmosphere, *Geophys. Res. Lett., 9*, 575–578, 1982.

VanZandt, T. E., Gravity waves, in *Atmospheric structure and its variation in the region 20 to 120 km, Handbook for MAP, 16*, 149–156, 1985.

VanZandt, T. E., Spectral description of the gravity wave field, *Adv. Space Res., 10*, 111–116, 1990.

VanZandt, T. E., and D. C. Fritts, A theory of enhanced saturation of the gravity wave spectrum due to increases in atmospheric stability, *Pure Appl. Geophys., 130*, 399–420, 1989.

VanZandt, T. E., S. A. Smith, T. Tsuda, D. C. Fritts, T. Sato, S. Fukao, and S. Kato, Studies of velocity fluctuations in the lower atmosphere using the MU radar, I, Azimuthal anisotropy, *J. Atmos. Sci., 47*, 39–50, 1990.

Vincent, R. A., Gravity-wave motions in the mesosphere, *J. Atmos. Terr. Phys., 46*, 119–128, 1984.

Vincent, R. A., Gravity waves in the southern hemisphere middle atmosphere: A review of observations, in *Dynamics, Transport and Photochemistry in the Middle Atmosphere of the Southern Hemisphere*, edited by A. O'Neill, 159–170, Kluwer Academic Publishers, Holland, 1990.

Vincent, R. A., Gravity-wave motions in the mesosphere and lower thermosphere observed at Mawson, Antarctica, *J. Atmos. Terr. Phys., 56*, 593–602, 1994.

Vincent, R. A., and S. D. Eckermann, VHF radar observations of mesoscale motions in the troposphere: Evidence for gravity wave Doppler shifting, *Radio Sci., 25*, 1019–1037, 1990.

Vincent, R. A., and D. C. Fritts, A climatology of gravity wave motions in the mesopause region at Adelaide, Australia, *J. Atmos. Sci., 44*, 748–760, 1987.

Vincent, R. A., and I. M. Reid, HF Doppler measurements of mesospheric gravity wave momentum fluxes, *J. Atmos. Sci., 40*, 1321–1333, 1983.

Wallace, J. M., General circulation of the tropical lower stratosphere, *Rev. Geophys. Space Phys., 11*, 191–222, 1973.

Wallace, J. M., and V. E. Kousky, Observational evidence of Kelvin waves in the tropical stratosphere, *J. Atmos. Sci., 25*, 900–907, 1968.

Weinstock, J., Saturated and unsaturated spectra of gravity waves and scale dependent diffusion, *J. Atmos. Sci., 47*, 2211–2225, 1990.

Whiteway, J. A., and T. J. Duck, Evidence for critical level filtering of atmospheric gravity waves, *Geophys. Res. Lett., 23*, 145–148, 1996.

Wilson, R., M. L. Chanin, and A. Hauchecorne, Gravity waves in the middle atmosphere observed by Rayleigh lidar, 2, Climatology, *J. Geophys. Res., 96*, 5169–5183, 1991.

Wunsch, C., Deep ocean internal waves: What do we really know?, *J. Geophys. Res., 80*, 339–343, 1975.

Wunsch, C., Geographical variability of the internal wave field: A search for sources and sinks, *J. Phys. Oceanogr., 6*, 471–485, 1976.

Wunsch, C., and S. Webb, The climatology of deep ocean internal waves, *J. Phys. Oceanogr., 9*, 235–243, 1979.

Yanai, M., and T. Maruyama, Stratospheric wave disturbances propagating over the equatorial Pacific, *J. Meteorol. Soc. Jpn., 44*, 291–294, 1966.

Zangvil, A., On the presentation and interpretation of spectra of large-scale disturbances, *Mon. Weather Rev., 105*, 1469–1472, 1977.

Zhu, X., A new theory of the saturated gravity wave spectrum for the middle atmosphere, *J. Atmos. Sci., 51*, 3615–3626, 1994.